Study of Hadronic Form Factors: essential inputs for the Hadronic Light-by-Light piece of muon's g − 2

Emilio José Estrada González

Advisor: Dr. Pablo Roig

Department of Physics
Centro de Investigación y de Estudios Avanzados del I.P.N

This dissertation is submitted for the degree of
PhD in Sciences in the Specialty of Physics

CINVESTAV January, 2026

Para mis papás, Rodolfo y Sandra.
Por favor, acepten esta tesis como un tributo a su amor.

Acknowledgements

To my home, Sandra, Rodolfo, Majo, José, la Luchis, Yuyus, Joel & Dino, por el apoyo incondicional y porque los extrañé mucho en estos 5 años.

To my family, Muno, Tita, Salvador, Conchi, uncles, aunts, cousins, & nephews, por el tiempo que vivimos antes de venirme acá y el que ya no se puede recuprar.

To Pablo Roig, por su incansable apoyo, y su intachable gestión como asesor; por la formación en cada aspecto de mi vida, la confianza de compartirme proyectos ambiciosos e interesantes y por la amistad que desarrollamos en estos 5 años.

To my other mentors, Sergi, Adolfo, Emilie & Antonio, por el acompañamiento que me dieron durante estos años, además de la gestión para invitarme a sus centros de investigación y compartir invaluables discusiones conmigo.

To my professors, por todo el conocimiento que transmitieron durante sus clases.

To the High-Energy Physics group at Cinvestav, por el buen ambiente académico y la disposición siempre a discutir temas de interés para convertirnos en mejores científicos.

To my friends and colleagues, Juanma & Diego, porque además de la amistad que compartimos en estos años, tuve el gusto y honor de haber trabajado junto a ustedes.

To my friends at Cinvestav, porque aunque el camino es personal, fue un gusto que por un tiempo los hayamos caminado juntos. Fueron mi familia lejos de casa estos 5 años.

To SECIHTI, Por el apoyo económico brindado para realizar mis estudios de pos-

grado, la educación superior pública debe defenderse y trabajarse.

To CINVESTAV, por todo el apoyo en mi estancia por estos rumbos, especialmente a Mariana, Salvador, Lupita y Jhovanny, por su increíble apoyo a toda la comunidad, especialmente a mi persona. Sin gente como ustedes, ningún instituto funciona.

To Sonbae Lindavista, por los grandes momentos vividos y todos los aprendizajes obtenidos en el *Do*.

Abstract

During this thesis, we have studied different hadronic form factors, and we have used them to compute contributions to the Hadronic Light-by-Light piece of the muon anomalous magnetic moment (this work has deserved the author membership of the Theory Initiative, thanks to his contributions to the second White Paper). Specifically, for the HLbL section, we have computed the pseudoscalar pole contributions in the first hybrid analysis (adding lattice to experimental data); we also computed the first baryonic contribution to HLbL, the proton-box; finally, we computed the tensor meson pole contributions, as a timely third determination due to the strong tension in previous determinations, claiming for the first time concrete evidence of new form factors in this sector, which shall require the development of a new basis in future complete evaluations of this contribution. We used Resonance Chiral Theory, dispersive representations, rational approaches, and parametrizations of experimental data, together with lattice QCD calculations, to describe these form factors, having thus made use of extensive theoretical resources for this thesis. All this work resulted in 3 papers, 1 short review, 1 collaboration report, and 1 project to be completed soon.

Resumen

Durante esta tesis, estudiamos distintos factores de forma hadrónicos, y los usamos para calcular contribuciones a la dispersión luz-por-luz hadrónica del momento magnético anómalo del muón como miembros de la Iniciativa Teórica, gracias al impacto de los trabajos realizados y a la contribución al segundo White Paper. Concretamente, en la sección de la dispersión luz-por-luz, calculamos las contribuciones de polos pseudoescalares en el primer análisis híbrido (añadiendo datos de lattice a los experimentales); también calculamos la primera contribución bariónica en HLbL, la caja de protones; finalmente, calculamos las contribuciones de polos tensoriales, como una determinación oportuna debido a la fuerte tensión entre determinaciones previas, declarando por primera vez evidencia concreta de nuevos factores de forma en este sector, que requerirán una nueva base para el cálculo completo de estas contribuciones en el futuro. Hemos usado Teoría de Resonancias Quirales, representaciones dispersivas, métodos racionales y parametrizaciones de datos experimentales; junto a cálculos de lattice QCD, para describir estos factores de forma, habiendo hecho uso de una extensa cantidad de recursos teóricos para la elaboración de esta tesis. Este trabajo produjo 3 artículos, 1 de revisión corta, 1 reporte de colaboración y un proyecto próximo a concluir.

Table of contents

Introduction

The Standard Model of Elementary Particles has been shown for the last 6 decades to be consistent with the experimental evidence. However, the SM cannot account for fundamental observations in the universe, as massive neutrinos, the matter-antimatter asymmetry, or the nature of Dark Matter. This opens the door for key searches for deviations from it, which we can separate into three kinds: precise tests within the Standard Model, phenomenology of new particles, and beyond the Standard Model physics parametrizations in Effective Field Theories.

The precise tests within the standard theory can be performed both in high-energy observables at LHC and low-energy precision measurements at high-intensity experiments, and require enormous efforts from the experimental and theory collaborations. Among the most relevant tensions between theory and experiment in recent years –so-called *anomalies*–, we can mention the muon anomalous magnetic moment [1–6], semi-leptonic B meson decays [7–16], measurements of the W boson mass [17–23], and many others [24].

During the work towards this Ph.D., we focused mainly on improving the precision of the theoretical determination of the anomalous magnetic moment of the muon within the Standard Model, contributing to the Theory Initiative and becoming an author of the White Paper 2025 [25], as a recognition of the relevance of the obtained results. The experimental uncertainty of the current experimental world average is 145×10^{-12} (124 ppb), which shows an enormous improvement with respect to the first results at the beginning of the century, 630×10^{-12} (540 ppb). Within the Standard Model, the Theory Initiative reported a precision of 430×10^{-12} in their first report and of 620×10^{-12} [1].

[1] The increase of the uncertainty in the theoretical determination is caused by the appearance of new data for the $e^+e^- \to$ hadrons, which worsened the tension between different datasets used to determine the Hadronic Vacuum Polarization piece (particularly, its most important contribution, coming from the di-pion cut) and made impossible a data-driven average at this point. The Lattice QCD average was used instead, which improved a lot from WP2020 to WP2025, but its uncertainty is still larger (though more reliable) than that of the data-driven average used in WP2020.

In contrast with the experimental determination, where the total $g-2$ is measured, the theory initiative uses the Standard Model to compute it, which is a Quantum Field Theory. This implies (particularly for the Hadronic light-by-light piece, see later discussion and the subsequent chapters) that contributions must be computed individually and summed, avoiding double-counting (See Refs. [26–85].). To achieve it, the contributions are separated into electromagnetic, electroweak, and QCD contributions. The first ones dominate the magnitude of a_μ, the second ones are small in magnitude and in error and the last ones dominate the uncertainty, because of two factors: having hadrons instead of gluons and quarks as intermediate states, and having –consequently– to deal with the non-perturbative regime of QCD below $E < 2\text{GeV}$.

The hadronic sector is divided into the dominant contribution –related to the Green function of two electromagnetic currents in pure QCD–, called Hadronic Vacuum Polarization (HVP) and the subdominant contribution –related to the Green function of four electromagnetic currents in pure QCD–, called Hadronic Light-by-Light (HLbL). From data-driven methods, the first one can be determined by the precise measurement of the cross section $\sigma(e^+e^- \to \text{hadrons})$ or –by means of an isospin rotation– the cross section of $\tau^- \to \pi^-\pi^0\nu_\tau$ [86–102] from datasets from BaBar [103, 104], CMD-3 [105], KLOE [106–108], SND20 [109], followed by CMD-2 [110–114], BESIII [115], and SND06 [116]); or ALEPH [117], CLEO [118], OPAL [119] and Belle [120], for the tau case. The HLbL piece, in contrast, cannot be obtained by measuring a single process. Instead, it has to be split into its hadronic intermediate states, one by one, relating each of them to on-shell observables, depending on the form factors, which encapsulate all dependence on hadrons production from QCD.

The tension between theory and experiment has changed more than once during the last 5 years, starting at 3.7 σ in 2020 with the appearance of the Theory Initiative White Paper [5], rising to 4.2σ when the first run of the FNAL was analyzed [2], reaching its maximum of 5.1σ in 2023, when the run 1-3 were analyzed [3] to finally decrease to its current status with the release of the final results of the FNAL experiment [4] and the WP 2025 of the Theory Initiative [6]. The current value of the (non-)tension is $38(63) \times 10^{-11}$, being compatible within 1 σ; however, the Hadronic Vacuum Polarization piece is still in internal tension between experimental inputs and Lattice QCD ones [26, 34, 38, 32, 35, 39, 28].

The status of this tension and the increase of the uncertainty on the theory side, does not mean –at all– that there have been no relevant improvements in

the determination of this observable within the Standard Model. Piece by piece, there have been significant advances. Three of them are included in this thesis: The determination of the pseudoscalar pole contributions [62] to the HLbL, the first determination of baryonic contributions to the Hadronic Light-by-Light piece [121], and finally, a timely third determination of the tensor meson pole contributions to the HLbL [122], which explored the gap between the other two determinations [67, 69]. We stress that the more reliable uncertainty of the second White Paper [6] should also be seen as a remarkable collective advance.

As a result of these works, a full evaluation of $a_\mu^{\rm HLbL}$ within Resonance Chiral Theory has become closer. The pseudoscalar-box contributions were computed for this thesis as part of a Review that outlines the recent progress and remaining pieces for achieving a full $R\chi T$ determination of the HLbL piece [123].

All these works have a common necessary ingredient: an accurate description of the hadronic form factors. These are the essential inputs to compute the HLbL contributions to $g-2$ with high precision. The main procedure for doing so is:

1. Construct a model for the Form Factors: in the works of [62, 122, 123], a theory based on the symmetries of QCD are used to construct a model for the form factor, *Resonance Chiral Theory* [2].

2. Impose the short-distance constraints: OPE provides a tool for computing the behavior of these form factors at high energies. Furthermore, the Light Cone Expansion offers a generalization of these results[124].

3. Fitting the free parameters: the parameters which could not be constrained by symmetries or SDCs, can be fitted –if available– to experimental information, and in some cases, to LQCD calculations.

4. Computing the a_μ contributions: With the help of computational tools such as VEGAS integrator [125], and the Master Formula developed in Refs. [126, 46, 48, 61] a value for the individual contributions can be obtained with the form factors.

5. Assessment of theory uncertainties: Most models cannot reproduce everything that the known theory predicts. The assessment of the theory uncertainties is fundamental for a computation to be reliable.

[2] In [121], accurate parametrizations of experimental data and LQCD calculations were available, which made steps unnecessary for this work.

As an extension of this thesis, an exploration of new physics contributions can be performed in the hadronic τ decays, which also rely on form factors to describe the processes. If we choose ideal angular observables, we can obtain an approximate cancellation and go 'beyond form factors', to study the effect of new physics directly from the experimental input, which is a cleaner approach, if feasible. This is a work in progress [127] in an advanced stage, which was presented at TAU2025 [128].

The outline of this thesis follows. We give an introductory overview to the tests within and beyond the Standard Model that we have performed during my PhD in Chapter 1. Later, we describe the Effective Field Theory that we have used for describing QCD at low energies in terms of the meson states, $R\chi T$, in Chapter 2. After the theoretical basis has been set, we describe our work on the pseudoscalar pole contributions to a_μ^{HLbL} in Chapter 3, on the proton-box in Chapter 4, on the tensor meson poles in Chapter 5, and on the status of a full evaluation of a_μ^{HLbL} within $R\chi T$ in Chapter 6. We finalize this thesis with the general conclusions and the perspectives for future works in Chapter 7. Two appendices have been included, completing the main material covered in this thesis. Appendix A details how to employ the 3 main Python libraries used for this thesis. Appendix B explores how to go beyond the form factors in hadronic tau decays (work in progress).

CHAPTER 1

Tests of The Standard Model

In this first chapter, we introduce our framework, the Standard Model of Elementary Particles (SM). In this thesis, we conducted tests within and beyond SM through phenomenological studies. The main part of this work, using the theory framework introduced in chapter 2, consists of precision calculations of hadron contributions to the hadronic light-by-light piece of muon g-2, which are discussed in chapters 3 to 6. We also introduce new physics tests in semileptonic tau decays (appendix B), which are relatively independent of hadron input, thereby providing a clean access to potential new physics contributions. For both types of applications, the SM is the stepping stone, the reason for which is briefly introduced in the following. Conclusions and perspectives of this Ph. D. Thesis are given in chapter 7. An appendix A guiding to useful computing tools complements the main material.

1.1 The Standard Model

The Standard Model of Elementary Particles [129–131] requires three elements to be defined: the interactions, the matter content, and the symmetries (including those of the vacuum, if they are different from the ones in the Lagrangian). All of these elements are related as the interactions are given by mediators which depend on the representation of the symmetry groups, the matter content fills representations of the symmetry groups, and all the physics is described by the possible operators constructed with the matter content, which are singlets under all of the symmetry groups of the SM. All these ideas are developed in several textbooks; I will follow the ones of Paul Langacker[132], Palash B. Pal[133], and Peskin & Schroeder [134],

which I strongly recommend for a PhD level of understanding of Particle Physics and the Standard Model.

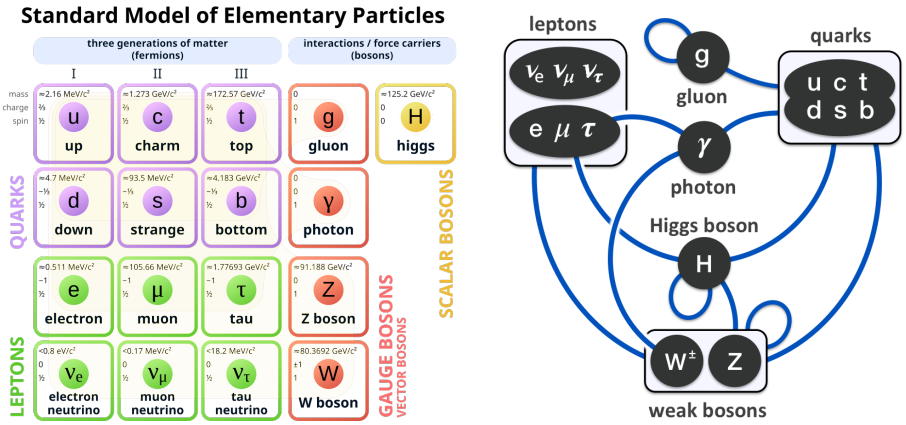

Fig. 1.1 The Standard Model of Elementary Particles and their interactions.

All the known universe –so far– has the particles displayed in the left-hand side of Figure 1.1 as its elementary constituents. We can classify them as: quarks, gauge bosons, leptons, and the Higgs boson. They interact as shown in the right-hand side of Figure 1.1.

Some remarks on the elementary particle classification are relevant at this point:

- The photon is the mediator of the electromagnetic interactions, which are experienced by all the charged particles. $W^{\pm}$ and Z^0 are the mediators of the weak interactions and are self-interacting, as coming from a non-Abelian theory. Gluons are the mediators of the strong interactions and are also self-interacting, for the same reason.

- The Higgs boson is the particle responsible for the mass of all particles via the Higgs mechanism[135–137] but –perhaps– the neutrinos.

- The quarks are the only particles that experience electromagnetic, weak, and strong interactions; however, they are not found free in nature due to a phenomenon called color confinement. They all carry color, and all free particles are colorless, a property which can be achieved by combinations of two (mesons) or three (baryons) (anti)quarks; these are called hadrons and are the main object of study of this thesis.

- The leptons are classified by families: electron(e), muon(μ), and tau(τ). These three families consist of a charged massive (MeV-GeV) particle and its neutrino,

which is massless in the Standard Model, but neutrino oscillations provide evidence of massive neutrinos, which can be accommodated in a minimal extension of the SM. τ is the only lepton massive enough to have hadronic decays, which provide a great scenario to test evidence of BSM physics (or to learn about hadronization) as we have outlined in appendix B.

They can also be classified by their spin: bosons are integer spin particles (Higgs is spin zero and mediators are spin one) and half spin particles (quarks and leptons are spin $1/2$).

1.1.1 Gauge Group of the Standard Model

After the brief introduction of the SM particles and their interactions, let us focus on the reason for most of the facts previously mentioned, the symmetry group. As mentioned above, the symmetry group of a field theory defines the interactions, as the mediators are in the adjoint representation. Consequently, the number of mediators (generators of the symmetry group) is equal to the dimension of the adjoint representation.

When the symmetry of the interactions is promoted from global to local, a set of new particles in the adjoint representation of the symmetry group is required to make the Lagrangian invariant. The corresponding set of transformations is called gauge transformations, and the group is now called the gauge group. The gauge group of the standard model is the direct product of three groups $SU(3)_C \times SU(2)_L \times U(1)_Y$. The main ideas and consequences of these interactions will be discussed in sections 1.1.2 and 1.1.3.

A very relevant feature of the gauge group is the intensity of the interactions, which is different for $SU(3)_C$ than for the other two and has fundamental implications on how we do calculations in one or another. This [139, 140] is the gauge couplings' energy dependence. The running of the effective gauge coupling is defined by the renormalization group equation, which, for QCD only, results in a growing coupling for low energies (see Figure 1.2), reaching a non-perturbative regime below $E < 2\,\text{GeV}$. This, on the one hand leads to infrared slavery at low energies, where strong interactions grow to be non-perturbative. On the other, it gives rise to asymptotic freedom, which explains the success of the parton model.

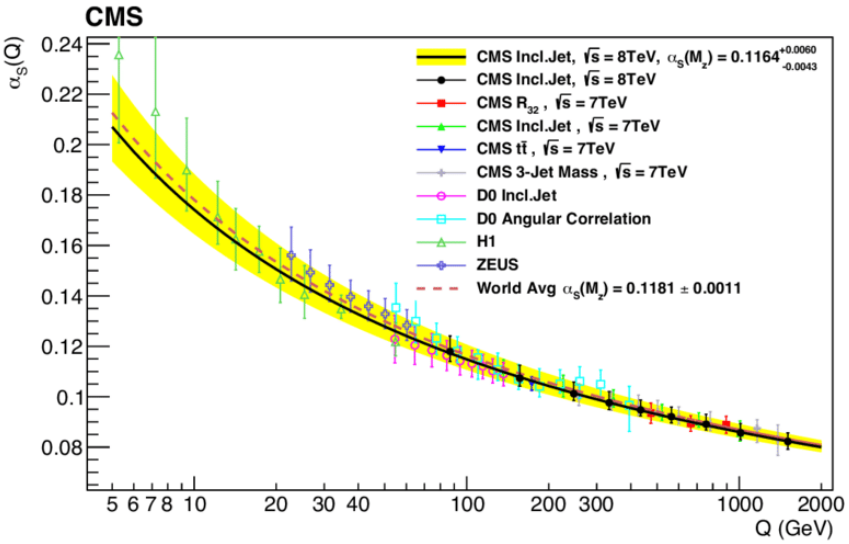

Fig. 1.2 The running of $\alpha_s(s)$, shows stronger interactions at low energies [138]. This results in a non-perturbative regime below energies of around 2 GeV.

1.1.2 Electro-weak interactions

The EW sector $(SU(2)_L \times U(1)_Y)$ has, as a key feature, different representations for left and right particle chiralities. The description of one family of quarks can be replicated to study the three of them, and the lepton sector as well. So, in general, the representations of fermions in the theory are:

$$\phi_1(x) = \begin{pmatrix} u \\ d \end{pmatrix}_L, \qquad \phi_2(x) = u_R, \qquad \phi_3(x) = d_R, \tag{1.1}$$

meaning that the left-hand fields do interact under the $SU(2)_L$ sector and the right-handed ones do not; also, their interactions are determined by their weak hypercharge, which is different for quarks, leptons, and the Higgs boson. Using these representations, the most general fermion Lagrangian can be built, determined by the invariance under global transformations of the EW group:

$$\mathscr{L} = \sum_{j=1}^{3} i\bar{\phi}_j(x)\gamma^\mu \partial_\mu \phi_j(x). \tag{1.2}$$

In order to generate interactions, the global symmetry needs to be promoted to a local one, according to the gauge principle. For this purpose, the theory requires one boson per each symmetry generator of the theory, so that the covariant derivatives

have the correct behavior under local transformations:

$$\begin{aligned} D_\mu \phi_1(x) &= \left[\partial_\mu + ig\frac{\sigma_i}{2}W_\mu^i(x) + ig' y_1 B_\mu(x)\right]\phi_1(x), \\ D_\mu \phi_2(x) &= [\partial_\mu + ig' y_2 B_\mu(x)]\phi_2(x), \\ D_\mu \phi_3(x) &= [\partial_\mu + ig' y_3 B_\mu(x)]\phi_3(x). \end{aligned} \tag{1.3}$$

Gauging the symmetry (making it local) gives rise to the right interactions, in agreement with experiment, as we intended. An important feature of this group is that it is non-abelian (their generators do not commute), so 3- and 4-boson interactions are predicted by the theory. Another important feature is the fact that it is not W^0 (or W^3) the weak neutral gauge boson, Z^0, nor B is γ, but orthogonal combinations of them: the weak eigenstates B and W^3 mix to yield the physical (mass eigenstates) γ and Z^0 states (with the mixing defined by the masslessness condition for the photon, in terms of the weak-mixing angle). The electromagnetic interactions are thus included in the EW theory. In fact, the pattern of spontaneous electroweak symmetry breaking warrants that the electroweak gauge group is broken to the $U(1)$ of QED at low energies, which is the symmetry group of the electroweak vacuum.

Since the Higgs is a doublet under the EW gauge group, interactions with the rest of the particles are allowed; the ones with the fermions are called Yukawa interactions. The couplings of these interactions are directly related to the mass of the fermions. The interactions with the gauge bosons come directly from gauging the theory and result in renormalizable mass terms for the vector bosons; this is the so-called Higgs mechanism.

With the three generations of matter (particularly of quarks) it is possible to violate the combined symmetry of charge conjugation and parity [141], which is one of the required conditions to understand our absolutely matter-dominated universe [142]. However, it is not enough to explain the measured baryon asymmetry, so new physics is required for this.

1.1.3 Strong Interactions

Strong interactions are the ones related to the stability of the atoms' nucleus and have a very rich phenomenology. Quantum Chromodynamics is the fundamental theory of the strong interactions. In the mid of the 1960's, working on the subject was hard, both theoretically and experimentally, since all observed particles are "colorless", meaning they are singlets under the gauge group. It is not intuitive

to introduce a force to which all asymptotic states are invisible to? This apparent paradox arises because the constituents of composite particles, protons and neutrons in nuclei, are not blind to this force, and so, they do interact strongly. Considering the fact that they interact but are confined inside the nucleons (and some other particles too), very high-energy processes should be studied in order to see the effects of this force. A historically important case exemplifying this need is the experimental ratio between $e^-e^+ \to \mu^-\mu^+$ to $e^-e^+ \to$ hadrons, which is sensitive to N_C and verifies that $N_C = 3$. Also, spin $\frac{1}{2}$ particles (quarks) in the fundamental representation and the conjugate representation for antiquarks can, together, form bound colorless integer spin particles (bosons). Also three spin $\frac{1}{2}$ particles in the fundamental representation can form bound colorless semi-integer spin particles (baryons) [133].
This success was both experimental and theoretical, and came in several pieces. First the Feynman's parton model [143] proposed that nucleons were constituted by smaller spin $\frac{1}{2}$ point-like particles which carry part of the nucleon's momenta (evidence of this statement was found in Deep Inelastic Scattering experiments) [132], then the quark model was proposed, which correctly predicted magnetic moments of nucleons. It, however, faced the challenge of the apparent non-existence of both quarks and gluons, which were not detected directly [133]. Indirect evidence for quarks and gluons eventually appeared, so that the theory could be considered "complete". Notwithstanding, the elementary particles of the theory could not be seen as free states (due to confinement). Despite of that, at very high energy, they behave as free particles (asymptotic freedom), which could only be understood after later work on quantum corrections in non-abelian field theories. These two facts appeared as major issues because the fundamental theory was not useful, in practice, from a QFT viewpoint [144], since perturbation theory could not be employed for computations in some (low enough) energy regimes.

Despite perturbation theory cannot be used for some calculations, the QCD Lagrangian can be the starting point to construct an EFT based on the symmetries of the underlying theory and the degrees of freedom of the effectively interacting particles (mesons and baryons), which can instead be used in these troublesome energy regimes. The $SU(3)_C$ locally invariant Lagrangian [145] is (we neglect gauge-fixing and ghost terms):

$$\mathscr{L}_{QCD} = -\frac{1}{4} G^i_{\mu\nu} G^{\mu\nu i} + \sum_r \bar{q}^\alpha_r i \not{D}^\beta_\alpha q_{r\beta} - \sum_r m_r \bar{q}^\alpha_r q_{r\alpha} + \frac{\theta_{QCD}}{32\pi^2} g_s^2 G^i_{\mu\nu} \tilde{G}^{\mu\nu i}, \qquad (1.4)$$

where the r index runs over the six quark flavors, α goes over three colors, and i runs over the eight gauge bosons, the gluons; g_s is the strong interaction coupling, and the field strength tensor is given by:

$$G^i_{\mu\nu} = \partial_\mu G^i_\nu - \partial_\nu G^i_\mu - g_s f_{ijk} G^j_\mu G^k_\nu, \tag{1.5}$$

where the quark gauge covariant derivative is:

$$D^{\mu\beta}_\alpha = \partial^\mu \delta^\beta_\alpha + \frac{i g_s}{\sqrt{2}} G^{\mu\beta}_\alpha, \tag{1.6}$$

with

$$G^\beta_\alpha = \sum_{i=1}^{8} G^i \frac{\lambda^{i\beta}_\alpha}{\sqrt{2}}, \tag{1.7}$$

and λ^i are the eight hermitian generators of $SU(3)_C$, the Gell-Mann matrices. More details on the implications of the symmetries of QCD will be given in Chapter 3, where a theory for hadrons in the non-perturbative regime is developed.

1.2 Tests within The Standard Model: muon's anomalous magnetic moment, a_μ

Both in Classical Electromagnetism and in Quantum Mechanics, a particle with an angular momentum interacts with a magnetic field. In the quantum case, it is not restricted to the orbital angular momentum but also to the particle's spin. The frequency of the Classical precession and the quantum one is related by a factor of g, which is called the gyromagnetic ratio.

In quantum field theory, for a charged lepton, this observable can be calculated by computing the amplitude of the process $\ell \to \gamma \ell$ as it can be seen in Figure. 1.3. The tree-level diagram results in $g = 2$, however, precision calculations can be computed with all possible intermediate states, which is represented by the blob in the right-hand side of Figure 1.3.

Since the quantum corrections to the tree-level calculations are infinite, one must truncate the calculation when the desired accuracy is achieved. Since this process is an electromagnetic interaction, we know that all contributions should respect the

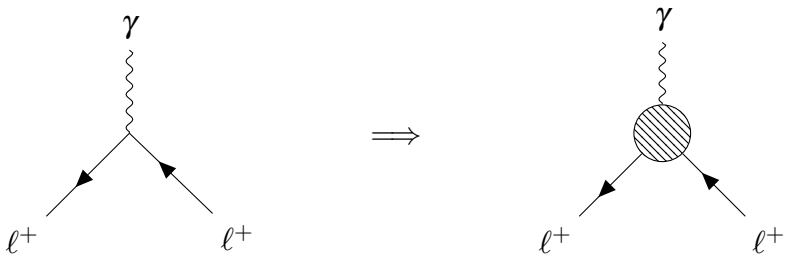

Fig. 1.3 l^+ interaction with a photon at tree-level in QED and generalized to all SM (and possibly BSM) interactions.

Ward identities, reducing the possible structure of all intermediate states to:

$$\bar{u}(p')\Gamma^{\mu}(p,p')u(p) = e\,\bar{u}(p')\left[\gamma^{\mu}F_1(q^2) + \frac{i\sigma^{\mu\nu}}{2m_\ell}q_\nu F_2(q^2)\right]u(p), \tag{1.8}$$

where the functions multiplying each possible tensor structure are called form factors. The first one is normalized to the (non-renormalized) electromagnetic charge, and the second one is related to the anomalous magnetic moment of the lepton by:

$$F_2(q^2=0) = \frac{(g-2)_\ell}{2} := a_\ell. \tag{1.9}$$

The first and dominant quantum correction, was computed by Julian Schwinger [146] and is the one related with the QED diagram shown in Figure 1.4. This term is equal for each of the 3 charged leptons; however, this is not true for all contributions to this process. Schwinger's result was historically very important, as it explained the recent Kusch-Foley measurement, being (together with the Lamb shift analogous calculation and measurement) the extremely solid foundation for all loop computations in QFT from then on.

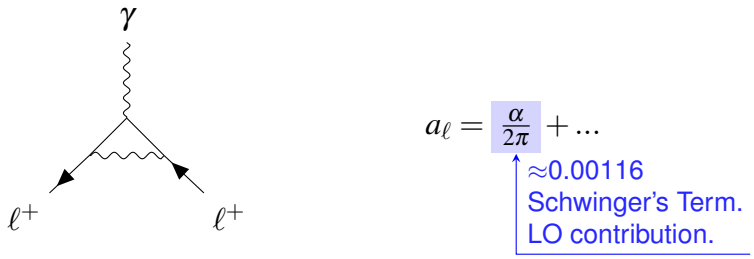

Fig. 1.4 First correction to $g_\ell - 2$. This is a photon exchange between the lepton in the initial and final states. The computation of this loop diagram is standard in QFT textbooks such as [147].

1.2.1 $g-2$ measurement: Past (CERN and BNL), Present (FNAL), and Future (J-PARC)

To understand the tension between experiment and theory, we must first comprehend the ideas of the observable we are describing. From quantum mechanics, we know that when a particle with spin interacts with a magnetic field, spin precession occurs with frequency

$$\omega_s = g_\mu \frac{eB}{2m_\mu} + \text{small corrections}. \tag{1.10}$$

Given the initial spin direction, we can measure ω_s and, consequently, g_μ [148].
Pion decay $\pi^\pm \to \mu^\pm \overset{(-)}{\nu}_\mu$ can help us to do it (it is easier to see it in pions rest frame). And the latter decay (in-flight) $\mu^+ \to e^+ \nu_e \bar{\nu}_\mu$ (if we consider maximum energy e^+'s)

$$\nu_\mu \xleftarrow[\vec{s}_{\nu_\mu} \to]{} \pi^+ \xrightarrow[\leftarrow \vec{s}_{\mu^+}]{} \mu^+$$

allows measuring μ's spin direction directly, as it is inherited by the electron [1]. In general, the Michel distribution [149] is used, for the higher-energy positrons.

$$\begin{array}{l} \bar{\nu}_\mu \\ \nu_e \end{array} \xleftarrow[\vec{s}_{\nu_e} \to]{\vec{s}_{\nu_\mu} \leftarrow} \mu^+ (\vec{s}_{\mu^+}) \xrightarrow[\vec{s}_{e^+}]{} e^+$$

At Brookhaven National Laboratory (BNL), the first measurement of a_μ at the level of ppm (parts per million) was performed [150–154, 1] [2]. The statistical and systematic errors have been greatly reduced at Fermi National Accelerator Laboratory (FNAL), reaching a final accuracy of 127 ppb [2–4]. The experimental setup was similar, and the results are shown in Figure 1.5.

The experiment consists of a magnet with a highly calibrated magnetic field which induces a circular motion of the muons (with angular frequency $\vec{\omega}_c = -\frac{q\vec{B}}{m_\mu \gamma}$). As mentioned above, this induces a precession on the muon's spin with frequency $\vec{\omega}_s = -g\frac{q\vec{B}}{2m_\mu} - (1-\gamma)\frac{q\vec{B}}{\gamma m_\mu}$. Due to the particle selection, if $g = 2$, the relative orientation of momentum and spin remains the same. Since this is not the case, there is a

[1] All neutrinos are left-handed (helicity and chirality are equal for massless particles) and antineutrinos are right-handed.

[2] Previous measurements on the muon $g-2$ were conducted at CERN in a series of three experiments, improving from 4300 to 10 ppm [155–157].

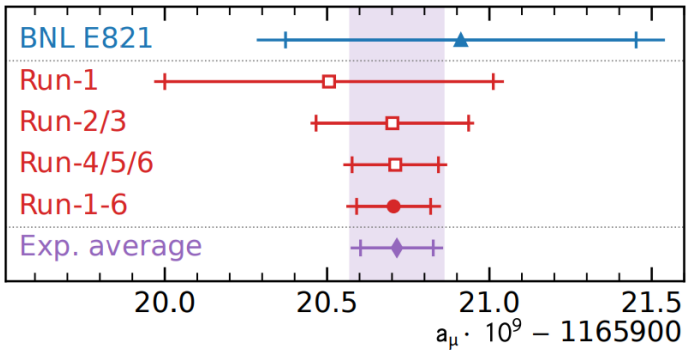

Fig. 1.5 Results for the experiment at BNL [1] and the different runs of FNAL [2–4] for the muon anomalous magnetic moment.

difference between the frequencies, which is sensitive directly to a_μ (working at the 'magic γ' value, ~ 29.3, which cancels the dependence on residual electric fields, see below):

$$\vec{\omega}_a = \vec{\omega}_s - \vec{\omega}_c = -a_\mu \frac{q\vec{B}}{m_\mu}. \tag{1.11}$$

The spin precession frequency is affected by the electric quadrupoles used to provide vertical focusing in the storage ring. In the presence of both electric and magnetic fields, for $\vec{\beta}$ perpendicular to both of them, the expression for the anomalous precession frequency becomes:

$$\vec{\omega}_a = -\frac{q}{m_\mu}\left(a_\mu \vec{B} - \left(a_\mu - \frac{1}{\gamma^2 - 1}\right)\frac{\vec{\beta}\times\vec{E}}{c}\right), \tag{1.12}$$

where the second term vanishes if $\gamma = 29.3$, this is the so-called magic momentum of 3.094 GeV/c. By measuring the magnitude of $\vec{B}$ and the difference of frequencies $\vec{\omega}_a$, it is possible to get a precise determination of a_μ. For the measurement of ω_a, the correlation between the spin of the parent muon and the daughter electron's direction should be used to infer the direction of muon's spin. This correlation function requires information on the 4-momentum of the produced electron. Since the muons inserted in the storage ring (see Figure 1.6) are highly relativistic, most of the decaying electrons are ultra-relativistic, and thus useful for the measurement.

Consequently, the electrons have high energies in the lab frame. By setting a laboratory threshold, it is possible to select the angles of the emitted electrons above this threshold, which is directly related with ω_a. The distribution of the electron counts over the threshold is shown in Figure 1.7, a fit to these data is performed

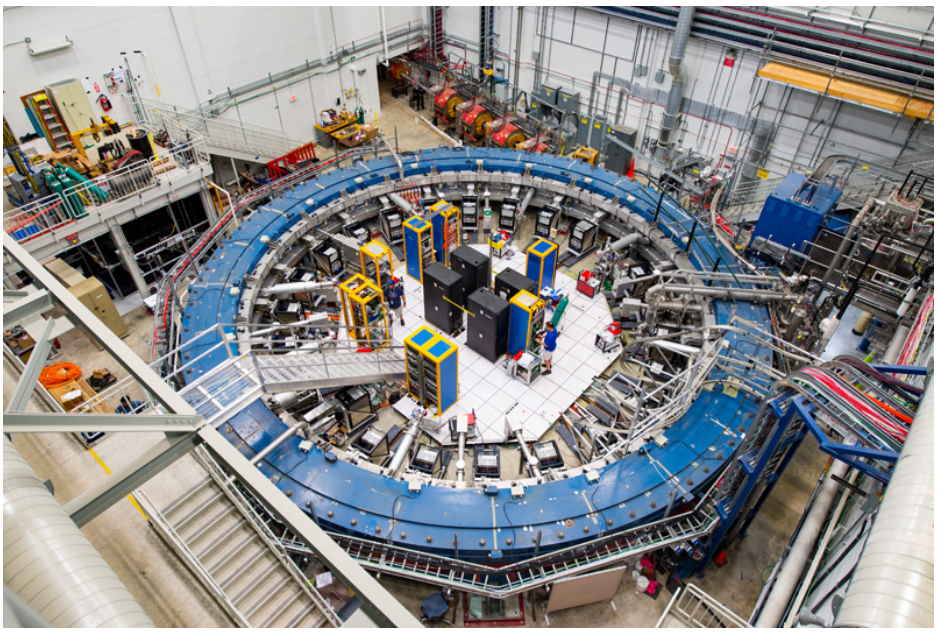

Fig. 1.6 Accelerator at FNAL, which uses the same magnet as the experiment in BNAL and a similar procedure to obtain a_μ.

and the difference of frequencies is obtained. In the most recent publications, there is not detailed information about the experiment, for understanding further the experimental setup, I would recommend to read Ref. [1]. With the analysis of all data, the experimental world average is:

$$a_\mu^{\text{Exp}} = a(exp) = 116\,592\,0715(145) \times 10^{-12} \quad (124\text{ppb}). \tag{1.13}$$

• J-PARC experiment: plans for the future.

Since the program at FNAL has been completed, and the goal of reaching a 140 ppb precision has been achieved, there is no expected change in the experimental value on the order of decades. However, the experiment *muon g - 2/EDM* **E34** is under construction at J-PARC in Japan [158, 159]. The experiment aims to perform ultra-precision measurements of $g-2$ and the electric dipole moment of the muon using a completely different method from those at BNL and FNAL, offering a test of these results, particularly of their systematic uncertainties.

The experimental principle will be recapitulated next: It starts obtaining muons from the decay of pions generated from the proton accelerator at J-PARC. By cooling and later accelerating the muons, E34 aims to obtain a low-emittance beam, thereby significantly reducing the systematics associated with a wide beam. An important feature of this experiment is that it does not require the muons to be calibrated to be

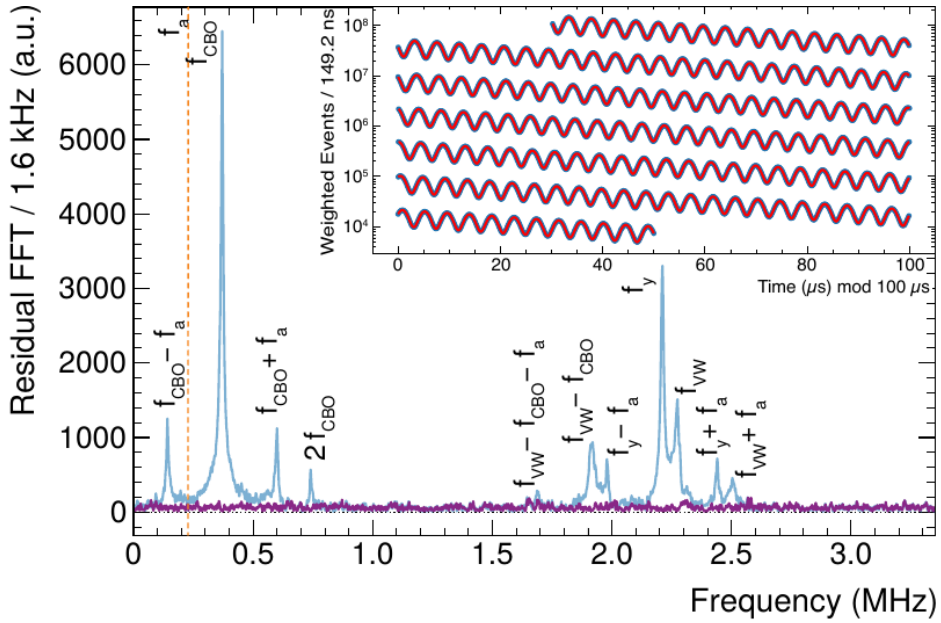

Fig. 1.7 Distribution of electrons as a function of time taken by the last analysis of the last 3 runs out of 6 taken in FNAL[4] is shown in the right upper corner plot. The rest of the plot displays the Fourier transforms of the residuals from the sum of the four fits to the Run-4/5/6 . Similar plots can be found in the BNL reports [150–154, 1].

at the *magic momentum*. A diagram of the experiment is shown in Figure 1.8. Recent progress on the experiment can be found in Ref. [160]. Currently, the muons are being accelerated to 100 keV, while the goal is to achieve 210 MeV. The data taking is expected to start in the next decade; currently, construction, design redefinition, ionization tests, and installation are being performed for the building, source, linear accelerator, storage ring, and detector [3].

1.2.2 Theory Initiative

The theory initiative is in charge of computing the anomalous magnetic moment of the muon within the standard model [5, 6]. The essential inputs for the most recent computation are found in Refs. [26–85]. However, with many computations still in dispute, and many others still not being computed completely or at all, there are more than 700 articles quoted, related to the calculation of this observable. This gives an idea of the complexity of achieving such precise theoretical prediction.

[3] Just before submitting the final version of this thesis, ref. [161] appeared, proposing the CANTON-μ experiment, that will reach the sub 0.1 ppm precision on the a_μ measurement.

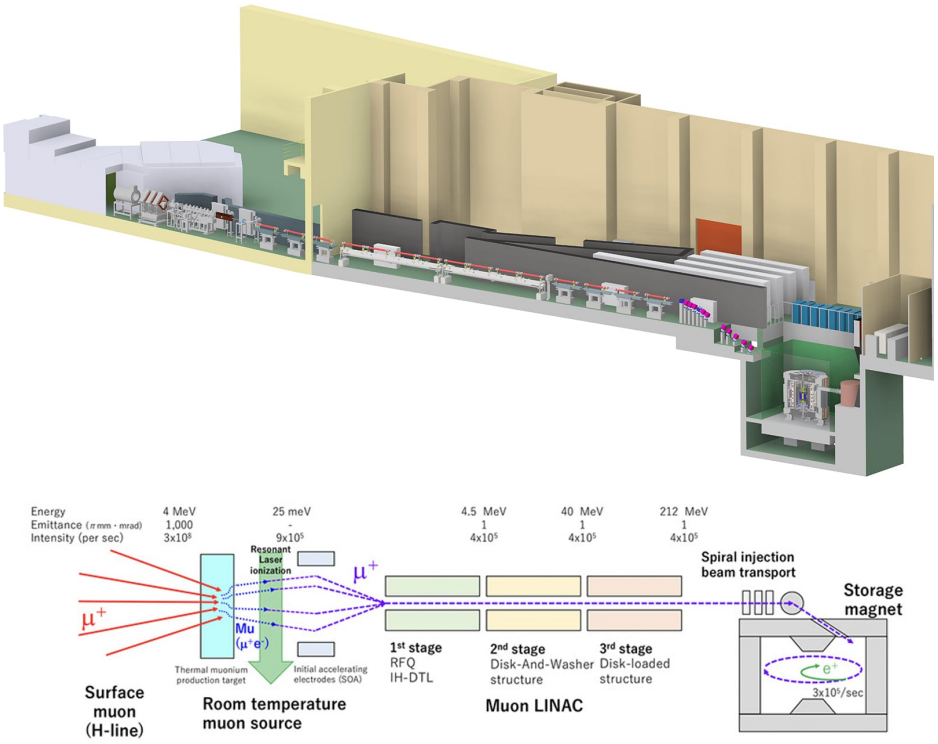

Fig. 1.8 Ultra cold muon experiment at J-PARC under construction. Muons are collected, cooled, accelerated, and inserted into a storage ring ∼20 times smaller than the one at BNL and FNAL.

The calculation is organized by the kind of interactions involved: electromagnetic, hadronic, and electroweak contributions. The electromagnetic contributions hold almost all the total a_μ, but the hadronic piece is responsible for most of the uncertainty due to the presence of intermediate hadronic states, which require form factors to be accounted for.

1.2.2.1 QED contributions

The QED contributions are organized by the lepton mass dependence, which means:

$$a_\mu^{\text{QED}} = A_1 + A_2(m_\mu/m_e) + A_2(m_\mu/m_\tau) + A_3(m_\mu/m_e, m_\mu/m_\tau), \tag{1.14}$$

and at the same time, each one of these contributions is split in the well-converging perturbative QED counting:

$$A_i = \left(\frac{\alpha}{\pi}\right)^n A_i^{(2n)}, \tag{1.15}$$

where the first contribution for A_1 is the well known Schwinger contribution [146], $A_1^{(2)} = 1/2$. By 2018, all terms up to eight orders have been computed by different groups and have been cross-checked. The mass independent contributions consist of 1, 7, 72, 891, and 12,672 diagrams for the first to fifth order in perturbation theory. Examples of the fourth and sixth order diagrams are found in Figure 1.9. The values for the $A_i^{(2n)}$ are of the same order, resulting in a smoothly convergent series in the QED counting[4].

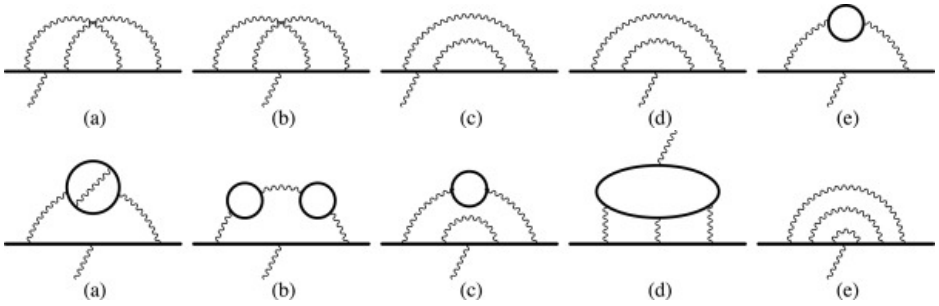

Fig. 1.9 Diagrams (split in different topology classes) at two and three loops contributing to the mass-independent parts of the QED piece of a_μ.

The fine-structure constant is a fundamental input to the complete calculation. It is taken from atom-interferometer experiments, resulting in tensions between the values obtained from the cesium atom mass (^{133}Cs) and the rubidium atom mass (^{87}Rb), with accuracies of ppb. In fact, the PDG review on the electroweak Standard Model and constraints on new physics [217] advises to take the weighted average of these measurements and the value coming from a_e (solving it for $\alpha(m_e)$) in order to get the recommended value of α. These differences are irrelevant for the precision needed in a_μ^{QED}.

The current value for the QED contributions is

$$a_\mu^{\text{QED}} = 116\,584\,718.8(2) \times 10^{-11}. \tag{1.16}$$

1.2.2.2 EW contributions

The electroweak contributions are the smallest of all in the SM [5] and also have a small error. The EW piece is composed by all SM contributions not included in

[4] See Refs. [146, 162–188] for the mass independent contributions, Refs. [189, 162, 190–193, 166, 194–216].

[5] This is important as they naturally set the expected size of NP contributions coming from chiral gauge theories, upon quadratic rescaling of the energy scales involved, with some room for varying the coupling strength with respect to the SM case.

pure QED, that are not of hadronic type either. An example of these contributions is shown in Figure 1.10. This computation is split perturbatively in EW by counting one-loop contributions, two-loop contributions with bosons and fermions, and higher-order corrections. The boson two-loop contributions consist of those without closed fermion loops; the fermion two-loop ones do contain closed fermion loop diagrams.

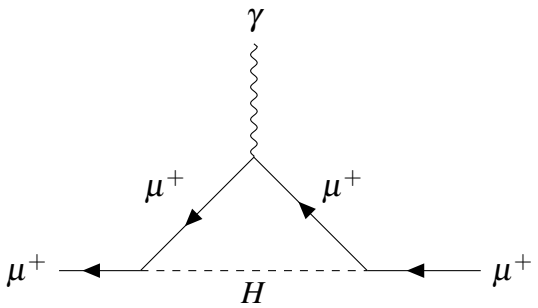

Fig. 1.10 μ^+ interaction with a photon including an $\mu - H - \mu$ loop. The accuracy of its contribution was greatly improved thanks to the Higgs boson discovery and its precise mass measurement [218, 219].

Altogether, this results in the value of [83, 220, 221, 85]:

$$a_\mu^{\mathrm{EW}} = 154.4(4) \times 10^{-11}. \tag{1.17}$$

1.2.2.3 QCD Contributions I: Hadronic Vacuum Polarization

The hadronic pieces are split into two contributions. The dominant one is the Hadronic Vacuum Polarization, which contains all contributions coming from an exchange of a photon between the muon's external legs with intermediate hadronic states in the middle, represented by the blob in Figure 1.11. The input for the hadronic piece of this contribution can be obtained by data-driven methods or Lattice-QCD calculations. Within the data-driven methods, we can separate between collider inputs $e^+e^- \to$ hadrons and τ decay inputs ($\tau \to 2\pi\nu_\tau$ mainly) [6].

The leading order contribution can be obtained by an HVP master formula [222–225]:

$$a_\mu^{\mathrm{HVP,LO}} = \left(\frac{\alpha m_\mu}{3\pi}\right)^2 \int_{s_{thr}}^{\infty} ds \frac{\hat{K}(s)}{s^2} R_{\mathrm{had}}(s), \tag{1.18}$$

where the kernel $\hat{K}(s)$ is the electromagnetic one and $R_{\mathrm{had}}(s) = \frac{3s}{4\pi\alpha^2}\sigma[e^+e^- \to \mathrm{hadrons}(+\gamma)]$, inclusive in final-state photon emission. Correspondingly, the lightest contributing

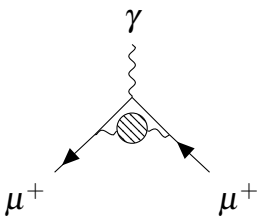

Fig. 1.11 Hadronic Vacuum Polarization diagram. These contributions consist of the exchange of a photon by the incoming and outgoing muon, with an hadronic intermediate state, represented by the blob.

cut is $e^+e^- \to \pi^0\gamma$. This master formula is obtained by means of the optical theorem [226].

The cross section of $e^+e^- \to$ hadrons needs to be measured with high precision in order to compete with the experimental accuracy. In Ref. [227], all available data at the moment were analyzed to compute a data-driven evaluation of eq. (1.18). This input for $R_{\rm had}(s)$ is shown in Figure 1.12. It can be seen that the process is dominated by the $\pi^+\pi^-$ channel. This piece can be obtained, alternatively, by an isospin rotation of the $\tau^- \to \pi^-\pi^0\nu_\tau$ cross section[86–90]. Important discrepancies

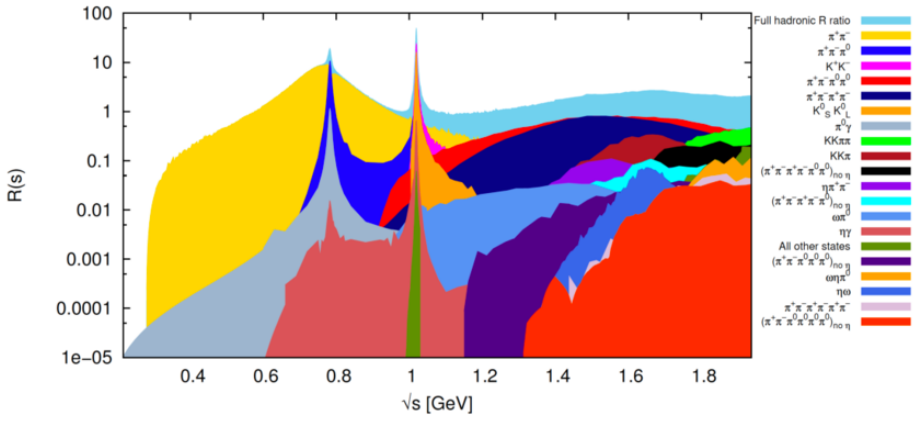

Fig. 1.12 The hadronic R ratio, split in all contributions to the process $e^+e^- \to$ hadrons.

between e^+e^- data sets and also with τ data have arisen, which can be appreciated in Figure 1.13. This made impossible to report an average of the data-driven results for $a_\mu^{\rm HVP,LO}$ at this point (White Paper 2, 2025 [6]). Proposals for solving this issue can be studied in Ref. [91]. For this reason, for WP2025, the Theory Initiative reported the LQCD average [26–42] as the value for $a_\mu^{\rm HVP,LO}$ (see also refs. [43–45]), resulting in agreement between theory and experiment. However, it is still important to

understand why a non-negligible difference exists between e^+e^- data, τ data, and LQCD results.

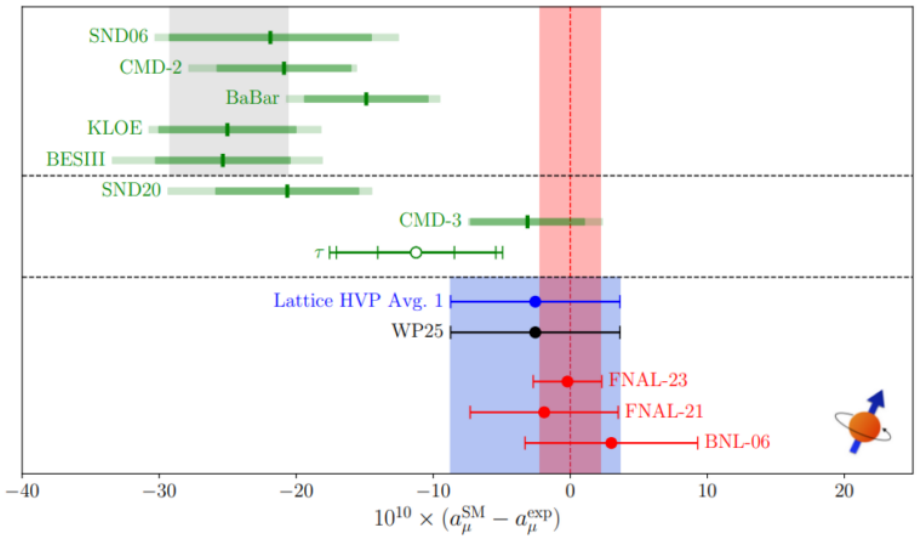

Fig. 1.13 Results for the $a_\mu^{SM} - a_\mu^{exp}$ difference with diverse HVP inputs. In green bars, the $e^+e^- \to$ hadrons results are displayed; in green lines, the τ data values are shown; in blue, the value of the LQCD HVP average is represented, and finally, in red are the experimental measurements.

By using the LQCD input for the leading contributions, it is obtained:

$$a_\mu^{HVP} = 7045(61) \times 10^{-11}, \tag{1.19}$$

which is higher than the value reported in WP2020 [5] and leads to agreement between theory and experiment. The difference $a_\mu^{SM} - a_\mu^{exp}$ has been used to set constraints on heavy new physics explanations within the EFT framework [228–235].

1.2.2.4 QCD Contributions II: Hadronic Light-by-Light

The Hadronic Light-by-Light (HLbL) piece of a_μ contains two more electromagnetic vertices than HVP, which makes it subleading. This process consists of three photons interacting with the muon and an external photon. The first three are virtual particles, and the last photon corresponds to the magnetic field that interacts with the muon. In the middle, pure QCD happens, which means that all intermediate states in the non-perturbative regime are hadrons (See Figure 1.14). In contrast to what happens with HVP, a Data-Driven determination of this observable cannot be obtained by

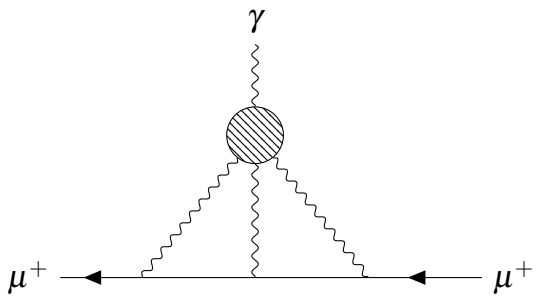

Fig. 1.14 Hadronic Light-by-Light piece of a_μ. Any intermediate hadron process can occur as an intermediate state, which is represented by the blob.

means of measuring a single inclusive process ($e^+e^- \to$ hadrons). Instead, it has to be split into its hadronic intermediate states one by one, avoiding redundancies by relating each of them to on-shell observables, depending on the form factors. For this purpose, it is convenient to study the HLbL tensor instead of the contribution to muon's $g-2$.

Any representation of the HLbL tensor in the light quark sector ($q = u,d,s$) can be computed from

$$\Pi^{\mu\nu\lambda\sigma}(q_1,q_2,q_3) = -i\int d^4x d^4y d^4z e^{-i(q_1\cdot x + q_2\cdot y + q_3\cdot z)} \langle 0|\, T\{j^\mu_{\rm em}(x) j^\nu_{\rm em}(y) j^\lambda_{\rm em}(z) j^\sigma_{\rm em}(0)\}\,|0\rangle\,, \tag{1.20}$$

where $j_{\rm em} := \bar{q}Q\gamma^\nu q$ and Q is the charge matrix. This object can be constructed from the amplitudes of any representation of the HLbL with the photon helicities amputated.

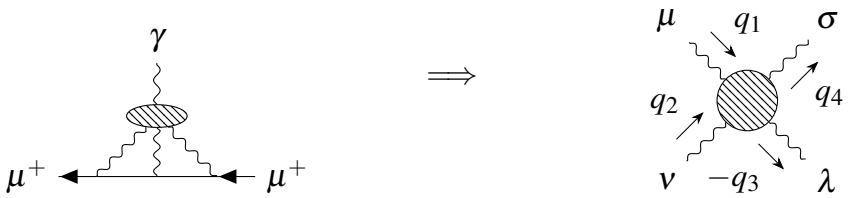

Fig. 1.15 The HLbL processes can be studied by means of the HLbL tensor, which can take different representations depending on the intermediate state under consideration.

On the contrary, a direct lattice calculation of the HLbL can be done –even though some studies are done in specific intermediate state contributions, the viability of computing a full contribution is convenient–. The counting is different in LQCD HLbL determination compared to the data-driven ones, making it difficult to compare something beyond the total HLbL contribution.

In this thesis, we have focused on the data-driven determinations. According to the second White Paper [6], the data-driven methods are split into four main sources: dispersive approach, the holographic QCD, model evaluations, and Schwinger Dyson/Bethe Salpeter equation solutions.

The full HLbL evaluations available are (in units of 10^{-11}):

$$a_\mu^{\text{HLbL: LQCD}} = 122.5(9.0), \tag{1.21}$$

$$a_\mu^{\text{HLbL: Dispersive}} = 105.9(8.8), \tag{1.22}$$

$$a_\mu^{\text{HLbL: R}\chi\text{T}} = 106.1(9.0). \tag{1.23}$$

We will give more details on the $R\chi T$ evaluation along this thesis. Our original contributions are collected in chapters 3 to 6.

1.2.3 How to sum HLbL contributions to a_μ? The Master formula

One can naively try to evaluate the HLbL contribution to a_μ in terms of the HLbL tensor [46] by extracting the form factor at zero virtuality $F_2(q^2=0)$:

$$\begin{aligned}\Gamma^{\sigma}_{\text{HLbL}}(p_1,p_2) = &-e^6\int\frac{dq_1^4}{(2\pi)^4}\frac{dq_2^4}{(2\pi)^4}\gamma_\mu\frac{(\not p_1+\not p_2+m_\mu)}{(p_1+p_2)^2-m_\mu^2}\gamma_\lambda\frac{(\not p_1-\not p_2+m_\mu)}{(p_1-p_2)^2-m_\mu^2}\gamma_\nu\\ &\times\frac{1}{q_1^2}\frac{1}{q_2^2}\frac{1}{(p_1-p_2-q_1-q_2)^2}\Pi^{\mu\nu\lambda\sigma}(q_1,q_2,p_1-p_2-q_1-q_2).\end{aligned} \tag{1.24}$$

However, we still have to use projector techniques and angular averages, which will result in taking a trace to obtain a_μ. For the case of the pseudoscalar poles, this can be done without too much trouble, but a much more general procedure becomes handy. The works by Colangelo, Hoferichter, Procura, and Stoffer are the basis for this methodology [126, 46, 48]. The inclusion of further representations has required the optimization of the basis used in these works; up to now, the best one is found in Ref. [61]. However, it still needs to be improved to account for the tensor meson poles, which is also being pursued in triangle kinematics [236]. Putting this forward this has been one important contribution of this thesis. This procedure will be described next, according to the Bardeen, Tung and Tarrach recipe [237, 238].

- **Tensor Decomposition.**

The first step is to decompose the HLbL tensor representation in the most general set of tensor structures of 4 indices, considering 4-momenta conservation only:

$$\begin{aligned}\Pi^{\mu\nu\lambda\sigma} =& g^{\mu\nu}g^{\lambda\sigma}\Pi_1 + g^{\mu\lambda}g^{\nu\sigma}\Pi_2 + g^{\mu\sigma}g^{\lambda\nu}\Pi_3 \\ &+ \sum_{\substack{k=1,2,4\\l=1,2,3}} g^{\mu\nu}q_k^\lambda q_l^\sigma \Pi_{kl}^4 + \sum_{\substack{j=1,3,4\\l=1,2,3}} g^{\mu\lambda}q_j^\nu q_l^\sigma \Pi_{jl}^5 + \sum_{\substack{j=1,3,4\\k=1,2,4}} g^{\mu\sigma}q_j^\nu q_k^\lambda \Pi_{jk}^6 \\ &+ \sum_{\substack{i=2,3,4\\l=1,2,3}} g^{\nu\lambda}q_i^\mu q_l^\sigma \Pi_{il}^7 + \sum_{\substack{i=2,3,4\\k=1,2,4}} g^{\nu\sigma}q_i^\mu q_k^\lambda \Pi_{ik}^8 + \sum_{\substack{i=2,3,4\\j=1,3,4}} g^{\lambda\sigma}q_i^\mu q_j^\nu \Pi_{ij}^9 \\ &+ \sum_{\substack{i=2,3,4\\j=1,3,4}} \sum_{k=1,2,4 l=1,2,3} q_i^\mu q_j^\nu q_k^\lambda q_l^\sigma \Pi_{ijkl}^{10} \\ :=& \sum_{i=1}^{138} L_i^{\mu\nu\lambda\sigma}\Xi_i. \end{aligned} \tag{1.25}$$

There are a total of 3 structures with two metric tensors, 54 structures with one metric tensor and two momenta, and 81 structures with four momenta. The 138 scalar functions multiplying the tensor structures are different for each HLbL tensor representation.

• **Imposing gauge invariance and Ward Identities.**

Due to gauge invariance and conservation of the electromagnetic current (Ward Identities), 95 linearly independent relations are imposed, leaving 43 independent tensor structures. To impose these conditions, the following projectors are used:

$$I_{12}^{\mu\nu} = g^{\mu\nu} - \frac{q_2^\mu q_1^\nu}{q_1\cdot q_2}, \quad I_{34}^{\lambda\sigma} = g^{\lambda\sigma} - \frac{q_4^\lambda q_3^\sigma}{q_3\cdot q_4}. \tag{1.26}$$

The HLbL tensor is invariant under the action of these projectors; however, as they enforce the Ward identities, only 43 linearly independent terms remain after applying the projectors:

$$\begin{aligned}\Pi^{\mu\nu\lambda\sigma} =& I_{12}^{\mu\mu'}I_{12}^{\nu\nu'}I_{34}^{\lambda\lambda'}I_{34}^{\sigma\sigma'}\Pi^{\mu'\nu'\lambda'\sigma'} \\ =& \sum_{i=1}^{138} I_{12}^{\mu\mu'}I_{12}^{\nu\nu'}I_{34}^{\lambda\lambda'}I_{34}^{\sigma\sigma'}L_i^{\mu'\nu'\lambda'\sigma'}\Xi_i = \qquad : \sum_{j=1}^{43}\bar{L}_{i_j}^{\mu\nu\lambda\sigma}\Xi_{i_j}, \end{aligned} \tag{1.27}$$

where the new tensor structures $\bar{L}_{i_j}^{\mu\nu\lambda\sigma}$ are the ones that do not vanish upon the imposition of the Ward identities, and Ξ_{i_j} are their respective scalar functions.

• **Removing the Kinematic Poles.**

Artificial kinematic poles were induced by the scalar products in the denominators of the projectors. This effect has to be non-physical, since the HLbL still has to be properly defined. The kinematic singularities should be removed by:

- Adding linear combinations which contain no poles to eliminate as many double poles as possible in the other parts.
- Multiplying the remaining double poles by the scalar product $q_1 \cdot q_2$ or $q_3 \cdot q_4$.
- Proceeding with the remaining double single and single double poles.

By doing this, kinematic singularities has been introduced in the scalar functions. However, they correspond to the degeneracies of the obtained basis in the limits $q_1 \cdot q_2 \to 0$ and/or $q_3 \cdot q_4 \to 0$. The null-space of these structures in these limits finds 11 new structures, which requires the basis to be expanded into a redundant one of 54 elements. This redundant basis will be the one used in the Master Formula.

• **Inverting the basis.**

This basis is invertible in the soft-photon limit, which is precisely the one we need to impose on the HLbL tensor, $q_4 \to 0$. In order to read the mapping from the appendices in [46], here is a practical guide –all references to equations in the following list refer to the mentioned reference–:

- The 138 scalar functions of the specific HLbL tensor representation, arranged in a non-uniform multi-dimensional Π, are written in a plain 138 1-D array Ξ_i.
- The Ξ_{i_j} are selected as in Appendix C, rearranging the i_j into $j \in [1, 43]$.
- The Ξ_{i_j} are rotated into the functions $\tilde{\Pi}_j$ by the matrix in eq. (C.3).
- The 54 scalar functions of the redundant basis, Π_j, are defined by taking the limits in eq. (F.8).
- The 12 final scalar functions entering in the Master Formula, $\bar{\Pi}_j$, are defined in eq. (D.2).

Finally, the contribution of the specific representation of the HLbL tensor can be accounted for in the Master Formula:

$$a_\mu^{\rm HLbL} = \int_0^\infty dQ_1 \int_0^\infty dQ_2 \int_{-1}^{1} d\tau \sqrt{1-\tau^2} Q_1^3 Q_2^3 \sum_{i=1}^{12} T_i(Q_1,Q_2,\tau)\bar{\Pi}_i(Q_1,Q_2,\tau), \qquad (1.28)$$

where the functions T_i are defined in the quoted reference and come from the angular integration by using Gegenbauer polynomial techniques [239]. The Q_i are the magnitudes of the euclidean 4-momenta $q_i^2 \to -Q_i^2$, and τ is the projection of Q_1 into Q_2, since Q_3 is defined by 4-momentum conservation but Q_3^2 depends on the relative orientations of $Q_{1,2}$: $Q_3^2 = Q_1^2 + Q_2^2 + 2Q_1Q_2\tau$.

Usually, only a few of the $\bar{\Pi}_i$ are given, since they obey the following relations:

$$\begin{aligned}
&\hat{\Pi}_2 = \mathscr{C}_{23}[\hat{\Pi}_1], \quad \hat{\Pi}_3 = \mathscr{C}_{13}[\hat{\Pi}_1], \quad \hat{\Pi}_5 = \mathscr{C}_{23}[\hat{\Pi}_4], \quad \hat{\Pi}_6 = \mathscr{C}_{13}[\hat{\Pi}_4],\\
&\hat{\Pi}_8 = \mathscr{C}_{12}[\hat{\Pi}_7], \quad \hat{\Pi}_9 = \mathscr{C}_{12}[\mathscr{C}_{13}[\hat{\Pi}_7]], \quad \hat{\Pi}_{10} = \mathscr{C}_{23}[\hat{\Pi}_7], \quad \hat{\Pi}_{13} = \mathscr{C}_{13}[\hat{\Pi}_7],\\
&\hat{\Pi}_{14} = \mathscr{C}_{12}[\mathscr{C}_{23}[\hat{\Pi}_7]], \quad \hat{\Pi}_{11} = \mathscr{C}_{13}[\hat{\Pi}_{17}], \quad \hat{\Pi}_{16} = \mathscr{C}_{23}[\hat{\Pi}_{17}], \quad \hat{\Pi}_{50} = -\mathscr{C}_{23}[\hat{\Pi}_{54}], \quad \hat{\Pi}_{51} = \mathscr{C}_{13}[\hat{\Pi}_{54}].
\end{aligned} \qquad (1.29)$$

Consequently, the only required scalar functions are $\hat{\Pi}_1$, $\hat{\Pi}_4$, $\hat{\Pi}_7$, $\hat{\Pi}_{17}$, and $\hat{\Pi}_{54}$, defining the $\bar{\Pi}$ functions of the Master Formula.

The optimized basis in ref. [61] includes non-redundantly the contributions of the Pseudoscalar, Scalar and Axial meson poles, and Pseudoscalar Boxes in terms of their form factors. For the tensor poles, only the cases of $\mathscr{F}_{1,3}$ and $\mathscr{F}_{2,3}$ are free of singularities. In Chapter 5 we show evidence of a need for a new basis that considers all 5 form factors for the tensor meson transition form factors.

CHAPTER 2

Resonance Chiral Theory: An Effective Field Theory for QCD around a GeV

2.1 Effective Field Theories

Quantum effective field theories (EFTs) are built to describe physics at low energies compared to a reference scale, Λ, which is characteristic of heavy degrees of freedom that are non-dynamical at long distances, and thus integrated out from the action. In this way, one achieves the simplest possible description of the relevant physics, based on the symmetries of the low-energy theory and on its light (masses m considerably smaller than Λ) degrees of freedom [1]. Basic references on the subject, where more detailed and pedagogical explanations can be found, are refs. [240–242].

We can summarize the main features of EFTs as follows [243, 244]:

- Low-energy physics is independent of short-distance properties. The only remnants of the high-energy theory can be found in the precise values of the low-energy constants and in symmetry relations.
- Vanishing ratios m/E and E/Λ are taken as first approximation, which can systematically be improved including perturbative corrections in powers of these ratios.
- Non-local exchanges mediated by heavy particles ($M \geq \Lambda$) are replaced by an infinite tower of local interactions between the light fields. These are order-by-

[1] The symmetry of the vacuum (either the full group or a subgroup of the Lagrangian's) also needs to be specified to characterize it completely.

order renormalizable (in the expansion parameter used to define the power counting of the EFT).

- The EFT represents the infrared dynamics up to a given accuracy (which can be estimated from its power-counting), in terms of a finite set of LECs. By construction, it has identical low-energy (but different short-distance) behaviour to the (more) fundamental theory.

The validity of the EFT description and its properties is ensured by Weinberg's theorem [245]: 'For a given set of asymptotic states, perturbation theory with the most general Lagrangian containing all terms allowed by the assumed symmetries will yield the most general S matrix elements consistent with analyticity, perturbative unitarity, cluster decomposition, and the assumed symmetries'. For our case of interest of RχT, it warrants that we can write a Lagrangian density with active fields creating/annihilating pions, Kaons, eta mesons and the light-flavored resonances, using chiral symmetry for the former and unitary symmetry for the latter and obtain as a result the most general observables consistent with these symmetries in the $E \sim 1$ GeV region.

2.2 Chiral Perturbation Theory

In this section, we will introduce Chiral Perturbation Theory (χPT), which is the low-energy EFT dual to QCD at low energies. Its construction was introduced in the seminal work by Weinberg [245] and was systematized by Gasser and Leutwyler [246, 247]. It follows the main idea: *"if one writes down the most general possible Lagrangian, including all terms consistent with assumed symmetry principles, and then calculates matrix elements with this Lagrangian to any given order of perturbation theory, the result will simply be the most general possible S-matrix consistent with analyticity, perturbative unitarity, cluster decomposition and the assumed symmetry principles.*

2.2.1 QCD and Chiral Symmetry

The QCD Lagrangian, for the three lightest quarks (whose masses are considerably smaller than typical hadron scales), $i = u, d, s$, is (we neglect the θ_{QCD}-term associated to a possible tiny violation of CP symmetry by the strong interactions)

$$\mathscr{L}_{QCD} - \mathscr{L}_{QCD}^{\text{gauge fixing}} = -\frac{1}{4} G^a_{\mu\nu} G^{\mu\nu,a} + \bar{q}_i (i\not{D} - m_{q_i}) q_i \,, \tag{2.1}$$

with $D_\mu = \partial_\mu - ig_s G^a_\mu$, introducing the strong coupling g_s and $a = 1, \ldots, N_C^2 - 1$ gluon fields, G^a_μ. For energies where these light quark mass effects are negligible, the massless QCD Lagrangian, $\mathscr{L}_0^{QCD}$, is a good approximation, with (we omit the gauge-fixing and gluon field-strength tensor terms below)

$$\mathscr{L}^0_{QCD} = i\left(\bar{q}_{i,L} \not{D} q_{i,R} + \bar{q}_{i,L} \not{D} q_{i,L}\right) , \tag{2.2}$$

which is trivially invariant under separate transformation of the left- and right-handed components in (three-)flavor space. The so-called 'chiral' symmetry group is then $G \equiv SU(3)_L \times SU(3)_R$ [2]. As a consequence of this symmetry, the hadrons spectrum should exhibit a parity symmetry, which is, however, severely violated. This is particularly so for the lightest pseudoscalar versus scalar mesons, where the pions are ~ 7 times lighter than the a_0 mesons. This breaking is milder for the lowest-lying spin-one states, where $m_{a_1}/m_\rho \sim 1.6$. The way out of this seeming conundrum goes through the second possibility of realizing a symmetry (the first one, à la Wigner-Weyl must happen in quantum mechanics, but not necessarily in quantum field theory) and corresponds to Lagrangian symmetries being reflected in the theory's spectrum. The other option is à la Nambu-Goldstone [250, 251], where the vacuum symmetry group, H, is only a subgroup of the $\mathscr{L}$ symmetry group, G. In our case of interest of low-energy QCD, both phenomenological observations made before suggest the pattern of spontaneous chiral symmetry breaking

$$G \equiv SU(3)_L \otimes SU(3)_R \to H \equiv SU(3)_V . \tag{2.3}$$

Indeed, in application of the Goldstone theorem [251, 252], there must exist a multiplet of massless states (as many as generators of the broken symmetries), with suitable quantum numbers to warrant the existence of an order parameter of the (chiral) symmetry breakdown (pseudoscalars in this case, as the chiral axial symmetries are broken). This explains why pion masses can be neglected (in first approximation) compared to the rest of hadron's and why parity is not a symmetry of the spectrum. In order to understand the small masses of the lightest octet of pseudoscalar mesons we need to account for $m_{q_i} \neq 0$, a small explicit chiral symmetry breaking that is implemented in χPT exactly like in QCD, by using appropriate spurion fields [246].

[2] Chiral symmetry also includes the $U(1)$ pieces associated to vector ($_V$) and axial-vector ($_A$) transformations, that is, $L+R \sim V$ and $-L+R \sim A$. The first one counts the number of quarks minus antiquarks, so it is proportional to the baryon number, which is conserved. The second one is broken by quantum corrections [248, 249] and dubbed, for this reason, anomalous.

In this way,

$$< 0|\bar{q}_i q_i|0 >\neq 0 \tag{2.4}$$

is the natural order parameter of spontaneous chiral symmetry breaking and $m_{q_i} \neq 0$ includes its explicit breakdown. Particularly enlightening and useful reviews on χPT are refs. [253–255], and the book [256].

2.2.2 Chiral Currents and Chiral Symmetry Breaking

The Lagrangian in eq. (2.2) is invariant under two independent global transformations:

$$\begin{aligned}
\begin{pmatrix} u_L \\ d_L \\ s_L \end{pmatrix} \to U_L \begin{pmatrix} u_L \\ d_L \\ s_L \end{pmatrix} &= \exp\left(-i\sum_{a=1}^{8}\Theta_{La}\frac{\lambda_a}{2}\right) e^{-i\Theta_L} \begin{pmatrix} u_L \\ d_L \\ s_L \end{pmatrix}, \\
\begin{pmatrix} u_R \\ d_R \\ s_R \end{pmatrix} \to U_R \begin{pmatrix} u_R \\ d_R \\ s_R \end{pmatrix} &= \exp\left(-i\sum_{a=1}^{8}\Theta_{Ra}\frac{\lambda_a}{2}\right) e^{-i\Theta_R} \begin{pmatrix} u_R \\ d_R \\ s_R \end{pmatrix},
\end{aligned} \tag{2.5}$$

where $U_{L(R)}$ are independent 3×3 complex rotations times a global phase, where the former (latter) can be identified with a $SU(3)$ ($U(1)$) transformation. In this way, eq. (2.2) is invariant under a global $SU(3)_L \times SU(3)_R \times U(1)_L \times U(1)_R$, which can be rewritten –restoring to completeness– by using a $(L,R) \to (V,A)$ basis change. It is convenient to proceed this way, because (V,A) have a definite behavior under parity transformation, which is a good label for the hadron multiplets. Chiral currents related to these symmetries can be written, according to Nöether's Theorem [256], as

$$\begin{aligned}
V_a^\mu &= \bar{q}\gamma^\mu \frac{\lambda_a}{2} q, \\
A_a^\mu &= \bar{q}\gamma^\mu\gamma_5 \frac{\lambda_a}{2} q, \\
V^\mu &= \bar{q}\gamma^\mu q, \\
A^\mu &= \bar{q}\gamma^\mu\gamma_5 q,
\end{aligned} \tag{2.6}$$

making 18 conserved currents. However, as mentioned in section 2.2.1, there is an observed asymmetry between particles with the same spin and opposite parity. This

property of nature hints to us that symmetry breaking must occur (otherwise these multiplets would be degenerate, according to the symmetries just discussed).

When the masses of light quarks are accounted for in the QCD Lagrangian, chiral symmetry is explicitly broken. The divergence of (almost all) chiral currents of eq. (2.2.2) becomes non-vanishing

$$\begin{aligned}
\partial_\mu V_a^\mu &= i\bar{q}\left[\mathscr{M}, \frac{\lambda_a}{2}\right] q, \\
\partial_\mu A_a^\mu &= i\bar{q}\gamma_5\left\{\mathscr{M}, \frac{\lambda_a}{2}\right\} q, \\
\partial_\mu V^\mu &= 0, \\
\partial_\mu A^\mu &= 2i\bar{q}\gamma_5\mathscr{M} q + \frac{3g_s^2}{32\pi^2}\varepsilon_{\mu\nu\rho\sigma}G_a^{\mu\nu}G_a^{\rho\sigma},
\end{aligned} \tag{2.7}$$

where the mass matrix is $\mathscr{M} = \mathrm{diag}\{m_u, m_d, m_s\}$. The second term in the RHS of $\partial_\mu A^\mu$ originates from quantum corrections (it is related to the extremely approximate CP symmetry of the strong interactions, which must be discussed in presence of the electroweak sector of the SM, and is not yet understood [257–262]). It is important to make some remarks regarding the inclusion of non-zero quark masses:

1. For any value of quark masses, the individual flavor currents $\bar{f}\gamma^\mu f$ are conserved in the strong interactions, which makes the strong coupling flavor independent.

2. All 18 currents, except the vector singlet current (baryon number is exactly conserved, but for anomalous effects), get a non-vanishing divergence for different quark masses.

3. For equal quark masses, the 9 vector currents (octet + singlet) are conserved.

4. Considering a more realistic case, $m_u = m_d \neq m_s$, the $SU(3)$ flavor symmetry is reduced to $SU(2)$ isospin symmetry.

5. $m_u - m_d$ (compared to the typical energy scale of a given process) is then a scale of (most of the times small) isospin symmetry breaking.

This information will become important when discussing the symmetry breaking in QCD at low energies.

2.2.3 Light Pseudoscalar Mesons as Pseudo-Goldsone bosons

Spontaneous symmetry breaking in the thoery of strong interactions is feasible because of the known experimental input just explained. Considering the chiral limit, a sufficient (although not necessary) condition for it to take place is $\langle \bar{q}q \rangle \neq 0$, the so-called *(non-vanishing) scalar singlet quark condensate*. This naming comes from the fact that $\bar{q}q$ stays invariant under the Lorentz group and transforms as a singlet under $SU(3)_V$. The "condensation" is a non-perturbative phenomenon of the QCD ground state, which is driven by the formation of quark-antiquark pairs. The definition of scalar and pseudoscalar densities will be practical:

$$\begin{aligned} S_a(y) &= \bar{q}(y)\lambda_a q(y), \\ P_a(y) &= i\bar{q}(y)\gamma_5\lambda_a q(y), \end{aligned} \tag{2.8}$$

with $a = 0, ..., 8$, $\lambda_0 = \sqrt{\frac{2}{3}} I_3$, and the other 8 generators are the usual Gell-Mann matrices. In the chiral limit, $\langle S_a \rangle = 0$, that, for the diagonal matrices, gives the relations

$$\begin{aligned} \langle \bar{\lambda}_1 \rangle &= \sqrt{\frac{2}{3}} \langle \bar{u}u + \bar{d}d + \bar{s}s \rangle = 0, \\ \langle \bar{\lambda}_3 \rangle &= \langle \bar{u}u - \bar{d}d \rangle = 0, \\ \langle \bar{\lambda}_8 \rangle &= \sqrt{\frac{1}{3}} \langle \bar{u}u + \bar{d}d - 2\bar{s}s \rangle = 0, \end{aligned} \tag{2.9}$$

$$\tag{2.10}$$

leading to the equality of all $\langle \bar{f}f \rangle$. If we then take a non-null singlet quark condensate, we obtain:

$$\langle \bar{q}q \rangle = 3 \langle \bar{f}f \rangle \,. \tag{2.11}$$

This implies that $P_a(y)$ has a non-vanishing matrix element between the vacuum and the massless one-particle state $|\phi_b\rangle$, meaning that chiral symmetry has been spontaneously broken, resulting in $SU_L(3) \times SU_R(3) \to SU_V(3)$, giving rise to 8 pseudoscalar Goldstone bosons. This fits perfectly with the explanation we are aiming at, yielding the construction of the pseudoscalar meson octet, which will have a different nature than its parity partner. The explicit symmetry breaking by quark masses will give rise instead –for these lightest pseudoscalars– to pseudo-Goldstone bosons.

2.2.4 χPT for Mesons

The observations of nature reviewed previously lead to the search for a mechanism spontaneously breaking the chiral symmetry. This will, in turn, provide us with a useful framework to build a theory with 8 pseudoscalar (pseudo)Goldstone bosons. Here, the lightest octet of pseudoscalar mesons (π, K, η) can be identified with each of the Goldstone bosons. Based on that, an effective theory describing their interactions can be constructed.

2.2.4.1 Transformation properties of the Goldstone Bosons

In order to build the effective field theory applicable to these Goldstone bosons, it is necessary to understand first how they do transform under the action of the symmetry group, and which object is the ideal one for this task [263, 264, 241]. The Goldstone bosons can be arranged in a n-dimensional vector $\vec{\Phi} = (\phi_1, ...\phi_n)$, which maps from Minkowski space to a vector space:

$$M_1 = \left\{ \vec{\Phi} : M^4 \to \mathscr{R}^n | \phi_i : M^4 \to \mathscr{R} \right\}. \tag{2.12}$$

For its utility in this construction, we will discuss some properties of all left co-sets, called the quotient G/H, which are defined as

$$G/H = \{gH | g \in G\}, \tag{2.13}$$

where, simultaneously, gH is defined as:

$$gH = \{gh | h \in H\}, \tag{2.14}$$

with G (H) the symmetry group of a dynamical Lagrangian system (its vacuum). A very relevant property in this context is that co-sets either completely overlap, or are completely disjoint. This allows us to map isomorphically the quotient G/H and the Goldstone boson fields. This mapping, φ, has an important property: any given element $g \in G$ can map a vector Φ to another, Φ'. This property can be applied to our chiral QCD case. The symmetry group of chiral QCD is $G = SU(3)_L \times SU(3)_R$ and of its vacuum is $H = SU(3)_V$. Let $\tilde{g} = (\tilde{L}, \tilde{R}) \in G$. A representative element of the left co-set can be characterized as $\tilde{g}H = (1, \tilde{R}\tilde{L}^\dagger)H$ following the convention where the identity matrix appears as the first argument. Under the action of an element, g, a

left co-set element $\tilde{g}$ transforms as

$$g\tilde{g}H = (L, R\tilde{R}\tilde{L}^\dagger)H = (1, R\tilde{R}\tilde{L}^\dagger L^\dagger)(L,L)H = (1, R(\tilde{R}\tilde{L}^\dagger)L^\dagger)H, \tag{2.15}$$

where, in the last step, we have used the fact that (L,L) belongs to $SU(3)_V$ and concerning group properties, it is mapped into H itself. The representative matrix $\tilde{g}$ is then transformed as

$$U(x) \to RU(x)L^\dagger, \tag{2.16}$$

under the action of the group element g. Thus, in order to construct a basis in which we can write any $SU(3)$ element, we must get a set of hermitian traceless 3×3 matrices. This can be done by using the exponential parametrization, and the fact that there is an isomorphism between the elements of the group G and the elements of the vector space spanned by the Goldstone bosons. So we can write an $SU(3)$ element as

$$U(x) = \exp\left(i\frac{\Phi(x)\cdot\lambda}{F_0}\right), \tag{2.17}$$

where

$$\phi = \Phi\cdot\lambda = \begin{pmatrix} \pi^0 + \frac{1}{\sqrt{3}}\eta_8 & \sqrt{2}\pi^+ & \sqrt{2}K^+ \\ \sqrt{2}\pi^- & -\pi^0 + \frac{1}{\sqrt{3}}\eta_8 & \sqrt{2}K^0 \\ \sqrt{2}K^- & \bar{K}^0 & -\frac{2}{\sqrt{3}}\eta_8 \end{pmatrix}, \tag{2.18}$$

and the constant F_0 is a energy scale introduced to make the argument of the exponential function dimensionless, and will be set by experimental input (it is the pion decay constant in the chiral limit). We can (and will) choose $R(x) = L^\dagger(x) = u(x)$ so that $u^2(x) = U(x)$ [265]. These elements transform under the action of the symmetry group ($g \in G$) as in eq. (2.16). This permits us to construct not just the building blocks of the EFT but also to look for all independent terms allowed by the theory at a given order in the perturbative expansion. Since the construction is made in (even) powers of $\frac{p}{\Lambda}$, which for this case is $\Lambda = 4\pi F_\pi \approx 1.170$ GeV [256] (where $F_\pi \sim F_0$ is now renormalized and includes chiral corrections), it will converge rather well at low energies. It useful to remark that $\partial_\mu U(x)$ terms are of order $\frac{p}{F_0}$ and $U(x)$ is of order p^0.

2.2.4.2 Large N_C limit

When computing chiral corrections and setting everything for the inclusion of vector meson resonances, the Large-N_C limit of QCD [266–268] is a very convenient tool. Taking this limit implies $F_0 \to F \sim F_\pi$, and leads to the inclusion of the η' in $U(x)$

of eq. (2.17) as the element corresponding to λ_0. Altogether, and because of the inconsistent values for the mixings in the chiral and in the Large-N_C limits for the $\eta - \eta'$ system [269], we will let them as free parameters, leading to (note the $\sqrt{2}$ factor difference in Φ, compared to eq. (2.18)):

$$\Phi = \begin{pmatrix} \frac{1}{\sqrt{2}}(C_\pi \pi^0 + C_q \eta + C'_q \eta') & \pi^+ & K^+ \\ \pi^- & \frac{1}{\sqrt{2}}(-C_\pi \pi^0 + C_q \eta + C'_q \eta') & K^0 \\ K^- & \bar{K^0} & -C_s \eta + C'_s \eta' \end{pmatrix} . \quad (2.19)$$

In eq. (2.19), $C_\pi = F/F_\pi$ in the large-N_C limit [270–272], with the physical pion decay constant $F_\pi = 92.1$ MeV [217]. $C^{(\prime)}_{q,s}$ describe the η-η' system in the two-angle mixing scheme [273]

$$C_q = \frac{F}{\sqrt{3}\cos(\theta_8 - \theta_0)} \left(\frac{\cos\theta_0}{f_8} - \frac{\sqrt{2}\sin\theta_8}{f_0} \right) , \quad (2.20a)$$

$$C'_q = \frac{F}{\sqrt{3}\cos(\theta_8 - \theta_0)} \left(\frac{\sqrt{2}\cos\theta_8}{f_0} + \frac{\sin\theta_0}{f_8} \right) , \quad (2.20b)$$

$$C_s = \frac{F}{\sqrt{3}\cos(\theta_8 - \theta_0)} \left(\frac{\sqrt{2}\cos\theta_0}{f_8} + \frac{\sin\theta_8}{f_0} \right) , \quad (2.20c)$$

$$C'_s = \frac{F}{\sqrt{3}\cos(\theta_8 - \theta_0)} \left(\frac{\cos\theta_8}{f_0} - \frac{\sqrt{2}\sin\theta_0}{f_8} \right) . \quad (2.20d)$$

The determination of these mixing parameters is discussed in chapter 4, where they are used as stabilization points in the fits.

2.2.5 χPT Lagrangian

With these elements in consideration, we can now construct a χPT Lagrangian with optimal conditions to further include different resonances. We must consider that the chiral low-energy constants vary from χPT to the case with resonances, as they are integrated out in the former and become active fields in the latter, thereby affecting the LECs directly.

The leading order terms compatible with the assumed symmetries, in each parity sector, are given by [3]:

$$\mathscr{L}_{\text{no } R} = \frac{F^2}{4}\langle u_\mu u^\mu + \chi_+\rangle + \mathscr{L}_{\text{WZW}}\,, \tag{2.21}$$

where the $\mathscr{L}_{\text{WZW}}$ is given by the Wess-Zumino-Witten [276, 277] term, which is obtained from the WZW action. This action needs to be defined in addition to the natural definition of χPT, as intrinsic parity is an accidental symmetry of its construction. Processes as $K^+K^- \to \pi^0\pi^+\pi^-$ and $P \to \gamma\gamma$ are not included in the even-intrinsic parity chiral Lagrangians, but occur –by strong interactions– in nature. Since the QCD Lagrangian has the chiral anomaly, this one must be implemented in its effective realization at low energies. The Wess-Zumino-Witten action, which accomplishes this task, is given by:

$$\begin{aligned} S_{WZW}[U,l,r] =& -\frac{iN_C}{240\pi^2}\int d\sigma^{ijklm} Tr\left[\Sigma_i^L\Sigma_j^L\Sigma_k^L\Sigma_l^L\Sigma_m^L\right] \\ & -\frac{iN_C}{48\pi^2}\int dx^4 \varepsilon_{\mu\nu\rho\sigma}\left(W(U,l,r)^{\mu\nu\rho\sigma} - W(1,l,r)^{\mu\nu\rho\sigma}\right), \end{aligned} \tag{2.22}$$

where $W(U,l,r)$ is defined as

$$\begin{aligned} W(U,l,r)^{\mu\nu\rho\sigma} =& Tr\Bigg[Ul^\mu l^\nu l^\rho U^\dagger r^\sigma + \frac{1}{4}Ul^\mu U^\dagger r^\nu U l^\rho U^\dagger r^\sigma \\ & + iU\partial^\mu l^\nu l^\rho U^\dagger r^\sigma + i\partial^\mu r^\nu U l^\rho U^\dagger r^\sigma - i\Sigma^{L\mu} l^\nu U^\dagger r^\rho U l^\sigma \\ & \Sigma^{L\mu} U^\dagger \partial^\nu r^\rho U l^\sigma - \Sigma^{L\mu}\Sigma^{L\nu} U^\dagger r^\rho U l^\sigma + \Sigma^{L\mu} l^\nu \partial^\rho l^\sigma + \Sigma^{L\mu}\partial^\nu l^\rho l^\sigma \\ & -i\Sigma^{L\mu} l^\nu l^\rho l^\sigma + \frac{1}{2}\Sigma^{L\mu} l^\nu \Sigma^{L\rho} l^\sigma - i\Sigma^{L\mu}\Sigma^{L\nu}\Sigma^{L\rho} l^\sigma\Bigg] - (L \leftrightarrow R), \end{aligned} \tag{2.23}$$

and $\Sigma_\mu^{L(R)}$ are

$$\Sigma_\mu^L = U^\dagger \partial_\mu U, \qquad \Sigma_\mu^R = U\partial_\mu U^\dagger, \tag{2.24}$$

where $L \leftrightarrow R$ means $\Sigma_\mu^L L \leftrightarrow R\Sigma_\mu^R$, $l_\mu \leftrightarrow r_\mu$ and $U \leftrightarrow U^\dagger$. This Lagrangian is of order p^4. In our context, contributions at chiral order p^6 are saturated by resonance exchange. Consequently, these operators must be included for consistency in our framework, as it is done in Chapter 3.

For the other operators, we have defined previously $U(x)$ and consequently $u(x)$, which are the building blocks for the inclusion of the pGBs. u_μ and $\chi_\pm$ are defined

[3] We do not include the next-to-leading order terms, that are saturated by resonance exchange in the antisymmetric tensor formalism that we will use [274, 275].

by [265]

$$u_\mu = i\left[u^\dagger(\partial_\mu - ir_\mu)u - u(\partial_\mu - il_\mu)u^\dagger\right], \quad \chi_\pm = u^\dagger\chi u^\dagger \pm u\chi^\dagger u, \tag{2.25}$$

in which the external (pseudo)scalar $(p)s$ spin-zero and (left)-right $(l_\mu)r_\mu$ spin-one sources appear. For the vector electromagnetic case,

$$r_\mu = l_\mu = -eQA_\mu + \cdots, \quad Q = \text{diag}\left(\frac{2}{3}, -\frac{1}{3}, -\frac{1}{3}\right). \tag{2.26}$$

Explicit chiral symmetry breaking is introduced like in QCD, through non-vanishing quark masses, by means of the scalar current, via

$$\chi = 2B(s+ip), \quad s = \text{diag}(m_u, m_d, m_s), \quad p = 0, \quad 2m = m_u + m_d, \tag{2.27}$$

where the last equality corresponds to the isospin symmetry limit [4].

Interactions between pGBs and with external sources can be studied in this setting. However, since we aim to define form factors with correct high-energy behavior, we need to go further and include massive spin 1 fields consistently within χPT. This is most conveniently done working them in the antisymmetric tensor formalism.

2.3 Chiral Lagrangians for Massive Spin 1 Fields

Chiral Perturbation Theory (χPT) emerged [246, 247], as dual to QCD at low enough energies, explaining pion, kaon and eta meson physics precisely (including the chiral anomaly [276, 277]). However, as one approaches the masses of the $\rho(770)$ meson and other resonances, going to higher orders in χPT [265, 278] is no longer effective, and other unitarization procedures need to be considered. Resonance Chiral Theory ($R\chi T$) [274, 275] extends the energy range of applicability of χPT beyond the lightest resonance masses, by including them as explicit degrees of freedom in the theory. This is done based on the large number of colors limit of QCD [266, 267], that is equivalent to a semiclassical expansion for meson fields. The theory is built upon chiral symmetry for the lightest pseudo-Goldstone boson particles and unitary symmetry for the resonance fields.

[4] The isospin symmetry limit corresponds to $m_u = m_d$, denoted here m, resulting in $m_u + m_d = 2m$.

The following two observations are important for understanding that the unknown couplings do not grow out of control. First, the number of resonance fields in the operators is limited by the specific problem under study. Second, there is a balance between the order of the chiral tensors involved and the fulfillment of QCD short-distance constraints that need to be required to ensure formalism-independence of the observables [274, 275]. In this way, the resonance regime smoothly interpolates between the known chiral and short-distance limits of the QCD results. The relations among the $R\chi T$ couplings that are obtained requiring the asymptotic QCD results increase the predictive power of the theory, as will be illustrated in the context of $a_\mu^{\rm HLbL}$ throughout this thesis.

In addition to the operators described in Section 2.2.5, we will make use of the following chiral tensor for the electromagnetic interactions (given in terms of the QED field-strength tensor, $F^{\mu\nu}$):

$$f_\pm^{\mu\nu} = uF_L^{\mu\nu}u^\dagger \pm u^\dagger F_R^{\mu\nu}u, \tag{2.28}$$

and the covariant derivative defined by the connection:

$$\Gamma_\mu = \frac{1}{2}\left[u^\dagger(\partial_\mu - ir_\mu)u + u(\partial_\mu - il_\mu)u^\dagger\right], \quad \nabla_\mu \cdot = \partial_\mu + [\Gamma_\mu, \cdot]. \tag{2.29}$$

In general, all resonances are included as chiral tensors which transform as $X \xrightarrow{G} hXh^\dagger$ with $h \in H$, where H, G ($G \subset H$) characterize the pattern of spontaneous symmetry breakdown

$$G \equiv SU(3)_L \otimes SU(3)_R \to H \equiv SU(3)_{V=L+R} \tag{2.30}$$

in low-energy QCD. The chiral tensor operators for the resonances $R = S, P, V, A$ can be found in Ref. [279] ([280]) for the even(odd)-intrinsic parity sector. For tensor resonances, the operators can be found in Refs. [281, 282, 122].

2.3.1 RχT Lagrangian: Vector Meson Resonances

The vector meson multiplet in the large-N_C limit is included in the antisymmetric tensor fields [246, 274] [5] (ideal $\omega^{0,8}$ meson mixing into the ω, ϕ mass eigenstates is

[5] The standard description of resonances in terms of a vector field requires that the $\mathcal{O}(p^6)$ terms in the chiral expansion are included to comply with low-energy symmetry requirements. Instead, this is not needed working with antisymmetric tensor fields, which is a quite convenient motivation to use them, as we do.

used):

$$V_{\mu\nu} = \begin{pmatrix} (\rho^0+\omega^0)/\sqrt{2} & \rho^+ & K^{*+} \\ \rho^- & (-\rho^0+\omega^0)/\sqrt{2} & K^{*0} \\ K^{*-} & \bar{K^{*0}} & \phi \end{pmatrix}_{\mu\nu} . \tag{2.31}$$

We will restrict ourselves now to the even intrinsic parity sector. There, the most general Lagrangian which -upon resonance integration- contributes to the $\mathscr{O}(p^4)$ chiral low-energy constants is determined by the vector meson resonances multiplet behavior under the chiral group. This yields :

$$\begin{aligned} \mathscr{L}_V^{kin} &= -\frac{1}{2}\langle \nabla_\lambda V^{\lambda\nu} \nabla^\rho V_{\rho\nu}\rangle + \frac{1}{4} M_V^2 \langle V_{\mu\nu} V^{\mu\nu}\rangle, \\ \mathscr{L}_V^{even} &= \frac{F_V}{2\sqrt{2}}\langle V_{\mu\nu} f_+^{\mu\nu}\rangle + \frac{\lambda_V}{\sqrt{2}}\langle V_{\mu\nu}\left\{f_+^{\mu\nu}, \chi_+\right\}\rangle + i\frac{G_V}{\sqrt{2}}\langle V_{\mu\nu} u^\mu u^\nu\rangle, \end{aligned} \tag{2.32}$$

where $\langle\rangle$ is an abbreviation for the flavor trace. These operators and their implications will be further discussed in the next chapter, where both intrinsic-parity sectors will be of relevance.

CHAPTER 3

π^0,η, η' transition form factors in resonance chiral theory and $a_\mu^{\mathrm{P-poles}}$

As mentioned in Chapter 1, the main contributions to the HLbL piece of a_μ are the ones of the pseudoscalar poles [283–289]. To compute them, the main input is the transition form factor (TFF), $\mathrm{P}\to\gamma^*\gamma^*$. This work aimed to improve the error of previous determinations [290, 291, 280, 47, 49, 292, 50, 293–299]($\sim 4\times10^{-11}$, around 20 % of the previous total error of the HLbL), and to correct systematic errors on previous determinations using the same framework, Resonance Chiral Theory (RχT) [280, 300–302], which previously failed to include chiral corrections or, more importantly, to reproduce some of the short-distance constraints (SDCs), which were in the quality criteria for including a computation in the muon $g-2$ Theory Initiative White Paper 2020 [5] due to its importance, as shown in [303]; consequently, RχT had space for improvement that motivated our present work.

In particular, including just one multiplet of vector mesons it was not possible to comply with the leading asymptotic behavior for double virtuality. In ref. [302], the associated error was estimated to be $\binom{+5.0}{-0.0}\times10^{-11}$, from the contribution of excited vector multiplets, which would restore the appropriate short-distance behavior for double virtuality. In this work, we have verified previous results and computed all new contributions associated to the first resonance excitations within this formalism, being consistent with the procedure of ref. [302] and complying now with the QCD short-distance behavior.

We have considered an RχT Lagrangian with two vector meson resonances as derived in [275, 280, 304, 279, 305–308] with the first order chiral corrections in order to fulfill the SDCs required by the muon $g-2$ Theory Initiative. The parameters and

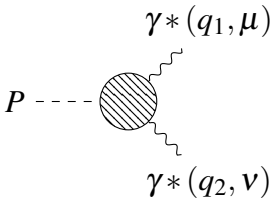

Fig. 3.1 Schematic representation of the $P \to \gamma^*\gamma^*$ ($P = \pi^0, \eta, \eta'$) Transition Form Factor.

couplings that were not constrained by QCD properties, were fitted to experimental data available on the TFFs, the radiative decay widths, Lattice QCD calculations in the doubly virtual sector and the best determinations of the $\eta - \eta'$ mixings.

3.1 Pseudoscalar Transition Form Factor ($P \to \gamma^*\gamma^*$): The essential input

Due to charge conservation, and strangeness conservation of electromagnetic interactions, π^0, $\eta - \eta'$ can decay into two photons via anomalous contributions, from the odd-intrinsic parity sector of QCD. For the π^0 and η, they are the main decay channels; for the η', they are not, but are still relevant. The decay of a pseudoscalar particle into two photons is described by the amplitude:

$$\langle \gamma^*(q_1,\lambda_1)\gamma^*(q_2,\lambda_2)|P(p)\rangle = i(2\pi)^4\delta^{(4)}(q_1+q_2-p)e^2\varepsilon_\mu^{\lambda_1^*}(q_1)\varepsilon_\nu^{\lambda_2^*}(q_2)\mathscr{M}^{\mu\nu}(q_1,q_2)\,, \tag{3.1}$$

where $\varepsilon_{\mu,\nu}^{\lambda_i^*}(q_i)$ are the polarization of the photons as given by the usual bibliography [134]:

$$\varepsilon_\pm(q) = \mp(0,1,\pm i,0)\,, \quad \varepsilon_0(p) = (0,0,0,1)\,. \tag{3.2}$$

Due to symmetries, there is only one possible tensor structure of $\mathscr{M}^{\mu\nu}(q_1,q_2)$, which results in:

$$\mathscr{M}^{\mu\nu}_{P\gamma^*\gamma^*} = \varepsilon^{\mu\nu\alpha\beta}q_{1\alpha}q_{2\beta}\mathscr{F}_{P\gamma^*\gamma^*}(q_1^2,q_2^2), \tag{3.3}$$

and it is pictorially represented by the Feynman Diagram in Fig. 3.1. All internal dynamics of the pseudoscalar mesons is encoded in $\mathscr{F}_{P\gamma^*\gamma^*}(q_1^2,q_2^2)$, the transition form factor (TFF), which must be symmetric under $q_1^2 \leftrightarrow q_2^2$ [1].

[1] Alternatively, we could have defined this form factor from the VVP Green function.

The asymptotic behavior of the pseudoscalar form factors is defined by [309–312], in the discrete cases of single and double virtuality, and by the Light-Cone-Expansion results in the full asymmetric cases [124]. In the single and double virtual case, the limits are:

$$\lim_{Q^2\to\infty} Q^2 \mathscr{F}_{\pi^0\gamma^*\gamma^*}(-Q^2,-Q^2) = \frac{2F_\pi}{3}\,, \tag{3.4a}$$

$$\lim_{Q^2\to\infty} Q^2 \mathscr{F}_{\pi^0\gamma^*\gamma^*}(-Q^2,0) = 2F_\pi\,, \tag{3.4b}$$

with $q^2 = -Q^2$. At leading order in the perturbative expansion, the results for the $\eta^{(\prime)}$ mesons are obtained multiplying those for the π^0, eqs. (3.4), by the flavor space rotation factor $\frac{5C_q-\sqrt{2}C_s}{3}$ $\left(\frac{5C'_q+\sqrt{2}C'_s}{3}\right)$, respectively. These 4 couplings are parametrized in the two-angle mixing scheme [269, 273, 313]. The asymptotic behavior for general asymmetries, parametrized by $w = \frac{q_1^2-q_2^2}{q_1^2+q_2^2}$, are given by [124]:

$$\mathscr{F}_{P\gamma^*\gamma^*}(q_1^2,q_2^2) = \frac{4\sum_a C_a F_P^a}{\tilde{Q}^2} f^P(w), \tag{3.5}$$

with the symmetric piece written in terms of $\tilde{Q}^2 = \frac{q_1^2+q_2^2}{2}$, and the asymmetry function, $f^P(w)$, is given by:

$$f^P(w) = -\frac{3}{2w^2}\left(1 + \frac{1-w^2}{2w}\log\frac{1-w}{1+w}\right), \tag{3.6}$$

with the limiting cases $f^P(0) = -1$ and $f^P(\pm 1) = -\frac{3}{2}$, matching the values found in eq. (3.4) when the values for the decay constants are substituted in eq. (3.5).

3.2 Pseudoscalar Pole Contributions

The pseudoscalar poles contribute to the HLbL amplitude by the diagrams in Fig. 3.2. These diagrams can be used to construct the HLbL tensor of this specific representation to obtain the scalar functions of eq. (1.28). The scalar functions are:

$$\bar{\Pi}_1(Q_1,Q_2,\tau) = -\frac{\mathscr{F}_{P\gamma^*\gamma^*}(-Q_1^2,-Q_2^2)\mathscr{F}_{P\gamma^*\gamma^*}(-Q_3^2,0)}{Q_3^2+m_P^2},$$

$$\bar{\Pi}_2(Q_1,Q_2,\tau) = -\frac{\mathscr{F}_{P\gamma^*\gamma^*}(-Q_1^2,-Q_3^2)\mathscr{F}_{P\gamma^*\gamma^*}(-Q_2^2,0)}{Q_2^2+m_P^2}. \tag{3.7}$$

$$\tag{3.8}$$

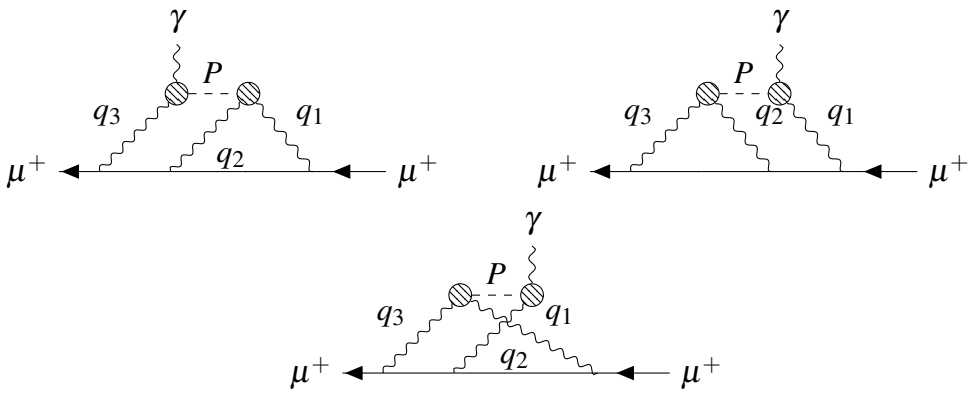

Fig. 3.2 Pseudoscalar pole diagrams contributing to the HLbL piece of a_μ. The different photon virtualities, q_1, q_2, q_3, are fixed to the side not in contact with the form factors, and all of the possible permutations are included in these three diagrams.

The rest of the scalar functions are zero. Due to the simplicity of the amplitude of the pseudoscalar poles, alternative derivations of the a_μ contributions were used before the procedure that lead to the Master Formula (See Refs. [290, 314, 315, 49]). It was previously discussed if it was the pseudoscalar pole or the exchange the one that should be used for computing this contribution. It was until the development of the dispersion relations for the HLbL that it was clear that the poles are the ones that should be used, as they correspond exactly to the one-pseudoscalar intermediate on-shell states, being this a systematic procedure of classifying contributions, free of ambiguities due to double-counting [46].

3.2.1 RχT Lagrangian: V+V'+P'

In this section, we describe the formalism used to compute the P transition form factors, within RχT,[2] which extends the energy domain of applicability of the χPT Lagrangian [246] by including the light-flavored resonances as explicit degrees of freedom [275] as discussed in Chapter 2. The leading contribution to the $P\gamma\gamma$ transition form factor (TFF) at low energies[3] is given by the Wess-Zumino-Witten (WZW) contact term [276, 277], which is completely specified by the chiral anomaly [248, 249], in terms of the number of colors of the QCD gauge group (N_C) and the pion decay

[2] A more extended discussion can be found in e.g. ref. [302].
[3] It is $\mathcal{O}(p^4)$ in the chiral expansion, where $p^2 \sim m_P^2$ [246].

constant in the chiral limit (F):

$$\mathscr{F}^{\mathrm{WZW}}_{P\gamma^*\gamma^*} = -c_P \frac{N_C}{12\pi^2 F}, \tag{3.9}$$

where c_P is the flavor space rotation coefficient, defined as $c_\pi = 1$, $c_\eta = \frac{5C_q - \sqrt{2}C_s}{3}$, $c_{\eta'} = \frac{5C'_q + \sqrt{2}C'_s}{3}$. Since this term is a constant, it cannot be a complete description of the TFFs, as it would violate analyticity and unitarity. Besides, it would obviously not reproduce the short distance constraints from eq. (3.4). To achieve the correct asymptotic behavior [302, 301], and a consistent description [280], we need to consider RχT with the lowest lying vector multiplet(V), the first excitation of those(V') and pseudoscalar resonances as well(P').

The complete basis of odd-intrinsic parity RχT operators, which -upon resonance integration- saturate most of the $\mathscr{O}(p^6)$ chiral low-energy constants (LECs), was found in ref. [280]. We will, however, use the basis in ref. [304] with a copy for the V' resonances, besides the interactions of this new set of resonances with the previous ones. This will be developed in more detail next.

We organize the Lagrangian describing the lightest pseudo-Goldstone bosons and their interactions in an increasing number of resonance fields, R:

$$\mathscr{L}_{\mathrm{R}\chi\mathrm{T}} = \mathscr{L}_{\mathrm{no}\,R} + \sum_R (\mathscr{L}^{\mathrm{Kin}}_R + \mathscr{L}^{\mathrm{Kin}}_{R'}) + \sum_{R,R'} \mathscr{L}_{R,R'} + \cdots . \tag{3.10}$$

We will further divide the RχT Lagrangian into its odd- and even-intrinsic parity sectors, including, in addition to the pseudo-Goldstone bosons (φ^a) and the photons (γ), the two lightest vector meson multiplets ($V^{(\prime)}$) and the first pseudoscalar excitations (P').

- **Operators with no resonance fields:**

We must note, however, that the values of the chiral LECs vary from χPT to this sector of RχT precisely by the fact that in the latter the resonance degrees of freedom are active, whereas they have been integrated out in the former. The relevant part of $\mathscr{L}_{\mathrm{no}\,R}$ in the even intrinsic parity are the ones coming from RχT, described in Chapter 2, and for the odd-intrinsic-parity are given by[265, 278]: [4]

[4]We include the $\mathscr{O}^W_j$ operators, which are subleading in the chiral expansion with respect to the WZW piece, to ensure the most general breaking of flavor symmetry.

j	O_j^W
7	$i\varepsilon^{\mu\nu\alpha\beta}\langle\chi_- f_{+\mu\nu} f_{+\alpha\beta}\rangle$
8	$i\varepsilon^{\mu\nu\alpha\beta}\langle\chi_-\rangle\langle f_{+\mu\nu} f_{+\alpha\beta}\rangle$
22	$\varepsilon^{\mu\nu\alpha\beta}\langle u_\mu\{\nabla_\gamma f_{+\gamma\nu}, f_{+\alpha\beta}\}\rangle$

Table 3.1 Chiral operators of order $\mathcal{O}(p^6)$ relevant for the description of the transition form factors of the pseudoscalar mesons, π^0, η, η'.

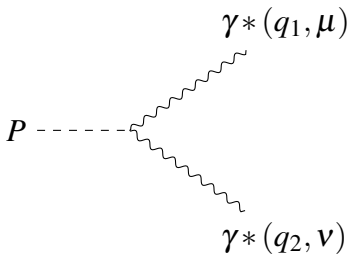

Fig. 3.3 Schematic representation of the non-resonant contributions to the $P\to\gamma^*\gamma^*$ ($P=\pi^0,\eta,\eta'$) Transition Form Factor.

$$\mathcal{L}_{\text{no }R}^{\text{odd}} = \mathcal{L}_{\text{WZW}} + \sum_{j=7,8,22} C_j^W \mathcal{O}_j^W\,, \tag{3.11}$$

where $\langle ...\rangle$ stands for a trace in flavor space. The 3 operators in eq. (3.11) are in table 3.1. Nevertheless, after our analysis of short-distance constraints is performed –shown in subsection 3.2.3–, all 3 C_j^W, vanish. The schematic representation of these contributions is shown in Fig. (3.3)

• **Operators with one vector resonance field:**

The inclusion of vector meson resonances to the chiral Lagrangian are described in Chapter 2. For the dynamic part, we start with the even-intrinsic parity sector, where we have

$$\mathcal{L}_V^{\text{even}} = \frac{F_V}{2\sqrt{2}}\langle V_{\mu\nu} f_+^{\mu\nu}\rangle + \frac{\lambda_V}{\sqrt{2}}\langle V_{\mu\nu}\{f_+^{\mu\nu}, \chi_+\}\rangle\,, \tag{3.12}$$

with the first term giving the leading contribution to the V^0-γ coupling and the second one including its flavor-symmetry breaking correction, proportional to quark masses.[5] The combination of these two terms will result in the Feynman rules for

[5]We note that $\lambda_V = \sqrt{2}\lambda_6^V$ in ref. [279].

j	$\mathscr{O}^j_{VJP}$
1	$\langle\{V^{\mu\nu}, f_+^{\rho\alpha}\}\nabla_\alpha u^\sigma\rangle$
2	$\langle\{V^{\mu\alpha}, f_+^{\rho\sigma}\}\nabla_\alpha u^\nu\rangle$
3	$i\langle\{V^{\mu\nu}, f_+^{\rho\sigma}\}\chi_-\rangle$
4	$i\langle V^{\mu\nu}[f_-^{\rho\sigma}, \chi_+]\rangle$
5	$\langle\{\nabla_\alpha V^{\mu\nu}, f_+^{\rho\alpha}\}u^\sigma\rangle$
6	$\langle\{\nabla_\alpha V^{\mu\alpha}, f_+^{\rho\sigma}\}u^\nu\rangle$
7	$\langle\{\nabla^\sigma V^{\mu\nu}, f_+^{\rho\alpha}\}u_\alpha\rangle$

Table 3.2 Odd-intrinsic parity operators with a vector resonance V, a vector current J and a light pseudoscalar, P. The common factor $\varepsilon_{\mu\nu\rho\sigma}$ is omitted in all operators.

the transition vertices of the relevant resonances:

$$\rho \to \gamma : F_V + 8m_\pi^2\lambda_V\,, \quad \omega \to \gamma : \frac{1}{3}(F_V + 8m_\pi^2\lambda_V)\,, \quad \phi \to \gamma : \frac{\sqrt{2}}{3}(F_V \to F_V + 8\Delta_{2K\pi}^2\lambda_V)\,, \tag{3.13}$$

where $\Delta_{2K\pi}^2 = 2m_K^2 - m_\pi^2$, and with an analogous primed version for the V'-γ vertices.

In the odd-intrinsic parity sector, one has

$$\mathscr{L}_V^{\text{odd}} = \sum_{j=1}^{7} \frac{c_j}{M_V}\mathscr{O}^j_{VJP}\,, \tag{3.14}$$

where the complete list of operators contributing to our processes of interest (via φ-γ-V vertices) is collected in table 3.2. Among these operators only $\mathscr{O}^3_{VJP}$ breaks chiral symmetry [6](the others will also give flavor-breaking contributions for real φs, once their wave functions renormalization and mixings are accounted for; with similar comments applying below). The schematic representation of these operators is shown in Fig. 3.4.

• **Operators with two vector resonance fields:**

These contributions are of the following type:

$$\mathscr{L}_{VV}^{\text{odd}} = \sum_{j=1}^{4} d_j\mathscr{O}^j_{VVP}\,, \tag{3.15}$$

[6]Although $\mathscr{O}^4_{VJP}$ also breaks chiral symmetry, its contribution vanishes for the processes studied here.

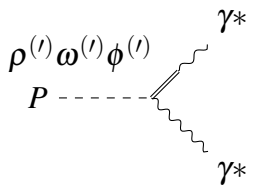

Fig. 3.4 Schematic representation of the contributions to the $P \to \gamma^*\gamma^*$ ($P = \pi^0, \eta, \eta'$) Transition Form Factors including one vector meson resonance. Only the neutral zero-strangeness resonances contribute, ρ, ω, ϕ.

j	$\mathcal{O}^j_{VVP}$
1	$\langle\{V^{\mu\nu}, V^{\rho\alpha}\}\nabla_\alpha u^\sigma\rangle$
2	$i\langle\{V^{\mu\nu}, V^{\rho\sigma}\}\chi_-$
3	$\langle\{\nabla_\alpha V^{\mu\nu}, V^{\rho\alpha}\}u^\sigma\rangle$
4	$\langle\{\nabla^\sigma V^{\mu\nu}, V^{\rho\alpha}\}u_\alpha\rangle$

Table 3.3 Odd-intrinsic parity operators with two vector resonances V and a light pseudoscalar, P. The common factor $\varepsilon_{\mu\nu\rho\sigma}$ is omitted in all operators.

where the basis of four operators is given in Table 3.3, but only the first three contribute to the decay of a pseudoscalar meson into two photons. Among these, $\mathcal{O}^2_{VVP}$ breaks unitary flavor symmetry. The operators of this kind are represented by diagrams as those in Fig. 3.5.

- **Operators with excited vector resonance fields:**

For the second vector multiplet, V', we repeat all operators that we had for the first one, V. That is, we add kinetic and dynamic terms for the excited vector mesons. In this way, we will have the new parameters (denoted by a prime) $M_{V'}, e_m^{V'}, F_{V'}, \lambda_{V'}, \{c_i'\}_{i=1}^7, \{d_j'\}_{j=1}^4$.

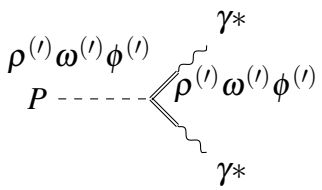

Fig. 3.5 Schematic representation of the contributions to the $P \to \gamma^*\gamma^*$ ($P = \pi^0, \eta, \eta'$) Transition Form Factors including two vector meson resonances. Only the neutral zero-strangeness resonances contribute, ρ, ω, ϕ.

j	$\mathscr{O}^{j}_{VV'P}$
a	$\langle\{V^{\mu\nu},V'^{\rho\alpha}\}\nabla_\alpha u^\sigma\rangle$
b	$\langle\{V^{\mu\alpha},V'^{\rho\sigma}\}\nabla_\alpha u^\nu\rangle$
c	$\langle\{\nabla_\alpha V^{\mu\nu},V'^{\rho\alpha}\}u^\sigma\rangle$
d	$\langle\{\nabla_\alpha V^{\mu\alpha},V'^{\rho\sigma}\}u^\nu\rangle$
e	$\langle\{\nabla^\sigma V^{\mu\nu},V'^{\rho\alpha}\}u_\alpha\rangle$
f	$i\langle\{V^{\mu\nu},V'^{\rho\sigma}\}\chi_-\rangle$

Table 3.4 Odd-intrinsic parity operators with one vector meson resonance, one excited vector meson resonance, and a pseudo-Goldstone boson [307]. A common $\varepsilon_{\mu\nu\rho\sigma}$ factor is omitted in all operators.

Additionally, we will also have new $VV'P$ interactions, which are [307]

$$\mathscr{L}^{\rm odd}_{VV'} = \sum_{j=a,b,c,d,e,f} d_j \mathscr{O}^{j}_{VV'P}\,, \tag{3.16}$$

with the $\mathscr{O}^{j}_{VV'P}$ shown in table 3.4. The diagrams for these operators are as the ones in Fig. 3.5, with one resonance from each multiplet.

- **Operators with pseudoscalar resonance fields:**

The pseudoscalar resonances, P' (with analogous flavor structure to the φ mesons), give subleading contributions via their mixing with the lightest pseudo-Goldstones, φ, that are suppressed as $m_P^2/m_{P'}^2$. However, the P' multiplet is crucial to recover the QCD-ruled short-distance behaviour on the VVP Green's function [280, 316]. Because of this, we must also take into consideration the pieces

$$\begin{aligned}\Delta\mathscr{L}^{\rm even}_P &= \frac{1}{2}\langle\nabla_\mu P'\nabla^\mu P'\rangle + i d_m\langle P'\chi_-\rangle\,,\\ \Delta\mathscr{L}^{\rm odd}_P &= \varepsilon_{\mu\nu\rho\sigma}\langle\kappa_5^P\left\{f_+^{\mu\nu},f_+^{\rho\sigma}\right\}P' + \kappa_3^{PV}\left\{V^{\mu\nu},f_+^{\rho\sigma}\right\}P' + \kappa^{PVV}V^{\mu\nu}V^{\rho\sigma}P'\rangle\,,\end{aligned} \tag{3.17}$$

which need to be repeated for $V\to V'$. The even parity sector induces transitions of the kind $P\to P'$, as the ones shown in Figure 3.6. The odd intrinsic parity ones will induce corrections to the diagrams shown in Figs. 3.3-3.5. The operator with coefficient $d_m^{(\prime)}$ vanishes in the chiral limit. There will also be a $VV'P'$ operator [308],

$$\Delta\mathscr{L}^{\rm odd}_{VV'P'} = \kappa^{VV'P'}\langle\{V^{\mu\nu},V'^{\mu\nu}\}P'\rangle\,, \tag{3.18}$$

that we need to include for consistency.

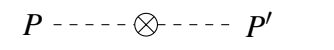

Fig. 3.6 Transitions of the kind $P \to P'$, which induce corrections to the contributions with zero, one and two resonances.

3.2.2 Transition Form Factors in RχT

The different contributions to $\mathscr{F}_{P\gamma^*\gamma^*}(q_1^2, q_2^2)$ considering only one vector resonance multiplet are described minutely in ref. [302], so we will not detail them here. Nonetheless, it is important to quote the redefinition of combinations of the coupling constants appearing in [302] that will also enter our results: [7]

$$c_{1235} \to c^*_{1235} = c_1 + c_2 + 8c_3^* - c_5\,, \tag{3.19a}$$

$$d_{123} \to d^*_{123} = d_1 + 8d_2^* - d_3\,, \tag{3.19b}$$

$$d_{abcf} \to d^*_{abcf} = d_a + d_b - d_c + 8d_f^*\,. \tag{3.19c}$$

The contributions from the second vector multiplet can be obtained by simply adding the same terms with primed couplings. We will concentrate here on the new terms that come from the $VV'P$ contributions to the two-resonances exchange diagrams.

The contributions coming from $\mathscr{L}_{VV'P}$, eq. (3.16), read

$$\begin{aligned}\mathscr{F}^{VV'P}_{\pi^0\gamma^*\gamma^*}(q_1^2, q_2^2) = \frac{2}{3F_\pi}\Bigg\{&(F_V + 8m_\pi^2\lambda_V)(F_{V'} + 8m_\pi^2\lambda_{V'})\left(m_\pi^2 d_{abcf} + d_{abc}q_1^2 + d_{abcd}q_2^2\right)\\ &\times\left(\frac{1}{(M_\rho^2 - q_1^2)(M_{\omega'}^2 - q_2^2)} + \frac{1}{(M_{\rho'}^2 - q_1^2)(M_\omega^2 - q_2^2)}\right) + (q_1 \leftrightarrow q_2)\Bigg\}\,,\end{aligned} \tag{3.20}$$

where we defined the combinations of couplings

$$d_{abcf} = d_a + d_b - d_c + 8d_f\,, \quad d_{abc} = d_a - d_b + d_c\,, \quad d_{abcd} = -d_a + d_b + d_c - 2d_d\,, \tag{3.21}$$

[7] This redefinition of coupling constants applies for both vector meson resonance multiplets, so the c's and the d's are also redefined in the same way.

and

$$\mathscr{F}^{VV'P}_{\eta\gamma^*\gamma^*}(q_1^2,q_2^2) = \frac{2}{3F}\left\{\left[5C_q\frac{2}{3}(F_V+8m_\pi^2\lambda_V)(F_{V'}+8m_\pi^2\lambda_{V'})\frac{d_{abcf}m_\eta^2+d_{abc}q_1^2+d_{abcd}q_2^2-8d_f\Delta_{\eta\pi}^2}{(M_{\rho'}^2-q_1^2)(M_\rho^2-q_2^2)}\right.\right.$$
$$\left.\left.+(\{5C_q\to-\sqrt{2}C_s,\Delta_{\eta\pi}\to-\Delta_{2K\pi\eta},\rho^{(\prime)}\to\phi^{(\prime)}\})\right]+(q_1\leftrightarrow q_2)\right\}, \tag{3.22}$$

where we introduced $\Delta_{\eta\pi}^2=m_\eta^2-m_\pi^2$ and $\Delta_{2K\pi\eta}^2=2m_K^2-m_\pi^2-m_\eta^2$. The pion wave-function renormalization has changed the global $1/F$ factor to $1/F_\pi$, for $N_C\to\infty$ [270–272], in eq. (3.20). In this equation. there is no ϕ contribution because ideal mixing for the vector meson resonances was used. For the $\eta^{(\prime)}$, ρ,ω,ϕ contribute; However, the isospin symmetry limit leads to $M_{\rho^{(\prime)}}=M_{\omega^{(\prime)}}$ so we have chosen to use $\rho^{(\prime)}$'s mass and propagator only. For the $\eta^{(\prime)}$ cases, the dependencies are on $C_{q/s}^{(\prime)}/F$, which are functions of $\{f,\theta\}_{8/0}$.

As always, an analogous expression is obtained for $\mathscr{F}_{\eta'\gamma^*\gamma^*}(q_1^2,q_2^2)$ by replacing $C_q\to C_q'$, $C_s\to -C_s'$ and $m_\eta\to m_{\eta'}$, and the $\eta^{(\prime)}$ expressions reduce to the π^0 one in the $U(3)$ flavor symmetry limit. In the chiral limit, our results for the P transition form factors reproduce those in refs. [280, 301]. Neglecting the contributions involving the V' multiplet we recover the results in ref. [302].

Since we want to make use of the short-distance constraints on the VVP Green's function derived in refs. [280, 301], the effect of the pseudoscalar resonance multiplet P' needs to be accounted for. The operator with coefficient d_m (from $\Delta\mathscr{L}_P^{\text{even}}$ in eq. (3.17)) introduces a mixing between the P' and φ states, proportional to quark masses, starting at $\mathscr{O}(m_P^2)$. As a result, the contribution from the P' states can be introduced by simply rescaling couplings as follows [302]:

$$C_7^W\to C_7^{W*}=C_7^W+\frac{4d_m\kappa_5^P}{3M_{P'}}, \tag{3.23a}$$

$$c_3\to c_3^*=c_3+\frac{d_mM_V\kappa_3^{PV}}{M_{P'}^2},^8 \tag{3.23b}$$

$$d_2\to d_2^*=d_2+\frac{d_m\kappa^{PVV}}{2M_{P'}^2}, \tag{3.23c}$$

$$d_f\to d_f^*=d_f+\frac{d_m\kappa^{PVV'}}{2M_{P'}^2}, \tag{3.23d}$$

[8] A short-distance constraint on κ_3^{PV} was found in ref. [280]. We will not use it, like in ref. [302], as it does no longer hold when the V' and P' multiplets are also considered.

where the last redefinition was not proposed before, to our knowledge. The remaining couplings do not need shifting.

3.2.3 Matching to Asymptotic QCD

As mentioned in 3.1, the high-energy behavior of the TFFs is defined by pQCD and the definition of the mixings. It is important to mention that by cutting the infinite tower of resonances, only a finite number of SDCs can be reproduced. Consequently, the logarithmic piece of eq. (3.5), is not achievable in this setting. We applied the single virtual and symmetric doubly virtual constraints, first in the chiral limit, and then including $\mathcal{O}(m_P^2)$ corrections. Our results were independent of considering corrections at this order to the LO values for the $C_{q/s}^{(\prime)}$ mixing coefficients, so we will keep them unexpanded throughout.

In addition to demanding the leading ultraviolet behaviour in the singly and doubly virtual limits of the transition form factors, we will also require the additional constraints derived from the short-distance analysis of the VVP Green's function. By matching the leading terms of the QCD OPE for infinite virtualities, within the chiral and large-N_C limits, Kampf and Novotny [280] obtain that the following (linear combinations of) constants vanish

$$C_{22}^W = C_7^{W*} = c_{125} = c'_{125} = c_{1235} = c'_{1235} = 0\,, \tag{3.24}$$

where we first used here $c_{125} = c_1 - c_2 + c_5$. Their remaining results are compatible with our findings that will be detailed next:

- Doubly Virtual π^0-TFF:
  - $\mathcal{O}(Q^0)$, $\mathcal{O}(m_P^0)$:

$$c'_{1256} = -M_{V'}\frac{M_V N_C + 32\sqrt{2}\pi^2 F_V c_{1256}}{32\sqrt{2}\pi^2 F_{V'} M_V}\,, \tag{3.25}$$

    where $c_{1256}^{(\prime)} = c_1^{(\prime)} - c_2^{(\prime)} - c_5^{(\prime)} + 2c_6^{(\prime)}$ appears (primed combinations of constants are defined analogously below).

  - $\mathcal{O}(Q^0)$, $\mathcal{O}(m_P^2)$:

$$\lambda_V = \lambda_{V'} = 0\,. \tag{3.26}$$

– $\mathcal{O}(Q^{-2})$, $\mathcal{O}(m_P^0)$:

$$c_{1256} = \frac{8d_3F_V + 4d_{abc}F_{V'} - \frac{F_\pi^2 M_V^2}{F_V(M_V^2 - M_{V'}^2)}}{4\sqrt{2}M_V}\,. \tag{3.27}$$

– $\mathcal{O}(Q^{-2})$, $\mathcal{O}(m_P^2)$:

$$c^*_{1235} = -e_m^V \frac{8d_3F_V + 4d_{abc}F_{V'} - \frac{F_\pi^2 M_V^2}{F_V(M_V^2 - M_{V'}^2)}}{\sqrt{2}M_V}\,. \tag{3.28}$$

- Singly Virtual π^0-TFF:

– $\mathcal{O}(Q^0)$, $\mathcal{O}(m_P^0)$:

$$d'_3 = \frac{-M_V^2 M_{V'}^2 N_C - 32\pi^2 d_{abcd}F_V F_{V'} M_V^2 - 64\pi^2 d_3 F_V^2 M_{V'}^2 - 32\pi^2 d_{abc}F_V F_{V'} M_{V'}^2}{64\pi^2 F_{V'}^2 M_V^2}\,. \tag{3.29}$$

– $\mathcal{O}(Q^0)$, $\mathcal{O}(m_P^2)$:

$$\begin{aligned} c^{*\prime}_{1235} = &-\frac{M_{V'}}{8\sqrt{2}\pi^2 F_{V'} M_V^4}(-e_m^{V'} M_V^4 N_C - 64\pi^2 d_3 e_m^{V'} F_V^2 M_V^2 - 32\pi^2 d_{abc} e_m^{V'} F_V F_{V'} M_V^2 \\ &+ 64\pi^2 d_3 e_m^V F_V^2 M_{V'}^2 + 32\pi^2 d_{abc} e_m^V F_V F_{V'} M_{V'}^2 + 8\sqrt{2}\pi^2 c^*_{1235} F_V M_V M_{V'}^2)\,. \end{aligned} \tag{3.30}$$

– $\mathcal{O}(Q^{-2})$, $\mathcal{O}(m_P^0)$:

$$d_{abc} = -\frac{-M_V^2 M_{V'}^4 N_C + 4\pi^2[4d_{abcd}M_V^2 F_V F_{V'}(M_V^2 - M_{V'}^2) + 16 d_3 F_V^2 M_{V'}^2 (M_V^2 - M_{V'}^2) + 5F_\pi^2 M_V^2 M_{V'}^2]}{16\pi^2 F_V F_{V'} M_{V'}^2 (M_V^2 - M_{V'}^2)}\,. \tag{3.31}$$

– $\mathcal{O}(Q^{-2})$, $\mathcal{O}(m_P^2)$:

$$d'^*_{123} = -\frac{F_V[2d^*_{123}F_V M_{V'}^2 + d^*_{abcf}F_{V'}(M_V^2 + M_{V'}^2)]}{2F_{V'}^2 M_V^2}\,. \tag{3.32}$$

We note that the relation $e_m^{V'} = e_m^V \frac{M_{V'}^2}{M_V^2}$, which stems from our assumption of identical flavor structure for the V and V' nonets, precisely cancels the $\mathcal{O}(Q^0)$, $\mathcal{O}(m_P^4)$ terms in the singly virtual asymptotic limit (in fact they are cancelled to all orders in m_P^2). We anyway recall that our computation only retains $\mathcal{O}(m_P^2)$ corrections.

We find additional constraints, coming from either the η or η' form factors, which are:

- Doubly Virtual η-TFF:
  - $\mathcal{O}(Q^0)$,$\mathcal{O}(m_P^0)$:
$$C_8^W = 0\,. \tag{3.33}$$
  - $\mathcal{O}(Q^{-2})$,$\mathcal{O}(m_P^2)$:
$$c_3^* = e_m^V \frac{16\pi^2 d_{abcd} F_V F_{V'} M_V^2 (M_V^2 - M_{V'}^2) + 32\pi^2 d_3 F_V^2 M_{V'}^2 (M_V^2 - M_{V'}^2) + 24\pi^2 F_\pi^2 M_V^2 M_{V'}^2}{32\sqrt{2}\pi^2 F_V M_V M_{V'}^2 (M_V^2 - M_{V'}^2)}\,. \tag{3.34}$$
- Singly Virtual η-TFF:
  - $\mathcal{O}(Q^0)$,$\mathcal{O}(m_P^2)$:
$$c_3'^* = \frac{M_{V'}^3 (\sqrt{2} e_m^V M_V N_C - 128\pi^2 c_3^* F_V)}{128\pi^2 F_{V'} M_V^3}\,. \tag{3.35}$$
  - $\mathcal{O}(Q^{-2})$,$\mathcal{O}(m_P^2)$:
$$d_2'^* = -\frac{F_V [2 d_2^* F_V M_{V'}^2 + d_f^* F_{V'} (M_V^2 + M_{V'}^2)]}{2 F_{V'}^2 M_V^2}\,. \tag{3.36}$$

We remark that our setting provides π^0, η, η' transition form factors which, in the chiral limit, follow the proportionality $1 : \frac{5C_q - \sqrt{2}C_s}{3} : \frac{5C_q' + \sqrt{2}C_s'}{3}$. This implies that it is not able to accommodate the corrections to eqs. (3.4) due to the anomalous dimension of the singlet axial current [317], which are relevant for the $\eta^{(\prime)}$ cases. Our fit results, however, will not hint to any need for improving on this point presently. Higher order corrections to the first of eqs. (3.4) have been computed using the OPE, and multiply it by $\left(1 - \frac{8}{9}\frac{\delta_P^2}{Q^2}\right)$. For the π^0, $\delta_\pi^2 = 0.20(2)$ GeV^2, determined from QCD sum rules [310]. For the $\eta^{(\prime)}$ the corresponding values have not been computed, although it is reasonable to expect that they deviate from the π^0 result by typical $U(3)$ (and large-N_C) breaking corrections, $\lesssim 30\%$ [47].

Our short-distance constraints on the RχT parameters are compatible with those found in $\tau^- \to P^-[\gamma]\nu_\tau$ [318–320] and $\tau^- \to (VP)^-\nu_\tau$ decays [321]. They are consistent with those derived studying the $\tau^- \to (KK\pi)^-\nu_\tau$ [322] and $\tau^- \to \eta^{(\prime)}\pi^-\pi^0\nu_\tau$ [323] decays provided $F_V = \sqrt{3}F$ [316], a relation that is also favored in $\tau^- \to (\pi\pi\pi)^-\nu_\tau$ decays [324–326], which is driven by the axial-vector current.

We will not quote the $\mathscr{F}_{P\gamma^*\gamma^*}$ form factors obtained after applying the short-distance constraints discussed previously, but after employing the next definitions. First, we introduce the following barred couplings:[9]

$$\bar{d}_{123} = \frac{F_V^2}{3F_\pi^2} d^*_{123}\,, \tag{3.37a}$$

$$\bar{d}_{abcf} = \frac{F_V F_{V'}}{6F_\pi^2} d^*_{abcf}\,, \tag{3.37b}$$

$$\bar{d}_2 = \frac{F_V^2}{3F_\pi^2} d^*_2\,, \tag{3.37c}$$

$$\bar{d}_f = \frac{F_V F_{V'}}{6F_\pi^2} d^*_f\,, \tag{3.37d}$$

$$\bar{d}_3 = \frac{F_V^2}{3F_\pi^2} d_3. \tag{3.37e}$$

Further, the dependence of our results on $\bar{d}_{123}(\bar{d}_2)$ and $\bar{d}_{abcf}(\bar{d}_f)$ suggests us to introduce their following convenient combinations

$$d_{s1} = \left(1 - \frac{M_V^2}{M_{V'}^2}\right)\left(\bar{d}_{abcf} + \frac{M_{V'}^2}{M_V^2}\bar{d}_{123}\right), \tag{3.38a}$$

$$d_{s2} = \left(1 - \frac{M_V^2}{M_{V'}^2}\right)\left(\bar{d}_f + \frac{M_{V'}^2}{M_V^2}\bar{d}_2\right), \tag{3.38b}$$

which appear for single and double virtuality, and

$$d_{d1} = \left(1 - \frac{M_{V'}^2}{M_V^2}\right)\left(\bar{d}_{abcf} + \bar{d}_{123}\right), \tag{3.39a}$$

$$d_{d2} = \left(1 - \frac{M_{V'}^2}{M_V^2}\right)\left(\bar{d}_f + \bar{d}_2\right), \tag{3.39b}$$

that enter only for double virtuality. It is also advantageous to employ

$$d_{d3} = \left(1 - \frac{M_{V'}^2}{M_V^2}\right)^2 \bar{d}_3, \tag{3.40}$$

[9] $\bar{d}_{123}$ and $\bar{d}_2$ were already used in ref. [302].

that is only sensitive to the doubly virtual photon case.

Altogether, this enables to recast the $\mathscr{F}_{P\gamma^*\gamma^*}$ form factors as

$$\begin{aligned}\mathscr{F}_{\pi^0\gamma^*\gamma^*}(q_1^2,q_2^2) =& \Big\{ 96\pi^2 F_\pi^2 (m_\pi^2 M_\rho^2 M_{\rho'}^2 d_{s1} + m_\pi^2 q_1^2 q_2^2 d_{d1} + 2M_\rho^2 q_1^2 q_2^2 d_{d3}) + N_C M_{V'}^2 M_{\rho'}^2 (q_1^2 q_2^2 - M_\rho^4) \\ &+ 4F_\pi^2 \pi^2 q_1^2 q_2^2 (q_1^2 + q_2^2 - 2M_\rho^2) + 24 F_\pi^2 \pi^2 M_{\rho'}^2 \left[(q_1^2+q_2^2) M_\rho^2 - 2 q_1^2 q_2^2 \right] \Big\} \\ &/ \left[24\pi^2 F_\pi (M_\rho^2 - q_1^2)(M_\omega^2 - q_2^2)(M_{\rho'}^2 - q_1^2)(M_{\omega'}^2 - q_2^2) \right] + (q_1 \leftrightarrow q_2)\,,\end{aligned} \tag{3.41}$$

and

$$\begin{aligned}\mathscr{F}_{\eta\gamma^*\gamma^*}(q_1^2,q_2^2) =& \frac{5C_q}{18F\pi^2 (M_\rho^2 - q_1^2)(M_\rho^2 - q_2^2)(M_{\rho'}^2 - q_1^2)(M_{\rho'}^2 - q_2^2)} \times \\ &\Big\{ \pi^2 F_\pi^2 \Big[24 m_\eta^2 d_{s1} M_\rho^2 M_{\rho'}^2 - 192 d_{s2} M_\rho^2 M_{\rho'}^2 \Delta_{\eta\pi}^2 + 24 m_\eta^2 q_1^2 q_2^2 d_{d1} - 192 q_1^2 q_2^2 d_{d2} \Delta_{\eta\pi}^2 + 48 q_1^2 q_2^2 d_{d3} M_\rho^2 \\ &- \left(q_1^2 q_2^2 (2M_\rho^2 - q_1^2 - q_2^2) + 6 M_{\rho'}^2 \left(2 q_1^2 q_2^2 - M_\rho^2 \left(q_1^2 + q_2^2 \right) \right) \right) \Big] + N_C \left(-\frac{M_{V'}^2}{4} \right) \left(M_{\rho'}^2 (M_\rho^4 - q_1^2 q_2^2) \right) \Big\} \\ &+ (q_1 \leftrightarrow q_2) + (5C_q \to -\sqrt{2} C_s, \rho \leftrightarrow \phi, \rho' \leftrightarrow \phi', \Delta_{\eta\pi}^2 \to -\Delta_{2K\eta\pi}^2)\,.\end{aligned} \tag{3.42}$$

The η' form factor is obtained by replacing $C_q \to C_q'$, $C_s \to -C_s'$ and $m_\eta \to m_{\eta'}$ in eq. (3.42).

As in the π^0 case (see the related explanation below eq. (3.22)), the $\eta^{(\prime)}$ transition form factors neither depend on the pion decay constant in the chiral limit, F. These are functions of $C_q^{(\prime)}/F$ and $C_s^{(\prime)}/F$, which in turn depend just on the two mixing angles $\theta_{8/0}$ and decay constants $f_{8/0}$.

3.2.4 TFF global fit

Let us recall the criteria required in the White Paper for taking an evaluation of $a_\mu^{P-\text{pole,HLbL}}$ into account, before dwelling on the details of our fits to the data. These conditions were that (quoting from ref. [5]):

1. in addition to the transition form factor normalization given by the real-photon decay widths, also high-energy constraints must be fulfilled;

2. at least the spacelike experimental data for the singly-virtual TFF must be reproduced;

3. systematic uncertainties must be assessed with a reasonable procedure.

As for the doubly-virtual transition form factor, the experimental data is still very scarce as there is only one measurement by BaBar consisting of five data points for the η' transition form factor with relatively large uncertainties. Therefore, we require our doubly-virtual transition form factors to be not only in accord with the BaBar data for the η' but also in line with the Lattice-QCD data released by the Budapest–Marseille–Wuppertal (BMW) collaboration for the π^0, η and η' doubly-virtual TFFs. As in the singly-virtual case, systematic uncertainties must also be reasonably assessed. We suggested that, for the second White Paper, one should demand –in addition to the three points above– consistency between data-driven P TFF and lattice QCD results, particularly for double virtuality, where these now constitute the best input. This proposal was followed by the Muon g-2 Theory Initiative.

We will start recapitulating the parametric dependence of our P transition form factors, eqs. (3.41) and (3.42), with appropriate substitutions for the η' case.

In principle, a couple of parameters are needed to specify the masses within each V multiplet, M_V, e_m^V, and their primed counterparts. However, our assumption of identical flavor structure for both nonets erases the dependence on $e_m^{V'}$. Therefore, the corresponding spectra will be specified by three independent parameters, that we choose to be $M_V, e_m^V, M_{V'}$. In addition to these, we will have the four parameters associated to the $\eta^{(\prime)}$ mixing, our choice being the decay constants and mixing angles $\{f, \theta\}_{8/0}$. The final five fitted parameters will be those specifying the functional dependence for single and double photon virtuality: $d_{s1,d1,d3}$ for $P = \pi^0$ and also $d_{s2,d2}$ for the $\eta^{(\prime)}$, for a total of 12 fitted parameters. Among them, only $M_{V^{(\prime)}}$ and d_{d3} are $U(3)$-symmetric, while the rest break this approximate flavor symmetry.

Since our focus is on the P-pole contributions to a_μ^{HLbL}, we will only fit spacelike data ($q^2 \leq 0$). The timelike region is more involved within RχT, because resonance widths are needed, which is a next-to-leading order effect in the $1/N_C$ expansion. Although it is phenomenologically clear that this is the leading next-to-leading order effect, other terms at this order may not be negligible and complicate the treatment. Additionally, radiative corrections can be more important in the timelike region, as discussed in [327].

We will use the following data:

- The decay widths $\Gamma(P \to \gamma\gamma)$, corresponding to the transition form factors evaluated for null virtuality (real photons),

$$\Gamma(P \to \gamma\gamma) = \frac{(4\pi\alpha)^2}{64\pi} m_P^3 |\mathscr{F}_{P\gamma\gamma}(0,0)|^2 , \tag{3.43}$$

  are helpful in the characterization of the η-η' mixing and constitute the normalization which receives chiral corrections for low virtualities. These inputs are taken from the PDG [328].[10]

- Transition form factor data from the BaBar [329, 330], Belle [331], CELLO [332], CLEO [333] and LEP [334] experiments, for the singly virtual case.

- There is only one measurement for double virtuality, by BaBar, in the η' channel [335], consisting of five points (which are insufficient to reliably fit our three parameters $d_{d1,d2,d3}$). We will increase the sensitivity to the doubly virtual regime by supplementing BaBar's with Lattice QCD results [294, 296, 297]. Specifically, from the z-expansion performed by the BMW collaboration in [294], we generate three points (at $Q_1^2 = Q_2^2 = 0.1\,, 1.0$, and 4.0 GeV^2) for all three P mesons.[11] These points are shown in Table 3.5. We would like to note here that at least the Lattice data for the η doubly-virtual transition form factor shall be included in the fits to obtain a satisfactory simultaneous description of all three mesons.

As in ref. [302], we will take advantage of stabilization points for the fit, using the results from a previous determination of the $\{f,\theta\}_{8/0}$ parameters [273, 269, 336–339][12]

$$\begin{gathered}\theta_8 = (-21.2 \pm 1.6)^\circ\,, \quad \theta_0 = (-9.2 \pm 1.7)^\circ, \\ f_8 = (1.26 \pm 0.04) F_\pi = (116.2 \pm 3.7)\text{MeV}, f_0 = (1.17 \pm 0.03) F_\pi = (107.9 \pm 2.8)\text{MeV}\,,\end{gathered} \tag{3.44}$$

[10] We are not taking $\Gamma(\eta' \to \gamma\gamma)$ as a separate data point, since it uses LEP data that we are fitting, see next item.

[11] Given that the z-expansion has 6 parameters (with their corresponding correlation) one can generate at most 6 points for having an invertible covariance matrix. Four our analysis, we only generate 3 *lattice* points for each P to avoid high correlations between (neighboring) points [328]. We note that 3 is the minimum number of points we need to fix the three doubly virtual parameters. Had we used 4, 5 or 6 data points we would have obtained highly correlated data, which implies a (close to) non-invertible covariance matrix, that over-represents the lattice information.

[12] The correlation between the fitted parameters describing the singly and doubly virtual behavior (now $d_{s1,s2,d1,d2}$) and $\{f,\theta\}_{8/0}$ is large, like with a single vector resonance multiplet (as in ref. [302]), which calls for adding these extra fit points in order to keep the fit within the physical region.

$Q_1^2 = Q_2^2$ [GeV^2]	0.1	1	4
π^0	0.0194(3)	0.0475(4)	0.0514(12)
0.1	1	0.2758	0.1556
1	0.2758	1	0.1222
4	0.1556	0.1222	1
η	0.0158(11)	0.0440(26)	0.0474(31)
0.1	1	0.6743	0.3006
1	0.6743	1	0.4615
4	0.3006	0.4615	1
η'	0.0251(30)	0.0920(100)	0.0934(114)
0.1	1	0.8658	0.3840
1	0.8658	1	0.4423
4	0.3840	0.4423	1

Table 3.5 Central values, uncertainties and correlation matrix for the doubly virtual transition for factors, generated at three representative values of $q_1^2 = q_2^2$ from the BMW results [294] and used in our fits.

which increase the χ^2 by barely more than unit.

The fits can compensate for the neglected higher V excitations by shifting any of the mass parameters M_V or M_V'. We choose to keep M_ρ close to its PDG value by adding it as a point in the cost function.

We will add to the χ^2 a final fit point, corresponding to $\delta_\pi^2 = 0.20(2)$ GeV^2 (see the discussion below eq. (3.36)).

The cost function for this fit will then be:

$$\chi^2_{\text{Global}} = \chi^2_{\pi^0_{\text{SV}}} + \chi^2_{\eta_{\text{SV}}} + \chi^2_{\eta'_{\text{SV}}} + \chi^2_{\pi^0_{\text{DV}}} + \chi^2_{\eta_{\text{DV}}} + \chi^2_{\eta'_{\text{DV}}} + \sum_{P}^{\text{ExtraPoints}} \left(\frac{P_{\text{exp}} - P_{\text{model}}}{\Delta P_{\text{exp}}} \right)^2 , \quad (3.45)$$

which includes the transition form factor data for single and double virtuality, SV and DV (where the latter incorporate lattice input) for the P channels, and the extra points given by: the $\Gamma(P \to \gamma\gamma)$ decay widths [328], the decay constants and mixing angles of the $\eta - \eta'$ system (3.44), M_ρ [328], and $\delta_\pi^2 = 0.20(2)$ GeV^2 [310].

Regarding the Lattice data, the correlations between the generated data were also considered in each of the $\chi^2_{P_{DV}^{\text{LQCD}}}$, so their contribution to the reduced χ^2 in eq. (3.45) is given by:

$$\chi^2_{P_{DV}^{\text{LQCD}}} = \sum_{i,j=1}^{3} \left(P_i^{\text{LQCD}} - P_i^{\text{R}\chi\text{T}} \right) \left(\text{Cov}_{ij}^{\text{LQCD}} \right)^{-1} \left(P_j^{\text{LQCD}} - P_j^{\text{R}\chi\text{T}} \right) , \quad (3.46)$$

where $P_{i(j)}^{\text{LQCD}}$ and $\left(\text{Cov}_{ij}^{\text{LQCD}}\right)^{-1}$ are, respectively, the central value and the inverse of the covariance matrix of the lattice data given in Table 3.5. [13]

Following previous analyses of the $\mathscr{F}_{P\gamma^*\gamma^*}$ form factors and their contributions to a_μ^{HLbL} [124, 301, 302, 340–352] and owing to our preliminary fits for this work, we will not include BaBar π^0 data in our reference fit, as it is inconsistent with Belle's, that appears more compatible with the predicted (Brodsky-Lepage) asymptotic limit.[14] Additionally, the chiral symmetry relations among the different P form factors data points at the largest measured energies are best satisfied without the BaBar π^0 data. The possible bias induced by excluding this dataset is included as a systematic error.

Our preliminary fits show a big correlation (close to one) of the pairs of parameters $\{d_{s1}, d_{s2}\}$ and $\{d_{d1}, d_{d2}\}$. This motivates us to consider instead their combinations

$$d_{s1} = \langle d_{s1}\rangle + \frac{\sigma_{d_{s1}}}{\sqrt{2}}\left(\sqrt{1+r_s}\, r_{s1} - \sqrt{1-r_s}\, r_{s2}\right), \tag{3.47a}$$

$$d_{s2} = \langle d_{s2}\rangle + \frac{\sigma_{d_{s2}}}{\sqrt{2}}\left(\sqrt{1+r_s}\, r_{s1} + \sqrt{1-r_s}\, r_{s2}\right), \tag{3.47b}$$

and analogously for the doubly virtual case ($s \to d$), in order to minimize their correlations (assuming small interdependences with the rest of the parameters, which is a good approximation). Eqs. (3.47) use the mean values of the preliminary fit ($\langle d_{s1}\rangle, \langle d_{s2}\rangle$) and their uncertainties ($\sigma_{d_{s1}}, \sigma_{d_{s2}}$). The new parameters are r_{s1}, r_{s2}, defined through the original correlation $r_s \sim 1$ (same with $s \to d$).

Our best fit results corresponding to the minimization of the cost function (3.45) are given in table 3.6 with the correlation matrix shown in table 3.7. The comparison of our $\mathscr{F}_{P\gamma^*\gamma^*}(q_1^2, q_2^2)$ to data for single and double virtuality are displayed in figures 3.7 and 3.8.

We will comment now on the big correlations that can still be seen in table 3.7. The redefinition in eq. (3.40) shows that we cannot make any further rotation of parameters to avoid the anticorrelation of -0.837 between M_V' and d_{d3}.[15] We rotated the parameters d_{s1} and d_{s2}, according to eq. (3.23), to minimize their correlation. We note that the rotated parameter r_{s1} has big correlations with both M_V and e_m^V (which is not the case for its partner rotated parameter, r_{s2}). Correlations between the η-η' mixing parameters are slightly larger than in ref. [302], but still reasonable. The large

[13] Taking the covariance matrix into account introduces extra degrees of freedom due to having non-diagonal entries different from zero equal. The additional d.o.f. equal the non redundant entries of the covariance matrix.

[14] We have checked that the fits are worse if these BaBar data is kept, like in ref. [302].

[15] Besides, the correlation between them is non-linear, so we could not proceed analogously.

Parameter	Fit Result
M_V [GeV]	0.752(2)
e_m^V	-0.32(4)
$M_{V'}$ [GeV]	1.933(4)
r_{s1}	0.0(0.6)
r_{s2}	0.0(0.9)
r_s	0.9976
$\langle d_{s1} \rangle$	-1.6(6)
$\langle d_{s2} \rangle$	-0.21(7)
θ_8 [°]	-18.5(6)
θ_0 [°]	-6.9(1.6)
f_8 [MeV]	118.8(4)
f_0 [MeV]	99.4(1.7)
r_{d1}	0.0(0.5)
r_{d2}	0.0(0.9)
r_d	0.9783
$\langle d_{d1} \rangle$	-2.8(2.0)
$\langle d_{d2} \rangle$	-0.31(24)
d_{d3}	-3.48(3)
χ^2_{Global}/d.o.f.	148.0/110

Table 3.6 Our best fit results, with uncertainties in parentheses. The input values of the rotations (3.47) are also given, where the errors in the $\langle d \rangle$ are the σ_d's.

	M_V	e_m^V	$M_{V'}$	r_{s1}	r_{s2}	θ_8	θ_0	f_8	f_0	r_{d1}	r_{d2}	d_{d3}
M_V	1	0.739	−0.035	0.501	−0.065	0.035	−0.008	−0.077	−0.025	0.357	−0.152	0.371
e_m^V	0.739	1	−0.106	0.614	−0.120	−0.009	0.019	−0.099	−0.053	0.300	−0.145	0.344
$M_{V'}$	−0.035	−0.106	1	−0.035	−0.114	−0.032	0.202	0.063	−0.030	−0.446	0.399	−0.837
r_{s1}	0.501	0.614	−0.035	1	0.226	0.335	0.029	−0.014	−0.113	0.217	−0.097	0.186
r_{s2}	−0.065	−0.120	−0.114	0.226	1	0.185	−0.219	0.089	0.431	0.026	0.211	0.082
θ_8	0.035	−0.009	−0.032	0.335	0.185	1	0.002	−0.657	−0.069	0.075	0.071	0.015
θ_0	−0.008	0.019	0.202	0.029	−0.219	0.002	1	−0.001	0.605	−0.069	−0.041	−0.187
f_8	−0.077	−0.099	0.063	−0.014	0.089	−0.657	−0.001	1	0.032	−0.047	0.002	−0.084
f_0	−0.025	−0.053	−0.030	−0.113	0.431	−0.069	0.605	0.032	1	−0.011	0.165	0.030
r_{d1}	0.357	0.300	−0.446	0.217	0.026	0.075	−0.069	−0.047	−0.011	1	−0.152	0.140
r_{d2}	−0.152	−0.145	0.399	−0.097	0.211	0.071	−0.041	0.002	0.165	−0.152	1	−0.392
d_{d3}	0.371	0.344	−0.837	0.186	0.082	0.015	−0.187	−0.084	0.030	0.140	−0.392	1

Table 3.7 Correlation matrix between the 12 fitted parameters of the best fit.

correlation between M_V and e_m^V is entirely a result of fixing M_ρ to its PDG value. In our preliminary fits, floating both parameters independently, their correlation was only ~ 0.22.

We will discuss next the central values of our reference fit:

- M_V is typically smaller than the results obtained in single resonance approximations ($\sim$ 800 MeV [312, 353]) but the value of $M_{\rho(\phi)}$ is still compatible, at 1(2) σ, with the PDG [328].

- As commented above, e_m^V is highly correlated with M_V because we are requiring that $M_V^2 - 4e_m^V m_\pi^2 \sim M_\rho^2$. Nevertheless, the value of this flavor symmetry breaking parameter is compatible at less than one standard deviation with the best fit result in ref. [302].

- One should not expect $M_{V'}^2 - 4e_m^{V'} m_\pi^2 \sim M_{\rho'}^2$, because $M_{V'}^2$ (we recall that we are assuming $e_m^{V'} M_V^2 = e_m^V M_{V'}^2$) absorbs the effect of the neglected higher V excitations, so its fitted value $M_{V'} \sim 1.933$ GeV appears reasonable.

- Concerning the η-η' mixing parameters, agreement of our fitted values with the input (3.44) is acceptable, with differences being $1.2(0.70)\sigma$ for $\theta_{8(0)}$, and $0.4(1.9)\sigma$ for $f_{8(0)}$.

- For our best fit values, eq. (3.40) implies that $d_{d3} \sim 30\bar{d}_3$, with $\bar{d}_3 \sim d_3$. Short-distance QCD constraints on the VVP Green's function [280, 316] determine $d_3 \sim -0.126$, corresponding to a d_{d3} with a deviation of less than 10% from our best fit value.

- Best fit values for the parameters $r_{s1,s2}$ and $r_{d1,d2}$ are compatible with zero. Little information is known on the couplings of the V' multiplet that enter the definition of the original couplings $d_{s1,s2}$ and $d_{d1,d2}$. If we set them to zero for a rough estimate and take into account that $\bar{d}_{123,2} \sim d_{123,2}$, we can use that $d_{123} \sim 1/24$ [280, 316] (again from the short-distance behaviour of the VVP Green's function), to estimate that $d_{s1} \sim 1/4$ and $d_{d1} \sim 5/4$, which agree within 1 and 3σ with our best fit. According to refs. [354–357] $d_2 = 0.08 \pm 0.08$, that again yields estimates d_{s2} and d_{d2} in agreement with our best fit results.

The comparison of the transition form factors corresponding to our best fit results (table 3.6) to data in the singly virtual regime for the π^0, η and η' mesons in fig. 3.7 is very satisfactory but for a few points that seem to be outliers, given the general trend shown by the data. At the largest measured virtualities our transition form factors seem to approach faster the Brodsky-Lepage limit than the data, that have large uncertainties there, anyway.

An analogous comparison for double virtuality is shown in fig. 3.8, where the relevance of the lattice data is evident -these data are extremely helpful in our analysis to constrain the doubly-virtual parameters $d_{d1,d2,d3}$. We note that a couple of low-energy points in the η (η') case are below (above) our curves, although the statistical significance of this tension is moderate. As a sanity check, we have verified that the comparison of our best fit results to lattice QCD exhibits a similar pattern

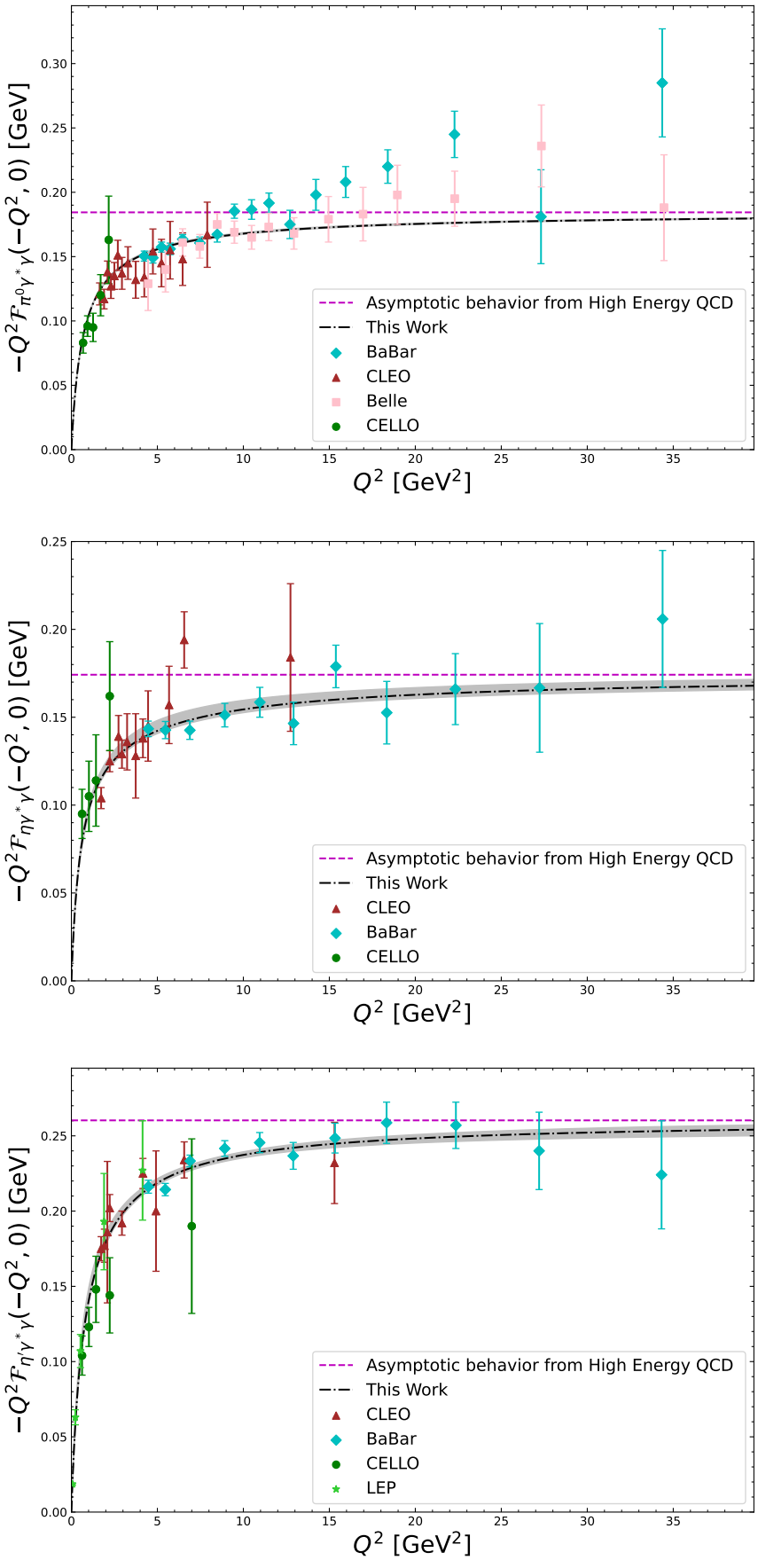

Fig. 3.7 The transition form factors corresponding to our best fit results (table 3.6) are compared to data in the singly virtual regime for π^0, η and η'. BaBar data for the π^0 case [329] is shown for completeness, but it was not used in our reference fits.

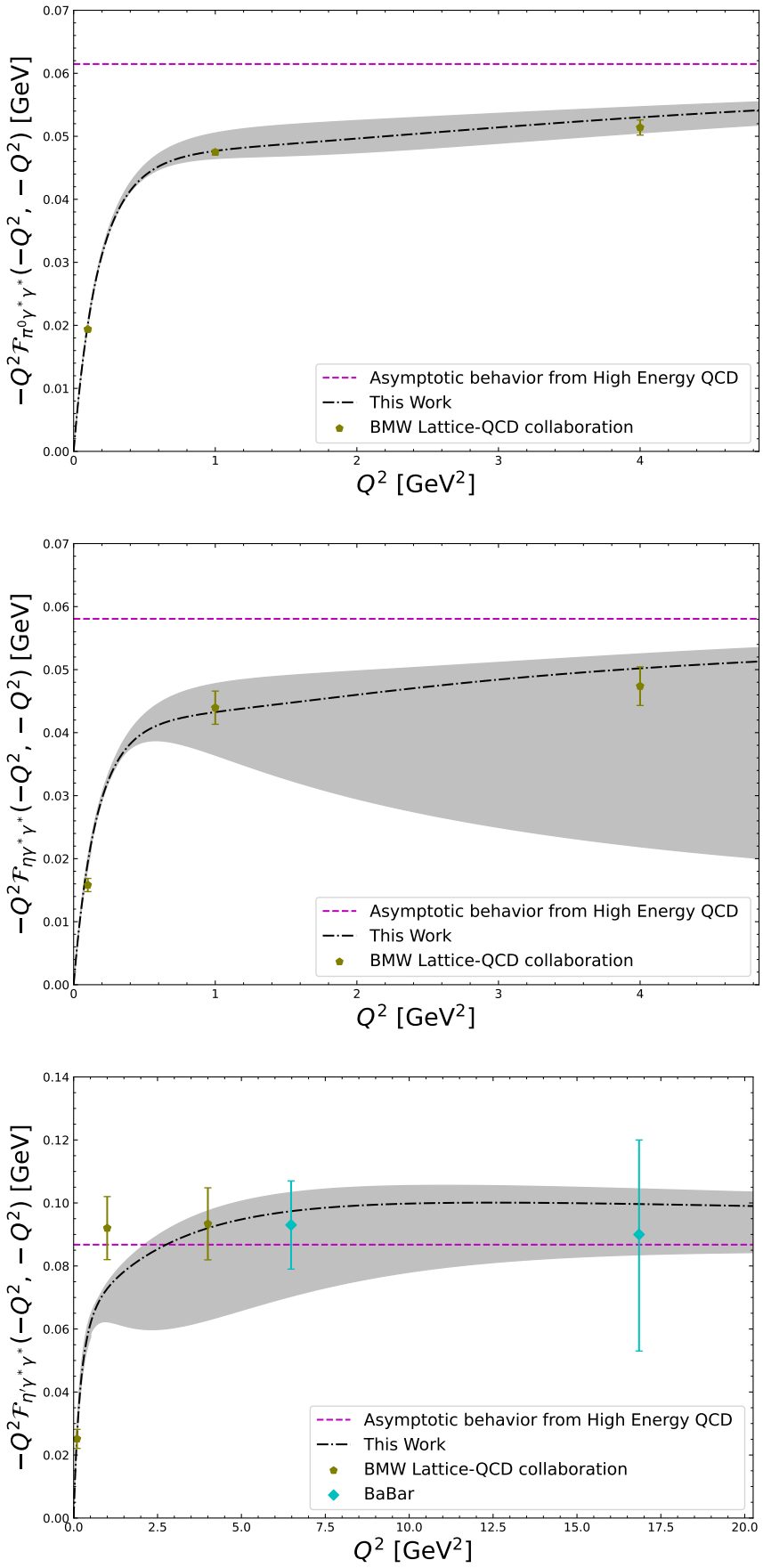

Fig. 3.8 The transition form factors corresponding to our best fit results (table 3.6) are compared to data in the doubly virtual regime for π^0, η and η'.

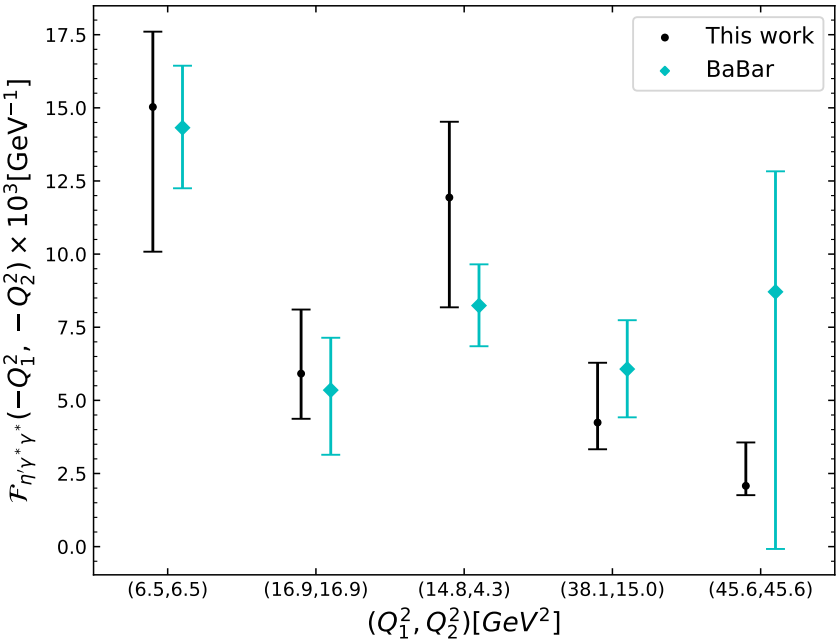

Fig. 3.9 BaBar data (cyan diamonds) for the η' doubly-virtual transition form factor [335] as compared to our best fit results (black circles) from table 3.6 including statistical and systematic errors.

in the singly virtual case.[16] In addition, in fig. 3.9 we show a comparison of the standalone BaBar measurements of the η' doubly-virtual transition form factor, which includes non-diagonal Q^2 data points, together with our best fit results. As seen, the results are in good agreement, while the experimental statistics is not sufficiently precise yet as to further constrain the parameters of double virtuality.

We have extracted the slope parameters, $\{b,c,d\}_P$, defined from

$$\lim_{Q^2\to 0} \mathscr{F}_{P\gamma^*\gamma}(-Q^2,0) = \mathscr{F}_{P\gamma\gamma}(0,0)\left(1-\frac{b_P}{m_P^2}Q^2+\frac{c_P}{m_P^4}Q^4-\frac{d_P}{m_P^6}Q^6+\cdots\right), \tag{3.48}$$

corresponding to our best fit results, and compared them to ref. [47] in table 3.8. As in this reference, we are not quoting our results for d_π, since the sensitivity of the data and our fit to this parameter is pretty small, because of chiral suppression. The agreement for b_P (and for c_π) is very satisfactory, while the accordance with the other parameters shown is quite good. In the last row shown for each channel, we recall

[16] We cannot add these data to our fit since they would be double counted (they are obtained from the double virtuality data, setting one photon on-shell). We could have decided to use this information for the singly virtual case, but it was much more useful to employ it for double virtuality in our case, as we did.

Parameter	Our result	Values in [47]	Difference between both
b_π	0.03163(16)	0.0321(19)	0.2σ
c_π	0.000862(6)	0.00104(22)	0.8σ
π_∞	$2F_\pi$	$2F_\pi$	0σ
b_η	0.600(10)	0.572(8)	1.6σ
c_η	0.316(7)	0.333(9)	1.1σ
d_η	0.164(4)	0.195(20)	1.3σ
η_∞[GeV]	0.174(3)	0.180(12)	0.4σ
$b_{\eta'}$	1.26(2)	1.31(3)	1.0σ
$c_{\eta'}$	1.86(4)	1.74(9)	0.9σ
$d_{\eta'}$	2.82(6)	2.30(22)	1.9σ
η'_∞[GeV]	0.260(4)	0.255(4)	0.6σ

Table 3.8 Low-energy slope parameters $\{b,c,d\}_P$ and Brodsky-Lepage parameter (P_∞) from our best fit result and their comparison with the values used in [47].

the coefficient of the $\mathcal{O}(1/Q^2)$ term in the single asymptotic (Brodsky-Lepage) limit (P_∞), see eq. (3.4b), for which both analyses agree within one standard deviation.

Finally, it is important to remark that, in addition to having reproduced the Short-Distance Constraints (SDC) for all 3 mesons and having a good agreement with the other successful descriptions at intermediate energies, the decay widths $\Gamma(P\to\gamma\gamma)$ are also in great accord with the experimental values -we have obtained a value of $7.67(9)$ eV for π^0 (which is only at 0.6σ from the measurements [358, 359]), $497(13)$ eV for the η (0.6σ from [360]) and $4.3(2)$ KeV for η' (merely 0.2σ from [334]). This agreement is noteworthy, given the slight tension (in the π^0 and η cases) between the lattice QCD results for these widths and the PDG values (see also our footnote 13).

3.3 Equivalence of RχT TFF with the Canterbury Approximants

In contrast with the case of the π^0 pole, where evaluations from many models had been done [290, 361, 47, 302, 292, 49, 50, 293, 294], in the White Paper 2020 of the muon $g-2$ theory initiative [5], the $\eta-\eta'$ contributions were taken from [47] and there were not other evaluations of these contributions satisfying the White Paper quality criteria by then. Recent determinations of these can be found in Refs. [294, 362, 62, 68, 363]. The rational approach of ref. [47] is based on the so called Canterbury Approximants [364–368]. We will translate our RχT description,

including two multiplets of vector resonances, to the CA language and comment on the corresponding implications in this section [17].

3.3.1 Definition of Canterbury Approximants

Canterbury Approximants (CAs) are described by a rational function $f(x,y)$ of polynomials which are analytic, symmetric under $x \leftrightarrow y$ and satisfy the accuracy-through-order conditions [47, 364–368]. A C_M^N is defined then as:

$$C_M^N(x,y) = \frac{R_N(x,y)}{Q_M(x,y)} = \frac{\sum_{i,j=0}^{N} a_{i,j} x^i y^j}{\sum_{i,j=0}^{M} b_{i,j} x^i y^j}\,. \tag{3.49}$$

Ref. [47] mentioned that both $C_{N+1}^N(Q_1^2,Q_2^2)$ and $C_N^N(Q_1^2,Q_2^2)$ work for describing the high-energy behavior prescribed by perturbative QCD [311, 312, 309, 310] on the pseudoscalar transition form factor, eqs. (3.4). Choosing one or the other depends on whether dropping the last term(s) of the polynomial from R_N or Q_M in eq. (3.49). Given this constraint, the convergence and Bose symmetry are guaranteed at arbitrary virtualities for both photons. Increasing N and/or M implies incrementing the freedom of the model, so that an optimal choice of them must be done with both freedom and over-fitting in mind.

3.3.2 CA to $R\chi T$ Mapping

In [47], a C_2^1 was used[18] (we do not write a subscript P in the α and β coefficients in eq. (3.50), although they are different for π^0,η,η'):

$$C_2^1(Q_1^2,Q_2^2) = \frac{\mathscr{F}_{P\gamma\gamma}(0,0)\left(1+\alpha_1(Q_1^2+Q_2^2)+\alpha_{1,1}Q_1^2Q_2^2\right)}{1+\beta_1(Q_1^2+Q_2^2)+\beta_{1,1}Q_1^2Q_2^2+\beta_2(Q_1^4+Q_2^4)+\beta_{1,2}Q_1^2Q_2^2(Q_1^2+Q_2^2)}. \tag{3.50}$$

[17] Unfortunately, it is impossible to relate analytically our framework to the dispersive approach [49], which currently provides the reference result for the pseudoscalar pole contributions.

[18] The $F_{P\gamma\gamma}(0,0)$ was factored out to provide with a physical meaning the normalization constant, given $a_0 = b_0 = 1$. Besides, the $\beta_{2,2}$ term was dropped -as commented before- in order to correctly account for the high-energy behavior.

The low-energy behavior, given by the $Q_1^2, Q_2^2 \to 0$ expansion [369], is:

$$\mathscr{F}_{P\gamma^*\gamma^*}(Q_1^2,Q_2^2) = \mathscr{F}_{P\gamma\gamma}(0,0)\left(1 - \frac{b_P}{m_P^2}(Q_1^2+Q_2^2) + \frac{c_P}{m_P^4}(Q_1^4+Q_2^4) + \frac{a_{P;1,1}}{m_P^4}(Q_1^2Q_2^2) - \frac{d_P}{m_P^6}(Q_1^6+Q_2^6) + \cdots\right), \tag{3.51}$$

and has been widely studied for all 3 particles (see Table VI of ref. [47]). The values of $\mathscr{F}_{P\gamma\gamma}(0,0)$, b_P and c_P, together with the high-energy behavior constraints

$$\lim_{Q^2\to\infty} \mathscr{F}_{P\gamma^*\gamma^*}(Q^2,Q^2) = \frac{P_\infty}{3}\left(\frac{1}{Q^2} - \frac{8}{9}\frac{\delta_P^2}{Q^4}\right) + \mathscr{O}(Q^{-6}), \tag{3.52a}$$

$$\lim_{Q^2\to\infty} \mathscr{F}_{P\gamma^*\gamma}(Q^2,0) = \frac{P_\infty}{Q^2}, \tag{3.52b}$$

impose 6 restrictions to the form factors in eq. (3.50), leaving only $\alpha_{1,1}$ as a free parameter.[19] However, $\alpha_{1,1}$ could not be fitted therein, since it is sensitive only to the doubly virtual case, for which no data was available by then.[20] Now, there are both experimental data [335] (only for η') and lattice QCD evaluations [294, 296, 297] which can be -as we pioneeringly illustrated in this work, ref. [62]- used to generate data in order to complete this description. An updated version of the CA study is included in this work, both for its intrinsic interest and for comparing to our results in the previous section.

Our form factors satisfying short-distance QCD constraints, eqs. (3.41) and (3.42) -with trivial changes for $\eta \to \eta'$- correspond to a C_2^2 and a C_4^4 CA, respectively. For the π^0 case the CA coefficients matching our parametrization eq. (3.41) are given in table 3.9.

We make the following important remarks concerning the results in table 3.9:

- The C_2^2 model has 4 more parameters than the C_2^1 model used in [47]. However, two of them vanish, consequently the degrees of freedom increase by two.
- By construction, our model based on RχT reproduces the dominant asymptotic behavior of the transition form factors, but the correction given by δ_π^2 is only included as a fit point in the χ^2, as opposed to the C_2^1 case, where it is used to fix a coefficient.

[19] For the $\eta^{(\prime)}$ cases, the asymptotic constraint on P_∞ in eq. (3.52b) was traded by the low-energy one on d_P (we recall there is no sensitivity to it for $P = \pi^0$), see table 3.8.

[20] In ref. [47] the range for $\alpha_{P\,1,1}$ was taken so as to avoid poles for the $C_2^1(Q_1^2,Q_2^2)$ in the spacelike region.

CA Coefficient	RχT result
$F_{\pi^0\gamma\gamma}(0,0)$	$\frac{8d_{s1}F_\pi m_\pi^2}{M_\rho^2 M_{\rho'}^2} - \frac{M_V^2 N_C}{12F_\pi M_\rho^2 \pi^2}$
$\alpha_1^\pi F_{\pi^0\gamma\gamma}(0,0)$	$-\frac{2F_\pi}{M_\rho^2 M_{\rho'}^2}$
$\alpha_{1,1}^\pi F_{\pi^0\gamma\gamma}(0,0)$	$-\frac{4F_\pi}{M_\rho^4 M_{\rho'}^2} + \frac{2F_\pi\left(-M_\rho^2+12d_{d1}m_\pi^2+24d_{d3}M_\rho^2\right)}{3M_\rho^4 M_{\rho'}^4} + \frac{M_V^2 N_C}{12F_\pi \pi^2 M_\rho^6}$
$\alpha_2^\pi F_{\pi^0\gamma\gamma}(0,0)$	0
$\alpha_{1,2}^\pi F_{\pi^0\gamma\gamma}(0,0)$	$-\frac{F_\pi}{3M_\rho^4 M_{\rho'}^4}$
$\alpha_{2,2}^\pi F_{\pi^0\gamma\gamma}(0,0)$	0
β_1^π	$M_\rho^{-2}\left(1+\frac{M_V^2}{M_{V'}^2}\right)$
$\beta_{1,1}^\pi$	$M_\rho^{-4}\left(1+\frac{M_V^2}{M_{V'}^2}\right)^2$
β_2^π	$M_\rho^{-2}M_{\rho'}^{-2}$
$\beta_{1,2}^\pi$	$M_\rho^{-4}M_{\rho'}^{-2}\left(1+\frac{M_V^2}{M_{V'}^2}\right)$
$\beta_{2,2}^\pi$	$M_\rho^{-4}M_{\rho'}^{-4}$

Table 3.9 Translation of our RχT result, eq. (3.41) to CA, for the π^0.

- The slope parameters from [369] are imposed on the C_2^1 up to c_π. In our case (RχT) they are not, rather we check (satisfactorily) compatibility with the results for them in ref. [47] for our best fit results (see table 3.8).

- For our RχT results, in the π^0 case, there are only two independent terms in the denominator of the CA, that we choose as β_1 and β_2. For the η' we have $\beta_{1,2,3,4}$, which are all independent. The others can be written as $\beta_{i,j} = \beta_i\beta_j$, so they are not quoted in the following.

- In general, there is only 1 free parameter in C_2^1 (3 for C_2^2) per channel, which can now be fitted to 3 points for the π^0 and η (from lattice), and 8 for the η' (from lattice and the BaBar measurement). In our RχT description there are 12 parameters which were simultaneously fitted to 122 data points[21] in the three channels, from different experiments [333, 332, 334, 329–331, 335] (including PDG [328]) and lattice data, generated from ref. [294].

For the $\eta^{(\prime)}$ cases, working with such a high order CA (C_4^4) is not feasible. For illustrative purposes, we obtained the corresponding CA in the chiral limit, which is a C_2^2. In fact, the same one describes the three cases (π^0, η, η'), provided we factor

[21] We included eight additional stabilization points, see the paragraphs before eq. (3.45).

out the overall $1:(5C_q-\sqrt{2}C_s)/3:(5C'_q+\sqrt{2}C'_s)/3$ dependence (c_P). The translation of the chiral limit of our results, eqs. (3.41) and (3.42), to CA is given in table 3.10.

CA Coefficient	Chiral THS coefficient
$F_{P\gamma\gamma}(0,0)$	$-\frac{c_P N_C}{12F_\pi\pi^2}$
$\alpha_1 F_{P\gamma\gamma}(0,0)$	$-\frac{2c_P F_\pi}{M_V^2 M_{V'}^2}$
$\alpha_{1,1} F_{P\gamma\gamma}(0,0)$	$c_P\left(\frac{16\bar{d}_3 F_\pi (M_V^2-M_{V'}^2)^2}{M_V^6 M_{V'}^4}+\frac{-\frac{8F_\pi^2(M_V^2+6M_{V'}^2)}{M_{V'}^4}+\frac{N_C}{\pi^2}}{12F_\pi M_V^4}\right)$
$\alpha_2 F_{P\gamma\gamma}(0,0)$	0
$\alpha_{1,2} F_{P\gamma\gamma}(0,0)$	$-\frac{c_P F_\pi}{3M_V^4 M_{V'}^4}$
β_1	$\left(\frac{1}{M_V^2}+\frac{1}{M_{V'}^2}\right)$
β_2	$\frac{1}{M_V^2 M_{V'}^2}$

Table 3.10 Translation of the chiral limit of our RχT result, eqs. (3.41) and (3.42), to CA, for $P=\pi^0,\eta,\eta'$.

In our updates of the CA results of ref. [47], to be presented below, we have decided to use the same methodology that was employed in this reference for the π^0 also for the $\eta^{(\prime)}$. That is, we will not trade the constraint on P_∞ (Brodsky-Lepage) by the one on d_P for $P=\eta^{(\prime)}$.[22] We will also consider the fits using C_2^2 enforcing the constraints that ensure that no poles be generated in the spacelike region.

Therefore, in this section we will be comparing the following fits to data:

- Our best fit result, described in sec. 3.2.4, dubbed RχT below.
- The results obtained considering the chiral limit of eqs. (3.41) and (3.42), which correspond to a C_2^2 CA, as indicated in table 3.10. This is christened χRχT in what follows.
- The update of the results in ref. [47], using a C_2^1. In this case, we change their procedure for the $\eta^{(\prime)}$ cases, as explained in the previous paragraph.

[22] We decided to do this because it is consistent with the RχT procedure, see the comparison in table 3.8. We have checked that proceeding in complete analogy to ref. [47] yields slightly larger χ^2 in the best fit results.

- The fit with a C_2^2 [23] demanding that no poles are generated in the unphysical region. This has also been done using the results in table 3.10 to determine the C_2^2.

The results of these fits are shown in table 3.11. According to them, the best agreement with data is obtained for RχT, and only C_2^2 yields fits with a reduced $\chi^2/\text{dof} \sim 1$ as well. Figures 3.10 and 3.11 extend Figs. 3.7 and 3.8 by adding the C_2^2 results. In the doubly virtual case, Fig. 3.11, it is clear that there are very few points to fit the three coefficients that are independent for each pseudoscalar in C_2^2, causing all 3 pseudoscalar mesons to have the parameter β_{22}^P at the limit of the allowed range; consequently, there are poles within the 1σ region of these parameterizations of the TFFs. On the contrary, the 3 couplings sensitive to double virtuality in RχT are related by flavor symmetry, so they are fitted to 14 data points, which prevents overfitting. This shows that, among the four options considered, $R\chi T$ is the best parametrization to account for all data.

Particle	$\chi^2_{\text{R}\chi\text{T}}/\text{dof}$	$\chi^2_{\chi\text{R}\chi\text{T}}/\text{dof}$	$\chi^2_{C_2^1}/\text{dof}$	$\chi^2_{C_2^2}/\text{dof}$
π^0	33.3/39	58.2/40	234.0/40	35.18/38
η	47.7/27	61.6/29	63.0/31	44.9/29
η'	50.3/36	208.5/38	42.39/40	33.6/38

Table 3.11 Our best fit (section 3.2.4) and its chiral limit are compared to the results obtained using CA. In the C_2^1, case we obtained $a_{P;1,1} = 0.0048(9), 0.75(13), 2.677(25)$ for $P = \pi^0, \eta, \eta'$, respectively.

3.4 π^0,η, η'-pole contributions to a_μ within $R\chi T$

The computation of the pseudoscalar contributions to a_μ^{HLbL} is performed by means of the Master Formula in eq. (1.28) with the scalar functions of eq. (3.8). However, as mentioned in sec. 3.2, before the development of the Master Formula, an equivalent expression had been found for the pseudoscalar poles. According to ref. [370]:

$$a_\mu^{P\text{-pole}} = -\frac{2\alpha^3}{3\pi^2}\int_0^\infty dQ_1 dQ_2 \int_{-1}^{1} dt\sqrt{1-t^2}Q_1^3Q_2^3\left[F_1P_6I_1(Q_1,Q_2,t) + F_2P_7I_2(Q_1,Q_2,t)\right], \tag{3.53}$$

[23] This was performed as a minimal extension of the work in [47], with the same updating procedure previously described. As mentioned before, this model has 3 free parameters sensitive exclusively to double virtuality data.

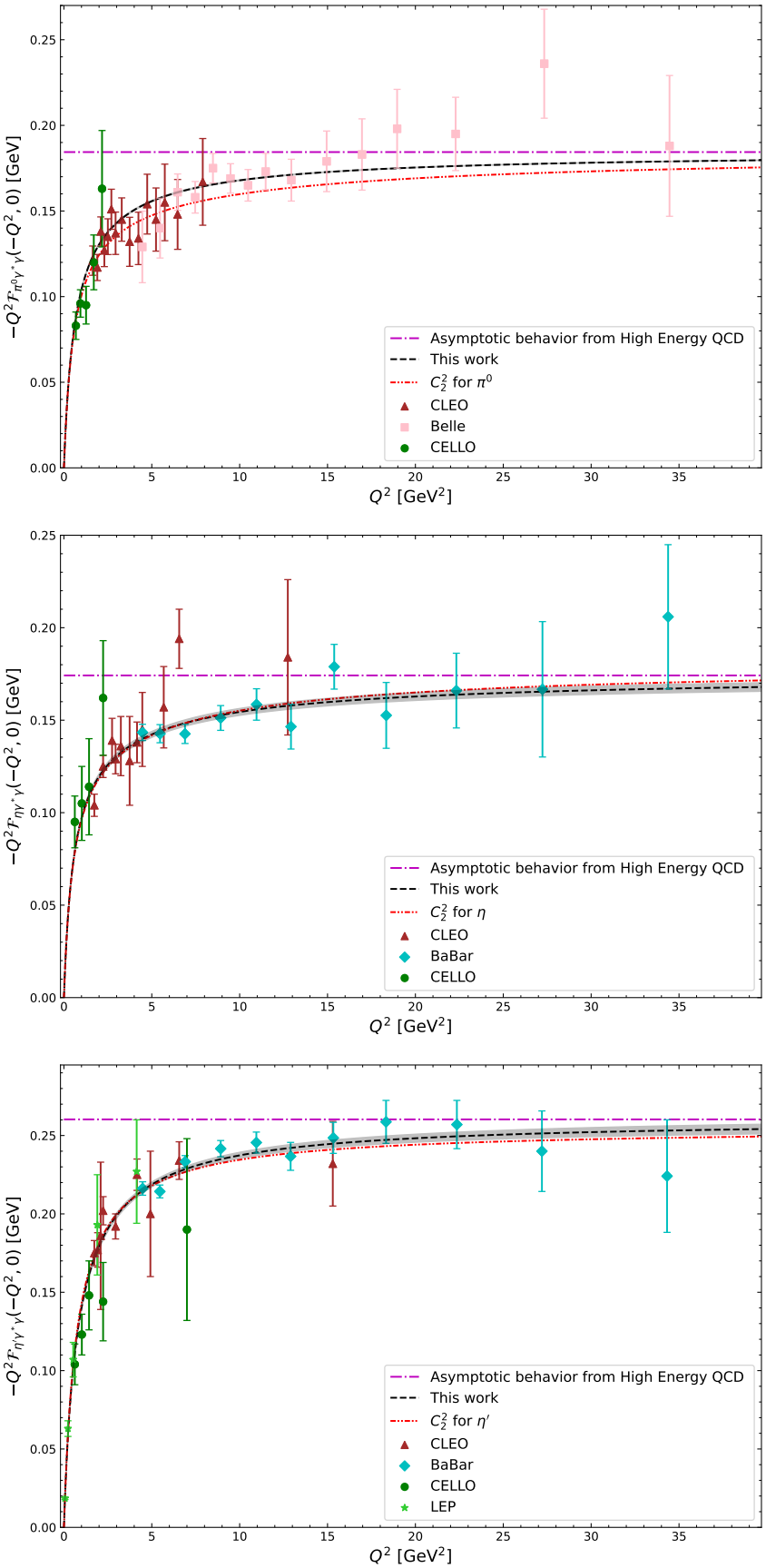

Fig. 3.10 The comparison between our best fit (table 3.6) for RχT and the C_2^2 results in the singly virtual regime for π^0, η and η'. In contrast with Figures 3.7 and 3.8, only the 1σ statistical errors are shown for the curve of our fit.

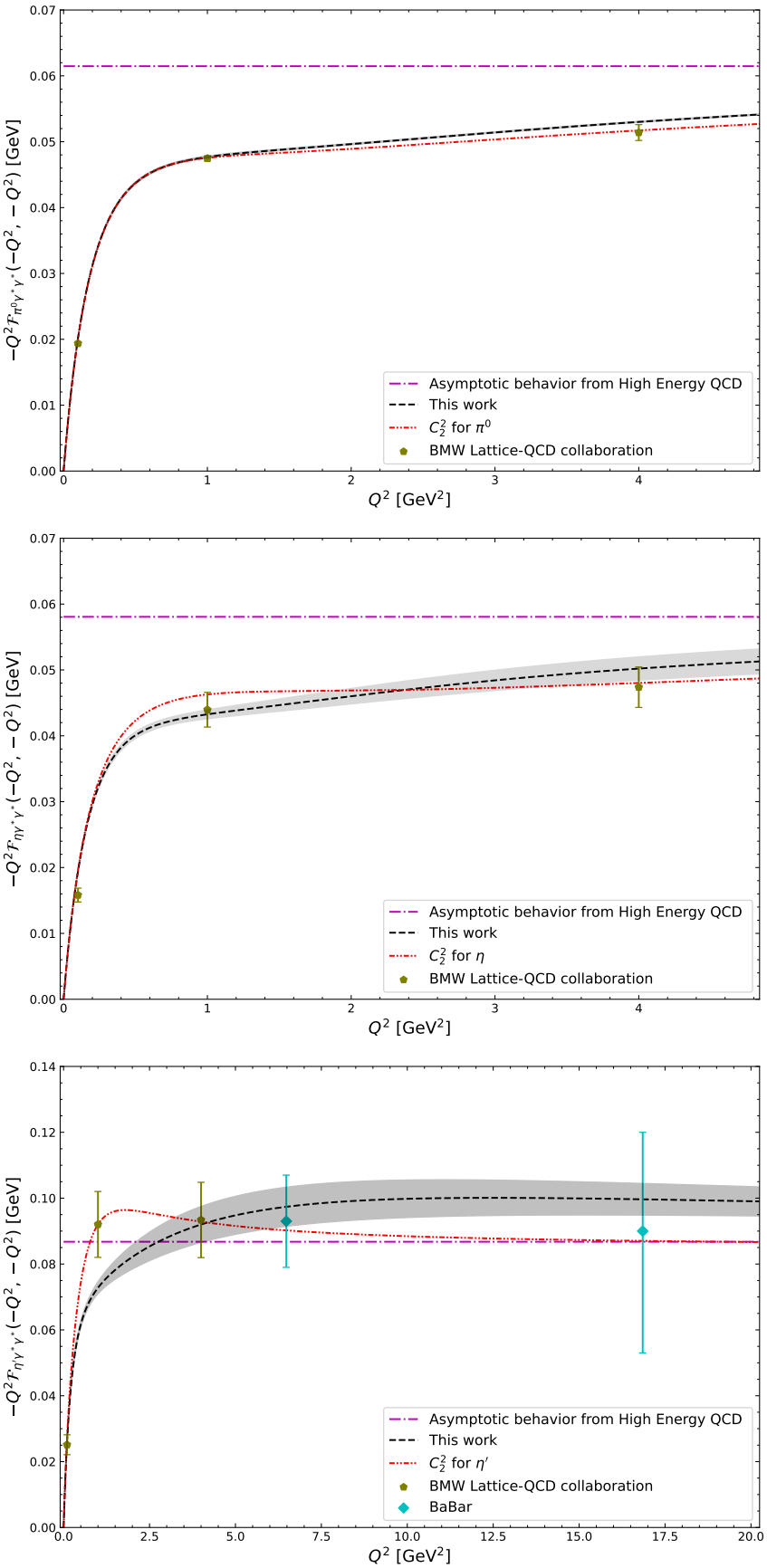

Fig. 3.11 The comparison between our best fit (table 3.6) for RχT and the C_2^2 results in the doubly virtual regime for π^0, η and η'. In contrast with Figures 3.7 and 3.8, only the 1σ statistical errors are shown for the curve of our fit.

where α is the fine structure constant, $Q_i = |Q_i|$, $t = \cos\theta$, $P_6 = \frac{1}{Q_2^2+m_\pi^2}$, $P_7 = \frac{1}{Q_3^2+m_\pi^2}$, $Q_3^2 = Q_1^2 + Q_2^2 + 2Q_1Q_2t$ and the $I_{1(2)}(Q_1, Q_2, t)$ are given in [370]. The information of the transition form factors is encoded in:

$$F_1 = \mathscr{F}_{P\gamma^*\gamma^*}(Q_1^2, Q_3^2)\mathscr{F}_{P\gamma^*\gamma}(Q_2^2, 0)\,. \tag{3.54a}$$

$$F_2 = \mathscr{F}_{P\gamma^*\gamma^*}(Q_1^2, Q_2^2)\mathscr{F}_{P\gamma^*\gamma}(Q_3^2, 0)\,. \tag{3.54b}$$

3.4.1 Assessment of systematic theory uncertainties

Besides the evaluation of the central value for the pole contributions and their respective propagation of statistical errors coming from the global fit, there are theory uncertainties induced by the limitations of our $R\chi T$ description of the P-TFFs.

Specifically, we will consider the one stemming from the use of different data sets (whether including/excluding BaBar π^0 single virtual data in the global fit), the one coming from cutting the infinite tower of V and P states to two multiplets, the one arising from neglecting subleading corrections in the large-N_C expansion and, finally, the one coming from including/excluding the Lattice QCD data for the doubly virtual TFF in our fits. We have verified that other corrections (from e.g. neglecting higher-order terms in m_P^2, modifying the η-η' mixing parameters according to the NNLO $U(3)$ χPT fit to lattice data of ref. [371], etc.) are negligible with respect to these (see also the related discussion in ref. [302], our relative errors on them are very similar to those reported therein).[24] Although its associated uncertainty is also negligible, we close this section by discussing the asymptotic behaviour for asymmetric double virtualities [25].

Use of all available experimental data

There are several data sets for the P-TFF. Analyses in the literature differ by including/excluding some experimental data or imposing cuts to the fitted data. In this work, as in ref. [302], BaBar data for the single virtual region of π^0 was excluded for the aforementioned reasons in the global fit of the three channels. An estimation of the error induced by this decision was computed by comparing the evaluation of

[24] Also negligible are the uncertainties associated to either using π^0 Lattice data from ref. [295] or [294], and to including or not additional subleading OPE constraints (see table 3.12).

[25] This last point refers to the fact that we have imposed a discrete amount of SDCs (single and symmetric doubly virtual), even though this behaviour is given for all asymmetries, as shown in eq. (3.5), which are not fulfilled exactly by our $R\chi T$ approach.

the $a_\mu^{P\text{-pole}}$ obtained by including or excluding these data. The obtained difference for each pseudoscalar meson is:

$$\left(\Delta a_\mu^{\pi^0\text{-pole}}\right)_{\text{Data Sets}} = +0.20 \times 10^{-11}, \tag{3.55a}$$

$$\left(\Delta a_\mu^{\eta\text{-pole}}\right)_{\text{Data Sets}} = -0.02 \times 10^{-11}, \tag{3.55b}$$

$$\left(\Delta a_\mu^{\eta'\text{-pole}}\right)_{\text{Data Sets}} = +0.02 \times 10^{-11}. \tag{3.55c}$$

As expected, the induced error occurs mainly in the evaluation of $a_\mu^{\pi^0\text{-pole}}$; however, small deviations are present for η and η' because RχT connects the TFFs of the 3 particles trough chiral symmetry.

Finite number of resonances

Even though the full RχT has an infinite tower of resonances in the $N_C \to \infty$ limit, cutting to a finite number of them is required for practical reasons (unless there exists an exact resummation mechanism, which usually only happens for the simplest toy models). This analysis includes -besides the pseudo-Goldstone bosons P- two resonance multiplet states for the vector mesons V, V', and one for the pseudoscalar mesons P'. A minimal extension to this model was performed earlier in ref. [298] -referred as three-multiplet resonance-, where a third V'' and P'' were included, albeit in the chiral limit, and only for the π^0 meson (where this approximation is more reliable).

An estimation of the systematic error caused by having a finite number of resonances was performed using the results from this three-multiplet resonance model and a fit to the data of our model in the chiral limit, χRχT. In ref. [298], the value of $a_\mu^{\pi^0\text{-pole}}$ was computed using the π^0 lattice data from ref. [295] up to $Q^2 = 4\text{GeV}^2$ to fit their free parameters, so an equivalent analysis (with the same dataset) was performed in χRχT to fit the 3 free parameters of table 3.10 -with the mixing parameters fixed to the results of our best fit– using only the π^0 lattice data points from ref. [294]. For η and η', there is no computation of the pole contributions to the HLbL piece of a_μ, so we cast the overall c_P flavor-space-rotation factor (defined just above table 3.10) to compute a fair estimate on these contributions within the three-multiplet resonance model. The resulting differences for each particle are:

$$\left(\Delta a_\mu^{\pi^0\text{-pole}}\right)_{\text{finite spectrum}} = +1.8 \times 10^{-11}, \tag{3.56a}$$

$$\left(\Delta a_\mu^{\eta\text{-pole}}\right)_{\text{finite spectrum}} = +1.0\times 10^{-11}\,, \tag{3.56b}$$

$$\left(\Delta a_\mu^{\eta'\text{-pole}}\right)_{\text{finite spectrum}} = +1.4\times 10^{-11}\,. \tag{3.56c}$$

Subleading corrections in $1/N_C$

We have considered the contributions at leading order in the large-N_C expansion in our computation. We have estimated the impact of neglected higher-order effects by considering the modification to the ρ propagator coming from pion and kaon loops at next-to-leading order (NLO).[26] Although a proper analysis of the SD behavior for the TFF should be done, we will use the result from the electromagnetic form factor of the pion [372], which will amount to the following replacement (the ρ propagator remains real in the whole space-like region, $q^2<0$)

$$M_\rho^2 - q^2 \to M_\rho^2 - q^2 + \frac{q^2 M_\rho^2}{96\pi^2 F_\pi^2}\left(A_\pi(q^2)+\frac{1}{2}A_K(q^2)\right)\,, \tag{3.57}$$

where

$$A_P(q^2) = \ln\frac{m_P^2}{M_\rho^2} + 8\frac{m_P^2}{q^2} - \frac{5}{3} + \sigma_P^3(q^2)\ln\left(\frac{\sigma_P(q^2)+1}{\sigma_P(q^2)-1}\right)\,, \tag{3.58}$$

with $\sigma_P(q^2)=\sqrt{1-\frac{4m_P^2}{q^2}}$. We will take its absolute value (there are other types of corrections at this order that we are disregarding, like those to the VVP vertex, that can have either sign) as the one standard deviation uncertainty induced by missing subleading corrections in the large-N_C limit. Then, we will have:

$$\left(\Delta a_\mu^{\pi^0\text{-pole}}\right)_{1/N_C} = \pm 1.5\times 10^{-11}\,, \tag{3.59a}$$

$$\left(\Delta a_\mu^{\eta\text{-pole}}\right)_{1/N_C} = \pm 0.5\times 10^{-11}\,, \tag{3.59b}$$

$$\left(\Delta a_\mu^{\eta'\text{-pole}}\right)_{1/N_C} = \pm 0.3\times 10^{-11}\,. \tag{3.59c}$$

[26] We have computed this modification up to 1 GeV. At higher energies other effects arise (like, e.g. those associated to inelasticities), with a relevant interplay to this one, which would need to be accounted for as well.

Combination of experimental and Lattice data

Finally, we evaluate the uncertainty on $a_\mu^{P\text{-poles}}$ that comes from neglecting Lattice QCD data in our fits. In this way, we quantify the difference between a fully data-driven analysis and a hybrid one. The differences, for every P, are:

$$\left(\Delta a_\mu^{\pi^0\text{-pole}}\right)_{\text{Hybrid analysis}} = +0.4\times 10^{-11}\,, \tag{3.60a}$$

$$\left(\Delta a_\mu^{\eta\text{-pole}}\right)_{\text{Hybrid analysis}} = -0.6\times 10^{-11}\,, \tag{3.60b}$$

$$\left(\Delta a_\mu^{\eta'\text{-pole}}\right)_{\text{Hybrid analysis}} = -0.8\times 10^{-11}\,. \tag{3.60c}$$

The π^0-pole contribution increases, while the η/η'-poles' decrease by including the Lattice data. To the best of our knowledge, this was the first quantification of the difference between a hybrid (including lattice information) and a fully data-driven analysis. It is possible here due to chiral symmetry, since the parameters d_{d1}, d_{d2} and d_{d3} appear in the π^0,η and η' TFFs with predicted relations between the three modes based on flavor symmetry. Even though the experimental data is available only for η', a joint description for all the 3 particles can be obtained. This situation contrasts with the case of the Canterbury Approximants analysis presented in table 3.11, where Lattice data cannot be excluded for π^0 nor for η.

Asymptotic Behavior for asymmetric double virtualities

Furthermore, in this work we have imposed the single virtual and symmetric double virtual SDCs, (3.4). However, from the light-cone expansion [312, 373, 342], the SDCs at leading order in pQCD and at leading-twist are given for general large asymmetric virtualities, which are equivalent to the results given in eq. (3.5), by:

$$\lim_{Q^2_{1(2)}\to\infty} \mathscr{F}_{P\gamma^*\gamma^*}(-Q_1^2,-Q_2^2) = \frac{P_\infty}{3}\int_0^1 dx \frac{\phi_P(x)}{xQ_1^2+(1-x)Q_2^2}, \tag{3.61}$$

where $\phi_P(x)$ is the pion distribution amplitude which -for large momenta- behaves as $\phi_P(x)\to 6x(1-x)$[312, 374]. The construction of the TFFs using RχT is limited to a polynomial description, which cannot reproduce the whole range of asymmetries in eq. (3.61). The asymmetric SDCs, $\lim_{Q^2\to\infty}\mathscr{F}_{P\gamma^*\gamma^*}(-Q^2,-\lambda Q^2)$, were compared -for $R\chi T$ and the light-cone expansion results- within the relevant region of the integration kernels for the $a_\mu^{\text{P}-\text{pole}}$, as it is shown in fig. 3.12. There is a bump in

the asymptotic behavior of eqs. (3.41) and (3.42) because the term reproducing the symmetric double virtual SDC of eq.(3.4) dominates the whole scale of asymmetries except for $\lambda \to 0$, and it behaves as $1/\lambda$. To quantify the effect in the evaluation of

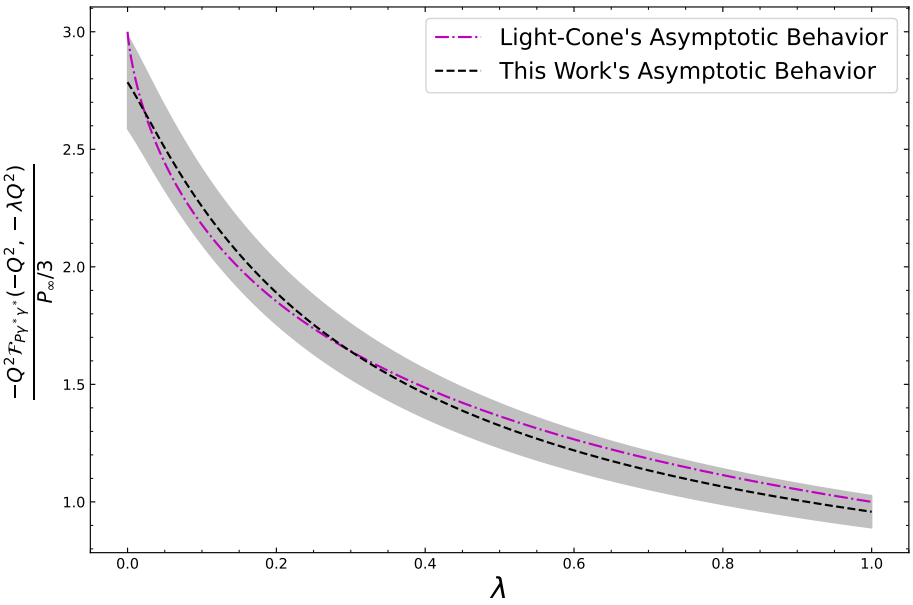

Fig. 3.12 Comparison between the asymptotic behavior of the light-cone expansion and this work's TFFs in terms of the ratio between the 2 squared momenta $\lambda = Q_1^2/Q_2^2$. Our one σ uncertainties are represented by the gray band.

$a_\mu^{\text{P-pole}}$ produced by this difference, a replacement of the dominant terms at high energies of eqs.(3.41) and 3.42) by the one of eq. (3.61) -as suggested in eq. (5.13) from [49]- was done, and the numerical difference was one order of magnitude smaller than the rest of the theory errors for the 3 pseudoscalar mesons. The change for the expression of the light-cone expansion was performed at a Q_1 value where the squared difference between this work's asymptotic behavior and eq. (3.61) is minimized.

3.4.2 Results

We implemented a numerical evaluation, using the VEGAS algorithm [375, 125]. For the computation of the statistical error, we generated 1000 sets of points in the parameter space from a normal multivariate distribution, given the central values and correlations from tables 3.6 and 3.7, which were used for the determination of the mean and standard deviation of each $a_\mu^{\text{P-pole}}$. With the four (independent) dominant uncertainties given by eqs. (3.55), (3.56), (3.59) and (3.60), we obtain the

following systematic theory error:

$$\left(\Delta a_\mu^{\pi^0\text{-pole}}\right)_{\text{theory}} = \left(^{+2.4}_{-1.5}\right) \times 10^{-11}\,, \tag{3.62a}$$

$$\left(\Delta a_\mu^{\eta\text{-pole}}\right)_{\text{theory}} = \left(^{+1.1}_{-0.8}\right) \times 10^{-11}\,, \tag{3.62b}$$

$$\left(\Delta a_\mu^{\eta'\text{-pole}}\right)_{\text{theory}} = \left(^{+1.4}_{-0.9}\right) \times 10^{-11}\,. \tag{3.62c}$$

Our final result, including statistical (cf. Figure 3.13) and the above systematic uncertainties [27] is:

$$a_\mu^{\pi^0\text{-pole}} = \left(61.9 \pm 0.6^{+2.4}_{-1.5}\right) \times 10^{-11} = \left(61.9^{+2.5}_{-1.6}\right) \times 10^{-11}\,, \tag{3.63a}$$

$$a_\mu^{\eta\text{-pole}} = \left(15.2 \pm 0.5^{+1.1}_{-0.8}\right) \times 10^{-11} = \left(15.2^{+1.2}_{-0.9}\right) \times 10^{-11}\,, \tag{3.63b}$$

$$a_\mu^{\eta'\text{-pole}} = \left(14.2 \pm 0.7^{+1.4}_{-0.9}\right) \times 10^{-11} = \left(14.2^{+1.6}_{-1.1}\right) \times 10^{-11}\,, \tag{3.63c}$$

with an uncertainty saturated by the model-dependence. Combining eqs. (3.63a), (3.63b) and (3.63c) we arrive at the following result for the pseudoscalar-pole contributions:

$$a_\mu^{\pi^0+\eta+\eta'\text{-pole}} = \left(91.3 \pm 1.0^{+3.0}_{-1.9}\right) \times 10^{-11} = \left(91.3^{+3.2}_{-2.1}\right) \times 10^{-11}\,. \tag{3.64}$$

3.4.3 Comparison with other approaches

In table 3.13 we collect different recent evaluations of $a_\mu^{\text{P}-\text{poles}}$, including ours. We underscore the good agreement between the diverse approaches, some of them with completely different systematics. This reinforces the reliability of this result.

Of particular interest is the comparison between our work and the results from another $R\chi T$ determination, which works with 3 multiplets of vector meson resonances [298]. We summarize the most important differences in table 3.12.

It is relevant to scrutinize where the differences among approaches are most important. To do so, the first slope parameter b_P and the asymptotic behavior parameter F^P_{asym} were computed for the main results in [6]. This comparison is shown in table 3.13, which shows high consistency between the dispersive, holographic, DSE/BSE, CA, and $R\chi T$ approaches for those two parameters.

[27] We always quote the systematic error after the statistical one.

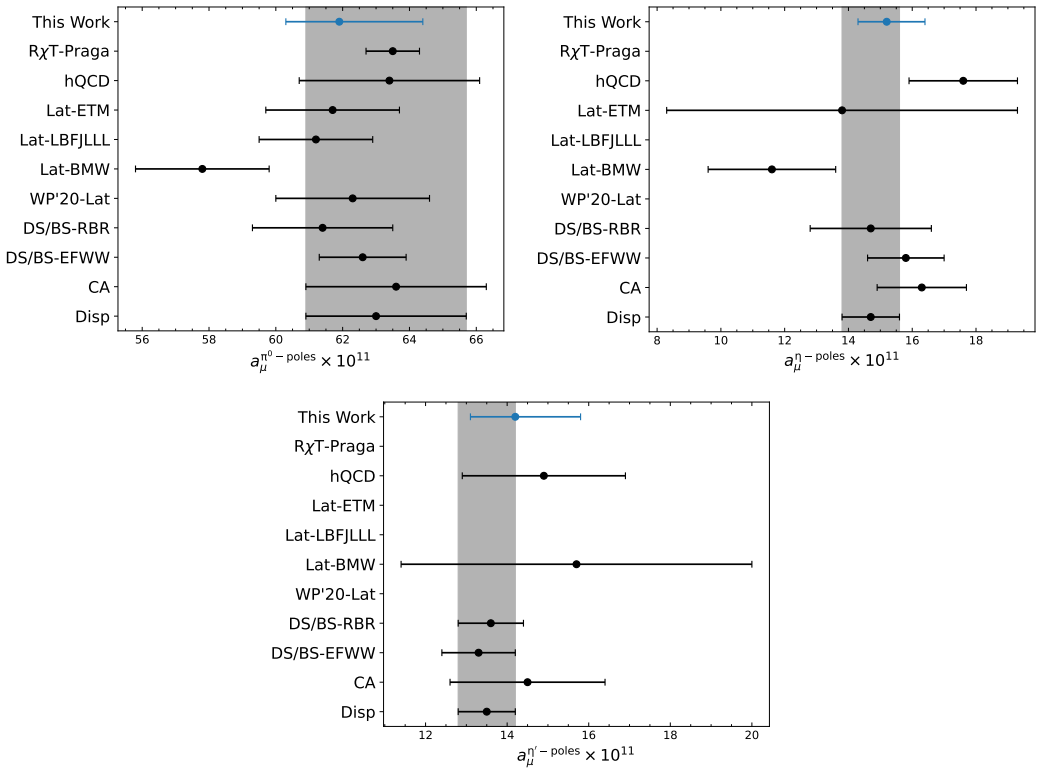

Fig. 3.13 Different recent evaluations of $a_\mu^{P\text{-poles}}$, $P = \pi^0, \eta, \eta'$, multiplied by 10^{11}. We collect the results quoted in the WP 2020 [5] and WP 2025 [6] as well as other relevant results such as those coming from other $R\chi T$ evaluations. Our results are shown in blue. The reference value for WP2025 is shown as a gray band.

Ref. [298]	This work
Ansätze	Computation from the RχT Lagrangian
3 resonance multiplets	2 resonance multiplets
Chiral Limit	Chiral symmetry breaking up to $\mathcal{O}(m_P^2)$
Only π^0 (for which χ-limit works quite well)	π^0, η, η'
More subleading OPE constraints	Only δ_π as subleading OPE constraint
2019 Lattice Calculations [295]	2023 Lattice Calculations [294]
Fit from [295] used	Only BaBar π^0 data not fitted

Table 3.12 Summary of the main differences between our study and ref. [298].

Finally, we can focus on the difference between approaches with polynomial form factors to study where there is more need for new experimental input relevant to a_μ. This can be done by different means; the first one is to compute the master integral truncated for $Q_i > \Lambda$. The results for this comparison are shown in Fig. 3.14 (which was originally done by the author for the second White Paper [6]) for all 3

	Disp. [292, 49, 363, 68]	CA [47]	RχT [62]	hQCD [59]	DSE/BSE [50]
b_{π^0} [GeV^{-2}]	1.73(5)	1.76(10)	1.74(1)	1.68(8)	1.71(1)
b_{η} [GeV^{-2}]	1.83(4)	1.91(3)	2.00(3)	1.53(3)	1.87(1)
$b_{\eta'}$ [GeV^{-2}]	1.49(3)	1.43(3)	1.37(2)	1.31(2)	1.54(3)
$\bar{F}^{\pi^0}_{\text{asym}}$	$2F_\pi$	$2F_\pi$	$2F_\pi$	$2F_\pi[\times 0.9]$	$2.6(4)F_\pi$
$\bar{F}^{\eta}_{\text{asym}}$ [GeV]	0.186(13)	0.180(12)	0.174(3)	0.194(14)	0.21(2)
$\bar{F}^{\eta'}_{\text{asym}}$ [GeV]	0.264(13)	0.255(4)	0.260(4)	0.32(4)	0.36(4)

Table 3.13 The slope and the asymptotic value of the pseudoscalar singly-virtual TFFs from the different approaches.

tensor mesons. The second one examines the difference between the integrands of eq. (3.53) for a given value of t. Since the integrand grows slowly for t close to 1 due to the $\sqrt{1-t^2}$ factor, the difference between the respective integrands is better represented by values near $t = 0$, in this case $t = -0.20$ was used for the π^0 case [28]. The plot shows that it is indeed the low-energy region that requires more data to make the a_μ determination less model-dependent. It is even more noteworthy that the main differences appear in low asymmetric virtualities, where there is a clear lack of data.

In fig. 3.15 we show the difference between CA [47] and $R\chi T$ [62] for the π^0 integrand of eq. (3.53). The relative maximum difference (in magnitude) is at the ~ 10 % level. These areas (in yellow and dark blue) are those where (lattice) data would be more helpful.

3.5 Conclusions and Outlook

In this work, we have presented a simultaneous description of the singly and doubly virtual π^0, η and η' transition form factors based on Resonance Chiral Theory that was included as one of the reference determinations in the White Paper 2025 of the muon $g-2$ Theory Initiative. Particularly, this calculation was included in the relevant inputs for the computation of a_μ^{SM} (Refs. [14-73] of the collaboration report [6]). This is the first (and up to now only) time that a result from a Thesis made in

[28]The difference between the integrand between the two approaches is uniform in t, when it approaches $t = \pm 1$ it is less intense, but with a similar distribution. At $t = -0.20$, the difference between approaches is maximized.

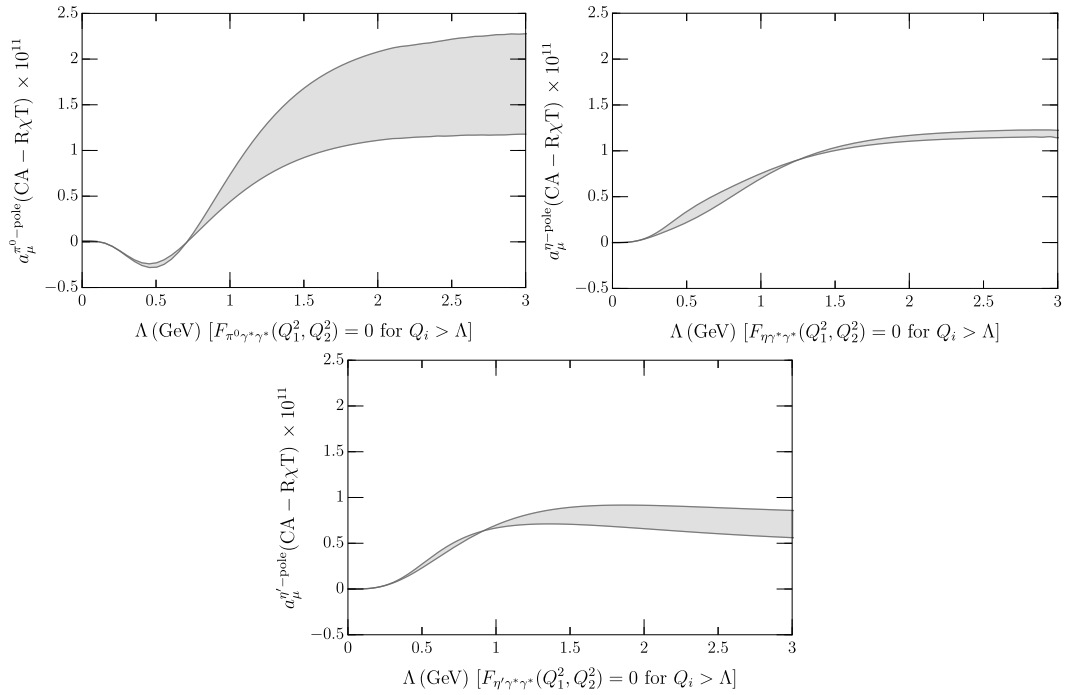

Fig. 3.14 The difference of the *CA* and $R\chi T$ approaches for the partial contribution to $a_\mu^{\text{HLbL:P}-\text{pole}}$ up to a given scale.

Mexico makes it to the list of essential SM inputs in the White Papers of this theory initiative.

In particular, we have shown that working within the two resonance multiplets saturation scheme we: satisfy leading (and some subleading) chiral and high-energy QCD constraints; get a normalization given by the two-photon partial decay width, $\Gamma(\pi^0/\eta/\eta' \to \gamma\gamma)$, that is fully compatible with experimental values; reproduce the singly virtual transition form factors experimental data in the spacelike region (see Fig. 3.7) and, last but not least; obtain a faithful description of the doubly virtual transition form factor for all three pseudoscalar mesons resulting from the use of the BaBar data in the η' channel in combination with Lattice-QCD results for the three mesons form factors (see Fig. 3.8). Our evaluation of the pole contributions to the hadronic light-by-light piece of the muon $g-2$ read: $a_\mu^{\pi^0\text{-pole}} = \left(61.9 \pm 0.6^{+2.4}_{-1.5}\right) \times 10^{-11}$, $a_\mu^{\eta\text{-pole}} = \left(15.2 \pm 0.5^{+1.1}_{-0.8}\right) \times 10^{-11}$ and $a_\mu^{\eta'\text{-pole}} = \left(14.2 \pm 0.7^{+1.4}_{-0.9}\right) \times 10^{-11}$, for a total of $a_\mu^{\pi^0+\eta+\eta'\text{-pole}} = \left(91.3 \pm 1.0^{+3.0}_{-1.9}\right) \times 10^{-11}$, where the first error is statistical and the second one is systematic (see Sec. 3.4.1).

Our determination for $a_\mu^{\pi^0\text{-pole}}$ is compatible at the level of 1σ with the dispersive evaluation, $a_\mu^{\pi^0\text{-pole}} = \left(63.0^{+2.7}_{-2.1}\right) \times 10^{-11}$ [5], the results based on Canterbury approx-

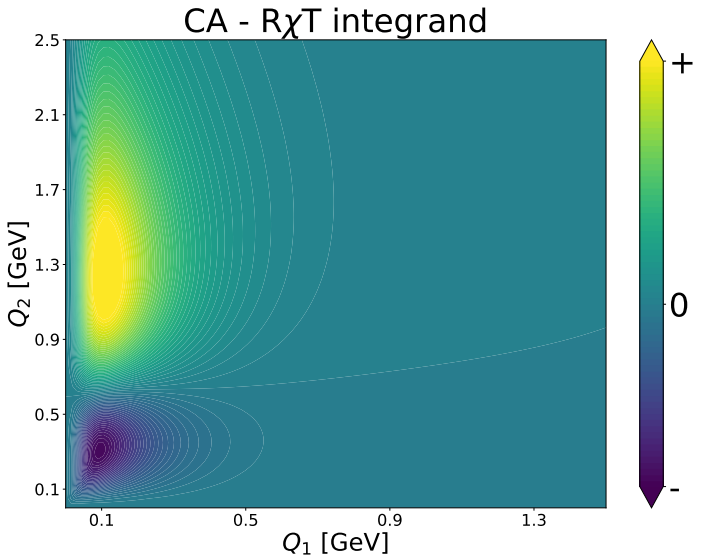

Fig. 3.15 Difference between the rational approach of [47] and RχT [62] for the integrand of eq. (3.53) in the π^0 case. The density plot shows relevant differences between these two models for low but asymmetric virtualities, reaching a maximum relative deviation of $\sim 10\%$ for all values of t in eq. (3.53).

imants, $a_\mu^{\pi^0\text{-pole}} = 63.6(2.7) \times 10^{-11}$ [47], and the most recent lattice QCD results, $a_\mu^{\pi^0\text{-pole}} = 61.2(1.7) \times 10^{-11}$ [376],and $a_\mu^{\pi^0\text{-pole}} = 61.7(2.0) \times 10^{-11}$[297]. Our outcomes for the $a_\mu^{\eta/\eta'\text{-pole}}$ contributions are particularly relevant, given that our approach complies with the leading asymptotic behavior for double virtuality and the good performance exhibited for describing the best doubly-virtual input at disposal, which is also reproduced by the recent results from hQCD [377] and Dispersive [68, 363] groups, which came after our publication. Interestingly enough, they are consistent with $a_\mu^{\eta/\eta'\text{-pole}} = [16.3(1.4)/14.5(1.9)] \times 10^{-11}$ from Canterbury Approximants [47] but with improved uncertainties, which however would need a C_4^4 to fully account for chiral symmetry constraints and their explicit breaking at leading order, that is non-negligible for the $\eta^{(\prime)}$ contributions (see section 3.3).[29] Our results are also compatible with the Lattice results $a_\mu^{\eta/\eta'\text{-pole}} = [11.6(2.0)/15.7(4.2)] \times 10^{-11}$ [294], although the η-pole contribution is in slight tension with our outcome due to the lower value for the normalization of their transition form factor.

We hope that our analysis strengthens the case for experimental measurements of the transition form factors of double virtuality for all three pseudoscalar mesons,

[29] At least a C_2^2 would be needed to describe the double virtuality data, instead of the C_2^1 used in ref. [47].

as they would allow constraining their functional form and reduce the uncertainty in $a_\mu^{P\text{-pole}}$.

To improve the results of this work and related data-driven ones, new data on the transition form factors are required. This work has shown that the double virtual η'-TFF data from [335] is not enough. Given the fact that δ_π^2 has been constrained by measurements, and η' doubly virtual data have already been taken, it would be of great interest to get η-TFF doubly virtual data[30]. Furthermore, studying the difference between the integrand of eqn. (3.53) of the Canterbury Approximants and $R\chi T$ showed that asymmetric doubly virtual data at low energies would also improve the determination of these contributions.

The BESIII collaboration mentioned in the Theory Initiative Workshops of 2024 and 2025 that data for the processes $\gamma^*\gamma^* \to \pi^0, \eta, \eta'$ is expected for $Q_1^2 \sim Q_2^2 \sim 1\mathrm{GeV}^2$ with the data analysis ongoing for the η and η' cases due to a favorable background situation. When these data become available, our results will be significantly improved, and the discrepancy between different models will be decreased, resulting in an even more reliable determination of $a_\mu^{\mathrm{HLbL:P-poles}}$.

[30]During this study, we considered different data sets. The minimal amount of LQCD input needed for a significant improvement on the fits was the one including $\mathscr{F}_{\eta\gamma^*\gamma^*}$ doubly virtual calculations.

CHAPTER 4

Proton-Box contribution to a_μ^{HLbL}

The current tension between the Standard Model prediction [6] and the experimental world average [4] is $36(63) \times 10^{-11}$, and the precision of both is of the same order. This implies that the subdominant contributions are becoming relatively more important each time. This raised the question of the importance of baryonic contributions in the HLbL piece.

The Heavy Mass Expansion (HME) method [378] provides us with a tool for computing point-like lepton-box contributions to a_μ. As a first approximation to the magnitude of the nucleon contributions, we obtained the values for the charged lightest baryons: $a_\mu^{\mathrm{p-box}} = 9.7 \times 10^{-11}$, $a_\mu^{\Sigma-\mathrm{box}} \approx 6.0 \times 10^{-11}$, $a_\mu^{\Xi-\mathrm{box}} \approx 4.9 \times 10^{-11}$. This result is comparable in magnitude to the tension between theory and experiment and their respective errors, thereby motivating a more realistic and precise analysis that incorporates the main effects of the structure of these compound objects. This requires information on their form factors, which is abundant for the proton and the neutron. As will be discussed later in this chapter, the proton-box contribution [121] is the most significant contribution to this observable, which is the reason why this work was focused on this baryon only.

4.1 Contribution to $a_\mu^{\rm HLbL}$

In order to compute the proton-box contribution to $a_\mu^{\rm HLbL}$, first we need to define the structure dependence of the $\gamma^* - p - p$ interaction:

$$\begin{aligned}\langle p^+(P_2)|J^\mu_{e.m.}(q)|p^+(P_1)\rangle &= \bar{u}(P_2)\Gamma^\mu(q)u(P_1)\\ &= \bar{u}(P_2)\left(F_1(q^2)\gamma^\mu + i\frac{F_2(q^2)}{2M_p}\sigma^{\mu\nu}q_\nu\right)u(P_1),\end{aligned} \tag{4.1}$$

where $F_{1,2}$ are the proton Dirac and Pauli form factors, respectively, and $q = P_2 - P_1$. In this analysis, the dominant term in eq.(4.1), is the one proportional to $F_1(q^2)$. This arises from the additional q_ν/M_p factor appearing in the tensor vertex, in such a way that, in the low momentum transfer regime (below 1 GeV), the tensor coupling behavior is significantly suppressed due to its momentum dependence, making it a valid approximation to consider only the vector coupling.[1] Conversely, at high photon virtuality (or even above 1 GeV), the $F_2(q^2)$ behavior becomes the suppression factor. In fact, in this case, also the $F_1(q^2)$ and kernel functions are highly suppressed, making the contributions of this q^2 region negligible. Indeed, due to the asymptotic constrains of the form factors F_1 and F_2 from p-QCD[311], which should behave as $\sim Q^{-4}, Q^{-6}$, respectively (satisfied by construction in both parametrizations employed in this work, as we discuss latter), the regime of high transferred momentum is free of divergences and we do not expect to have any significant error coming from this approximation [2].

Therefore, as a suitable first approximation, we will work only with the vector coupling in eq.(4.1) as input for the scattering amplitude computation shown in Fig. 4.1. The decomposition of the HLbL tensor for the proton-box representation results in the scalar functions:

$$\bar{\Pi}_i = F_1(Q_1^2)F_1(Q_2^2)F_1(Q_3^2)\,\frac{1}{16\pi^2}\int_0^1 dx\int_0^{1-x} dy\, I_i(Q_1,Q_2,\tau,x,y), \tag{4.2}$$

[1] This simplification is commonly taken, consistently in many other processes, such as electron-proton scattering in the same momentum transfer region. Similarly, in the proton-loop contribution to HVP, incorporating a non-zero F_2 leads to a 0.02% modification of the central value, which remains significantly smaller than the current uncertainty (consistent with the results reported in ref. [43]).

[2] In this sense, we have: $\Gamma^\mu(q)|_{q\to\infty} = \gamma^\mu A\, q^{-4} + iB\sigma^{\mu\nu}\hat{q}_\nu(2q^5M_p)^{-1}$, with $\hat{q}_\nu \equiv q_\nu/q$ a normalized four-vector and A and B being constants.

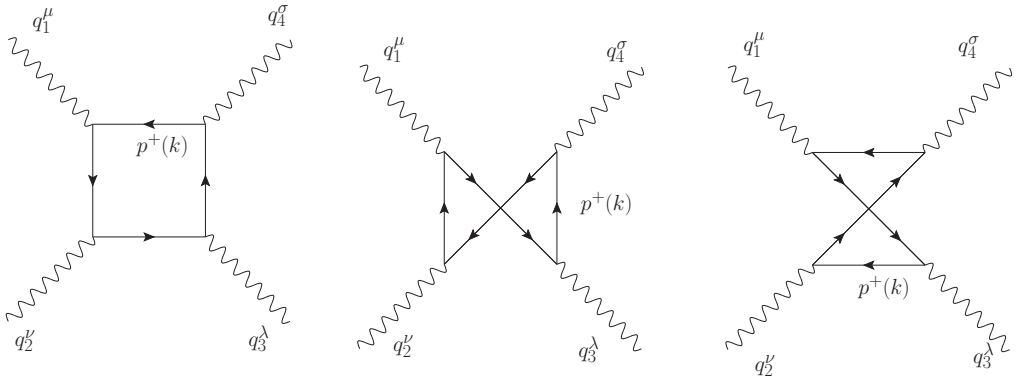

Fig. 4.1 Feynman diagrams for light-by-light scattering induced by a proton-box loop (and the corresponding diagrams with exchanged fermion fluxes inside the loop).

with the loop functions I_i being:

$$
\begin{aligned}
I_1 =& -\frac{16x(1-x-y)}{\Delta_{132}^2} - \frac{16xy(1-2x)(1-2y)}{\Delta_{132}\Delta_{32}},\\
I_3 =& \frac{32xy(1-2x)(x+y)(1-x-y)^2(q_1^2-q_2^2+q_3^2)}{\Delta_{312}^3}\\
&- \frac{32(1-x)x(x+y)(1-x-y)}{\Delta_{312}^2} - \frac{32xy(1-2x)(1-2y)}{\Delta_{312}\Delta_{12}},\\
I_5 =& -\frac{64xy^2(1-x-y)(1-2x)(1-y)}{\Delta_{132}^3},\\
I_9 =& -\frac{32x^2y^2(1-2x)(1-2y)}{\Delta_{312}^2\Delta_{12}},\\
I_{10} =& \frac{64xy(1-x-y)((2x-1)y^2+xy(2x-3)+x(1-x)+y)}{\Delta_{132}^3},\\
I_{12} =& -\frac{16xy(1-x-y)(1-2x)(1-2y)(x-y)}{\Delta_{312}\Delta_{12}}\left(\frac{1}{\Delta_{312}}+\frac{1}{\Delta_{12}}\right),
\end{aligned}
\tag{4.3}
$$

(4.4)

where $\Delta_{ijk} = m_p^2 - xyq_i^2 - x(1-x-y)q_j^2 - y(1-x-y)q_k^2$ and $\Delta_{ij} = m_p^2 - x(1-x)q_i^2 - y(1-y)q_j^2$. The rest of the scalar functions are obtained by means of permutations of the ones presented.

4.2 Proton Form Factors

The first main contribution to the proton-box to a_μ^{HLbL}. We need to obtain a proper description of the form factors in eq. (4.1) for accounting for this contribution. Contrary to what we have done for the pseudoscalars, the tensors, and other contributions, we did not perform an RχT description for this case, since the descriptions from experimental data [379] and Lattice QCD calculations [380] parametrizations have a detailed methodology, reliable error computation, and correct asymptotic behavior. Both approaches fitted parametrizations to the electric (G_E) and magnetic (G_M) proton form factors data, which are related to the Dirac and Pauli base by:

$$\begin{aligned} G_E(Q^2) &= F_1(Q^2) - \frac{Q^2}{4M_p^2} F_2(Q^2), \\ G_M(Q^2) &= F_1(Q^2) + F_2(Q^2). \end{aligned} \tag{4.5}$$

4.2.1 Data-Driven Form Factors

The electric and magnetic form factors are obtained in Ref.[379] after fitting the experimental data to a z-expansion parametrization of order 12 [381], where sum-rule constraints were applied on each form factor to warrant the asymptotic scaling $G_{E,M} \sim Q^{-4}$ and the correct normalization at null photon virtuality. [3] The statistical and systematic errors of their work are related to the fitting procedure to the world electron scattering data and additional uncertainties to account for tensions between different data sets and uncertainties in radiative corrections. Detailed information on the error computation, the data used for the fit and the obtained parameters is given in their *Appendix A: supplementary material* of their work, available in the journal version only.

In this way, the proton form factors can be written as:

$$G_E^{(p)}(Q^2), \frac{G_M^{(p)}(Q^2)}{\mu_p} = \sum_{i=0}^{12} a_i^{\{E,M\}} z^i, \tag{4.6}$$

[3] Other parametrizations, as the ones reported in Refs.[382, 383], have been considered for the $a_\mu^{\mathrm{p-box}}$ numerical evaluation, being consistent with the one used in this work within less than 1σ.

	E	M
a_0^X	0.239163298067	0.264142994136
a_1^X	−1.109858574410	−1.095306122120
a_2^X	1.444380813060	1.218553781780
a_3^X	0.479569465603	0.661136493537
a_4^X	−2.286894741870	−1.405678925030
a_5^X	1.126632984980	−1.356418438880
a_6^X	1.250619843540	1.447029155340
a_7^X	−3.631020471590	4.235669735900
a_8^X	4.082217023790	−5.334045653410
a_9^X	0.504097346499	−2.916300520960
a_{10}^X	−5.085120460510	8.707403067570
a_{11}^X	3.967742543950	−5.706999943750
a_{12}^X	−0.981529071103	1.280814375890

Table 4.1 z-expansion proton form factor fitted parameters, taken from Ref.[379].

where a_i are fitting parameters shown in table 4.1, and z is defined as follows:

$$z \equiv \frac{\sqrt{t_{\text{cut}} + Q^2} - \sqrt{t_{\text{cut}} - t_0}}{\sqrt{t_{\text{cut}} + Q^2} + \sqrt{t_{\text{cut}} - t_0}}, \tag{4.7}$$

with $t_0 = -0.7$ GeV^2, $t_{\text{cut}} = 4m_\pi^2$ and the form factors normalization fixed by the proton's electric charge non-renormalization and magnetic moment in Bohr magneton units, $G_E^p(0) = 1$ and $G_M^p(0) = \mu_p = 2.793$, in turn.

4.2.2 Lattice QCD Form Factors

Lattice QCD have become very important in the Theory Initiative White Paper 2025 [6], in contrast with the White Paper 2020 [5]. This was mainly due to the increase of LQCD groups which managed to perform more complete and partial evaluations of $g-2$ with great accuracy. Consequently, we considered a LQCD model for the neutron and proton form factors. In [380], the Lattice data for the form factors can be parametrized using a simple dipole approximation: [4]

$$G^{\{E,M\}}(Q^2) = G^{\{E,M\}}(0)/(1 + Q^2/\Lambda)^2, \tag{4.8}$$

[4] A z-expansion was performed as well, but no significant difference was found with respect to the simple dipole approximation.

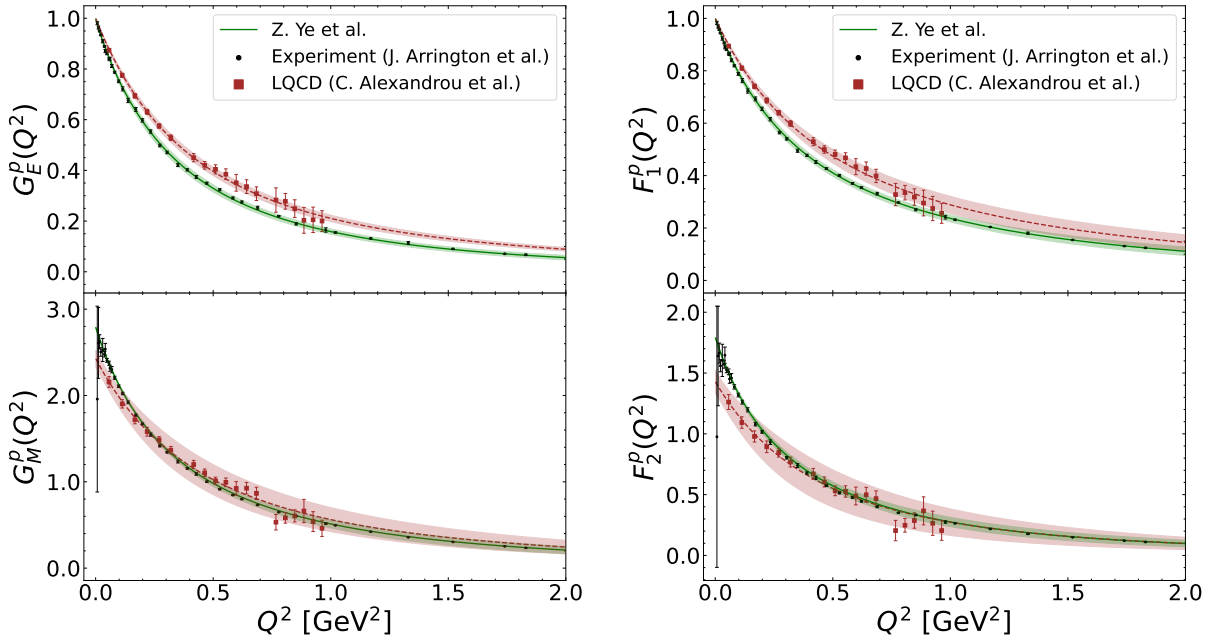

Fig. 4.2 G_E and G_M (F_1 and F_2) proton form factors. In black we show the experimental points taken from Ref.[379], meanwhile, red dots correspond to the Lattice QCD results of Ref.[380].

where Λ is related to the electric and magnetic radii by $\Lambda = 12/\langle r^2_{\{E,M\}}\rangle$ and the normalization is $G_E(0) = 1$ and $G_M(0) = \mu_p$. It is important to remark that this parametrization automatically fulfills the QCD-ruled asymptotic behavior for large values of Q^2. The numerical values required in eq.(4.8) are shown in table 4.2, where the normalization at null photon virtuality is automatically fulfilled for the electric form factor by setting $G_E^p(0) \to 1$. As explained in [380], there is an underestimation of the electric r.m.s. radius, due to the slower decay of the electric form factor. Besides, the magnetic moment of the proton is undervalued, which could be caused by a combination of residual volume effects and multi-hadron contributions.

$\sqrt{\langle r_E^2\rangle}$[fm]	$\sqrt{\langle r_M^2\rangle}$ [fm]	μ_p
$0.742 \pm 0.013 \pm 0.023$	$0.710 \pm 0.026 \pm 0.086$	$2.43 \pm 0.09 \pm 0.04$

Table 4.2 Numerical values of eq.(4.8) according to Ref.[380]. The uncertainties stand for the statistic and systematic errors, respectively.

As we show in Fig.4.2, the z-expansion reported in [379] is in good agreement with the data set of $G_M(Q^2)$ and $G_E(Q^2)$ from [383] extracted from the world's data

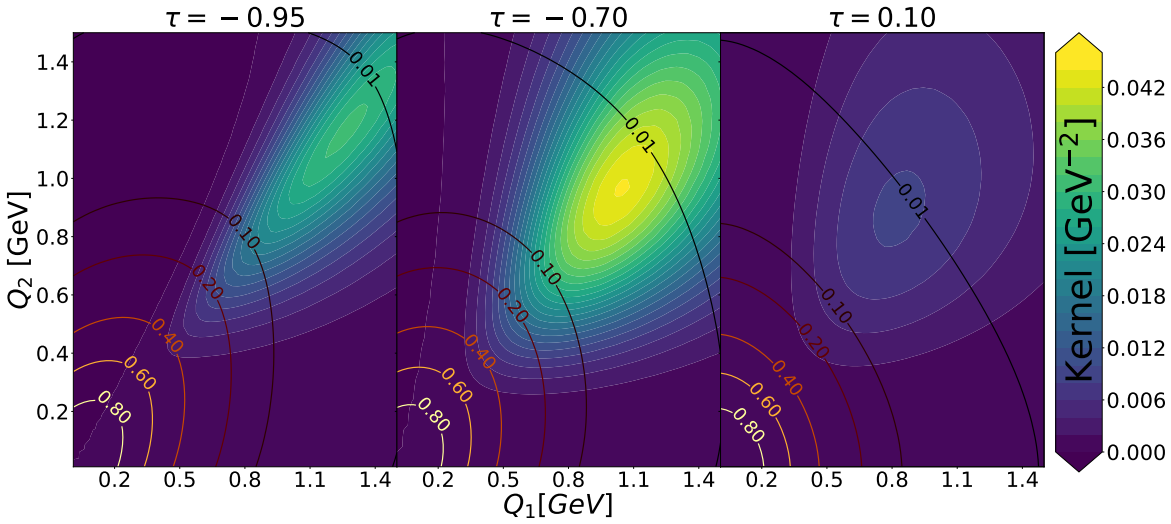

Fig. 4.3 Integral kernel (density plot) versus form factors dependence (contour plot) at relevant different virtualities for the off-shell photons, as described in the text.

on elastic electron-proton scattering and calculations of two-photon exchange effects. We also compared the former fit and the one obtained from Lattice QCD results with a $N_f = 2+1+1$ ensemble, reported in Ref.[380]. Finally, due to the small deviations between the two data sets, in the $Q^2 < 1\,\mathrm{GeV}^2$ region, it seems interesting to analyze both frameworks separately during the numerical evaluation of eq.(1.28).

4.3 Results and Outlook

The full integral kernel of the master integral eq. (1.28), which has $\bar{\Pi}_i$ general for all leptonic contributions, $\sqrt{1-\tau^2}\,Q_1^3\,Q_2^3 T_i \bar{\Pi}_i$, [5] without accounting for any form factor, primarily contributes to the overall integral at low momentum transfers (below 1 GeV), as illustrated by the density plot in Fig. 4.3 for three different τ values. Furthermore, the vector proton form factors term alone $F_1(Q_1^2)F_1(Q_2^2)F_1(Q_3^2)$, [6] acquires its maximum value within the same momenta region, as shown by the contour curves in the figure, being maximum at $Q_i = 0$ and decreasing as the momenta increase. Due to the mismatch between the kernels and form factors' maximum values, a significant decrease in the HME approximation result of around 2 orders of magnitude is expected for both approaches.

[5] The explicit dependence of T_i and $\bar{\Pi}_i$ on Q_1, Q_2 and τ has been omitted and the Einstein sum notation is understood.

[6] Evaluated using the dependence on Q^2 as a z-expansion (setup 1), see section 4.2 for details.

In order to obtain the explicit a_μ^{HLbL} contribution via the master integral, we implemented a numerical evaluation, using the VEGAS algorithm [375, 125].

For a first consistency test of the integration method, we reproduced all previously well-known results, being in complete agreement with all of them (π-pole, π-box, c-loop, etc.). Specifically, we corroborate that the use of the quark-loop scalar functions, without any form factors included, leads to the same result as the HME approximation for the proton case, getting a central value of 9.4×10^{-11} compared to the HME estimation of 9.7×10^{-11}.

Once the corresponding vector form factor $F_1(Q^2)$ is included in the analysis, we get the following results for the different setups described above: [7]

$$a_\mu^{\mathrm{p-box}} = 1.82(7) \times 10^{-12} \quad \textbf{(Data-Driven)}, \tag{4.9}$$

$$a_\mu^{\mathrm{p-box}} = 2.38(16) \times 10^{-12} \quad \textbf{(Lattice)}, \tag{4.10}$$

where both the systematic and statistical uncertainties were considered to estimate the error for each setup. The disagreement between the results can be inferred by the difference in the slope of the upper plot of Fig. 4.2

As mentioned above, there is a 2 orders of magnitude suppression with respect to the HME result, caused by the effect of the form factors. This behavior can be further discussed by understanding it in different regions of the parameter τ, the relative projection between the external momenta Q_1 and Q_2 [8]. First, we can see that close to ± 1, the $\sqrt{1-\tau^2}$ factor suppresses the values of the integral kernel. Also, as τ increases, Q_3 does as well, and the T_i functions decrease[48], causing the kernel to start diluting after its maximum value is reached, and to be almost negligible for positive values of τ. Finally, the maximum values of the integration kernel appear in $\tau \in [-0.85, -0.65]$, as shown in the supplemental material. For this value of τ, the relevant region of the kernel and the effect of the form factors in the numerical evaluation of eq. (1.28) can be analyzed.

In the case of the data-driven parametrization, both statistical and systematic errors were computed for $F_1^p(Q^2)$ for each value of Q^2 as discussed in [379], and these $\Delta F_1^p(Q^2)$ were used for the error propagation of eq. (1.28) considering the structure of eq. (4.2) in terms of the form factors. For the LQCD form factors, a numerical computation of the Jacobian matrix of eq. (1.28) within this setup was

[7] Using a different parametrization [382] of the same data, as the setup 1, a result of $a_\mu^{\mathrm{p-box}}$=1.79(5)$\times 10^{-12}$ was found, consistent with the results using [379].

[8] Even though the behavior in these regions can be seen in Fig. 4.3, it is better appreciated in the ancillary files of [121], where the comparison of all the range of τ is presented.

performed, and it was combined to obtain both the statistical and the systematic error by assuming a maximal correlation of the magnetic form factor parameters.[9]

Even though there is an underestimation of μ_p using a lattice QCD form factor, the slower decay of G_E^p compared with the data-driven one, compensates for this, and it results in a higher $F_1^p(Q^2)$ for the lattice QCD result, as explained in Ref.[380] and visible in Fig. 4.2. Consequently, the LQCD result for $a_\mu^{\text{p-box}}$ is larger than that of the data-driven determination. Therefore, in this work, we will adopt the data-driven $a_\mu^{\text{p-box}}$ approximation as our central value, awaiting more precise lattice results anticipated in the near future.

In this work, we have computed a first approximation of the proton-box contribution to the HLbL piece of a_μ. We discussed the corresponding proton form factor results, including a couple of different approaches, and got mutually consistent results from all of them.

It would be of great interest to study the contributions of –at least– the lightest multiplet of baryons. This would be possible by performing a tensor decomposition of the full amplitude –which also includes the form factor $F_2^N(Q^2)$–. This is technically difficult, however, possible. This contribution is expected to be sub-leading for the proton, but relevant for the neutral baryons, as the neutron. By performing this decomposition, a new set of scalar functions $\bar{\Pi}_i$ will be obtained, and a number for the baryonic contributions to the HLbL will be attainable.

[9]The uncertainty associated with the numerical integration method is sub-leading, of order $\mathcal{O}(10^{-15})$.

CHAPTER 5

Tensor Meson Pole Contributions to a_μ^{HLbL} within RχT

In this chapter, we study the construction of the transition form factors of the neutral non-strange tensor mesons into two photons ($T \to \gamma^*\gamma^*$) and their pole contributions to the HLbL piece of the anomalous magnetic moment of the muon. For this purpose, we work in the framework of RχT with the following conditions: we work in the chiral limit ($m_q \to 0$), at leading order in the $1/N_C$ counting, with two multiplets of vector meson resonances in three specific scenarios: without operators with derivatives (besides the unavoidable ones of the electromagnetic field-strength tensor), allowing for operators with derivatives of the form $T\partial V\partial V$, and allowing a full consistent set of operators with derivatives. By doing so, we obtained amplitudes with 1, 2, and all 5 possible tensor structures, respectively. We used these results to compare with those available using a simple quark model(QM)[67] and a holographic QCD Hard-Wall model(hQCD) [69]. We obtain compatible results with the QM and hQCD when only one form factor ($\mathscr{F}_1$) is considered, with hQCD when two form factors ($\mathscr{F}_{1,3}$) are accounted for, and a first estimation on the effect of having all non-zero transition form factors. Other computations of these contributions can be found in Refs. [384–388].

5.1 Tensor Meson Transition Form Factors ($T \to \gamma^*\gamma^*$)

A neutral, non-strange tensor meson can decay into two photons. And even though these processes are not their main channels [217], they are relevant when accounting for the T-pole contributions to $g-2$. The radiative decay of a massive tensor meson

is described by the matrix element [67]:

$$\langle\gamma^*(q_1,\lambda_1)\gamma^*(q_2,\lambda_2)|T(p,\lambda_T)\rangle = i(2\pi)^4\delta^{(4)}(q_1+q_2-p)e^2\varepsilon_\mu^{\lambda_1^*}(q_1)\varepsilon_\nu^{\lambda_2^*}(q_2)\varepsilon_{\alpha\beta}^{\lambda_T}(p)\mathscr{M}^{\mu\nu\alpha\beta}(q_1,q_2)\,, \tag{5.1}$$

where $\varepsilon_{\mu,\nu}^{\lambda_i^*}(q_i)$ are the polarizations of the photons (see e. g. ref. [134]):

$$\varepsilon_\pm(q) = \mp(0,1,\pm i,0)\,,\quad \varepsilon_0(p) = (0,0,0,1)\,, \tag{5.2}$$

And the $\varepsilon_{\alpha\beta}^{\lambda_T}(p)$ is the polarization tensor of a massive spin-2 meson, given by:

$$\begin{aligned}
\varepsilon_{\alpha\beta}^{\pm 2} &= \varepsilon_\alpha^\pm(p)\varepsilon_\beta^\pm(p),\\
\varepsilon_{\alpha\beta}^{\pm 1} &= \frac{1}{\sqrt{2}}\left(\varepsilon_\alpha^\pm(p)\varepsilon_\beta^0(p)+\varepsilon_\alpha^0(p)\varepsilon_\beta^\pm(p)\right),\\
\varepsilon_{\alpha\beta}^{0} &= \frac{1}{\sqrt{6}}\left(\varepsilon_\alpha^0(p)\varepsilon_\beta^0(p)+\varepsilon_\alpha^+(p)\varepsilon_\beta^-(p)+\varepsilon_\alpha^-(p)\varepsilon_\beta^+(p)\right),
\end{aligned} \tag{5.3}$$

where the polarization vectors are the same as for the photon in eq. (5.2). These polarizations obey the following sum rule:

$$\sum_\lambda \varepsilon_{\mu\nu}(k;\lambda)\varepsilon^*_{\rho\sigma}(k;\lambda) = \frac{1}{2}\big(P_{\mu\rho}P_{\nu\sigma}+P_{\nu\rho}P_{\mu\sigma}\big)-\frac{1}{3}P_{\mu\nu}P_{\rho\sigma}, \tag{5.4}$$

where $P_{\mu\nu} = g_{\mu\nu}-\frac{k_\mu k_\nu}{M_T^2}$. The reduced amplitude $\mathscr{M}^{\mu\nu\alpha\beta}$ [1] can be decomposed in five tensor structures [67]:

$$\mathscr{M}^{\mu\nu\alpha\beta} = \sum_{i=5}^{5} T_i^{\mu\nu\alpha\beta}\frac{1}{M_T^{n_i}}\mathscr{F}_i^T(q_1^2,q_2^2), \tag{5.5}$$

where $n_1 = 1$ and $n_{i\neq 1} = 3$, and the tensor structures are:

$$\begin{aligned}
T_1^{\mu\nu\alpha\beta} &= g^{\mu\alpha}P_{21}^{\nu\beta}+g^{\nu\alpha}P_{12}^{\mu\beta}+g^{\mu\beta}P_{21}^{\nu\alpha}+g^{\nu\beta}P_{12}^{\mu\alpha}+g^{\mu\nu}(q_1^\alpha q_2^\beta+q_1^\beta q_2^\alpha)-q_1\cdot q_2(g^{\mu\alpha}g^{\nu\beta}+g^{\nu\alpha}g^{\mu\beta}),\\
T_2^{\mu\nu\alpha\beta} &= (q_1^\alpha q_1^\beta+q_2^\alpha q_2^\beta)P_{12}^{\mu\nu},\\
T_3^{\mu\nu\alpha\beta} &= P_{11}^{\mu\alpha}P_{22}^{\nu\beta}+P_{11}^{\mu\beta}P_{22}^{\nu\alpha},\\
T_4^{\mu\nu\alpha\beta} &= P_{12}^{\mu\alpha}P_{22}^{\nu\beta}+P_{12}^{\mu\beta}P_{22}^{\nu\alpha},\\
T_5^{\mu\nu\alpha\beta} &= P_{21}^{\nu\alpha}P_{11}^{\mu\beta}+P_{21}^{\nu\beta}P_{11}^{\mu\alpha},
\end{aligned} \tag{5.6}$$

[1] This reduced amplitude comes from requiring Bose symmetry (invariance under $q_1\leftrightarrow q_2$ and $\alpha\leftrightarrow\beta$) and for the tensor to be non-vanishing under contraction in the sum-rules for $\varepsilon_{\alpha\beta}^{\lambda_T}(p)$.

where the $P_{ij}^{\mu\nu}$ are defined as:

$$P_{ij}^{\mu\nu} = g^{\mu\nu} q_i \cdot q_j - q_i^\nu q_j^\mu . \tag{5.7}$$

These tensor structures, together with the scalar functions $T_i^{\mu\nu\alpha\beta}$, define the interaction vertex in Fig. 5.1, and can be constructed using different approaches.

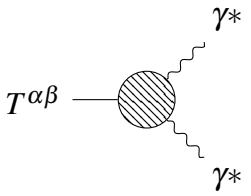

Fig. 5.1 Tensor Meson transition FF, which gives the radiative decay with both photons on-shell.

5.1.1 High-Energy behavior of the Form Factors

The high-energy behavior of these form factors is given by the Light-Cone-Expansion[124]. This is split in the symmetric and asymmetric pieces, which are parametrized by[2]:

$$\tilde{Q}^2 = \frac{q_1^2 + q_2^2}{2}, \quad w = \frac{q_1^2 - q_2^2}{q_1^2 + q_2^2}. \tag{5.8}$$

Then, the high-energy behavior of the transition form factors is given by:

$$\begin{aligned} \lim_{\tilde{Q}^2\to\infty} \mathscr{F}_1^T(q_1^2, q_2^2) &= \frac{4\sum_a C_a F_T^a M_T^3}{\tilde{Q}^4} f_1^T(w), \\ \lim_{\tilde{Q}^2\to\infty} \mathscr{F}_i^T(q_1^2, q_2^2) &= \frac{4\sum_a C_a F_T^a M_T^5}{\tilde{Q}^6} f_i^T(w), \quad i \in 2,3,4,5, \end{aligned} \tag{5.9}$$

the common constant $4\sum_a C_a F_T^a$ has been studied before [389–391] in the framework of LCSRs, which provides the non-strange dominant contribution, since the value used in this work–taken from [282]– as the one considered in [124], is close to ideal

[2] It was necessary to implement a new convention for the symmetric squared momenta to avoid confusion or mixing of different notations in the literature, as Q^2 was already used to define the positive squared momenta in the space-like region (which is the relevant one for the $g-2$ evaluation). This is different than in [67, 69, 122] where Q^2 was used in both cases.

mixing, resulting in:

$$F_T^{\rm eff} = 4\sum_a C_a F_T^a = \frac{5\sqrt{2}}{9} F_T^q = 79(8)\text{MeV}. \tag{5.10}$$

Furthermore, the asymmetric pieces of the SDCs, are given by the 5 functions:

$$\begin{aligned}
f_1^T(w) =& \frac{5(1-w^2)}{8w^6}\Big(15-4w^2+\frac{3(5-3w^2)}{2w}\log\frac{1-w}{1+w}\Big),\\
f_2^T(w) =& -\frac{5}{8w^6}\Big(15-13w^2+\frac{3(1-w^2)(5-w^2)}{2w}\log\frac{1-w}{1+w}\Big),\\
f_3^T(w) =& -\frac{5}{8w^2}\Big(15-w^2-\frac{w^4+6w^2-15}{2w}\log\frac{1-w}{1+w}\Big),\\
f_4^T(w) =& -\frac{5}{24w^6}\Big(45+30w-21w^2-8w^3+\frac{3(1+w)(15-5w-7w^2+w^3)}{2w}\log\frac{1-w}{1+w}\Big),\\
f_5^T(w) =& f_4^T(w)|_{w\to -w},
\end{aligned} \tag{5.11}$$

where in the last relation, $w\to -w$ is also $q_1^2 \leftrightarrow q_2^2$. This is extremely relevant, as $\mathscr{F}_4^T$ goes into $\mathscr{F}_5^T$ under the same exchange. These form factors are thus connected by Bose symmetry [3].

5.1.2 Helicity Basis

There is an analogous basis to the one presented in eq. (5.1), which is the one used by experimentalists to report the measurements [392]. This is given by the Helicity Amplitudes, which are obtained from projecting the total amplitude into specific polarization states of the different particles:

$$H_{\lambda_1\lambda_2;\lambda_T} = \varepsilon_\mu^{\lambda_1^*}(q_1)\varepsilon_\nu^{\lambda_2^*}(q_2)\varepsilon_{\alpha\beta}^{\lambda_T}(p)\mathscr{M}^{\mu\nu\alpha\beta}(q_1,q_2). \tag{5.12}$$

[3] It is important to stress this fact at this early stage, as it will allow us to infer information from one form factor from the experimental measurements of the other one.

The helicity amplitudes in terms of the form factors are[124]:

$$\begin{aligned}
H_{++;0} = H_{--;0} =& \frac{(q_1^2-q_2^2)^2 - M_T^2(q_1^2+q_2^2)}{\sqrt{6}M_T^3}\mathscr{F}_1^T - \frac{\lambda_{T12}(M_T^2-q_1^2-q_2^2)}{2\sqrt{6}M_T^5}\mathscr{F}_2^T - \sqrt{\frac{2}{3}}\frac{q_1^2q_2^2}{M_T^3}\mathscr{F}_3^T \\
& - \frac{q_2^2(M_T^2-q_1^2-q_2^2)}{\sqrt{6}M_T^3}\mathscr{F}_4^T - \frac{q_1^2(M_T^2-q_1^2-q_2^2)}{\sqrt{6}M_T^3}\mathscr{F}_5^T, \\
H_{+-;+2} = H_{-+;-2} =& -\frac{M_T^2-q_1^2-q_2^2}{M_T}\mathscr{F}_1^T - \frac{2q_1^2q_2^2}{M_T^3}\mathscr{F}_3^T - \frac{q_2^2(M_T^2-q_1^2-q_2^2)}{M_T^3}\mathscr{F}_4^T - \frac{q_1^2(M_T^2-q_1^2-q_2^2)}{M_T^3}\mathscr{F}_5^T,
\end{aligned}$$

$$\begin{aligned}
H_{+0;+1} = H_{-0;-1} =& \frac{q_2^2}{\sqrt{q_2^2}}\left(\frac{M_t^2+q_1^2-q_2^2}{\sqrt{2}M_T^2}\mathscr{F}_1^T + \frac{q_1^2(M_T^2-q_1^2+q_2^2)}{\sqrt{2}M_T^4}\mathscr{F}_3^T\right. \\
& \left. + \frac{(M_T^2-q_1^2-q_2^2)(M_T^2-q_1^2+q_2^2)}{2\sqrt{2}M_T^4}\mathscr{F}_4^T + \frac{q_1^2(M_T^2+q_1^2-q_2^2)}{\sqrt{2}M_T^4}\mathscr{F}_5^T\right) \\
H_{0+;-1} = H_{0-;+1} =& -\frac{q_1^2}{\sqrt{q_1^2}}\left(\frac{M_t^2-q_1^2+q_2^2}{\sqrt{2}M_T^2}\mathscr{F}_1^T + \frac{q_2^2(M_T^2+q_1^2-q_2^2)}{\sqrt{2}M_T^4}\mathscr{F}_3^T\right. \\
& \left. + \frac{q_2^2(M_T^2-q_1^2+q_2^2)}{\sqrt{2}M_T^4}\mathscr{F}_4^T + \frac{(M_T^2-q_1^2-q_2^2)(M_T^2+q_1^2-q_2^2)}{2\sqrt{2}M_T^4}\mathscr{F}_5^T\right), \\
H_{00;0} =& \frac{q_1^2q_2^2}{\sqrt{q_1^2}\sqrt{q_2^2}}\left(\sqrt{\frac{2}{3}}\frac{2}{M_T}\mathscr{F}_1^T - \frac{\lambda_{T12}}{\sqrt{6}M_T^5}\mathscr{F}_2^T + \frac{M_T^4-(q_1^2-q_2^2)^2}{\sqrt{6}M_T^5}\mathscr{F}_3^T\right. \\
& \left. + \frac{(M_T^2-q_1^2+q_2^2)^2}{\sqrt{6}M_T^5}\mathscr{F}_4^T + \frac{(M_T^2+q_1^2-q_2^2)^2}{\sqrt{6}M_T^5}\mathscr{F}_5^T\right),
\end{aligned} \tag{5.13}$$

where $\lambda_{T12} = \lambda(M_T^2, q_1^2, q_2^2)$ is the Källen function[393] and the momenta dependence is implied when writing the form factors. It is important to notice that when exchanging $q_1^2 \leftrightarrow q_2^2$ and $\mathscr{F}_4^T \leftrightarrow \mathscr{F}_5^T$, we get invariance in the helicity amplitudes [4]. A particular case of these form factors is the one observed in the detectors, the single virtual case:

$$\mathscr{F}_{\lambda_T=0}^T = \frac{Q^2}{\sqrt{6}M_T^2}\mathscr{F}_1^T(-Q^2,0) - \frac{(M_T^2+Q^2)^2}{2\sqrt{6}M_T^4}\mathscr{F}_2^T(-Q^2,0) + \frac{Q^2}{\sqrt{6}M_T^2}\mathscr{F}_5^T(-Q^2,0),$$

[4] It is trivial in the first two and the last case, however in the $\lambda_T = \pm 1$ case, it is necessary to exchange also $\lambda_1 \leftrightarrow \lambda_2$ to see the connection between the form factors 4 and 5. This will allow us to connect the form factors and consequently, obtain information of both when only one of them is observed.

$$\mathscr{F}^T_{\lambda_T=1} = \frac{\sqrt{Q^2}}{\sqrt{2}M_T}\mathscr{F}^T_1(-Q^2,0) + \frac{\sqrt{Q^2}(M_T^2-Q^2)}{2\sqrt{2}M_T^3}\mathscr{F}^T_5(-Q^2,0),$$

$$\mathscr{F}^T_{\lambda_T=2} = -\mathscr{F}^T_1(-Q^2,0) + \frac{Q^2}{M_T^2}\mathscr{F}^T_5(-Q^2,0). \tag{5.14}$$

As it can be seen, the single virtual case probes $\mathscr{F}_4$ or $\mathscr{F}_5$ depending on which one we tag as the real photon and which one as the virtual one. We have exchanged the notation with respect to the one used in [392], where $\frac{q_1^2-M_T^2}{M_T}$ was factored out from the Helicity Amplitudes.

5.2 Tensor Pole Contributions

The pole contributions of the tensor mesons come from the 3 diagrams of Figure 5.2. The amplitude generated by these diagrams can be decomposed into the different tensor structures (and their respective scalar functions) of the Hadronic Light-by-Light tensor with the procedure described in [61]. By doing so, the T-pole contributions to $a_\mu^{\rm HLbL}$ can be computed. Given the 5 Form Factors, an evaluation of

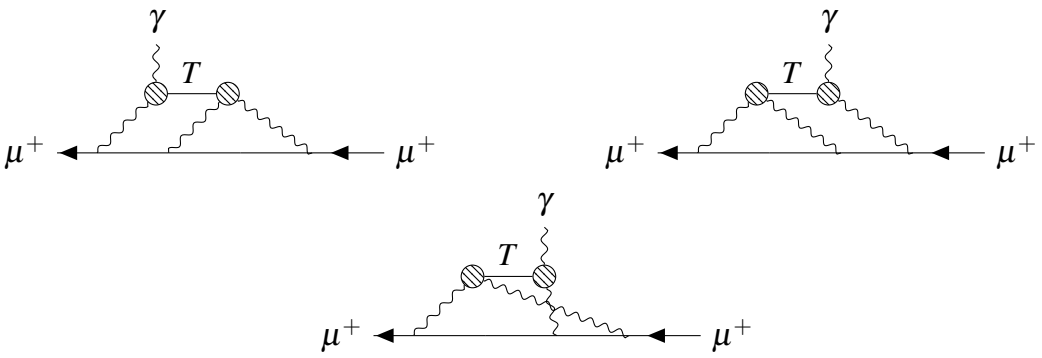

Fig. 5.2 Diagrams that contribute to the HLbL piece of the anomalous magnetic moment of the muon, which include tensor meson poles.

the Master Formula of eq. (1.28) is difficult due to the presence of kinematic singularities ($q_i \to 0$) in 4-point kinematics[61], in contrast with the case of the pseudoscalar, scalars and axial mesons, where these are absent in the current standard basis. An effort is being made to account for the Tensor meson pole contributions in triangle kinematics[236]. However, if only the combination of form factors $\mathscr{F}^T_{1,3}$ or $\mathscr{F}^T_{2,3}$ are different from zero, we can evaluate these contributions straightforwardly from the Master Formula. The first one is particularly interesting to study, as the 3 most recent determinations [67, 69, 122] have a non-zero $\mathscr{F}^T_{1,3}$, where the last one corresponds to

original work of this thesis.
The scalar functions for the Master Formula in the case $\mathscr{F}^T_{1,3} \neq 0$, $\mathscr{F}^T_{2,4,5} = 0$ are free of kinematic singularities and are given by:

$$\hat{\Pi}_1(q_1^2,q_2^2,q_3^2) = \frac{\mathscr{F}_1^T(q_2^2,0)}{M_T^6}\left(-M_T^2\mathscr{F}_1(q_1^2,q_3^2) + (q_1^2 - M_T^2)\mathscr{F}_3(q_1^2,q_3^2)\right) + q_1 \leftrightarrow q_2,$$

$$\begin{aligned}\hat{\Pi}_4(q_1^2,q_2^2,q_3^2) =& \frac{\mathscr{F}_1^T(q_3^2,0)}{3M_T^8(M_T^2-q_3^2)}\Big(8M_T^4q_3^2\mathscr{F}_1^T(q_1^2,q_2^2) + \Big[6M_T^6 + 3M_T^4(q_1^2+q_2^2) - 3M_T^2(q_1^2-q_2^2)^2 \\ & - q_3^2(4M_T^4 + 5M_T^2(q_1^2+q_2^2) + (q_1^2-q_2^2)^2)\Big]\Big) \\ & + \Big(\Big[\left(M_T^4 + 2M_T^2q_3^2 - q_3^2(q_1^3+2q_2^3+q_3^3) - q_1^2q_2^2\right)\mathscr{F}_3^T(q_1^2,q_3^2) \\ & + M_T^2\left(-4M_T^2 + q_1^2 + 3q_2^2 + q_3^3\right)\mathscr{F}_1^T(q_1^2,q_3^2)\Big]\frac{\mathscr{F}_1^T(q_2^2,0)}{M_T^6(M_T^2-q_2^2)} + q_1 \leftrightarrow q_2\Big),\end{aligned}$$

$$\begin{aligned}\hat{\Pi}_{17}(q_1^2,q_2^2,q_3^2) =& \Big[\Big(2q_3^2(M_T^2+q_1^2+q_2^2) + 3M_T^2(q_1^2+q_2^2)\Big)\mathscr{F}_3^T(q_1^2,q_2^2) \\ & - 2M_T^2(3M_T^2+2q_3^2)\mathscr{F}_1^T(q_1^2,q_2^2)\Big]\frac{\mathscr{F}_1^T(q_3^2,0)}{3M_T^8(M_T^2-q_3^2)} \\ & + \Big((q_3^2-q_1^2)\mathscr{F}_3^T(q_1^2,q_3^2)\frac{\mathscr{F}_1^T(q_2^2,0)}{M_T^6(M_T^2-q_2^2)} + q_1 \leftrightarrow q_2\Big),\end{aligned}$$

$$\begin{aligned}\hat{\Pi}_{54}(q_1^2,q_2^2,q_3^2) =& (q_1^2-q_2^2)\mathscr{F}_3^T(q_1^2,q_2^2)\frac{\mathscr{F}_1^T(q_3^2,0)}{M_T^6(M_T^2-q_3^2)} \\ & \Big(\Big[2M_T^2\mathscr{F}_1^T(q_1^2,q_3^2) - (q_1^2+q_3^2)\mathscr{F}_3^T(q_1^2,q_3^2)\Big]\frac{\mathscr{F}_1^T(q_2^2,0)}{M_T^6(M_T^2-q_2^2)} - q_1 \leftrightarrow q_2\Big).\end{aligned} \tag{5.15}$$

The remaining scalar functions are given by their symmetry relations. The remaining piece for computing these contributions are the form factors.

5.3 RχT Lagrangian: V+V′+P′+T

The form factors for this process will be given by Resonance Chiral Theory, where extra operators will be included to the ones previously used in Chapters 2 and 3 to include the interaction with the tensor mesons. We start with the Lagrangian that

includes the Tensor Mesons ($J^{PC} = 2^{++}$) in the symmetric hermitian rank-2 tensor field representation [281, 282]:

$$T_{\mu\nu} = \sum_{i=0}^{8} \frac{T^i_{\mu\nu}\lambda_i}{\sqrt{2}} = \begin{pmatrix} \frac{a_2}{\sqrt{2}} + \frac{f_2^8}{\sqrt{6}} + \frac{f_2^0}{\sqrt{3}} & a_2^+ & K_2^{*+} \\ a_2^- & -\frac{a_2}{\sqrt{2}} + \frac{f_2^8}{\sqrt{6}} + \frac{f_2^0}{\sqrt{3}} & K_2^{*0} \\ K_2^{*-} & \bar{K}_2^{*0} & -\frac{2f_2^8}{\sqrt{6}} + \frac{f_2^0}{\sqrt{3}} \end{pmatrix}_{\mu\nu}, \tag{5.16}$$

which is the same flavor structure as in the pseudoscalar and vector cases. The flavor states will be mixed, as the mass states are the ones for which the decay width is well defined. With this representation of the tensor mesons, the following kinetic term can be constructed:

$$\mathscr{L}_{\mathrm{kin}} = -\frac{1}{2}\langle T_{\mu\nu} D^{\mu\nu,\rho\sigma} T_{\rho\sigma}\rangle, \tag{5.17}$$

with

$$\begin{aligned} D^{\mu\nu,\rho\sigma} =& (\Box + M_T^2)\Big[\frac{1}{2}(g^{\mu\rho}g^{\nu\sigma} + g^{\mu\sigma}g^{\nu\rho}) - g^{\mu\nu}g^{\rho\sigma}\Big] + g^{\mu\nu}\partial^\rho\partial^\sigma + g^{\rho\sigma}\partial^\mu\partial^\nu \\ & - \frac{1}{2}\Big(g^{\mu\sigma}\partial^\nu\partial^\rho + g^{\mu\rho}\partial^\nu\partial^\sigma + \mu \leftrightarrow \nu\Big), \end{aligned} \tag{5.18}$$

being the covariant derivative that ensures the invariance of the term under unitary transformations. For the on-shell case, we get a mass term:

$$\mathscr{L}_m^{(0)} = -\frac{M_T^2}{2}\langle T_{\mu\nu} T^{\mu\nu}\rangle. \tag{5.19}$$

The superscript refers to the zeroth order in the chiral expansion. In [282], they go beyond the chiral limit as it is possible to fix the couplings when the only purpose is to reproduce the decay widths and masses of a_2, f_2 and f_2' [5]. The mass term recalls the need for a parametrization of the mixing of the flavor states when written in terms of the mass eigenstates. As it was done in [282], this can be given in terms of a

[5] It is necessary to mention that chiral corrections are not included in this work, since there will be more couplings that the ones which can be fixed when including vector meson resonances which are required for reproducing correctly the high-energy behavior. These chiral corrections are small and accounted for by our uncertainties.

single-angle parametrization:

$$\begin{aligned} f_2^8 &= \sin\theta_T f_2 + \cos\theta_T f_2', \\ f_2^0 &= \cos\theta_T f_2 - \sin\theta_T f_2', \end{aligned} \tag{5.20}$$

where θ_T parametrizes the mixing.

The final ingredient of the basic Lagrangian–which is only χPT+T– is the one of the tensor mesons interactions with the pGbs. In the chiral limit, the interactions compatible with the assumed symmetries are given by the term:

$$\mathscr{L}_{\text{TPP}}^{(0)} = g_T \langle T_{\mu\nu}\{u^\mu, u^\nu\}\rangle, \tag{5.21}$$

where the u^μ were defined in Chapter 2.

5.3.1 Minimal Lagrangian: No Derivatives

It can easily be seen that, without including the vector meson resonances, the form factors obtained from RχT cannot fulfill the SDCs from eq. (5.9). For obtaining a $1/\tilde{Q}^4$ behavior, at least 2 multiplets of tensor meson resonances need to be included, and even a $\sim 1/\tilde{Q}^6$ is required in the double virtual case. The propagators coming from the exchange of these vector mesons–determined by the same Feynman Rules as in the pseudoscalar meson TFF of chapter 3– produce the setup to impose the SDCs to the TFFs obtained from RχT.

The first case to be studied is the minimal: to include the vector mesons without considering additional derivatives to the ones coming from the electromagnetic fields, $f_+^{\mu\nu}$ ($F^{\mu\nu}$, equivalently).

We have considered the most general Lagrangian consistent with the symmetries of RχT, at leading order in the $1/N_C$ expansion, in the chiral limit ($m_{u,d,s} \to 0$) and –by assumption– without derivatives (we have reconsidered, see table 5.2, this hypothesis). In the minimal realization, which includes pseudoscalar mesons, vector meson resonances, photons, tensor mesons, and their interactions, only 6 operators contribute – in this approximation– to the radiative tensor decays, which are collected in Table 5.1. Their real coupling constants are named according to the interaction vertices they describe and are not fixed by symmetry requirements. With this set of operators, we obtained only $\mathscr{F}_1^T$ different from zero for the 3 contributing neutral

Coupling constant	Operator
$C_{T\gamma\gamma}$	$\langle T^{\mu\nu}\{f_{+\mu}^{\alpha}, f_{+\alpha\nu}\}\rangle$
$C_{T\gamma V}$	$i\langle T^{\mu\nu}\{f_{+\mu}^{\alpha}, V_{\alpha\nu}\}\rangle$
$C_{T\gamma V'}$	$i\langle T^{\mu\nu}\{f_{+\mu}^{\alpha}, V'_{\alpha\nu}\}\rangle$
C_{TVV}	$\langle T^{\mu\nu}\{V_{\mu}^{\alpha}, V_{\alpha\nu}\}\rangle$
$C_{TV'V'}$	$\langle T^{\mu\nu}\{V'^{\alpha}_{\mu}, V'_{\alpha\nu}\}\rangle$
$C_{TVV'}$	$\langle T^{\mu\nu}\{V_{\mu}^{\alpha}, V'_{\alpha\nu}\}\rangle$

Table 5.1 Relevant RχT Operators at leading order in the $1/N_C$ expansion and in the chiral limit, neglecting operators with derivatives. We note that $C_{T\gamma V^{(\prime)}}$ are dimensionless, while $(C_{T\gamma\gamma})\ C_{TV^{(\prime)}V^{(\prime)}}$ have (inverse) energy dimensions.

tensor mesons:

$$\begin{aligned}\mathscr{F}_1^{a_2}(q_1^2,q_2^2) =& -\frac{M_{a_2}}{2}\left[\frac{\sqrt{2}}{3}C_{T\gamma\gamma}+C_{T\gamma V}\frac{4F_V}{3}\left(D_{M_V}^{-1}(q_1^2)+D_{M_V}^{-1}(q_2^2)\right)\right.\\ &\left.+C_{TVV}\frac{2\sqrt{2}F_V^2}{3}D_{M_V}^{-1}(q_1^2)D_{M_V}^{-1}(q_2^2)+C_{TVV'}\frac{2\sqrt{2}F_VF_{V'}}{3}D_{M_V}^{-1}(q_1^2)D_{M_{V'}}^{-1}(q_2^2)+V\leftrightarrow V'\right],\end{aligned}$$

$$\begin{aligned}\mathscr{F}_1^{f_2}(q_1^2,q_2^2) =& -\frac{M_{f_2}}{2}\left[\frac{\sqrt{2}}{3\sqrt{3}}C_{T\gamma\gamma}\left(\sin\theta_T+2\sqrt{2}\cos\theta_T\right)\right.\\ &+C_{T\gamma V}\left(8\sin\theta_T+11\sqrt{2}\cos\theta_T\right)\frac{2\sqrt{3}F_V}{27}\left(D_{M_V}^{-1}(q_1^2)+D_{M_V}^{-1}(q_2^2)\right)\\ &+C_{TVV}\left(\sin\theta_T+2\sqrt{2}\cos\theta_T\right)\frac{2\sqrt{2}F_V^2}{3\sqrt{3}}D_{M_V}^{-1}(q_1^2)D_{M_V}^{-1}(q_2^2)\\ &\left.+C_{TVV'}\left(\sin\theta_T+2\sqrt{2}\cos\theta_T\right)\frac{2\sqrt{2}F_VF_{V'}}{3\sqrt{3}}D_{M_V}^{-1}(q_1^2)D_{M_{V'}}^{-1}(q_2^2)+V\leftrightarrow V'\right],\\ \mathscr{F}_1^{f_2'}(q_1^2,q_2^2) =& \left.\mathscr{F}_1^{f_2}(q_1^2,q_2^2)\right|_{\sin\theta_T\to\cos\theta_T,\cos\theta_T\to-\sin\theta_T,M_{f_2}\to M_{f_2'}},\end{aligned}\tag{5.22}$$

where $D_{M_R}(q_i^2)=M_R^2-q_i^2$.

Since in a model with finite resonances only a discrete amount of short-distance constraints (SDCs) can be imposed, for the $\mathscr{F}_1^T$ FF we choose to fix the symmetric double virtual case and the single virtual $1/Q^4$ behavior

$$\begin{aligned}\lim_{Q^2\to\infty}\mathscr{F}_1^T(-Q^2,-Q^2) &= -\frac{3F_T^{\rm eff}M_T^3}{14Q^4},\\ \lim_{Q^2\to\infty}\mathscr{F}_1^T(-Q^2,0) &\sim \frac{1}{Q^4},\end{aligned}\tag{5.23}$$

where $Q_i^2 = -q_i^2$, and $F_T^{\rm eff}$ has the value from eq. (5.10) . We note that the magnitude of $\mathscr{F}_1^T$ is overestimated this way, since for one finite and another asymptotic photon virtuality, $\mathscr{F}_1^T$ should vanish as $\sim \ln Q^2/Q^6$ (which we will approximate as $\sim 1/Q^4$ because we are working with the rational approximant). However, with two multiplets of vector meson resonances (and also with three of them), we get $\mathscr{F}_1^T \sim 1/Q^2$ in this mixed region, which we consider as a systematic error when computing $a_\mu^{\rm HLbL:T-pole}$. The resulting FFs, after imposing the high-energy constraints mentioned above, are:

$$\mathscr{F}_1^T(q_1^2,q_2^2) = c_T M_T \frac{9F_T^{\rm eff}\tilde{M}_T^2(M_V^4 - q_1^2q_2^2)/\tilde{c}_T - 14\sqrt{2}C_{TVV}F_V^2(M_V^2 - M_{V'}^2)^2}{42\,D_{M_V}(q_1^2)D_{M_V}(q_2^2)D_{M_{V'}}(q_1^2)D_{M_{V'}}(q_2^2)}, \tag{5.24}$$

where c_T is a flavor space coefficient, given by: $c_{a_2} = 1$, $c_{f_2} = \frac{\sin\theta_T + 2\sqrt{2}\cos\theta_T}{\sqrt{3}}$, $c_{f_2'} = \frac{\cos\theta_T - 2\sqrt{2}\sin\theta_T}{\sqrt{3}}$. There is a difference between M_T and $\tilde{M}_T$, c_T and $\tilde{c}_T$ since the first ones come from the definition of the TFFs and the second ones stem from the short distance constraints, as we shall discuss later. The only free parameters left are the combination $C_{TVV}F_V^2$ and the mixing angle θ_T. These two parameters can be used to normalize the form factors to reproduce the radiative decay widths as was done in ref. [282]. We will take their chiral limit value for the mixing angle, $\theta_T = (27.2 \pm 1.1)^\circ$, and fix $C_{TVV}F_V^2 = (0.110 \pm 0.005)\ \text{GeV}^3$, from the measured value of $\Gamma(a_2 \to \gamma\gamma)$.

Given the SDCs imposed to the TFF from eq. (5.22) we get the following relation between couplings:

$$\begin{aligned} C_{T\gamma R} &= 0, \quad R \in \gamma, V, V' \\ F_V F_{V'} C_{TVV'} &= \frac{9F_T^{\rm eff}\tilde{M}_T^2 M_V^2/\tilde{c}_T}{14\sqrt{2}\left(M_V^2 - M_{V'}^2\right)} - F_V^2 C_{TVV}, \\ F_{V'}^2 C_{TV'V'} &= F_V^2 C_{TVV} - \frac{9F_T^{\rm eff}\tilde{M}_T^2\left(M_V^2 + M_{V'}^2\right)/\tilde{c}_T}{14\sqrt{2}\left(M_V^2 - M_{V'}^2\right)}, \end{aligned} \tag{5.25}$$

which makes also possible to evaluate the other couplings, namely: $C_{TVV'}F_V F_{V'} = -(0.121 \pm 0.005)\,\text{GeV}^3$ and $C_{TV'V'}F_{V'}^2 = (0.195 \pm 0.010)\,\text{GeV}^3$ [6]. These 5 constraints, together with the determination of $C_{TVV}F_V^2$ and θ_T, fix the 6 coupling constants and the mixing parameter, leading to a fully determined $\mathscr{F}_1^T$ for all $T = a_2, f_2, f_2'$. As mentioned before, there are two masses, one coming from the definition of the form factors, which is the mass of each tensor(M_T), and the one coming from these

[6] The corresponding uncertainties are negligible with respect to the one obtained in the systematic and statistical obtained for the computation of the $a_\mu^{\rm HLbL:T-poles}$.

SDCs, which can only be imposed once. Consequently, $\tilde{M}_T$ and $\tilde{c}_T$ are choices; the systematic error induced by choosing one of the three masses or the isospin average of them for $\tilde{M}_T$ and $\tilde{c}_T$ is addressed later in this section.

For the remaining parameters of eqs. (5.24), we use the PDG input [217] for the tensor meson masses and their radiative decay widths. The effective masses of the vector meson multiplets are obtained from the study of $a_\mu^{\rm P-pole}$, within $R\chi T$, in ref. [62]. Thus, with all parameters fixed -within uncertainties- we complete our description of the tensor mesons $\mathscr{F}_1^T$.

5.3.1.1 Systematic and Statistical errors

The statistical errors come from the propagation of errors of the parameters and couplings in eq. (5.24). The systematic ones come –in principle– from two main sources:

- first, the asymptotic term in eq. (5.23) can be fixed for only one of the tensor mesons, as all couplings are common; consequently, one must choose either one of them. This will result in a factor of $\tilde{c}_T$ dividing the first term of the numerator in eq. (5.24), and setting $\tilde{M}_T$ to $M_{a_2}, M_{f_2}, M_{f_2'}$ or $\bar{M}$, the isospin average. We have chosen $T = a_2$, since it has the middle value of c_T and M_T; consequently, the mismatch of the asymptotic behavior of the non-chosen ones will be reduced to a minimum. In order to compute the error induced by this choice, we studied all 3 possibilities and considered an error bar that contains the 3 curves.

- second, fulfilling all known SDCs is impossible in our setting with a finite amount of resonances. In the limiting case when one momentum is asymptotic and the other one is finite, we get a $1/Q^2$ behavior, but it should scale as $\frac{\ln Q^2}{Q^6}$. In order to estimate this error–in the same fashion as in [47]– we used a Canterbury Approximant which behaves as similar as possible to this limit, $1/Q^4$.

The second point needs to be written more explicitly. For this purpose, the minimal choice is a $C_2^0(Q_1^2, Q_2^2)$:

$$\mathscr{F}_1^T(Q_1^2, Q_2^2) = \frac{\mathscr{F}_1^T(0,0)}{1 + \beta_1^T(Q_1^2 + Q_2^2) + \beta_{1,1}^T Q_1^2 Q_2^2 + \beta_2^T(Q_1^4 + Q_2^4)}, \tag{5.26}$$

where we omit the terms with $\beta^T_{1,2}$ and $\beta^T_{2,2}$ coefficients, as they contribute to orders $1/Q^6$ and $1/Q^8$ in the asymptotic behavior. All single virtual, double virtual, and mixed asymptotic behaviors, $\sim (1/Q^4)$, can be reproduced by the condition:

$$\beta^T_2 = \frac{-14\mathscr{F}^T_1(0,0) - 3\beta_{1,1}F^{\text{eff}}_T M^3_T}{6F^{\text{eff}}_T M^3_T}. \tag{5.27}$$

The 2 remaining constants, β^T_1 and $\beta^T_{1,1}$, will be fixed by matching the first two low-energy-expansion constants from our model and the considered $C^0_2(Q^2_1, Q^2_2)$, eq. (5.26) [7]:

$$\frac{\mathscr{F}^T_1(Q^2_1, Q^2_2)}{\mathscr{F}^T_1(0,0)} \approx 1 - \frac{a^T_1}{M^2_T}(Q^2_1 + Q^2_2) + \frac{b^T_{1,1}}{M^4_T}Q^2_1 Q^2_2 + ..., \tag{5.28}$$

leading to the following relations:

$$\beta^T_1 = \frac{1}{M^2_\Lambda} = \frac{1}{M^2_V} + \frac{1}{M^2_{V'}},$$

$$\beta^T_{1,1} = \frac{1}{M^4_{\Lambda'}} = \frac{14\sqrt{2}C_{TVV}F^2_V(M^4_V - M^4_{V'})^2 - 9F^{\text{eff}}_T\tilde{M}^2_T M^4_V(M^4_V + 2M^2_V M^2_{V'} + 2M^4_{V'})/\tilde{c}_T}{M^4_V M^4_{V'}\left[14\sqrt{2}C_{TVV}F^2_V(M^2_V - M^2_{V'})^2 - 9F^{\text{eff}}_T\tilde{M}^2_T M^4_V/\tilde{c}_T\right]}, \tag{5.29}$$

where we introduced the two scales that are similar in magnitude to the mass of the first vector meson resonance, $M_\Lambda \sim M_{\Lambda'} \sim M_\rho$. It is important to remember that $\tilde{M}_T$ is the mass chosen for imposing the SDCs, and that only appears when matching the low energy constants, since the SDCs are imposed independently for each meson in this approach.

Moreover, the asymptotic behavior of the Canterbury Approximant is given by:

$$\lim_{\tilde{Q}^2\to\infty} \mathscr{F}^T_1(q^2_1, q^2_2) \to \frac{4\sum_a C_a F^a_T M^3_T}{\tilde{Q}^4}\left(-\frac{3\mathscr{F}^T_1(0,0)M^4_{\Lambda'}}{14\mathscr{F}^T_1(0,0)M^4_{\Lambda'}(w^4+6w^2+1) + 24F^{\text{eff}}_T M^3_T w^2}\right). \tag{5.30}$$

With the systematic and statistical errors being discussed, we obtained a model for the transition form factor $\mathscr{F}^T_1$, which is shown in figure 5.3, where it is compared with the models used for the $a_\mu^{\text{HLbL:T}-\text{poles}}$ and with the Canterbury Approximant previously discussed.

[7] These constraints will produce a good description at low energies, which is desired when working with a_μ.

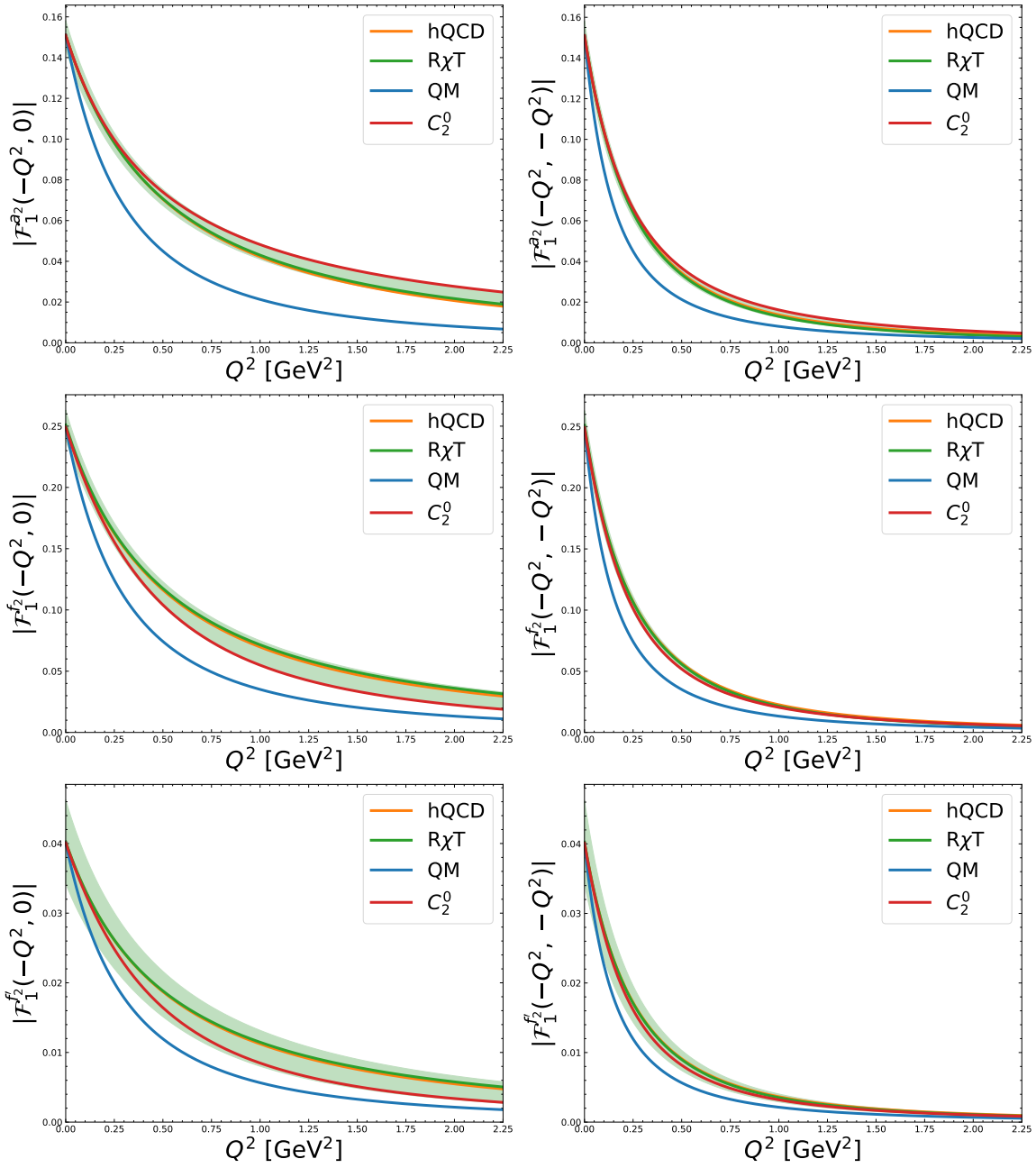

Fig. 5.3 Comparison between the simple quark model (QM) [387] used in the dispersive determination [67], the holographic QCD (hQCD) hard-wall model [69], the RχT model used in this work and the C_2^0 of eq. (5.26) for the single and symmetric double virtual form factor $\mathcal{F}_1^T$, for all 3 tensor mesons: $a_2(1320)$, $f_2(1270)$ and $f_2'(1525)$. Our one σ uncertainties are displayed by the green band.

There is scarce related experimental information to validate our model. However, Belle [392] measured the single virtual form factors for the $f_2(1270)$ tensor meson

in the helicity basis of eq. 5.14. In this minimal case, this is reduced as only $\mathscr{F}_1^T$ is different from zero. The comparison of these data with the quark model used in [67], the Hard-Wall model used in [69], and our results is shown in Figure 5.4. Our model exhibits good agreement with the experimental data.

It is important to remark that –by construction– these TFFs fulfill the doubly

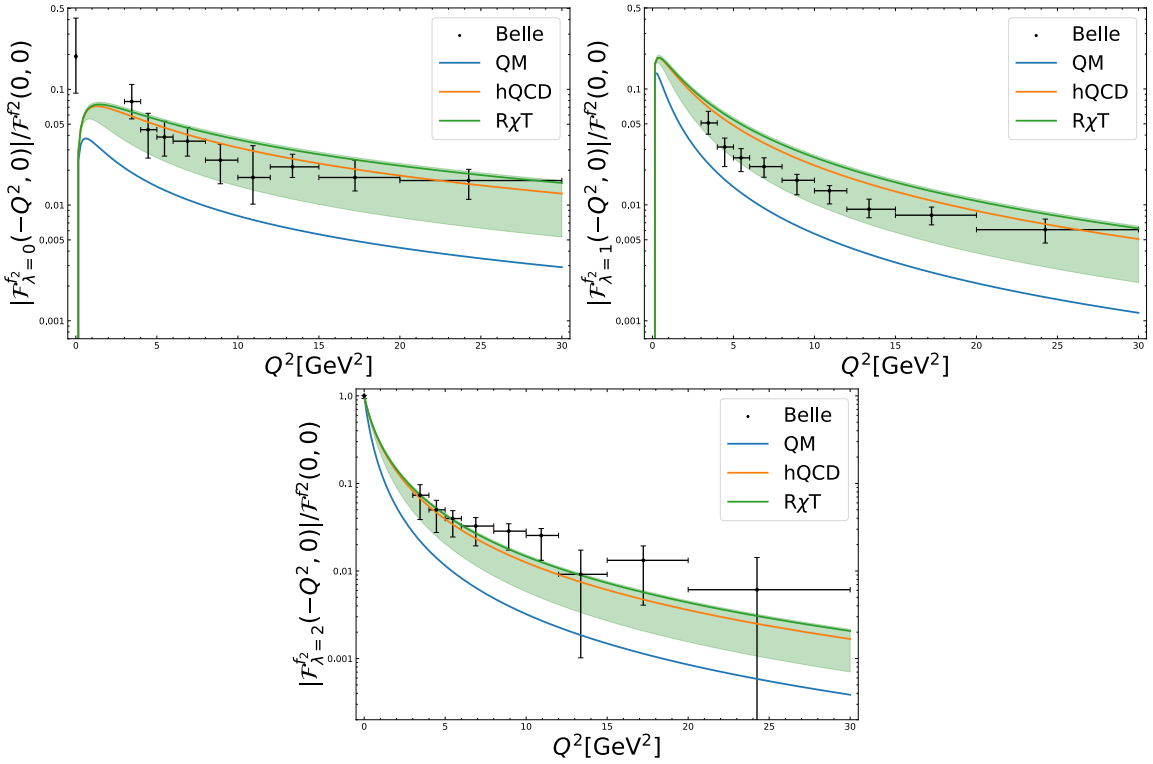

Fig. 5.4 Comparison between the simple quark model (QM) [387] used in ref. [67], the hard-wall model (hQCD) [69] and this work ($R\chi T$) with the Belle data [392] in the helicity basis of eq. (5.14) for the $f_2(1270)$ tensor meson, normalized by $\mathscr{F}^{f_2}(0,0) = \sqrt{\frac{5\Gamma_{T\gamma\gamma}}{\pi\alpha^2 M_T}}$. Our one σ uncertainties are displayed by the green band.

virtual asymptotic behavior given in ref. [124]. However, for arbitrary asymmetries –parametrized by $w = \frac{q_1^2-q_2^2}{q_1^2+q_2^2}$, so that $\mathscr{F}_i^T(q_1^2,q_2^2) = \mathscr{F}_i^T(\tilde{Q}^2) f_i^T(w)$–, for $\tilde{Q}^2 = \frac{q_1^2+q_2^2}{2} \to \infty$, we get:

$$\lim_{\tilde{Q}^2\to\infty} \mathscr{F}_1^T(q_1^2,q_2^2) \to \frac{4\sum_a C_a F_T^a M_T^3}{\tilde{Q}^4}\left(-\frac{3}{14}(1-w^2)^{-1}\right), \tag{5.31}$$

which is simpler than the ones obtained by refs. [124] and [69]. One reason for the lack of structure of our result is the truncation of the infinite tower of interactions to two vector and the lightest tensor meson multiplets. If the infinite tower of

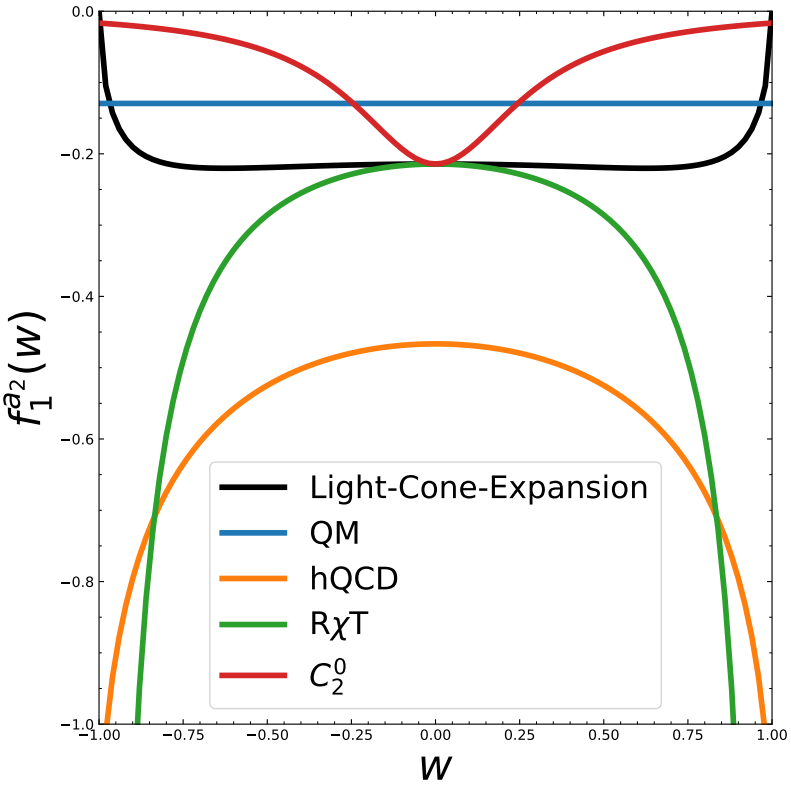

Fig. 5.5 Comparison of the full asymmetry range of the asymptotic behavior of $f_1^{a_2}(w)$ given by ref. [124] using the Light-Cone-Expansion, the quark model (QM) [387] used in ref. [67], the hard-wall model of ref. [69] (hQCD) and this work ($R\chi T$ in green and C_2^0 in red).

resonances were not integrated out, a logarithmic term would be expected, as in the quoted refs.

The comparison between the asymmetry functions for the a_2 –which is representative for all tensor mesons–, is shown in Figure 5.5, where it is clear that none of the 3 models that have been used for computing the $a_\mu^{\mathrm{HLbL:T-poles}}$ fulfills the asymmetric asymptotic behavior predicted by ref. [124] for f_1^T, being generally worse as the asymmetry approaches the single virtual case. However, noticeably, in the purely hadronic region where these contributions are computed, the high-energy behavior does not significantly influence the resulting contributions to a_μ. The matching at $Q_0 = 1.5$ GeV is shown in the left plot of Figure 5.6 for $\mathscr{F}_1^T$. There it can be seen, again, that the single virtual asymptotic behavior ($\lambda = 0$) is not reproduced. Near the symmetric ($\lambda = 1$) asymptotic behavior, a better transition is achieved –as expected– for higher values of the matching scale $Q_0 = 7.5\,\mathrm{GeV}$, as it can be appreciated in the right plot of Figure 5.6.

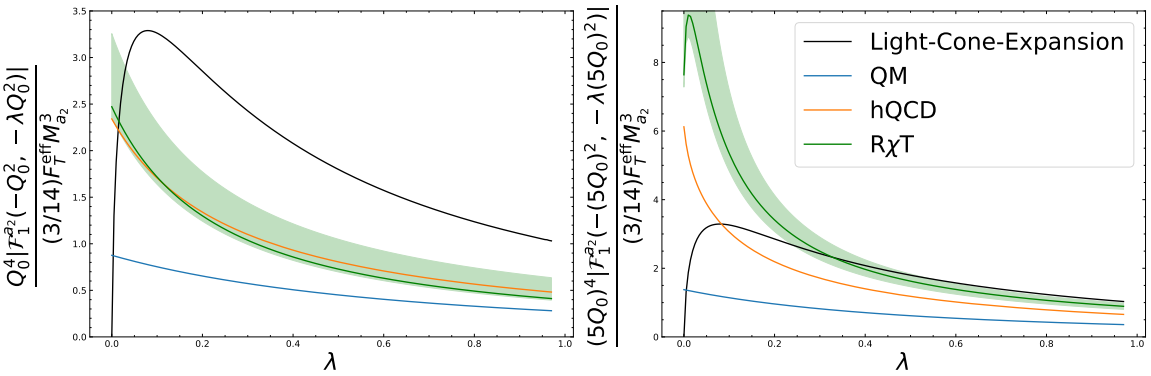

Fig. 5.6 Transition from the purely hadronic to the asymptotic region as a function of the relative virtuality of both photons, λ, at the matching scale $Q_0 = 1.5\,\text{GeV}$(left) and $5Q_0$(right) for the 3 models considered for $\mathscr{F}_1^T$ and the Light-Cone-Expansion. Our one σ uncertainties are displayed by the green band.

For the a_μ computation, we use the master formula provided in ref. [46], using the optimized basis in ref. [61] with the scalar functions from eq. (5.15), which allows for an evaluation of the tensor meson poles without kinematic singularities for specific cases, including the one where only $\mathscr{F}_1^T$ is non-vanishing: In this way, we got the following results:

$$a_\mu^{\text{a}_2-\text{pole}} = -\left(1.09(10)_{\text{stat}}\left(^{+0.11}_{-0.00}\right)_{\text{syst}}\right)\times 10^{-11}, \tag{5.32a}$$

$$a_\mu^{\text{f}_2-\text{pole}} = -\left(3.4(3)_{\text{stat}}\left(^{+0.0}_{-0.4}\right)_{\text{syst}}\right)\times 10^{-11}, \tag{5.32b}$$

$$a_\mu^{\text{f}_2'-\text{pole}} = -\left(0.046(14)_{\text{stat}}\left(^{+0.000}_{-0.008}\right)_{\text{syst}}\right)\times 10^{-11}, \tag{5.32c}$$

$$a_\mu^{a_2+f_2+f_2'-\text{pole}} = -\left(4.5^{+0.3}_{-0.5}\right)\times 10^{-11}. \tag{5.32d}$$

These results are compatible with those from [67] and [69]–when evaluating only the contribution coming from $\mathscr{F}_1^T$– and the average done for the White Paper of the muon's $g-2$ Theory Initiative [6]–where the holographic results included the contributions from $\mathscr{F}_3^T$–.

5.3.2 Minimally Extended Model: $T\partial V\partial V$

We further considered an ad hoc extension consisting in the operators of the kind $\langle T^{\mu\nu}\{\nabla_\alpha R_\mu^\alpha, \nabla_\lambda R_\nu^{(\prime)\lambda}\}\rangle$–with $R, R' = f, V, V'$ as in Table 5.1–, resulting in 6 additional

operators, which are displayed in Table 5.2 [8]. We choose this particular extension since it generates a non-zero $\mathscr{F}_T^3$ TFF, as put forward in [69]. This allows for an evaluation of $a_\mu^{\rm HLbL:\,T-poles}$ which is free of kinematic singularities in the optimized basis of Ref. [61] (contrary to what happens in a more general treatment, that deserves further study). This study intends to confirm the sign change in the evaluation of the tensor meson pole contributions when a non-zero $\mathscr{F}_3^T$ is present. The $\mathscr{F}_3^T$ FF is obtained straightforwardly, noting that

Coupling constant	Operator
$g_{T\gamma\gamma}$	$\langle T^{\mu\nu}\{\nabla_\alpha f_{+\mu}^\alpha, \nabla_\lambda f_{+\nu}^\lambda\}\rangle$
$g_{T\gamma V}$	$i\langle T^{\mu\nu}\{\nabla_\alpha V_\mu^\alpha, \nabla_\lambda f_{+\nu}^\lambda\}\rangle$
$g_{T\gamma V'}$	$i\langle T^{\mu\nu}\{\nabla_\alpha V_\mu'^\alpha, \nabla_\lambda f_{+\nu}^\lambda\}\rangle$
g_{TVV}	$\langle T^{\mu\nu}\{\nabla_\alpha V_\mu^\alpha, \nabla_\lambda V_\nu^\lambda\}\rangle$
$g_{TV'V'}$	$\langle T^{\mu\nu}\{\nabla_\alpha V_\mu'^\alpha, \nabla_\lambda V_\nu'^\lambda\}\rangle$
$g_{TVV'}$	$\langle T^{\mu\nu}\{\nabla_\alpha V_\mu^\alpha, \nabla_\lambda V_\nu'^\lambda\}\rangle$

Table 5.2 RχT Operators that are obtained adding two derivatives to those in Table 5.1, which only generate $\mathscr{F}_T^3$. The energy dimension of the coefficients of the operators with zero, one and two resonances is -3, -2 and -1, respectively.

$$\mathscr{F}_3^T(q_1^2,q_2^2) = M_T^2 \mathscr{F}_1^T(q_1^2,q_2^2)|_{C_T\to g_T}. \tag{5.33}$$

However, the SDCs for these form factors are different from the ones for $\mathscr{F}_1^T$ as can be seen in eq. (5.9). For the $\mathscr{F}_3^T$, we have chosen to fix the doubly virtual behavior, both symmetric and asymmetric, to their leading power law, and in the case of double virtuality, we matched the coefficient to the one given by the Light-Cone-Expansion in ref. [124]:

$$\begin{aligned}\lim_{Q\to\infty} \mathscr{F}_3^T(-Q^2,-Q^2) &= -\frac{8}{21}\frac{F_T^{\rm eff} M_T^5}{Q^6},\\ \lim_{Q^2\to\infty} \mathscr{F}_3^T(-Q^2,-\lambda Q^2) &\sim \frac{1}{Q^6}, \quad \lambda\in(0,1).\end{aligned} \tag{5.34}$$

This happens for the same reasons as in $\mathscr{F}_1^T$, as a result of the impossibility of imposing the symmetric double virtual constraint to the 3 tensor mesons simultaneously and having to choose only one that determines the rest. Analogously to the $\mathscr{F}_1^T$ case,

[8] The covariant derivatives are constructed as in refs. [247, 274]. However, for the case at hand, $\nabla_\lambda \to \partial_\lambda$.

we have chosen a_2 and get the following constraints on the parameters:

$$\begin{aligned} g_{T\gamma R} &= 0, \quad R \in \gamma, V, V', \\ F_V^2 g_{TVV} &= -\frac{21\mathscr{F}_{a_2}^3(0,0)M_V^4 M_{V'}^4 + 8F_T^{\rm eff} M_{a_2}^5 M_V^2}{7\sqrt{2}M_{a_2}^3\left(M_V^2 - M_{V'}^2\right)^2}, \\ F_V F_{V'} g_{TVV'} &= \frac{21\mathscr{F}_{a_2}^3(0,0)M_V^4 M_{V'}^4 + 4F_T^{\rm eff} M_{a_2}^5\left(M_V^2 + M_{V'}^2\right)}{7\sqrt{2}M_{a_2}^3\left(M_V^2 - M_{V'}^2\right)^2}, \\ F_{V'}^2 g_{TV'V'} &= -\frac{21\mathscr{F}_{a_2}^3(0,0)M_V^4 M_{V'}^4 + 8F_T^{\rm eff} M_{a_2}^5 M_{V'}^2}{7\sqrt{2}M_{a_2}^3\left(M_V^2 - M_{V'}^2\right)^2}, \end{aligned}$$

which results in [9]

$$\mathscr{F}_3^T(q_1^2,q_2^2) = c_T\left(\frac{M_T^3}{M_{a_2}^3}\right)\frac{\frac{4}{21}F_T^{\rm eff}M_{a_2}^5\left(q_1^2+q_2^2\right) + \mathscr{F}_3^{a_2}(0,0)M_V^4 M_{V'}^4}{D_{M_V}(q_1^2)D_{M_V}(q_2^2)D_{M_{V'}}(q_1^2)D_{M_{V'}}(q_2^2)}. \tag{5.35}$$

There is a ratio between the normalization of the form factors given by the flavor space rotation factor c_P and a mass factor, $\left(\frac{M_T^3}{M_{a_2}^3}\right)$, induced by imposing the SDCs to $\mathscr{F}_3^{a_2}$, which also appears in the high-energy term.

It can be seen that, in contrast to the $\mathscr{F}_1^T$ case, we have 6 constraints instead of 5 from the SDCs and one for the normalization. This is due to the main source of error: The lack of knowledge of $\mathscr{F}_3^T(0,0)$. A convenient notation has been used to make this evident, and –once again– only one of the normalizations can be imposed; the rest of them are given by the mixing angle θ_T.

The asymptotic behavior of $\mathscr{F}_3^T$ is given by

$$\mathscr{F}_3^T(q_1^2,q_2^2) \to \frac{4\sum_a C_a F_T^a M_T^5}{\tilde{Q}^6}\left(\frac{8}{21}(1-w^2)^{-2}\right), \tag{5.36}$$

where once more we observe the fact that with a finite amount of vector meson resonances, it is impossible to obtain the rich structure that is present in refs. [124, 69]. The comparison between these 3 results for the asymmetric piece of the asymptotic behavior of $\mathscr{F}_3^T$ is shown in Figure 5.7. We can see that the asymmetric piece of the asymptotic behavior of this form factor within RχT and hQCD is in less tension than for $\mathscr{F}_1^T$.

[9] The aforementioned behavior is achieved for all asymmetries except $\lambda = 0$. In this case, the symmetric part of the SDCs in ref. [124] behaves as $\frac{1}{Q^6}$, but in our approach it goes as $\frac{1}{Q^2}$. We account for this as a systematic uncertainty.

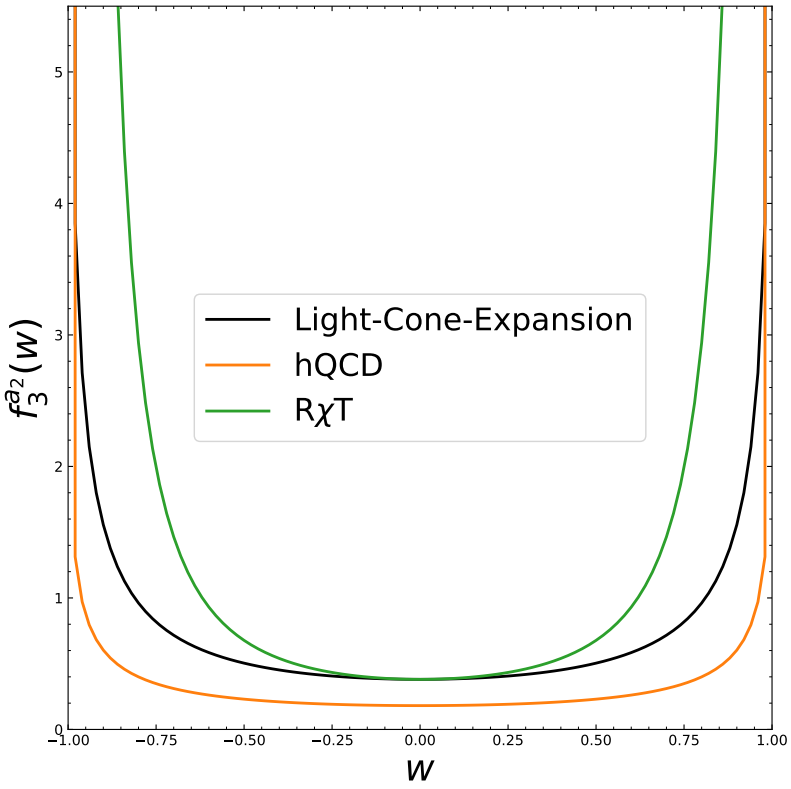

Fig. 5.7 Comparison of the full asymmetry range of the asymptotic behavior of $f_3^{a_2}(w)$ given by ref. [124] using the Light-Cone-Expansion, the hard-wall model of ref. [69] (hQCD) and this work ($R\chi T$).

5.3.2.1 $\mathscr{F}_3^T(0,0)$ ballpark within RχT

The lack of information on the normalization of the third form factor is the main problem for an RχT description of them. In [69], a value for $\mathscr{F}_3^T(0,0)$ was obtained within their formalism. However, we cannot cast their value to solve this issue, as it is not data-driven as the rest of our study. Instead, we performed an interpolation from the normalization of $\mathscr{F}_1^T(0,0)$. This procedure is based on the fulfillment of the SDCs coming from the Light-Cone-Expansion[124] results at different scales. We require that the ratio of the RχT and the LCE one is matched for $\mathscr{F}_1^T$ and $\mathscr{F}_3^T$ at a scale Q_λ. This matching depends on $\mathscr{F}_3^T(0,0)$, specifically for the a_2 case, since it defines the rest of the normalizations, as mentioned above. Consequently, floating the matching scale leads to different values for the normalization. We will take the average of the upper and lower limit and use an error that spans the whole region of results for $\mathscr{F}_3^{a_2}(0,0)$. The matching condition is then:

$$\frac{\mathscr{F}_3^{a_2-\mathrm{R}\chi\mathrm{T}}(Q_\lambda^2,Q_\lambda^2)}{\mathscr{F}_3^{a_2-\mathrm{LCE}}(Q_\lambda^2,Q_\lambda^2)}=\frac{\mathscr{F}_1^{a_2-\mathrm{R}\chi\mathrm{T}}(Q_\lambda^2,Q_\lambda^2)}{\mathscr{F}_1^{a_2-\mathrm{LCE}}(Q_\lambda^2,Q_\lambda^2)}. \tag{5.37}$$

The results for the matching for the 3 neutral tensor mesons are shown in Fig. 5.8. It can be seen that the value of the hQCD is included in the possible region for the normalization coming directly from RχT inference. The region is wide; however, it is a conservative approach given the lack of information on the normalization of the FFs.

As it can be seen, this procedure spans a wide range of possible *negative* values for $\mathscr{F}_3^T(0,0)$. This sign implies that we do not expect a sign change in the form factor, as the asymptotic behavior is also negative. The values for the normalizations are:

$$\begin{aligned}\mathscr{F}_3^{a_2}(0,0)&=-(0.106\pm0.101),\\ \mathscr{F}_3^{f_2}(0,0)&=-(0.165\pm0.156),\\ \mathscr{F}_3^{f_2'}(0,0)&=-(0.038\pm0.036).\end{aligned}$$

The rest of the parameters are the same ones as in the $\mathscr{F}_1^T$ case. The remaining statistical and systematic errors are negligible with respect to the one coming from the RχT interpolation for the normalization. The results are shown in the Figure. 5.10 and are compared with the ones from hQCD. It can be seen that the central values of a_2 and f_2 of the two approaches are close; however, for f_2' the hQCD curve is closer to the upper bound of RχT.

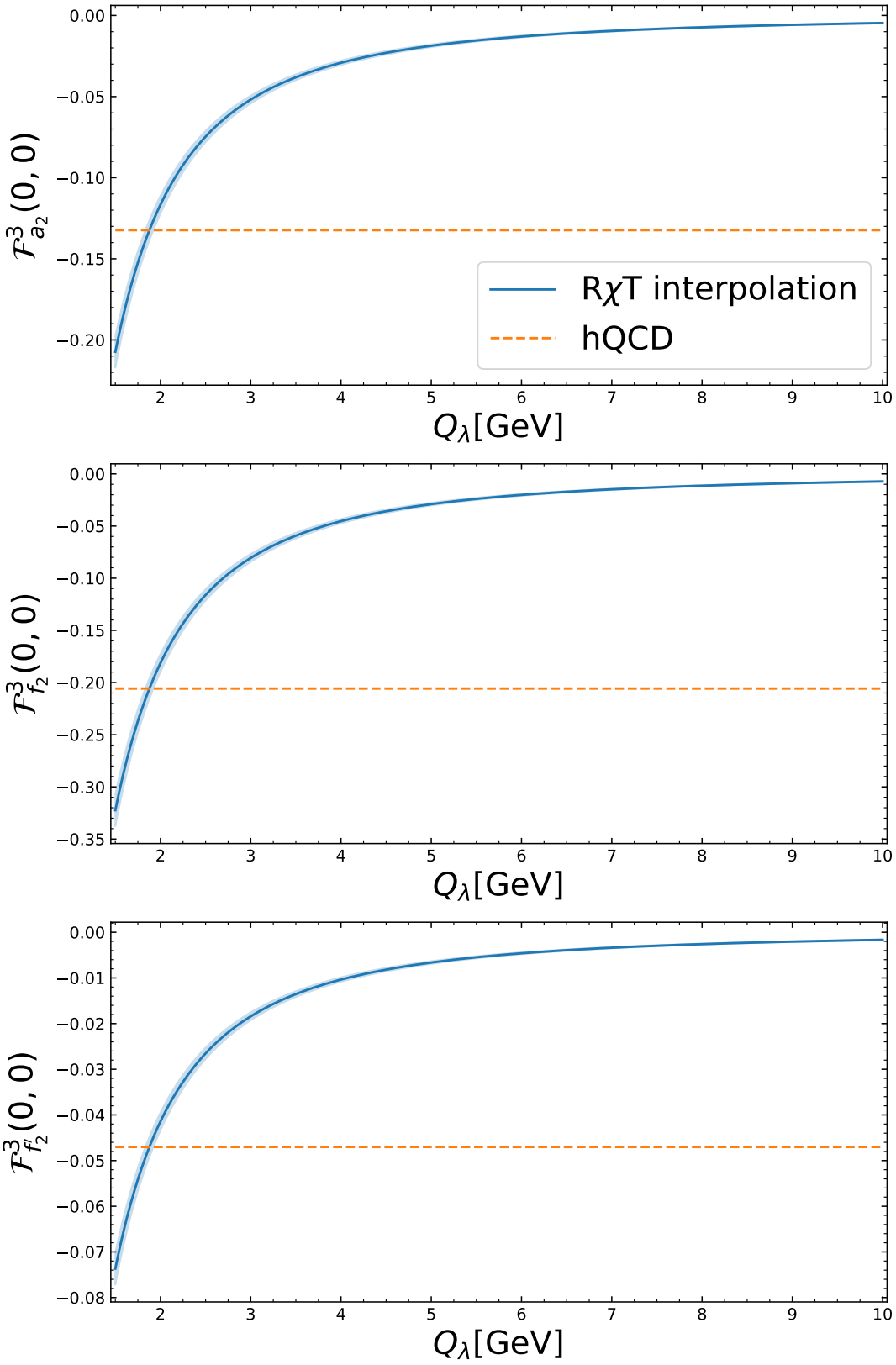

Fig. 5.8 Inferred value of $\mathscr{F}_3^T(0,0)$ from $\mathscr{F}_1^T(0,0)$ within RχT for all 3 neutral tensor mesons(blue) with our 1σ error and the value given by the hQCD approach[69](orange).

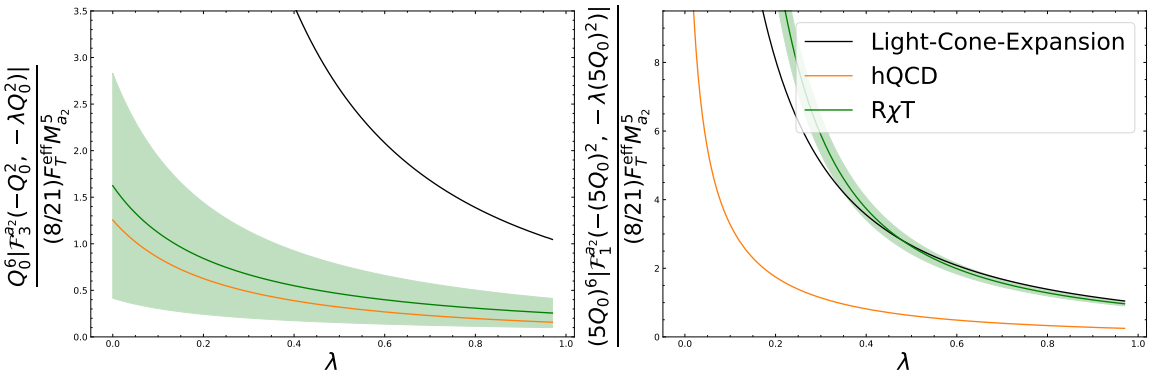

Fig. 5.9 Transition from the purely hadronic to the asymptotic region as a function of the relative virtuality of both photons, λ, at the matching scale $Q_0 = 1.5\,\text{GeV}$(left) and $5Q_0$(right) for the 2 models considered for $\mathcal{F}_3^T$ and the Light-Cone-Expansion. Our one σ uncertainties are displayed by the green band.

Given the normalizations, a comparison between the transition from the purely hadronic to the asymptotic region is possible, and it is shown in Figure 5.9. It is natural to find similar results in $\lambda = 1$ to the results in Figure 5.6, since that was the point where the matching of $\mathcal{F}_3^T(0,0)$ was performed. It is no surprise the fact that at a matching scale $5Q_0 = 7.5\text{GeV}$, the transition from RχT to the asymptotic region is smoother. It is relevant to mention that $\mathcal{F}_3^T$ can only be probed in the double virtual scenario, as it can be seen from eqs. (5.13) and (5.14). The plots from Figure 5.1 are then unchanged by the presence of a non-zero $\mathcal{F}_3^T$. This is, once again, a fair call for the experimentalist to look into the double virtual sector in the photo-production of tensor mesons.

The evaluation of the a_μ contribution of the tensor meson poles is obtained once more by evaluating the master formula with the scalar functions given in eq. (5.15). The optimized basis from [61] considers this specific case of a non-zero $\mathcal{F}_{1,3}^T$ only. For this case, we got the results:

$$a_\mu^{\text{a}_2-\text{pole}} = +0.5(1.4)_{\text{stat}}(^{+0.00}_{-0.07})_{\text{syst}} \times 10^{-11},$$

$$a_\mu^{\text{f}_2-\text{pole}} = +2(5)_{\text{stat}}(^{+0.12}_{-0.29})_{\text{syst}} \times 10^{-11},$$

$$a_\mu^{\text{f}_2'-\text{pole}} = +0.02(5)_{\text{stat}}(^{+0.001}_{-0.000})_{\text{syst}} \times 10^{-11},$$

$$a_\mu^{a_2+f_2+f_2'-\text{pole}} = +2.3(5.2) \times 10^{-11}.$$

These results confirm the fact stated by the hQCD group. When we have the presence of $\mathcal{F}_3^T$, we get a change of sign. However, we must mention that within the

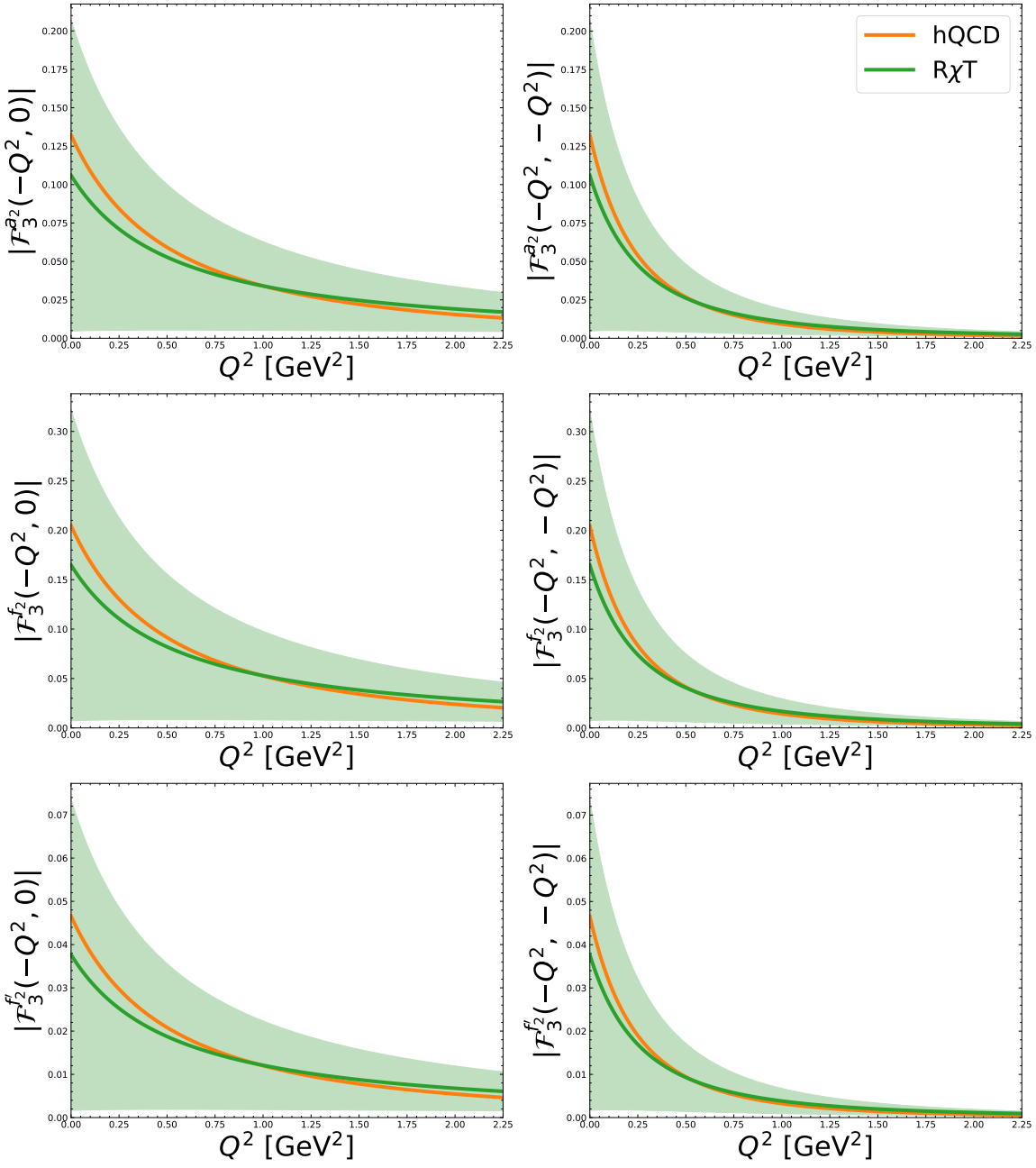

Fig. 5.10 Comparison between the holographic QCD (hQCD) hard-wall model [69], the RχT model used in this work for the single and symmetric double virtual form factor $\mathscr{F}_3^T$, for all 3 tensor mesons: $a_2(1320)$, $f_2(1270)$ and $f_2'(1525)$. Our uncertainties dominated by the lack of information on $\mathscr{F}_3^T(0,0)$ are displayed by the green band.

uncertainty band, negative values are allowed when the normalization of this last form factor is very small compared to the one from $\mathscr{F}_1^T$. In this small-normalization case, the results are very similar to the ones of the previous section, as expected. These results are shown in Figure 5.11, where it is shown that the lack of information on $\mathscr{F}_3^T$ normalization spans a wide range of positive and negative values for the tensor meson pole contribution to the HLbL piece of a_μ.

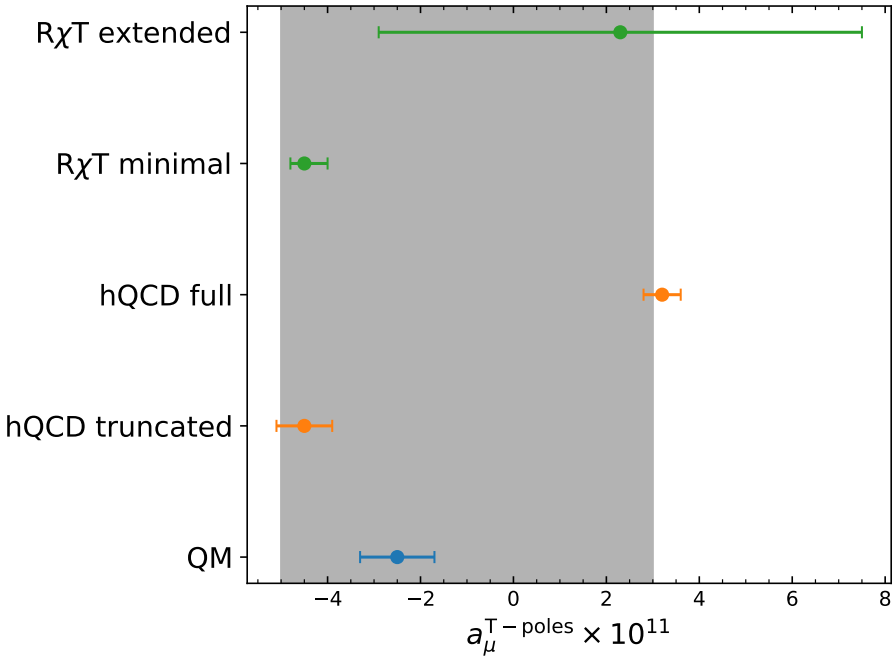

Fig. 5.11 Comparison of this work in the minimal and extended scenarios with the two determinations of the tensor meson pole contributions to a_μ^{HLbL} considered for the WP2025[6]: a Hard-Wall hQCD model [69] and a Simple Quark Model [67]. The value reported in the WP2025 is shown with a gray band.

5.4 Complete Extension: A full consistent account of operators with derivatives

So far, we have considered different scenarios within RχT for the description of the transition of a tensor meson into two photons. However, in the first case, we neglected–by choice– the operators with derivatives. In the second case, we included ad-hoc operators with two additional derivatives which induced $\mathscr{F}_3^T$ only. This is useful if one wishes to compare an RχT prediction for the $g-2$ with those of the

other two approaches currently available; however, there are more operators of the same order in $1/N_C$ which were not included, resulting in an inconsistency of the study. A full, consistent computation within RχT must consider these operators.

As in the case with no derivatives and its ad-hoc extension, we must consider operators with zero, one, and two resonances. This study is still a work in progress, for which we will only explain the case with no resonances for sketching the procedure.

5.4.1 Counting of Operators and their contributions

Because all indices must be contracted and the operators of the kind $T\gamma^*\gamma^*$ contain an even number of indices, we must include at least two derivatives when considering operators of higher order. Since total derivatives do not contribute to the Lagrangian, we can generate the terms with two derivatives from $\partial(\partial TVV)$, $\partial(T\partial VV)$, $\partial(TV\partial V)$. We can classify these operators by the number of derivatives contracted with the indices of $T_{\mu\nu}$.

• **0 contractions** All derivatives of these terms are contracted with the indices of the electromagnetic tensors or with themselves. By the null dynamical effect of the total derivative (which does not give rise to a topological contribution), one of the terms will be omitted, as it is not independent ('LI' below) of the others related to the same total derivative. We will choose to drop the term with the higher order of derivatives acting on $T_{\mu\nu}$. Every new operator will be written in green. First we consider the terms where both derivatives are contracted between them, The trace over flavor is implicit for all operators.

$$\partial_\lambda(\partial^\lambda T_{\mu\nu} f_+^{\mu\alpha} f_{+\alpha}{}^{\nu}) = \underbrace{\partial^2 T_{\mu\nu} f_+^{\mu\alpha} f_{+\alpha}{}^{\nu}}_{\text{Proportional to } C_{T\gamma\gamma}} + \partial_\lambda T_{\mu\nu}\partial^\lambda f_+^{\mu\alpha} f_{+\alpha}{}^{\nu} + \underbrace{\partial_\lambda T_{\mu\nu} f_+^{\mu\alpha}\partial^\lambda f_{+\alpha}{}^{\nu}}_{\text{already considered in previous term by Bose symmetry } (\mu\leftrightarrow\nu)}, \tag{5.39a}$$
ommited - not LI due $\partial()$

$$\partial_\lambda(T_{\mu\nu}\partial^\lambda f_+^{\mu\alpha} f_{+\alpha}{}^{\nu}) = \underbrace{\partial^\lambda T_{\mu\nu}\partial_\lambda f_+^{\mu\alpha} f_{+\alpha}{}^{\nu}}_{\text{2nd term of prev}} + \underbrace{T_{\mu\nu}\partial^2 f_+^{\mu\alpha} f_{+\alpha}{}^{\nu}}_{\text{ommited - not LI due } \partial()} + T_{\mu\nu}\partial_\lambda f_+^{\mu\alpha}\partial^\lambda f_{+\alpha}{}^{\nu}, \tag{5.39b}$$

$$\partial_\lambda(T_{\mu\nu} f_+^{\mu\alpha}\partial^\lambda f_{+\alpha}{}^{\nu}) = \underbrace{\partial^\lambda T_{\mu\nu} f_+^{\mu\alpha}\partial_\lambda f_{+\alpha}{}^{\nu}}_{\text{3rd term of 1a}} + \underbrace{T_{\mu\nu}\partial^\lambda f_+^{\mu\alpha}\partial_\lambda f_{+\alpha}{}^{\nu}}_{\text{3rd term of 1b}} + \underbrace{T_{\mu\nu}\partial_\lambda f_+^{\mu\alpha}\partial^\lambda f_{+\alpha}{}^{\nu}}_{\text{ommited - not LI due } \partial()}. \tag{5.39c}$$

Now we consider the terms where the derivatives are contracted with different dummy indices of the photon fields.

$$\partial_\lambda(\partial_\alpha T_{\mu\nu} f_+^{\alpha\mu} f_+^{\lambda\nu}) = \partial_\lambda\partial_\alpha T_{\mu\nu} f_+^{\alpha\mu} f_+^{\lambda\nu} + \partial_\alpha T_{\mu\nu}\partial_\lambda f_+^{\alpha\mu} f_+^{\lambda\nu} + \partial_\alpha T_{\mu\nu} f_+^{\alpha\mu}\partial_\lambda f_+^{\lambda\nu}, \quad (5.40a)$$

↑ ommited - not LI due $\partial()$

$$\partial_\lambda(T_{\mu\nu}\partial_\alpha f_+^{\alpha\mu} f_+^{\lambda\nu}) = \partial_\lambda T_{\mu\nu}\partial_\alpha f_+^{\alpha\mu} f_+^{\lambda\nu} + T_{\mu\nu}\partial_\lambda\partial_\alpha f_+^{\alpha\mu} f_+^{\lambda\nu} + T_{\mu\nu}\partial_\alpha f_+^{\alpha\mu}\partial_\lambda f_+^{\lambda\nu}, \quad (5.40b)$$

↑ ommited - not LI due $\partial()$

$$\partial_\lambda(T_{\mu\nu} f_+^{\alpha\mu}\partial_\alpha f_+^{\lambda\nu}) = \partial_\lambda T_{\mu\nu} f_+^{\alpha\mu}\partial_\alpha f_+^{\lambda\nu} + T_{\mu\nu}\partial_\lambda f_+^{\alpha\mu}\partial_\alpha f_+^{\lambda\nu} + T_{\mu\nu} f_+^{\alpha\mu}\partial_\lambda\partial_\alpha f_+^{\lambda\nu}. \quad (5.40c)$$

↑ ommited - not LI due $\partial()$

↑ already in $\mu \leftrightarrow \nu$

• **1 contraction** Now one of the derivatives will be contracted with one of the indices of $T_{\mu\nu}$, it is irrelevant to choose either μ or ν because T is symmetric in the exchange of those indices. This requires that the photon fields have one contraction between themselves. Three different global derivative terms appear when one contraction is done with the tensor meson operator.

$$\partial_\lambda(\partial^\mu T_{\mu\nu} f_+^{\lambda\alpha} f_{+\alpha}{}^{\nu}) = \partial_\lambda\partial^\mu T_{\mu\nu} f_+^{\lambda\alpha} f_{+\alpha}{}^{\nu} + \partial^\mu T_{\mu\nu}\partial_\lambda f_+^{\lambda\alpha} f_{+\alpha}{}^{\nu} + \partial^\mu T_{\mu\nu} f_+^{\lambda\alpha}\partial_\lambda f_{+\alpha}{}^{\nu} \quad (5.41a)$$

↑ ommited - not LI due $\partial()$

$$\partial_\lambda(T_{\mu\nu}\partial^\mu f_+^{\lambda\alpha} f_{+\alpha}{}^{\nu}) = \partial_\lambda T_{\mu\nu}\partial^\mu f_+^{\lambda\alpha} f_{+\alpha}{}^{\nu} + T_{\mu\nu}\partial_\lambda\partial^\mu f_+^{\lambda\alpha} f_{+\alpha}{}^{\nu} + T_{\mu\nu}\partial^\mu f_+^{\lambda\alpha}\partial_\lambda f_{+\alpha}{}^{\nu} \quad (5.41b)$$

↑ ommited - not LI due $\partial()$

$$\partial_\lambda(T_{\mu\nu} f_+^{\lambda\alpha}\partial^\mu f_{+\alpha}{}^{\nu}) = \partial_\lambda T_{\mu\nu} f_+^{\lambda\alpha}\partial^\mu f_{+\alpha}{}^{\nu} + T_{\mu\nu}\partial_\lambda f_+^{\lambda\alpha}\partial^\mu f_{+\alpha}{}^{\nu} + T_{\mu\nu} f_+^{\lambda\alpha}\partial^\mu\partial_\lambda f_{+\alpha}{}^{\nu} \quad (5.41c)$$

↑ ommited - not LI due $\partial()$

• **2 contractions** Finally, we study the operators that have the two derivatives contracted with the tensor meson field:

$$\partial^\mu(\partial^\nu T_{\mu\nu} f_+^{\alpha\beta} f_{+\alpha\beta}) = \partial^\mu\partial^\nu T_{\mu\nu} f_+^{\alpha\beta} f_{+\alpha\beta} + \partial^\nu T_{\mu\nu}\partial^\mu f_+^{\alpha\beta} f_{+\alpha\beta} + \partial^\nu T_{\mu\nu} f_{+\alpha\beta}\partial^\mu f_+^{\alpha\beta}. \tag{5.42a}$$

ommited - not LI due $\partial()$

anticommutator, same coefficient

$$\partial^\mu(T_{\mu\nu}\partial^\nu f_+^{\alpha\beta} f_{+\alpha\beta}) = \partial^\mu T_{\mu\nu}\partial^\nu f_+^{\alpha\beta} f_{+\alpha\beta} + T_{\mu\nu}\partial^\mu\partial^\nu f_+^{\alpha\beta} f_{+\alpha\beta} + T_{\mu\nu}\partial^\nu f_{+\alpha\beta}\partial^\mu f_+^{\alpha\beta}. \tag{5.42b}$$

already in 2nd term of 4a with

ommited - not LI due $\partial()$

$$\partial^\mu(T_{\mu\nu} f_+^{\alpha\beta}\partial^\nu f_{+\alpha\beta}). \tag{5.42c}$$

complete term anticommmutator of eq 4b

This makes a total of 14 different operators that generate higher order terms in the amplitude of $\mathbf{T} \to \gamma^*\gamma^*$. It is necessary now to compute the amplitude to check the form factors they contribute to.

5.4.2 Contribution to the TFFs

The 14 independent operators lead to 14 different Feynman rules. Each one of them will be considered as an anticommutator and with contractions with both of the external photon legs. They will be labeled as operator i, $i \in [1,14]$. The independent operators and the form factors they contribute to are

1. $T_{\mu\nu}\{\partial_\lambda f_+^{\mu\alpha}, \partial^\lambda f_{+\alpha}{}^\nu\}$: contributes to F_1^T at order Q^2, SDCs will force the coupling constant to be zero. However, vector meson resonances might contribute to SDCs at different Q^{-2n} orders.

2. $\partial_\alpha T_{\mu\nu}\{\partial_\lambda f_+^{\alpha\mu}, f_+{}^{\lambda\nu}\}$: It contains F_4, F_5 $2(q_1\cdot q_2)F_1$ and a piece similar to $2T_2$ with the exchange $q_1^\alpha q_1^\beta + q_2^\alpha q_2^\beta \to q_1^\alpha q_2^\beta + q_2^\alpha q_1^\beta$. These two structures are not independent since $p^\alpha p^\beta = S_1 + S_2$ and when the tensor meson is on-shell, $p^\alpha p^\beta$ is annihilated. Then it contains -2F_2.

3. $\partial_\alpha T_{\mu\nu}\{f_+^{\alpha\mu}, \partial_\lambda f_+{}^{\lambda\nu}\}$: It contains 2 F_3, F_4 and F_5.

4. $T_{\mu\nu}\{\partial_\lambda\partial_\alpha f_+^{\alpha\mu}, f_+{}^{\lambda\nu}\}$: Contributes to T_4 and T_5.

5. $T_{\mu\nu}\{\partial_\alpha f_+^{\alpha\mu}, \partial_\lambda f_+{}^{\lambda\nu}\}$: Contributes to F_3^T.

6. $T_{\mu\nu}\{\partial_\lambda f_+^{\alpha\mu}, \partial_\alpha f_+{}^{\lambda\nu}\}$: contributes to F_1^T at order Q^2 ($q_1\cdot q_2 F_1^T$), SDCs will force the coupling constant to be zero. As in Op. 1, this should not be the case for vector meson resonances operators. It also contains $-2F_2$ With the same arguments as in Op. 2.

7. $\partial^\mu T_{\mu\nu}\{\partial_\lambda f_+^{\lambda\alpha}, f_{+\alpha}{}^\nu\}$: This structure does not possess double metric tensors, so the only possible structure is T_2, however, it is not present.

8. $\partial^\mu T_{\mu\nu}\{f_+^{\lambda\alpha}, \partial_\lambda f_{+\alpha}{}^\nu\}$: It is proportional to $p^\alpha p^\beta$, which is zero when contracted with the on-shell propagator.

9. $T_{\mu\nu}\{\partial_\lambda\partial^\mu f_+^{\lambda\alpha}, f_{+\alpha}{}^\nu\}$:Contributes to F_4, F_5 and $-(q_1^2+q_2^2)F_1$.

10. $T_{\mu\nu}\{\partial^\mu f_+^{\lambda\alpha}, \partial_\lambda f_{+\alpha}{}^\nu\}$: Contributes to F_2 the same way that Op. 2, so it originates -F_2.

11. $T_{\mu\nu}\{\partial_\lambda f_+^{\lambda\alpha}, \partial^\mu f_{+\alpha}{}^\nu\}$: This structure do not possess double metric tensors, so the only possible structure is T_2, however it is not present.

12. $T_{\mu\nu}\{f_+^{\lambda\alpha}, \partial_\lambda\partial^\mu f_{+\alpha}{}^\nu\}$: Contributes to F_2^T.

13. $\partial^\nu T_{\mu\nu}\{\partial^\mu f_+^{\alpha\beta}, f_{+\alpha\beta}\}$: It is proportional to $p^\alpha p^\beta$, which is zero when contracted with the on-shell propagator.

14. $T_{\mu\nu}\{\partial^\nu f_+^{\alpha\beta}, \partial^\mu f_{+\alpha\beta}\}$: Contributes to F_2 the same way that Op. 2, so it contributes to -F_2.

To complete the study, these contributions need to be expanded to the case with one and two resonances. Furthermore, there are many more independent operators. The model parameters will then be constrained by the Short Distance Constraints of all 5 TFFs, and the rest will be obtained by a global fit to the Belle single virtual data on f_2 [392].

5.4.3 Toy Fit

The SDCs from eq. (5.9) can be imposed on the obtained TFFs. However, with two multiplets of tensor meson resonances, the best that can be achieved is a $1/Q^4$ damping, which is not the $1/Q^6$ predicted by [124]. This fact makes the fitting procedure fail, as it can be understood from eq. (5.14) that if $\mathscr{F}_2^T$ scales in that way,

$\mathscr{F}^T_{\lambda_T=0}$ cannot go asymptotically to zero as the Light-Cone Expansion prediction and the data suggest.

This implies that at least 3 vector meson resonance multiplets must be included. This is a more extensive work, which will be continued after the presentation of this thesis, and will give a first complete and consistent study of the tensor meson resonances transition form factors within RχT. For the moment, a model with two vector meson resonances is good for a toy fit for $\mathscr{F}^T_{1,5}$, but not for $\mathscr{F}^T_2$. This exploratory study aims to obtain scales for the effective masses and the normalization of the form factors. Consequently, an ansatz for the form factors will be used to explore these parameters:

$$\mathscr{F}_1^T(q_1^2,q_2^2) = c_T\frac{3F_T^{\mathrm{eff}}M_T^3(q_1^2+q_2^2) - 14\mathscr{F}_1^T(0,0)M_V^4M_{V'}^4}{14D_{M_V}(q_1^2)D_{M_V}(q_2^2)D_{M_{V'}}(q_1^2)D_{M_{V'}}(q_2^2)}, \tag{5.43a}$$

$$\mathscr{F}_2^T(q_1^2,q_2^2) = \frac{\mathscr{F}_2^T(0,0)}{1-\beta_1^{\mathscr{F}_2}(q_1^2+q_2^2)+\beta_2^{\mathscr{F}_2}(q_1^4+q_2^4)-\frac{4\mathscr{F}_2(0,0)}{5F_T^{\mathrm{eff}}M_T^5}(q_1^6+q_2^6)}, \tag{5.43b}$$

$$\mathscr{F}_5^T(q_1^2,q_2^2) = \frac{\mathscr{F}_5^T(0,0)}{1-\beta_1^{\mathscr{F}_5}(q_1^2+q_2^2)+\beta_2^{\mathscr{F}_5}(q_1^4+q_2^4)-\frac{12\mathscr{F}_5(0,0)}{5F_T^{\mathrm{eff}}M_T^5}(q_1^6+q_2^6)}. \tag{5.43c}$$

As mentioned at the beginning of the chapter, an exchange of momenta $(q_1^2 \to q_2^2)$ will give us information of $\mathscr{F}_4^T$ from that of $\mathscr{F}_5^T$; consequently, they have the same normalization. The results for the global fit and the Form Factors are shown in figs. 5.12 and 5.13.

Concluding remarks from this exploratory study are:

- There is evidence of a non-zero $\mathscr{F}_2^{f_2}(0,0)$, which can be used to obtain the normalization of the other two form factors.
- There is no sensitivity in the current data to the normalization of $\mathscr{F}_5^T$ and, consequently, to $\mathscr{F}_4^T$.
- No conclusion on the form factors can be obtained until we construct a full and consistent description within RχT where all SDCs are taken into account, and double virtual data are measured.

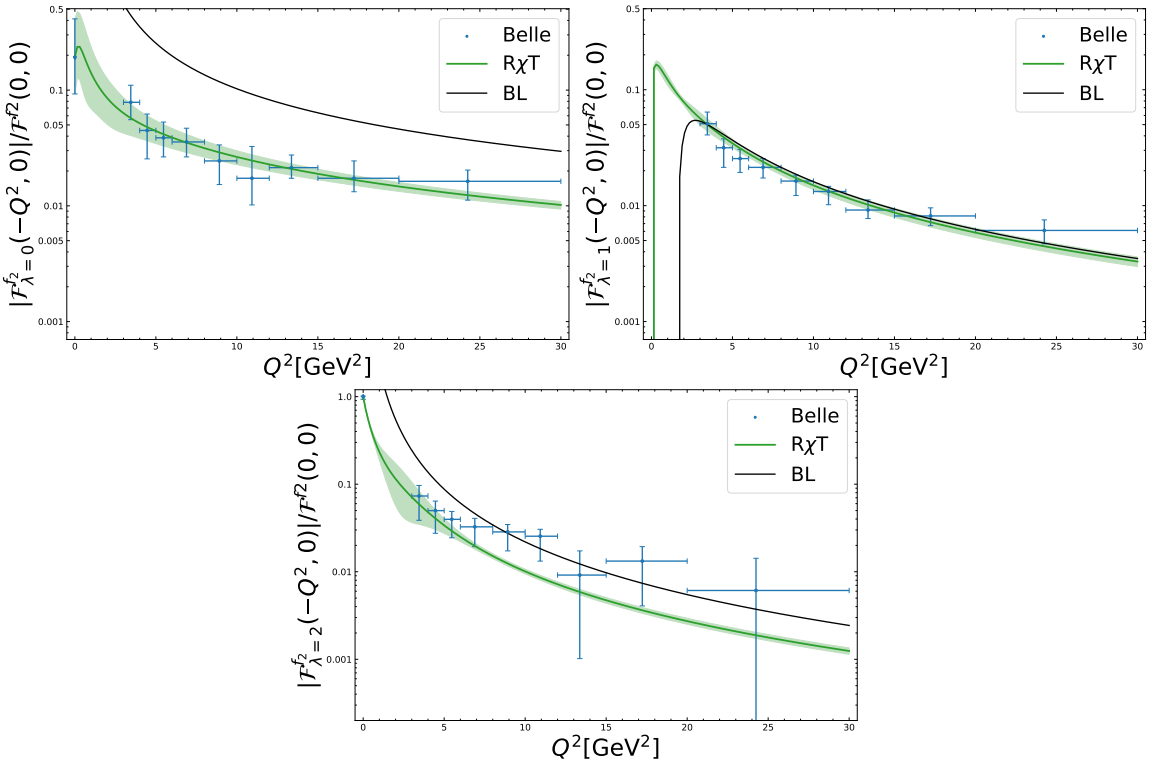

Fig. 5.12 Toy Fit results compared with the Brodsky-Lepage limit and the data from Belle[392].

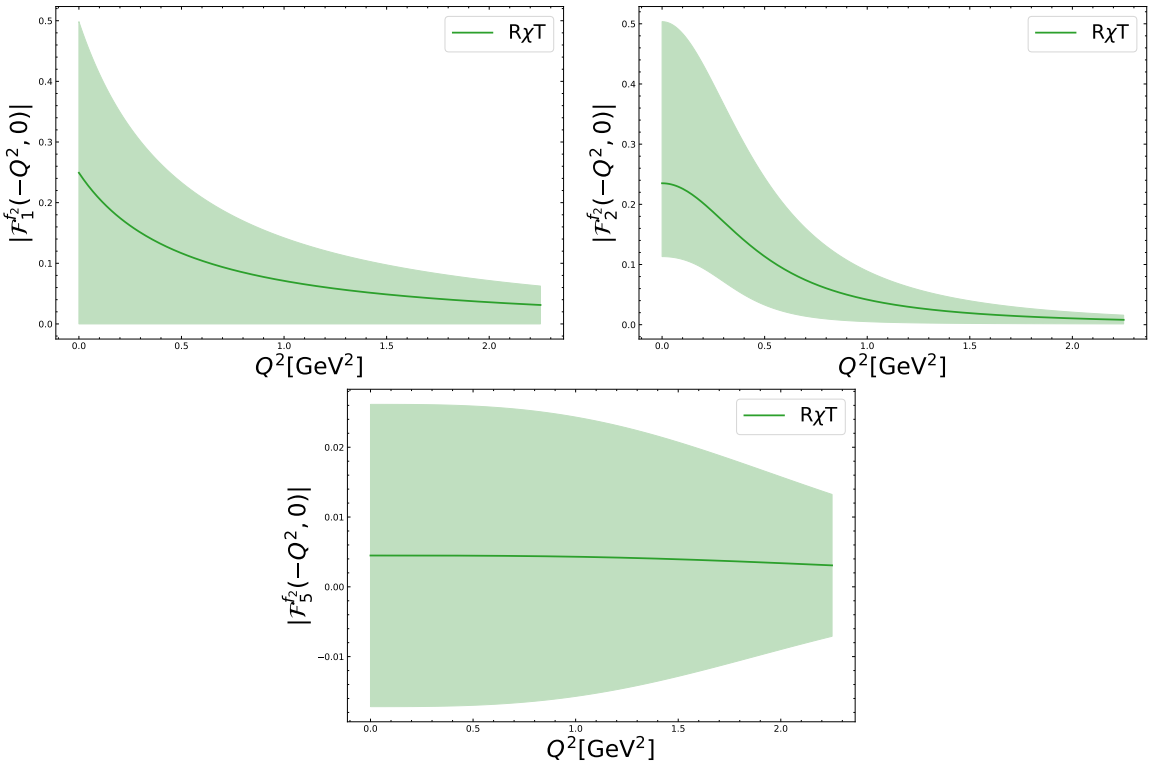

Fig. 5.13 Toy fit results for the transition form factors $\mathscr{F}_{1,2,5}$.

CHAPTER 6

Towards a full evaluation of $a_\mu^{\rm HLbL}$ within RχT

After performing the computations on the pseudoscalar and the tensor pole contributions to the HLbL, we are set to study the plausibility of a full study of this piece within Resonance Chiral Theory and its agreement with the rest of the full evaluations [67, 59, 69, 50, 394, 65]. Other relevant and sub-leading contributions were considered as well for a short review, which will be published soon in EPJ ST [123] [1]. So far, the pseudoscalar poles [301, 302, 62], axial poles [399], and tensor poles contributions [122] had been studied in the framework of RχT. The first and third were part of this thesis. The second one is not part of this thesis but will be included for completeness.

6.1 Pseudoscalar Box Contributions

As in the previous contributions, the main ingredient to compute these contributions are the form factors. In the box contributions case, it is the electromagnetic form factor, the one that defines the interaction of a pseudoscalar meson with a virtual photon ($\gamma^* \to PP$), see Figure 6.1. Since these form factors have only one off-shell photon, their only degree of freedom is its virtuality, Q^2. The scalar functions of the Master Formula, eq. (1.28), are written in terms of these form factors:

$$\overline{\Pi}_i^{\rm P-box}(Q_1^2,Q_2^2,Q_3^2) = F_P(Q_1^2)F_P(Q_2^2)F_P(Q_3^2)\frac{1}{16\pi^2}\int_0^1 {\rm d}x\int_0^{1-x}{\rm d}y I_i(x,y)\,, \qquad (6.1)$$

[1] This publication also reviewed the computation of $a_\mu^{HVP,LO}$ within $R\chi T$. See refs. [87, 88, 90, 395–398, 92].

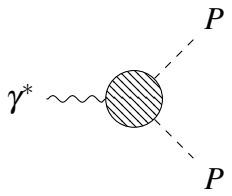

Fig. 6.1 Electromagnetic form factor of a pseudoscalar meson. This form factor defines the interaction of a pseudoscalar meson and a photon, which appears in every vertex of the pseudoscalar-box contributions.

with I_i being the functions of the two-dimensional Feynman parameter integral[48], defined as:

$$
\begin{aligned}
I_1(x,y) &= \frac{8xy(1-2x)(1-2y)}{\Delta_{123}\Delta_{23}},\\
I_4(x,y) &= \frac{4(1-x-y)(1-2x-2y)\Delta_{21}}{\Delta_{321}^2}\left(\frac{(1-2x-2y)^2}{\Delta_{321}}-\frac{1-x(3-2x)-y(3-2y)}{\Delta_{21}}\right)\\
&\quad+\frac{16xy(1-2x)(1-2y)}{\Delta_{321}\Delta_{21}},\\
I_7(x,y) &= -\frac{8xy(1-x-y)(1-2x)^2(1-2y)}{\Delta_{123}^3},\\
I_{17}(x,y) &= \frac{16xy^2(1-2x)(1-2y)}{\Delta_{123}\Delta_{23}}\left(\frac{1-x-y}{\Delta_{123}}+\frac{1-y}{\Delta_{23}}\right),\\
I_{39}(x,y) &= \frac{8xy(1-x-y)(1-2x)(1-2y)(1-2x-2y)}{\Delta_{123}^3},\\
I_{54}(x,y) &= -\frac{8xy(1-x-y)(1-2x)(1-2y)(x-y)}{\Delta_{123}\Delta_{21}}\left(\frac{1}{\Delta_{321}}+\frac{1}{\Delta_{21}}\right),
\end{aligned}
\tag{6.2}
$$

where

$$
\begin{aligned}
\Delta_{ijk} &= M_P^2-xyq_i^2-x(1-x-y)q_j^2-y(1-x-y)q_k^2,\\
\Delta_{ij} &= M_P^2-x(1-x)q_i^2-y(1-y)q_j^2.
\end{aligned}
\tag{6.3}
$$

Once again, the remaining scalar functions are obtained from the crossing relations between them.

The dispersively-defined vector form factor of the pion has been widely studied in the context of Resonance Chiral Theory [400–402]. The pion form factor $F_V^\pi(s)$ is defined as:

$$
\langle\pi^+(p)\pi^-(p')|V_\mu^3|0\rangle = (p-p')_\mu F_V^\pi(s),
\tag{6.4}
$$

where $s=(p+p')^2$ and V_μ^3 is the third component of the vector current associated with the approximate $SU(3)_V$ flavor symmetry of the QCD Lagrangian. This form factor can be described using a dispersive framework, with an RχT phaseshift seed, as in the previously cited refs. The first work uses a VMD in the zero-width approximation:

$$F_V^\pi(s)=\frac{M_\rho^2}{M_\rho^2-s}, \tag{6.5}$$

However, it can be improved by including χPT corrections at $\mathcal{O}(p^4)$ and by resumming the $\pi\pi$ and KK final-state interactions to all orders, relying on unitarity and analyticity constraints. Finally, to describe the region of the ρ peak, its on-shell (and slightly off-shell) behaviour must be correctly described. All of these facts were considered in [402], leading to:

$$F_V^\pi(s)=\frac{M_\rho^2}{M_\rho^2-s-iM_\rho\Gamma_\rho(s)}\exp\left(-\frac{s}{96\pi^2F_\pi^2}\mathrm{Re}\left[A_\pi(s,\mu^2)+\frac{1}{2}A_K(s,\mu^2)\right]\right), \tag{6.6}$$

where the energy-dependent width is defined as [2]:

$$\Gamma_\rho(s)=-\frac{M_\rho s}{96\pi F_\pi^2}\mathrm{Im}\left[A_\pi(s)+\frac{1}{2}A_K(s)\right]. \tag{6.7}$$

The two-pseudoscalar loop-functions accounting for the unitary corrections are given by[3]:

$$A_P(s,\mu^2)=\log\frac{m_P^2}{\mu^2}+\frac{8m_P^2}{s}-\frac{5}{3}+\sigma_P^3(s)\log\left(\frac{\sigma_P(s)+1}{\sigma_P(s)-1}\right), \tag{6.8}$$

and $\sigma_P(s)=\sqrt{1-\frac{4m_P^2}{s}}$. Due to the region of relevance of the a_μ ($E<1$ GeV), there is no need to go further and explore the influence of higher resonances in this case. This is the seed for the phaseshift in order to perform a thrice-subtracted dispersion relation for the form factor:

$$F_V^\pi(s)=\exp\left[\alpha_1 s+\frac{1}{2}\alpha_2 s^2+\frac{s^3}{\pi}\int_{4m_\pi^2}^{s_{\mathrm{cut}}}ds'\frac{\delta_1^1(s')}{s'^3(s'-s-i\varepsilon)}\right], \tag{6.9}$$

[2]There is a scale dependence in this piece, which cancels out with the scale dependence of the LEC $L_9^r(\mu^2)$. For this reason, the μ^2 will be taken as $\mu^2=M_\rho^2$ and omitted from the expressions after this point.

[3]Further details on the definitions and effects of the loop-functions are given in [247] and in the appendix of [401].

where the phase is given by the RχT seed:

$$\tan\delta_1^1(s) = \left.\frac{{\rm Im}F_V^\pi(s)}{{\rm Re}F_V^\pi(s)}\right|_{\rm R\chi T}. \tag{6.10}$$

For the form factor of the K, we have introduced the dominant $1/N_C$ correction to the vector meson propagators in the VMD Form Factor:

$$F_V^K(s) = \frac{1}{2}\left(\frac{M_\rho^2}{M_\rho^2 - s}\right)\exp\left[-\frac{s}{192\pi^2 F_\pi^2}\left(A_\pi(s) + 2A_K(s)\right)\right] + \frac{1}{3}\left(\frac{M_\omega^2}{M_\omega^2 - s}\right) + \frac{2}{3}\left(\frac{M_\phi^2}{M_\phi^2 - s}\right). \tag{6.11}$$

With this input, we obtain

$$a_\mu^{\pi-{\rm box}} = -15.8(3)\times 10^{-11}, \quad a_\mu^{K-{\rm box}} = -0.51(3)\times 10^{-11}, \tag{6.12}$$

which compares well with the WP2 numbers [6], taken from Refs. [48, 58],

$$a_\mu^{\pi-{\rm box}} = -15.9(2)\times 10^{-11}, \quad a_\mu^{K-{\rm box}} = -0.48(1)\times 10^{-11}, \tag{6.13}$$

These results are also supported by Dyson-Schwinger evaluations [403, 404].

We do not consider here other smaller box contributions, like those coming from excited pseudoscalars [405] and baryons [121].

6.2 Axial Pole Contributions

The contribution of axial-vector resonances to a_μ gained much interest after the celebrated Melnikov-Vainshtein work [303], which put forward that all short-distance QCD constraints relevant for the HLBL could not be satisfied only with pseudoscalar exchanges, which could be healed by the axial contributions. The importance of Ref. [399], which evaluated $a_\mu^{\rm axial-poles}$ within $R\chi T$, lies more in clarifying some issues about bases and satisfaction of high-energy constraints (see also e. g. ref. [406]) than in the actual number that was obtained, as we will explain.

A very important result of this paper is the derivation of a dictionary to translate between the four existing bases [407–409] (two different helicity bases, one quark-model inspired and another one first used in the study of the $<VVA>$ Green's function) in the literature that were used to compute $a_\mu^{\rm axials}$ previously [4], which

[4]Later on, a different basis, optimized for the dispersive analysis, was proposed [61, 67].

is non-trivial, given the off-shellness. This happens because of the Landau-Yang theorem [410, 411], whose fulfillment in the Melnikov-Vainshtein analysis [303] was shown in Ref. [399], contrary to the claims in Refs. [412, 408].

This work [399] also emphasized the role of axial-vector mesons in saturating the short-distance anomaly constraints, which became a hot topic for the g-2 community since then. However, working at leading order in $1/N_C$, $R\chi T$ only contributes to antisymmetric form factors, which give suppressed contributions to a_μ. Even including the effects of higher orders in the chiral and large-N_C expansions, this works finds a result of

$$a_\mu^{(a_1+f_1+f_1')-\text{poles}} = (0.8^{+4.1}_{-0.8}) \times 10^{-11}\,, \tag{6.14}$$

which is clearly smaller than the WP2 number [6]

$$a_\mu^{(a_1+f_1+f_1')-\text{poles}} = (12.2 \pm 4.3) \times 10^{-11}\,, \tag{6.15}$$

based on the dispersive analysis [67], that is supported by those of holographic QCD [53, 52], Regge theory [54] and Dyson-Schwinger equations [65]. Improved measurements of the axial transition form factors would be instrumental in reducing the above uncertainty.

Given the preceding explanations, it seems that an $R\chi T$ evaluation of these contributions would need to be constructed on the basis of the continuation to the timelike of the successful description of the axial current coupling to three-pion states in the spacelike [324, 326], which would be challenging anyway.

6.3 Scalar Pole Contributions

In principle, the scalar pole contributions to a_μ^{HLBL} could be evaluated using the master integrals derived in Ref. [394], which can be computed knowing the two form factors that appear in the general decomposition of the $<SVV>$ Green function. These have been computed in $R\chi T$ in Ref. [413], using the Lagrangian including the interactions in Ref. [279]. Upon imposing short-distance QCD constraints, one form factor depends on a single unknown coupling. The other one, however, depends on seven different (combinations of) couplings. With current knowledge on this

sector of the Lagrangian it is impossible to comply with all known high-energy QCD constraints while keeping predictive power [5].

For completeness, we quote that in the WP2 [6], the contribution of the lightest degrees of freedom in the scalar sector are split as

$$a_\mu^{\rm S-waves} = -9.1(1.0)\times 10^{-11}\,, \tag{6.16}$$

including the $I=0,1,2$ $\pi\pi, \bar{K}K, \pi\eta$ rescattering [48, 414, 57]. Therein, the dominant $I=0$ component can be understood as the $f_0(500)$ contribution, in terms of two-pion states, within the dispersive framework.

6.4 Other Contributions

Approximately 2/3 of the whole $a_\mu^{\rm HLBL}$ is given by the low-energy contributions, coming from the lightest pseudoscalar poles (Chap. 3) and boxes (Sec. 6.1), as well as their rescattering contributions (Sec. 6.3), which are dominated by sub-GeV physics. The remaining parts (including the lightest axial and tensor poles in Sec. 6.2 and Chap. 5) can be classified according to the different energy regions probed.

It has become standard to divide the momentum space between the short-distance regime (with all photon momenta in the HLBL with magnitude larger than 1.5 GeV), the low-energy contributions (all with modulus smaller than this quantity) and the mixed regime.

The pure short-distance (SD) region is very well-known, by applying repeatedly the OPE to the electromagnetic currents in the HLBL tensor [303, 51, 55, 415, 416, 66], yielding the result

$$a_\mu^{\rm SD} = \left(6.2^{+0.2}_{-0.3}\right)\times 10^{-11}\,. \tag{6.17}$$

The contribution of the charm quark loop uses to be quoted separately,

$$a_\mu^{\rm c-loop} = 3(1)\times 10^{-11}\,. \tag{6.18}$$

In the $N_C\to\infty$ limit of QCD an infinite tower of mesons is predicted per set of quantum numbers. Although contributions from the lightest states dominate $a_\mu^{\rm HLBL}$, the effects of their excitations are sizable, and accounted for, e. g. within holographic QCD [52, 53, 362, 59, 69] or Regge models [54]. The results used in the WP2 [6] for

[5] Ref. [394] used VMD form factors (violating QCD short-distance behaviour), to find $a_\mu^{\rm a_0+f_0+f_0'} = (-3\pm 2)\times 10^{-11}$.

these regions are

$$a_\mu^{\mathrm{A,S',T,...-low}} = 12.5(5.9)\times 10^{-11}\,, \quad a_\mu^{\mathrm{mixed}} = 15.9(1.7)\times 10^{-11}\,. \tag{6.19}$$

We note that the former result agrees extremely well with the WP2 number for the lightest axials and tensors, which also provides $\sim 86\%$ of the quoted uncertainty.

6.5 Comparison with other approaches

The sum of the different contributions in Eqs. (3.63), (6.13), (6.16), (6.17), (6.18) and (6.19), accounting for an additional uncertainty (of 5.0 units) in the matching of the different regions, yields the WP2 number

$$a_\mu^{\mathrm{HLBL,\,WP2}} = 103.3(8.8)\times 10^{-11}\,. \tag{6.20}$$

Using the $R\chi T$ results for the P-poles and -boxes and (more importantly) for the tensors instead, according to Eqs. (3.63), (6.12) and (5.38) would yield

$$a_\mu^{\mathrm{HLBL,\,with}\,R\chi T\,\mathrm{results}} = 106.1(9.0)\times 10^{-11}\,, \tag{6.21}$$

which is closer to the Lattice QCD number (based on Refs. [71–74]) in the WP2 [6]

$$a_\mu^{\mathrm{HLBL,\,lattice}} = 122.5(9.0)\times 10^{-11}\,. \tag{6.22}$$

6.6 Conclusions and outlook

We have reviewed the foundations of $R\chi T$ and its use in computing hadronic light-by-light contributions to a_μ, which benefit from measurements of the relevant form factors, whose prospects for improvement have been underlined. $R\chi T$ obtains very competitive results for the lightest pseudoscalar pole and box. Notably, for the tensor pole contributions, it favors the holographic results, which would require shifting the WP2 number for this contribution. This would imply closer agreement with the lattice a_μ^{HLBL} result.

CHAPTER 7

Conclusions and Perspectives

Conclusions

This thesis, titled *Study of Hadronic Form Factors: essential inputs for the Hadronic Light-by-Light piece of muon's* $g-2$, contains 3 completely original articles, 1 short review, 1 collaboration report, and 1 work in progress in its final stages. During the elaboration of this work, I worked with different hadronic form factors: Transition Form Factor of the Pseudoscalar Mesons $\mathscr{F}_{P\to\gamma^*\gamma^*}$, Dirac form factor of the proton F_1^p, Transition Form Factor of the Tensor Mesons $\mathscr{F}_{T\to\gamma^*\gamma^*}$, Electromagnetic form factor of the Pseudoscalar mesons F_V^P and the Scalar and Vector Form Factors of two Pseudoscalar mesons: $F_{V,S}^{\pi\pi}$, $F_{V,S}^{K\pi}$. In these works, dispersive representations, experimental and LQCD calculation parametrizations, Canterbury Approximants, and Resonance Chiral Theory were used to describe the form factors, leading to a rich set of techniques that adapt to the necessities of each problem. Also, the limits of a model can be quantified by means of (the) others, which allowed us to do a rigorous and systematic assessment of the theory errors induced by the limitations of each technique.

For our first project, we described the transition form factors of the pseudoscalar mesons $P\to\gamma^*\gamma^*$ using Resonance Chiral Theory with two vector meson resonance multiplets and a multiplet of pseudoscalar resonances, in addition to the lightest pseudoscalar nonet, at order m_P^2 in chiral symmetry breaking and leading order in $1/N_C$. In this framework, we imposed the Brodsky-Lepage limit together with the symmetric double virtual asymptotic limit (SDCs). The parameters not fixed by symmetries or SDCs were fitted to the available data: the single virtual data of the π^0, η, η' mesons, the double virtual data for η', LQCD points for π^0, η, η', the radiative

decay widths as well as ρ mass and $\eta - \eta'$ mixing parameters as stabilization points in a global analysis. The resulting form factors, with a reasonable computation of statistical errors, were used to calculate the pseudoscalar pole contributions to the HLbL piece of a_μ (in units of 10^{-11}): $a_\mu^{\pi^0\text{-pole}} = 61.9 \pm 0.6^{+2.4}_{-1.5}$, $a_\mu^{\eta\text{-pole}} = 15.2 \pm 0.5^{+1.1}_{-0.8}$ and $a_\mu^{\eta'\text{-pole}} = 14.2 \pm 0.7^{+1.4}_{-0.9}$, for a total of $a_\mu^{\pi^0+\eta+\eta'\text{-pole}} = 91.3 \pm 1.0^{+3.0}_{-1.9}$, where the first error is statistical and the second one is systematic. These results are in agreement with other determinations, with the innovative use of the double virtual data for η' from BaBar [335] and the combination of experimental data and LQCD calculations (so-called hybrid approach), with competing uncertainties. This result was recognized as essential input for the SM contribution of a_μ in the second White Paper [6] of the Theory Initiative.

For our second project, we studied the proton-box contributions to the HLbL piece of a_μ in the reduced scenario where only the Dirac form factor was taken into account, due to the suppression of the Pauli form factor. In this case, we used the form factors parametrizations of experimental data [379] and LQCD calculations [380] that fulfill the sum-rules imposed by QCD at high energies. The results for this contribution were $1.82(7) \times 10^{-12}$ (Data-Driven) and $2.38(16) \times 10^{-12}$ (LQCD), being one order of magnitude below the current error of the total HLbL piece. However, they are the first baryonic contribution to this process and might be relevant in the future. We note that LQCD still acknowledges room for improvement in the calculation of this form factor, that is currently more accurate (including all systematic uncertainties) in a data-driven way.

In our third project, we constructed the transition form factors of the tensor mesons within $R\chi T$. In contrast with the only form factor appearing in the pseudoscalar case, the rich structure of the propagator and vertices of the tensor mesons results in 5 possible tensor structures and their corresponding form factors. Besides, the scarce data make it difficult to think in a global fit of the scale of the pseudoscalar mesons (data quantity and quality). The best possible framework currently is that of two vector meson multiplets of resonances in the chiral limit. This allowed us to impose some of the SDCs (computing systematic errors for the ones we could not fulfill) and the normalization of the form factors. We worked in two scenarios, the first one neglecting operators with additional derivatives –by assumption– which generated $\mathscr{F}_1^T$ only, and the second one with an ad-hoc extension considering the operators with additional derivatives that generate $\mathscr{F}_3^T$ only. With these two sets of operators, we constructed the transition form factors that reproduce the results of the quark model and the hard-wall model of holographic QCD. The lack of data

in the doubly virtual sector made it impossible to obtain the normalization of $\mathscr{F}_3^T$. We performed a reasonable ballpark estimate of this normalization within $R\chi T$. Our results were (in units of 10^{-11}):

- with $\mathscr{F}_1^T$ only: $a_\mu^{\mathrm{a}_2-\mathrm{pole}} = -\left(1.02(10)_{\mathrm{stat}}(^{+0.00}_{-0.12})_{\mathrm{syst}}\right)$, $a_\mu^{\mathrm{f}_2-\mathrm{pole}} = -\left(3.2(3)_{\mathrm{stat}}(^{+0.0}_{-0.4})_{\mathrm{syst}}\right)$ and $a_\mu^{\mathrm{f}_2'-\mathrm{pole}} = -\left(0.042(13)_{\mathrm{stat}}\right)$, which add up to $a_\mu^{a_2+f_2+f_2'-\mathrm{pole}} = -\left(4.3^{+0.3}_{-0.5}\right)$.
- with $\mathscr{F}_1^T$ and $\mathscr{F}_3^T$: $a_\mu^{\mathrm{a}_2-\mathrm{pole}} = +0.47(1.43)_{\mathrm{norm}}(3)_{\mathrm{stat}}(^{+0.06}_{-0.00})_{\mathrm{syst}}$, $a_\mu^{\mathrm{f}_2-\mathrm{pole}} = +1.18(4.18)_{\mathrm{norm}}$ $(12)_{\mathrm{stat}}(^{+0.24}_{-0.00})_{\mathrm{syst}}$ and $a_\mu^{\mathrm{f}_2'-\mathrm{pole}} = +0.040(78)_{\mathrm{norm}}(2)_{\mathrm{stat}}$, summing to $a_\mu^{a_2+f_2+f_2'-\mathrm{pole}} = +1.7(4.4)$.

Previous uncertainties are dominated by the lack of knowledge of $\mathscr{F}_3^T(0,0)$. These results help to explain why there is an urgent need to measure doubly virtual data in the transition of a tensor meson to two photons. Finally, as an extension of this work, we have studied the consistent full set of operators with two additional derivatives, showing that all 5 form factors appear in RχT. A toy fit showed that at least $\mathscr{F}_2^T$ is non-zero and that $\mathscr{F}_{4,5}^T$ is not sensitive to the existing data. The evidence of new form factors different than the ones considered so far calls for a new basis in the Master Formula, since within the current basis, the contribution to a_μ^{HLbL} can only be evaluated in the case with nonvanishing $\mathscr{F}_1^T$ and $\mathscr{F}_3^T$.

These results contributed to the improvement of the Theory Initiative computation of the HLbL piece of a_μ, reducing the uncertainty from 19×10^{-11} to 8.8×19^{-11}. Our main contributions were: the reduction of errors, the implementation of new data, the first hybrid analysis in the HLbL, the computation of new contributions, and the understanding of tensions between different groups. We have advanced significantly towards an RχT evaluation on the HLbL piece of $g-2$ as it can be seen in Table 7.1.

Beyond form factors, we studied non-standard interactions in τ hadronic decays, where all possible structures were considered, and only the tensor ones are not absorbed in the standard parameters (for the measurable quantities considered here). We defined clean angular observables for which direct data input can be used to test the tensor contributions due to form factor cancellation. In the $\pi\pi$ channel, this can be done directly due to the absence of a sizable scalar form factor. For the $K\pi$ channel, $\frac{|F_S(s)|^2}{|F_V(s)|^2}$ –computed in Resonance Chiral Theory, and dispersive representations– was used as an expansion parameter to include small corrections. This is a work in progress which will be published soon.

I can conclude that my journey into hadronic form factors to perform tests within and beyond the Standard Model was successful, and allowed me to discover a set

	Dispersive	CA	RχT	hQCD	DSE/BSE
π^0-pole	$63.0^{+2.7}_{-2.1}$	63.6(2.7)	$61.3^{+2.5}_{-1.6}$	63.4(2.7)	62.6(1.3)
η-pole	14.7(9)	16.3(1.4)	$15.2^{+1.2}_{-0.9}$	17.6(1.7)	15.8(1.1)
η'-pole	13.5(7)	14.5(1.9)	$14.2^{+1.6}_{-1.1}$	14.9(2.0)	13.3(8)
π^0-box	$-15.9(2)$	-	$-15.8(3)$	-	$-15.6(4)$
K-box	$-0.484(11)$	-	$-0.51(3)$	-	$-0.48(6)$
$A = f_1, f_1', a_1$	12.2(4.3)	-	$0.8^{+4.1}_{-0.8}$	13.1(1.5)	8.6(2.6)
$S = f_0(1370), a_0(1450)$	-0.7(4)	-	-	-	-0.8(3)
$T = f_2, f_2', a_2$	-2.5(8)	-	+1.7(4.4)	3.2(6)	2.8 (6)

Table 7.1 Comparison between the main approaches to the individual contributions to the HLbL piece of $g-2$. The dispersive results were taken from refs. [292, 49, 363, 68, 48, 58, 67], the CA results from ref. [47], the RχT results were taken from [301, 302, 62, 123, 54, 399, 122] –original results from this thesis in blue–, the hQCD results were taken from refs. [59, 377, 69, 417] and the DSE/BSE results were taken from the two independent groups [50, 403–405, 65].

of techniques and theoretical foundations to continue my career in particle physics phenomenology while making significant original contributions to the scientific community. I feel pleased with my PhD experience at Cinvestav and look forward to new projects.

Future Work

In all projects, we did the best we could with the available data and the current theoretical tools; however, many of the studies can be updated or improved, as it is inherent in science. Some of the projects I plan for the future with different colleagues include continuations of these works, others are ideas we discussed, but time is finite, so we could not carry them out during the PhD. I plan to continue working on tests of the Standard Model with concrete goals:

• Tests within the Standard Model

- To describe the transition of tensor mesons into two photons ($a_2, f_2, f_2' \to \gamma^*\gamma^*$) within $R\chi T$ and to modify the tensor HLbL basis to account for the tensor pole contributions to the a_μ consistently with the rest of the HLbL piece.

  Currently, the available descriptions of this process are simplified cases due to the impossibility of evaluating the a_μ contribution in the most general case, as non-physical divergences are induced by imposing gauge invariance.

A description within $R\chi T$ can make use of the chiral symmetry of QCD to maximize the utility of available experimental information. The modification of the HLbL tensor basis is required to account for the general case. I aim to achieve the correct modification during this study. Currently, there are differences in the signs of the determinations of the tensor pole contributions to a_μ due to different simplifications applied. This study can solve this tension by considering a scenario where all previous studies are contained and can be recovered, as limiting cases.

This would also allow us to decompose the HLbL tensor in the appropriate basis to evaluate the baryonic-box contributions. At present, only the proton-box contribution has been computed, due to the suppression of the dipolar form factor, which simplifies the calculation. However, if this general decomposition is performed in the new basis, all baryons can be accounted for, which is also a research plan for the future. Noting the importance of baryon states in the large-N_C limit of QCD, this can be impactful considering the fulfilment of short-distance constraints on the full four-point HLbL tensor with an on-shell external photon, corresponding to the a_μ case.

- To use the longitudinal constraints on the HLbL tensor to describe the transition form factors of the pseudoscalar excited states within $R\chi T$ and evaluate their contributions to a_μ^{HLbL}. There is no experimental information available for these processes, for which constraints from low-energy and high-energy QCD must be imposed to obtain reasonable descriptions for these form factors. Specifically, the missing piece of the high-energy constraints on the longitudinal part of the HLbL tensor can be saturated by these particles (together with improved input from other sectors, as noted in the previous items).

- Given the experience we have gained on computing uncertainties for hadron processes in the muon's $g-2$ theory initiative collaboration, it is reasonable to organize an international workshop focused on improving uncertainties in hadron processes.

• Beyond the Standard Model probes

- To study possible deviations from the lepton decays $l \to l' \nu \bar{\nu}$ which cannot be easily distinguished from the standard case experimentally. This will result in generalized Michel parameters [418], which could be probed in particle colliders.

- To study relevant η and η' processes to ongoing experiments as JLab η Factory and future ones as REDTOP [419]. It is possible to establish limits to the hypothetical dark scalar which violates isospin [420] and mediates the processes $\eta^{(\prime)} \to \pi\gamma\gamma$ [421]. Also, the tensor contributions to similar processes $\eta^{(\prime)} \to \pi l^+ l^-$ can be probed [422]. Furthermore, the availability of CP-violating processes as $\eta^{(\prime)} \to \pi\mu^+\mu^-$ [423] can be updated within the framework of SMEFT and the expected statistics of the REDTOP experiment. Finally, it is possible to update the limits on the hypothetical leptophobic boson which mediates $\eta^{(\prime)} \to \pi^0\gamma\gamma$, considering tensor exchanges and the recent data of KLOE [424].

Hopefully, I can work on all these projects during the two years of a post-doc, but we will see how long it takes to complete all these goals. In any case, there is still a lot of fascinating physics to work on!

APPENDIX A

Guide for useful computational tools

One of the main tools we acquired during the realization of a PhD are the computational ones. Here I summarize and briefly describe the 3 most important ones that I used for this thesis, all implemented in Python.

All these 3 computational tools together with Wolfram Mathematica result in a powerful combination to perform numerical evaluations and error analysis in physics.

Optimization tools: iMinuit, Minuit for Python

The CERN-developed optimizer, Minuit, has been used for decades by particle physicists in different programming languages. In this thesis, I have used its implementation in Python, iMinuit [425].
To use it as an optimizer, a requirement is a cost function that depends on the parameters to be fitted. Furthermore, initial values for them are required. Common cost functions are included, but arbitrary cost functions can be defined, as long as they have the fitted parameters as arguments and return a real value.
To declare an optimization object based on the cost function *cost* with initial parameters a_0, b_0, ..., we require the following code:

```
m = Minuit(cost, a=a_0, b=b_0, ...)
```

Then, limits on the parameter values, or even if they are fixed, can be given to the object once it is declared. After that, different optimization processes can be done to the object *m*: scan, simplex, gradient, migrad and minos. The last two are the most important, as *migrad* is the most accurate optimizing procedure and *minos* computes

errors on the optimal parameters and the covariance matrix. It is important to mention the main outputs of the procedure: the fitted parameters (with quality tests), confidence intervals, and the covariance matrix. These outputs are required for later propagation of uncertainties.
It is recommended to use it in a *Jupyter Notebook* to maximize its benefits.

Numerical Integrations: VEGAS

For multidimensional numerical integration, the VEGAS integrator [125] has been used for a long time.
It requires defining an integrand [1], together with the variables to be integrated and their limits. First, the integrator must be set by the code:

```
integral= vegas.Integrator([[a_0,a_f], [b_0,b_f], [c_0,c_f],...], nproc=1)
```

where *a*,*b*,*c*, ... are the integrated variables and *nproc* is the number of processors to be used. Then, the integration can be performed for an integrand in terms of the integrated variables and other variables as well:

```
result=integral(lambda vars : integrand(vars,params_1,params_2, ...), nitn=10, neval=10000)
```

where vars is an array of the integrated variables, and *params_i* are the parameters of the integrator which are not integrated out. These parameters are the ones that can be used to compute a numerical propagation of errors. *nitn* is the number of computations of the integral, and *neval* is the number of evaluations per computation.

Numerical propagation of errors: the Jacobi library

The propagation of errors can be easy sometimes; however, when your parameters (with uncertainties and correlations) are input for integrals of very complicated expressions, a numerical tool for propagating errors can become handy. I have used during this thesis the Jacobi Library [426], which –for the skeptical– is from one of the developers of iMinuit [425].
The required inputs for performing an error propagation are: a function of the parameters, the central value of the parameters and the covariance matrix between them:

[1] It is desirable to define the integrand with the fitted parameters as arguments, since it makes possible a numerical propagation of errors.

```
central_value,covariance=propagate(lambda p: function(*p),params,cov)
error=np.sqrt(covariance)
```

The output is the central value of the function and the covariance of the point, which can be used to compute the error. This last step seems pointless for a single value; however, this can be used for a function of some variable(s) x with some parameters with errors. Then the code for the propagator becomes:

```
central_value,covariance=propagate(lambda p: function(*p,x),params,cov)
error=np.sqrt(covariance)
```

and the output is a list of central values for all values of the array x and the covariance matrix of the points in the array.

APPENDIX B

Beyond Form Factors: Precise Angular Tests in Hadronic τ Decays

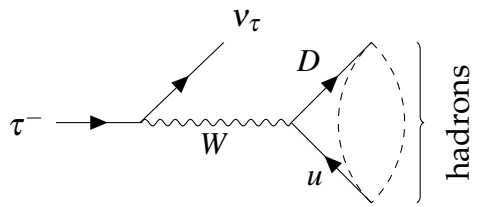

Fig. B.1 Feynman diagram sketching the hadronic decay of the τ.

Semileptonic tau decays [427–429] offer an ideal probe of hadronization (See Figure B.1) in the GeV region thanks to the clean environment provided by the lepton decay. In this sense, the tau is privileged, since it is the only lepton able to decay this way, thanks to its mass, $M_\tau \sim 1.8$ GeV. This allows to study the properties of the exchanged resonances mediating these processes and also –provided we control well enough the hadron input in the SM and radiative corrections– to constrain possible new physics contributions. In this chapter we explore the possibility to set these limits quite independently of form factor information for conveniently defined observables.

Tau decays can be well understood from the effective field theory perspective given by the Fermi-type Lagrangians, with ($D = d, s$ for these semileptonic processes)

$$\mathscr{L} = -\frac{G_F V_{uD}}{\sqrt{2}} \left[\bar{\nu}_{\tau,L} \gamma^\mu \tau_L\right] \left[\bar{D}_L \gamma_\mu u_L\right] + \text{h.c.} \tag{B.1}$$

From this Lagrangian, it is straightforward to write the matrix element for the τ decays under study

$$\mathscr{M} = -\sqrt{2} G_F V_{uD}^* L_\mu H^\mu \,, \tag{B.2}$$

where the lepton current is

$$L_\mu = \bar{u}_{\nu_\tau,L} \gamma_\mu \tau_L \,, \tag{B.3}$$

and the hadron vector is

$$H^\mu = 2\langle H^- | \bar{u}_L \gamma^\mu D_L | 0 \rangle \,. \tag{B.4}$$

For unpolarized taus, averaging over the decaying tau polarizations and summing over that of the neutrino yields ($\varepsilon^{0123} \equiv +1$)

$$\overline{|\mathscr{M}|}^2 = 2G_F^2 |V_{uD}|^2 (p_\tau^\alpha p_{\nu_\tau}^\beta + p_{\nu_\tau}^\alpha p_\tau^\beta - p_\tau \cdot p_{\nu_\tau} g^{\alpha\beta} - i\varepsilon^{\alpha\beta\gamma\delta} p_{\tau,\gamma} p_{\nu_\tau,\delta}) H_\beta^\dagger H_\alpha \,. \tag{B.5}$$

It is useful to introduce the virtual W momentum, $q = p_\tau - p_{\nu_\tau}, q^2 = s$, which corresponds to the momentum of the hadron system. Using it, we can decompose the hadron tensor $H_{\alpha\beta}(q) \equiv H_\beta^\dagger H_\alpha$ in terms of its longitudinal ($_L$) and transverse ($_T$) components as

$$H_{\alpha\beta}(q) = (-g_{\alpha\beta} q^2 + q_\alpha q_\beta) H_T(s) + q_\alpha q_\beta H_L(s) \,. \tag{B.6}$$

These can be obtained by applying the respective projectors to $H_{\alpha\beta}(q)$ ($-g_{\alpha\beta} q^2 + q_\alpha q_\beta$ and $q_\alpha q_\beta$ respectively). This allows us to write a very compact expression for the differential decay width in the unpolarized case

$$\frac{\mathrm{d}\Gamma}{\mathrm{d}s} = \frac{M_\tau^3}{16\pi} G_F^2 |V_{uD}|^2 \left(1 - \frac{s}{M_\tau^2}\right)^2 \left[H_L + H_T \left(1 + \frac{2s}{M_\tau^2}\right)\right] . \tag{B.7}$$

In the following sections, we will discuss the relevant one- and two-meson tau decay channels (in this case we will present the general distributions, including angular information, that are obtained). We will also comment on the inclusive case and then consider the original application of the WEFT for the two-hadron case, minimizing the dependence on form factor information.

B.1 Weak Effective Field Theory

Besides the tests within the SM mentioned in Chapter 1, there are tests of physics that are not contained in our framework; however, they can be studied as its extensions,

because it describes most of the physics we can observe in experiments. The possible expansions are of many kinds, for example: proposals of phenomenology associated with hypothetical light weakly-coupled particles, parametrizations of plausible new interactions with the SM particles, and the SM as an Effective Field Theory (the last two can generally parametrize effects induced by heavy new stuff).

Within these extensions, of our particular interest is the study of semileptonic processes beyond the standard model[430] in a model-independent way. Specifically, the hadronic τ decays and the constriction of the parameters of the Weak Effective Field Theory (WEFT) for $\tau \to \nu_\tau PP'$. For these processes, by integrating out the Higgs, SM weak bosons, and heavy quarks, we can construct local terms involving only light (active in tau decays) fields, containing the τ lepton, its neutrino, and the u, D ($D = d, s$) quarks. However, if we consider all possible particles beyond the SM mediators, we can write in the same fashion the most general Lagrangian with these degrees of freedom integrated out [429]:

$$\mathscr{L}_{\text{eff}} = -\frac{G_\mu V_{uD}}{\sqrt{2}}\Big[(1+\varepsilon_L^{D\tau})\bar{\tau}\gamma_\mu(1-\gamma_5)\nu_\tau\,\bar{u}\gamma^\mu(1-\gamma_5)D + \varepsilon_R^{D\tau}\bar{\tau}\gamma_\mu(1-\gamma_5)\nu_\tau\,\bar{u}\gamma^\mu(1+\gamma_5)D$$
$$+\tau(1-\gamma_5)\nu_\tau\,\bar{u}(\varepsilon_S^{D\tau}-\varepsilon_P^{D\tau}\gamma_5)D + \frac{1}{4}\hat{\varepsilon}_T^{D\tau}\bar{\tau}\sigma_{\mu\nu}(1-\gamma_5)\nu_\tau\,\bar{u}\sigma^{\mu\nu}(1-\gamma_5)D\Big] + \text{h.c.}, \quad \text{(B.8)}$$

where the $\varepsilon_\Gamma^{D\tau}$ contains the possible new physics. In the SM case all these coefficients vanish and $G_\mu = G_F$. These new physics effects should not be searched for in suppressed decays, but instead in observables in which there is very good control of the SM contribution, in order to obtain a beyond percent level of precision in the SM piece and consequently, clean probes of these parameters. Alternatively, one can search for processes where the SM piece is suppressed, and the BSM piece is not. For this thesis, we worked with clean angular observables (minimizing the dependence on hadron input) in the $\tau \to \nu_\tau K\pi$ decays (both $\bar{K}_0\pi^-$ and $K^-\pi^0$ are considered) as we detail next.

B.2 One Hadron Modes

The theoretically easiest semileptonic tau decays only have a meson, either a charged pion or Kaon, in the final state. The one-pion(Kaon) decay has a branching ratio of $\sim 10.8(0.70)\%$. Their corresponding hadron matrix element defines the meson decay

constant, $f_{P=\pi,K}$

$$H^\mu = 2\langle P^-(p)|\bar{D}_L\gamma^\mu u_L|0\rangle = -i\sqrt{2}f_P p^\mu\,, \tag{B.9}$$

with $f_\pi = 92.1(0.8)$ MeV and $f_K = 110.1(0.2)$ MeV [217]. We note that due to parity conservation of the strong interactions [1], only the axial current contributes to eq. (B.9). In this case, energy-momentum conservation forces $H^{\alpha\beta}$ to be proportional to $q^\alpha q^\beta$, that is, fully longitudinal. The full decay width is explicitly obtained as

$$\Gamma(\tau\to P^-\nu_\tau) = \frac{M_\tau^3}{16\pi}G_F^2|V_{uD}|^2 f_P^2\left(1-\frac{m_P^2}{M_\tau^2}\right)^2. \tag{B.10}$$

Virtual radiative corrections to these decays have recently been improved, working with $R\chi T$ [319, 320], completing the work done for real radiation [318, 431, 432]. Writing them as

$$\Gamma(\tau\to P^-\nu_\tau[\gamma]) = \Gamma(\tau\to P^-\nu_\tau)^0(1+\delta_{\tau P})\,, \tag{B.11}$$

where ^{0} denotes the Born result and the LHS is inclusive in photons, it is found [319, 320]

$$\delta_{\tau\pi} = (-0.24\pm0.56)\%\,,\quad \delta_{\tau K} = (-0.15\pm0.57)\%, \tag{B.12}$$

where the uncertainties are saturated by the counterterms scale-dependence.

B.3 Two Hadron Modes

In this case, the hadron matrix element reads ($s = q^2 = (p_1+p_2)^2$)

$$\langle P_1^- P_2^0|\bar{D}\gamma^\mu u|0\rangle = C_{P_1P_2}\left\{\left[(p_1-p_2)^\mu - \frac{\Delta_{P_1P_2}}{s}q^\mu\right]F_V^{P_1P_2}(s) + q^\mu F_S^{P_1P_2}(s)\right\}, \tag{B.13}$$

where $F_V^{P_1P_2}(0) = 1$ at leading order in the chiral expansion and $C_{\pi^-\pi^0} = \sqrt{2}$ (the others can be derived from flavor symmetry). Using the Dirac equation it is easily seen that

$$F_S(s) = \frac{m_D - m_u}{s}\langle P_1^- P_2^0|\bar{D}u|0\rangle\,, \tag{B.14}$$

relating the scalar form factor to the matrix element of the scalar density.

Radiative corrections to the tree-level results are available, including the model-independent part and the real structure-dependent part evaluated within $R\chi T$ (the virtual one is still missing) [433, 434, 90, 396].

[1] The axial anomaly starts contributing to processes with three mesons, or equivalent.

B.3.1 General Distributions

The most general doubly differential distributions in the hadron system invariant mass squared, s, and in the angle between the tau and the charged meson in the tau rest frame, α [435] is given by

$$\begin{aligned}\frac{\mathrm{d}\Gamma}{\mathrm{d}s\,\mathrm{d}\cos\alpha} =& \frac{G_F^2|V_{uD}|^2 M_\tau^3}{512\pi^3}\lambda^{1/2}\left(1,\frac{m_1^2}{s},\frac{m_2^2}{s}\right) S_{\mathrm{EW}}^{\mathrm{had}}|C_{P_1P_2}|^2\left(1-\frac{s}{M_\tau^2}\right)^2 \\ &\times\left[\mathscr{P}_0(s)+\mathscr{P}_1(s)\cos\alpha+\mathscr{P}_2(s)\cos^2\alpha\right], \end{aligned} \tag{B.15}$$

with [436]

$$\begin{aligned}&\mathscr{P}_0(s)=|F_S(s)|^2+|F_V(s)|^2\lambda\left(1,\frac{m_1^2}{s},\frac{m_2^2}{s}\right)\frac{s}{M_\tau^2}, \quad \mathscr{P}_1(s)=-2\,\mathrm{Re}[F_V(s)^* F_S(s)]\lambda^{1/2}\left(1,\frac{m_1^2}{s},\frac{m_2^2}{s}\right), \\ &\mathscr{P}_2(s)=|F_V(s)|^2\lambda\left(1,\frac{m_1^2}{s},\frac{m_2^2}{s}\right)\left(1-\frac{s}{M_\tau^2}\right), \end{aligned} \tag{B.16}$$

being λ the Källen function, $\lambda(a,b,c)=a^2+b^2+c^2-2(ab+ac+bc)$ [393].

In the previous equation, the factor S_{EW} resums the universal short-distance electroweak corrections for semileptonic tau decays [437–439], $S_{EW}^{had}\sim 1.02$ Its angular integration trivially gives the invariant mass distribution

$$\begin{aligned}\frac{\mathrm{d}\Gamma}{\mathrm{d}s} =& \frac{G_F^2|V_{uD}|^2 M_\tau^3}{768\pi^3}\lambda^{1/2}(s,m_1^2,m_2^2) S_{\mathrm{EW}}^{\mathrm{had}}|C_{P_1P_2}|^2\left(1-\frac{s}{M_\tau^2}\right)^2 \\ &\times\left[3|F_S(s)|^2+|F_V(s)|^2\lambda\left(1,\frac{m_1^2}{s},\frac{m_2^2}{s}\right)\left(1+\frac{2s}{M_\tau^2}\right)\right]. \end{aligned} \tag{B.17}$$

B.3.2 The $\pi\pi$ channel

Basically, one out of four tau leptons decay into the di-pion mode, which has the largest branching ratio. Due to parity, in the SM it can only be produced via the vector current and the scalar contribution is negligible, as it is suppressed by (m_d-m_u). Besides, the scalar density matrix element is forbidden in the very approximate limit of G-parity symmetry. Therefore, to an excellent approximation, it suffices to consider the pion vector form factor

$$\langle\pi^-\pi^0|\bar{d}\gamma^\mu u|0\rangle\approx\sqrt{2}(p_- - p_0)^\mu F_V^{\pi^-\pi^0}(s) \tag{B.18}$$

to fully characterize hadronization in this process. Correspondingly simplified expressions for this decay mode can be obtained trivially from the results in the two previous subsections.

As it was mentioned in the introductory chapter, an isospin rotation relates this charged form factor (probed in weak processes, like the tau decay) to the neutral form factor, which is accessed electromagnetically (and also from the neutral weak current, mediated by a Z^0) [2]

$$\frac{1}{2}\langle\pi^+\pi^-|\bar{u}\gamma^\mu u - \bar{d}\gamma^\mu d|0\rangle = F_V^{\pi^+\pi^-}(s)(p_+ - p_-)^\mu \,. \tag{B.19}$$

We recapitulate known properties of this form factor in the following:

- $\lim_{Q^2\to\infty} F_V(Q^2 = -s) = \frac{16F_\pi^2\alpha_S(Q^2)}{Q^2}$, the Brodsky-Lepage limit [312], obtained from the leading order behaviour in QCD for electromagnetic meson form factors, using the asymptotic results for the corresponding distribution amplitudes.

- $F_V(s)$ is analytic in the whole complex plane except for a cut starting at the two-pion threshold, $s = 4m_\pi^2$. Consequently, one can write dispersion relations for this object [3] using $\frac{1}{s'^n(s'-s-i\varepsilon)}$, where n represents the number of subtractions (one sets $F_V(0) = 1$ according to vector current conservation). Each additional subtractions increases the weight of the low-energy region and reduces that of the asymptotic regime, where short-distance QCD constraints become easier to fulfill. However, each of them brings an additional uncertainty through a new subtraction constant, not fixed by symmetry requirements -unlike the first one-. Therefore, n shall be kept as low as possible to increase predictability.

- The elastic region is defined as the one where no other states than 2π are possible. Neglecting the very small electromagnetic effect, the first inelastic contribution is 4π. This, and higher multiplicity pion states are large-N_C suppressed as intermediate states (higher order in the loop expansion), which explains why the onset of Kaon anti-Kaon contributions is really the one which starts introducing sizable inelastic effects. In the elastic region, unitarity of the S-matrix relates the imaginary part of the pion form factor to the $\pi\pi$ (isovector

[2] G-parity suppresses the isoscalar part, so only the isovector one was considered.

[3] One way of expressing it corresponds to the fact that the full form factor can be reconstructed from the knowledge of its phase at all energies. A famous realization of this idea corresponds to the Omnès representation [440], where it is obtained as an exponential of a dispersion integral of the scattering phase, which is exact in the elastic region.

and spin vector) scattering amplitude. Explicitly, ($\sigma_\pi(s) = \sqrt{1-\frac{4m_\pi^2}{s}}$)

$$\mathrm{Im}\, F_V(s) = \sigma_\pi(s) F_V(s) T_1^1(s)\,, \tag{B.20}$$

which shows that the form factor and scattering phase are identical in the elastic region.

- Its low-energy behaviour is determined from the results obtained within χPT. In the isospin limit, at next-to-leading order, one has

$$F_V(s) = 1 + \frac{2L_9^r(\mu)}{f_\pi^2} s - \frac{s}{96\pi^2 f_\pi^2}\left[A_\pi(s,\mu^2) + \frac{1}{2}A_K(s,\mu^2)\right], \tag{B.21}$$

in terms of the renormalized LEC $L_9^r(\mu^2)$ and the loop function [246]

$$A_P(s,\mu^2) = \log\left(\frac{m_P^2}{\mu^2}\right) + \frac{8m_P^2}{s} - \frac{5}{3} + \sigma_P^3(s)\log\frac{\sigma_P(s)+1}{\sigma_P(s)-1}\,. \tag{B.22}$$

As it must be, the dependence on the renormalization scale μ cancels between the LEC and the loop function.

- $R\chi T$ can provide a useful input phase for the dispersion relation, which -in the $N_C \to \infty$ limit- would include a sum over an infinite number of ρ-like states. The results for the lightest state exemplify how $R\chi T$ resums an infinite tower of interactions in χPT. Procedures based on this result include up to two ρ excitations [372, 400, 441, 442, 401, 402]. These were mostly interested in improving the description of hadronization and in determining resonance properties, most notably their pole positions. New physics analyses, using this input have also been performed in refs. [443, 444, 444].

The most precise branching fraction measurement of di-pion tau decays still comes from ALEPH [117] and the most accurate spectrum was measured by Belle [120]. Other measurements were obtained by CLEO [118] and OPAL [119]. It is expected that Belle-II [445] will improve on these results soon.

According to ref. [402], $\tau^- \to K_S K^- \nu_\tau$ BaBar data [446] (which can be related to the $\pi\pi$ case under $SU(3)$ flavor symmetry) show indications of violations of this symmetry [4]. In the advent of more precise data, separate descriptions of the $\pi^\pm\pi^0$ and $K^\pm K_S$ vector form factors will need to be used. Since the phase space for the

[4]The scalar form factor is similarly suppressed in the $K\bar{K}$ case, as with $\pi\pi$.

$K\bar{K}$ channel is completely in the inelastic regime of $\pi\pi$, the vector and tensor form factors do not coincide, leaving more space for new physics contributions [447, 436].

The other non-strange two-meson tau decays, $\tau^- \to \eta^{(\prime)}\pi^-\nu_\tau$, are suppressed by G-parity [448–452], and have not been measured yet, with branching ratio upper limits on the ballpark of $10^{-4,5}$ [453, 454], which are one or two orders of magnitude larger than the theory predictions. In these processes, radiative corrections which are suppressed by α but not by G-parity may compete with the Born contributions, making an accurate SM prediction even more challenging [455–457]. It is also worth to note that a good control on backgrounds, particularly the allowed decays including an additional π^0 [323], needs to be achieved; while the Belle measurement of the $\eta\pi^-\pi^0$ channel [458] is in tension with e^+e^- measurements [459] and with known pion vector precise data [458]. With these caveats in mind, possible new physics effects are large [460] and Belle-II has this search as one of its priorities [445].

B.3.3 The $K\pi$ channel

For the $\pi^-\bar{K}^0$ and $K^-\pi^0$ channels ($\sim 1\%$ and $\sim 0.5\%$ BR respectively), we can have a non-zero $F_S(s)$, which is still suppressed with respect to the $F_V(s)$ for most values of s. Still, it is relevant near the threshold, and the FFs ratio can be used in the rest of the domain as an expansion parameter for the observables we aim to describe. At leading order in χPT, we get $C_{\pi K} = \frac{1}{\sqrt{2}}$ [427] [5].

The form factors can be obtained from different sources, one of them is directly from the Belle spectrum of the $\tau \to K_S\pi^-\nu_\tau$ decays [461–465] and the other one is the $K_{\ell 3}$ decays [466, 467, 463, 464], also phaseshift measurements help to describe them [468] and others are computed from Resonance Chiral theory (which can also be used to give input phaseshift to the dispersive representation) [469–472, 396].

For the vector form factor, there is no significant variation between form factors due to the abundance of data in the $\tau \to K_S\pi^-\nu_\tau$ decays from Belle [473] and the high sensitivity to this form factor in particular. This information can be extracted by means of the differential decay width:

$$\frac{\mathrm{d}\Gamma_{K\pi}}{\mathrm{d}\sqrt{s}} = \frac{G_F^2|V_{us}|^2 m_\tau^3}{96\pi^3 s} S_{\mathrm{EW}} \left(1 - \frac{s}{m_\tau^2}\right) \left[\left(1 + 2\frac{s}{m_\tau^2}\right) q_{K\pi}^3 |F_V^{K\pi}(s)|^2 + \frac{3\Delta_{K\pi}^2}{4s} q_{K\pi} |F_S^{K\pi}|^2\right], \tag{B.23}$$

where isospin invariance is assumed, and a sum over $\bar{K}^0\pi^-$ and $K^-\pi^0$ channels was performed. $S_{\mathrm{EW}} \sim 1.02$ is the universal short-distance electroweak correction

[5] It is a convention that the first pseudoscalar P_1 is the charged one.

factor [437–439], $\Delta_{K\pi} = m_K^2 - m_\pi^2$ and $q_{K\pi}$ is defined as:

$$q_{K\pi} = \frac{2}{2\sqrt{s}}\sqrt{\left(s-(m_k^2+m_\pi^2)\right)\left(s-(m_k^2-m_\pi^2)\right)}\cdot\theta\Big(s-(m_k^2+m_\pi^2)\Big). \tag{B.24}$$

In this work, we have taken the description from [465] due to the availability of the correlation matrix for the fitted parameters, which will be used for the numerical error propagation. For this form factor, an $R\chi T$ with two vector meson resonances phaseshift seed was used, given by the normalized form factor [462]:

$$\tilde{F}_V^{K\pi}(s) = \frac{m_{K^*} - \kappa_{k^*}\tilde{H}_{K\pi}(0) + \gamma s}{D(m_{K^*},\gamma_{K^*})} - \frac{\gamma s}{D(m_{K^{*\prime}},\gamma_{K^{*\prime}})}, \tag{B.25}$$

where

$$D(m_n,\gamma_n) = m_n^2 - s - \kappa_n\tilde{H}_{K\pi}(s), \tag{B.26}$$

and

$$\kappa_n = \frac{192\pi}{\sigma_{K\pi}(m_n^2)^3}\frac{\gamma_n}{m_n}, \tag{B.27}$$

with $\sigma_{K\pi} = 2q_{K\pi}/\sqrt{s}$. All masses and γ_ns are fit parameters (which can be related to pole parameters, as done in the quoted references). Finally, the scalar one loop function $\tilde{H}_{K\pi}(s)$ is the isospin average of the two channels:

$$\tilde{H}_{K\pi}(s) = \frac{2}{3}\tilde{H}_{K^0\pi^-}(s) + \frac{1}{3}\tilde{H}_{K^-\pi^0}(s), \tag{B.28}$$

with this function being defined as [474, 471] $\tilde{H}(s) = H(s) - 2L_9^r s/(3F_\pi^2) = [sM^r(s) - L(s)]/F_\pi^2$, however removing the F_π^2 because of the definition of κ_n in terms of γ_n. The functions M_r and $L(s)$ are defined in [474] and can be checked in the code of Appendix A in ref. [469].

As in the $\pi\pi$ vector form factor, the $K\pi$ one can be described by an Omnès representation with an $R\chi T$ phaseshift seed given by:

$$\tan\delta_1^{K\pi}(s) = \frac{\mathrm{Im}\tilde{F}_V^{K\pi}(s)}{\mathrm{Re}\tilde{F}_V^{K\pi}(s)}, \tag{B.29}$$

the dispersion relation is three times subtracted, meaning:

$$\tilde{F}_V^{K\pi}(s) = \exp\left[\alpha_1\frac{s}{m_\pi^2} + \frac{1}{2}\alpha_2\frac{s^2}{m_\pi^4} + \frac{s^3}{\pi}\int_{s_{K\pi}}^{s_{\mathrm{cut}}} ds'\frac{\delta_1^{K\pi}(s')}{(s')^3(s'-s-i0)}\right], \tag{B.30}$$

where the α_i are fit parameters too. With this, the vector form factor is described accurately enough to match present data. Results of this description, which also includes the $\tau \to K^- \eta \nu_\tau$ channel, are found in Figure B.2.

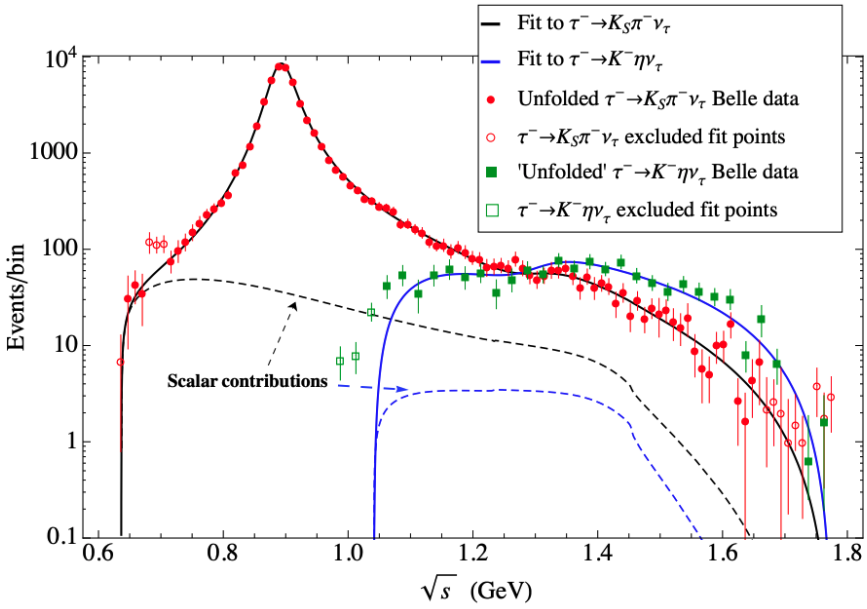

Fig. B.2 Belle $\tau \to K_S \pi^- \nu_\tau$ (red solid circles) [473] and $\tau \to K^- \eta \nu_\tau$ (green solid squares) [458] measurements as compared to the best fit in Ref. [465] (solid black and blue lines, respectively) obtained in combined fits to both data sets. The dashed lines correspond to the scalar form factor contributions, and the empty circles and squares are the data not used in the analysis.

For the scalar form factor, we have considered three sources [466, 468, 463], with the main differences described in Table B.1 and the results shown in Figure B.3. We considered all models with an error band that includes all of them, accounting for their respective uncertainties. The normalization of the form factors was taken from the FLAG collaboration in the $N_f = 2+1+1$ and $N_f = 2+1$ cases [475].

For our central curve, we have considered Refs. [463] and [466]. Since the study in [463] is restricted to the elastic region, a smooth transition from this solution to the solution of [466] can be done in the $[1.3-1.4]$ GeV region, according to estimated inelastic effects, as it is shown in Figure B.3. The relation between both form factors for the matching is done by means of:

$$F_S^{K\pi}(s) = F_S^{\rm JOP}(s) \mathrm{T_F}(s,+) + F_S^{\rm BBP}(s) \mathrm{T_F}(s,-), \tag{B.31}$$

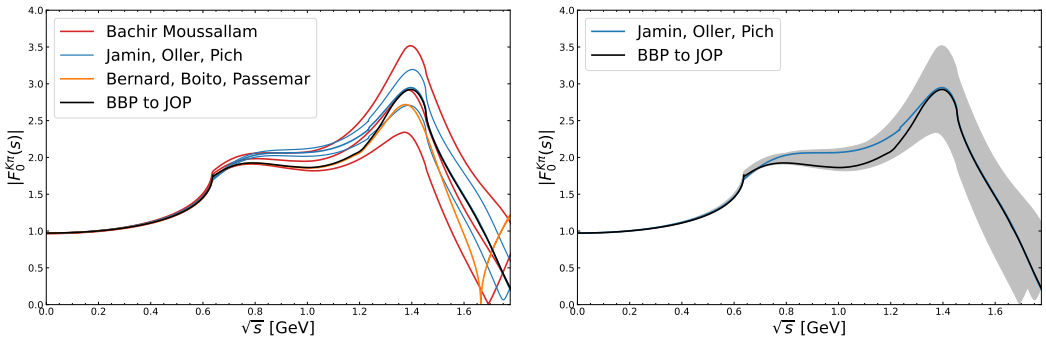

Fig. B.3 All considered models for $K\pi$ SFF. The central value is a continuation from Ref.[463] in the elastic region to [466] in the inelastic region. An error band that includes all curves with errors (variations of the parameters that determine de curves) will be considered for our error computation.

where the function $\mathrm{T_F}(s,\pm)$ is the one that defines the transition:

$$\mathrm{T_F}(s,\pm) = \frac{1}{\pi}\left(\arctan\left(\pm\frac{s-(s_f+s_0)/2}{a(s_f-s_0)}\right)+\frac{\pi}{2}\right), \tag{B.32}$$

and a is the factor that defines how smooth or strong the transition between s_0 and s_f is. For our case, we have chosen $a = 0.15$, $s_0 = 1.2\,\mathrm{GeV}$ and $s_f = 1.4\mathrm{GeV}$.

Model	Obtained from τ data	Source	s Domain
Dispersive representation [463] Bernard, Boito, Passemar	$\ln C = \ln(\tilde{f}_0(\Delta_{K\pi}))$ and λ_0' are fitted to τ data.	data points Provided by the authors	$[0,3.2]\mathrm{GeV}^2$
Dispersive Representation, LDC and SDC [466] Jamin, Oller, Pich	No, taken from S-wave $K\pi$ scattering	Data Points Provided by the authors	Inelastic case included
Dispersive representation coupled Form Factors [468] Moussallam	No, but validated by τ data	code	Inelastic case included provided by the author

Table B.1 Scalar Form Factors $F_S^{K\pi}$ from different models.

Interest in these decays grew thanks to the anomalous BaBar measurement of the CP asymmetry in $\tau \to K_S\pi\nu_\tau$ decays [476]. Effective field theory methods have shown that barring extreme fine-tuning, this result cannot be explained by heavy new physics [477–479] coming from an antisymmetric tensor current. Belle(-II) [445] are working on these and related decays (including an additional π^0, or with a $K^\pm$ instead of the $\pi^\pm$) to confirm or refute this unexpected result. In the double differential distribution including angular information, BSM effects in the scalar form factor can also pop up, which are being searched as well for by these experiments. It is in this context (particularly for the latter analyses) where we hope this work to be useful.

$K\eta^{(\prime)}$ tau decays were addressed, using a similar framework, in refs. [480, 465]. The corresponding vector form factors can be obtained from the $K\pi$ one, and their

scalar form factors enter the three coupled channels solutions discussed previously. We note that for ideal $\eta - \eta'$ meson mixing, the $K\eta$ scalar form factor vanishes at leading order in the chiral expansion, which results in its considerable suppression. This is the reason why the two coupled channel solution where it is effectively neglected is a good approximation to the $K(\pi, \eta')$ cases. Therefore, the BaBar measurement of the $K\eta$ mode [453] only tests the vector form factor, while there is only an upper limit at the level of 10^{-6} for the $K\eta'$ decays, obtained by BaBar [454].

B.4 WEFT for Two Hadron modes

When considering integrating out all possible BSM degrees of freedom (and the SM particles which are inaccessible in tau decays), we end up with the effective Lagrangian in eq.(B.8), which will induce other contributions to the amplitude, which will benefit from the following parametrizations:

$$\begin{aligned} H = \langle PP'|\bar{D}u|0\rangle =& C_{PP'}\frac{\Delta_{PP'}}{m_D - m_u}F_S^{PP'}(s), \\ H^\mu = \langle PP'|\bar{D}\gamma^\mu u|0\rangle =& C_{PP'}\left[\left(p_- - p_0 - \frac{\Delta_{PP'}}{s}q\right)^\mu F_V^{PP'}(s) + q^\mu \frac{\Delta_{PP'}}{s}F_S^{PP'}(s)\right], \\ H^{\mu\nu} = \langle PP'|\bar{D}\sigma^{\mu\nu}u|0\rangle =& -iF_T^{PP'}(p_-^\mu p_0^\nu - p_-^\nu p_0^\mu). \end{aligned} \tag{B.33}$$

For unpolarized taus, in the isospin limit, we found for the di-pion tau decays:

$$\begin{aligned} \frac{\mathrm{d}\Gamma}{\mathrm{d}s\,\mathrm{d}\cos\theta} =& \frac{m_\tau^3}{512\pi^3}G_\mu^2|V_{ud}|^2 C_{\pi\pi}^2 S_{\mathrm{EW}}\lambda_{\pi\pi}^{1/2}\left(1-\frac{s}{m_\tau^2}\right)^2\left[\frac{\lambda_{\pi\pi}s}{m_\tau C_{\pi\pi}}\mathrm{Re}\left(\hat{\varepsilon}_T^d F_V^{\pi\pi}F_T^{\pi\pi *}\right)\right. \\ &+ \left[1+2\mathrm{Re}\left(e_L^d + e_R^d\right)\right]\lambda_{\pi\pi}\left[\frac{s}{m_\tau^2} + \left(1-\frac{s}{m_\tau^2}\right)\cos\theta\right]|F_V^{\pi\pi}|^2 \\ &\left. - 2\frac{\lambda_{\pi\pi}^{1/2}}{m_\tau(m_d - m_u)}\mathrm{Re}\left(\varepsilon_S^d F_V^{\pi\pi}F_S^{\pi\pi *}\right)\cos\theta\right]G_{LD}(s), \end{aligned} \tag{B.34}$$

where θ is the angle between the τ^- and the π^- momenta in the hadronic rest frame, $\lambda_{\pi\pi} = \lambda(s, m_\pi^2, m_\pi^2)/s^2$, being λ the Källen function [393], and $G_{LD}(s)$ has the information on the long-distance radiative corrections [87].

B.4.1 Angular Observables of the Two-Hadron Mode in the WEFT

We can define the angular observables, *momenta*, from the differential decay widths:

$$I_{2n} = \langle \cos^{2n}\theta \rangle = \int_{-1}^{1} \mathrm{d}\cos\theta \frac{\mathrm{d}^2\Gamma}{\mathrm{d}s\mathrm{d}\cos\theta} \cos^{2n}\theta. \tag{B.35}$$

Due to the integrals of trigonometric functions, all momenta can be expressed in terms of just the first two:

$$I_{2n} = 3\frac{(n-1)I_0 + 5nI_2}{(2n+1)(2n+3)}. \tag{B.36}$$

At order $\mathscr{O}(\hat{\varepsilon}_T^2)$, we can write I_2 in terms of I_2:

$$I_2 = \frac{I_0}{5}\left(\frac{3m_\tau^2+2s}{m_\tau^2+2s}\right)\left(1 - 4\mathrm{Re}(\hat{\varepsilon}_T^d)\frac{F_T^{\pi\pi(0)} m_\tau s(m_\tau^2-s)}{C_{\pi\pi}(m_\tau^2+2s)(3m_\tau^2+2s)}\right), \tag{B.37}$$

which we can integrate to obtain directly deviations from the SM and non-SM differential decay rate:

$$J_2 = \int_{4m_\pi^2}^{m_\tau^2} ds I_2, \quad J_0 = \int_{4m_\pi^2}^{m_\tau^2} ds I_0. \tag{B.38}$$

These integrated momenta can be taken to the SM value by setting $\hat{\varepsilon}_T^d \to 0$, and we can obtain a clean observable to probe this parameter:

$$J_2 = J_2^{\mathrm{SM}}(1 - a\mathrm{Re}(\hat{\varepsilon}_T^d)), \quad J_0 = \Gamma_{\pi\pi}(1 - b\mathrm{Re}(\hat{\varepsilon}_T^d)), \tag{B.39}$$

with

$$\begin{aligned} a &= 4\frac{F_T^{\pi\pi}}{C_{\pi\pi}} m_\tau \int_{4m_\pi^2}^{m_\tau^2} ds I_0 \frac{s(m_\tau^2-s)}{(m_\tau^2+2s)^2}\left(\int_{4m_\pi^2}^{m_\tau^2} ds I_0 \frac{3m_\tau^2+2s}{m_\tau^2+2s}\right)^{-1}, \\ b &= 4\frac{F_T^{\pi\pi}}{C_{\pi\pi}} m_\tau \int_{4m_\pi^2}^{m_\tau^2} ds I_0 \frac{s(m_\tau^2-s)}{(m_\tau^2+2s)(3m_\tau^2+2s)}\left(\int_{4m_\pi^2}^{m_\tau^2} ds I_0\right)^{-1}. \end{aligned} \tag{B.40}$$

For the $K\pi$ case, the scalar form factor becomes non-negligible near the threshold, but can still be considered smaller than the vector form factor, so small corrections of the order $\frac{|F_S(s)|^2}{|F_V(s)|^2}$ to the momenta $I_{0,2}$ shall be considered.

In this way, one obtains ($\delta_V \equiv 2\,\mathrm{Re}(\varepsilon_L^D + \varepsilon_R^D)$)

$$I_0 = \frac{M_\tau^3}{768\pi^3} G_\mu^2 |V_{us}|^2 C_{\pi\bar{K}}^2 |F_V^{K\pi}(s)|^2 (1+\delta_V) \lambda_{K\pi}^{3/2} \left(1 - \frac{s}{M_\tau^2}\right)^2 \left\{ \frac{3sF_T^{K\pi}(0)}{M_\tau C_{\pi\bar{K}}} \mathrm{Re}\,\varepsilon_T^s + 1 + \frac{2s}{M_\tau^2} \right\} (1+\delta_0)\,, \tag{B.41}$$

with the small correction given by

$$\delta_0 = \frac{3\Delta_{K\pi} M_\tau^2 \left(1 + \frac{2s\,\mathrm{Re}\,\varepsilon_S^s}{M_\tau(m_s - m_u)}\right)}{\lambda_{K\pi} \left[-3M_\tau s F_T^{K\pi}(0)\,\mathrm{Re}\,\varepsilon_T^s + (M_\tau^2 + 2s)\right]} \frac{\left|F_0^{K\pi}(s)\right|^2}{\left|F_V^{K\pi}(s)\right|^2}\,. \tag{B.42}$$

Proceeding analogously for the second moment, it is found that

$$I_2 = \frac{M_\tau^3}{3840\pi^3} G_\mu^2 |V_{us}|^2 C_{\pi\bar{K}}^2 |F_V^{K\pi}(s)|^2 (1+\delta_V) \lambda_{K\pi}^{3/2} \left(1 - \frac{s}{M_\tau^2}\right)^2 \left\{ \frac{5sF_T^{K\pi}(0)}{M_\tau C_{\pi\bar{K}}} \mathrm{Re}\,\varepsilon_T^s + 3 + \frac{2s}{M_\tau^2} \right\} (1+\delta_2)\,, \tag{B.43}$$

with

$$\delta_2 = \frac{5\Delta_{K\pi} M_\tau^2 \left(1 + \frac{2s\,\mathrm{Re}\,\varepsilon_S^s}{M_\tau(m_s - m_u)}\right)}{\lambda_{K\pi} \left[-5M_\tau s F_T^{K\pi}(0)\,\mathrm{Re}\,\varepsilon_T^s + (3M_\tau^2 + 2s)\right]} \frac{\left|F_0^{K\pi}(s)\right|^2}{\left|F_V^{K\pi}(s)\right|^2}\,. \tag{B.44}$$

Thus, we can use eq. (B.37) also for the $K\pi$ case, provided we correct it with the factor $1 + \delta_2 - \delta_0$.

This is a work in progress, which was the main project for Santiago Paz's Master's Thesis, presented at TAU2025 [128], and will be published soon [127].

References

[1] MUON $g-2$ collaboration, *Final Report of the Muon E821 Anomalous Magnetic Moment Measurement at BNL*, *Phys. Rev. D* **73** (2006) 072003 [hep-ex/0602035].

[2] MUON $g-2$ collaboration, *Measurement of the Positive Muon Anomalous Magnetic Moment to 0.46 ppm*, *Phys. Rev. Lett.* **126** (2021) 141801 [2104.03281].

[3] MUON $g-2$ collaboration, *Measurement of the Positive Muon Anomalous Magnetic Moment to 0.20 ppm*, *Phys. Rev. Lett.* **131** (2023) 161802 [2308.06230].

[4] MUON $g-2$ collaboration, *Measurement of the Positive Muon Anomalous Magnetic Moment to 127 ppb*, *Phys. Rev. Lett.* **135** (2025) 101802 [2506.03069].

[5] T. Aoyama et al., *The anomalous magnetic moment of the muon in the Standard Model*, *Phys. Rept.* **887** (2020) 1 [2006.04822].

[6] R. Aliberti et al., *The anomalous magnetic moment of the muon in the Standard Model: an update*, *Phys. Rept.* **1143** (2025) 1 [2505.21476].

[7] S. Descotes-Genon, J. Matías, M. Ramín and J. Virto, *Implications from clean observables for the binned analysis of $B->K*\mu^+\mu^-$ at large recoil*, *JHEP* **01** (2013) 048 [1207.2753].

[8] LHCB collaboration, *Measurement of CP-Averaged Observables in the $B^0 \to K^{*0}\mu^+\mu^-$ Decay*, *Phys. Rev. Lett.* **125** (2020) 011802 [2003.04831].

[9] HPQCD collaboration, *Standard Model predictions for $B \to K\ell+\ell-$, $B \to K\ell 1-\ell 2+$ and $B \to K\nu\nu^-$ using form factors from Nf=2+1+1 lattice QCD*, *Phys. Rev. D* **107** (2023) 014511 [2207.13371].

[10] LHCB collaboration, *Branching Fraction Measurements of the Rare $B_s^0 \to \phi\mu^+\mu^-$ and $B_s^0 \to f_2'(1525)\mu^+\mu^-$ Decays*, *Phys. Rev. Lett.* **127** (2021) 151801 [2105.14007].

[11] N. Gubernari, M. Reboud, D. van Dyk and J. Virto, *Improved theory predictions and global analysis of exclusive $b \to s\mu^+\mu^-$ processes*, *JHEP* **09** (2022) 133 [2206.03797].

[12] G. Isidori, Z. Polonsky and A. Tinari, *Semi-inclusive $b \to s\ell^-\ell$ transitions at high q2*, *Phys. Rev. D* **108** (2023) 093008 [2305.03076].

[13] A.J. Buras, *Standard Model predictions for rare K and B decays without new physics infection*, *Eur. Phys. J. C* **83** (2023) 66 [2209.03968].

[14] M. Ciuchini, M. Fedele, E. Franco, A. Paul, L. Silvestrini and M. Valli, *Constraints on lepton universality violation from rare B decays*, *Phys. Rev. D* **107** (2023) 055036 [2212.10516].

[15] M. Algueró, A. Biswas, B. Capdevila, S. Descotes-Genon, J. Matías and M. Novoa-Brunet, *To (b)e or not to (b)e: no electrons at LHCb*, *Eur. Phys. J. C* **83** (2023) 648 [2304.07330].

[16] BELLE-II collaboration, *Evidence for $B+\to K+\nu\nu^-$ decays*, *Phys. Rev. D* **109** (2024) 112006 [2311.14647].

[17] ATLAS collaboration, *Measurement of the W-boson mass in pp collisions at $\sqrt{s} = 7$ TeV with the ATLAS detector*, *Eur. Phys. J. C* **78** (2018) 110 [1701.07240].

[18] CMS collaboration, *Measurement of the weak mixing angle with the Drell-Yan process in proton-proton collisions at the LHC*, *Phys. Rev. D* **84** (2011) 112002 [1110.2682].

[19] LHCB collaboration, *Measurement of the forward-backward asymmetry in $Z/\gamma^* \to \mu^+\mu^-$ decays and determination of the effective weak mixing angle*, *JHEP* **11** (2015) 190 [1509.07645].

[20] LHCB collaboration, *Measurement of the W boson mass*, *JHEP* **01** (2022) 036 [2109.01113].

[21] ALEPH, DELPHI, L3, OPAL, LEP ELECTROWEAK collaboration, *Electroweak Measurements in Electron-Positron Collisions at W-Boson-Pair Energies at LEP*, *Phys. Rept.* **532** (2013) 119 [1302.3415].

[22] J. de Blas, M. Pierini, L. Reina and L. Silvestrini, *Impact of the Recent Measurements of the Top-Quark and W-Boson Masses on Electroweak Precision Fits*, *Phys. Rev. Lett.* **129** (2022) 271801 [2204.04204].

[23] ALEPH, DELPHI, L3, OPAL, SLD, LEP ELECTROWEAK WORKING GROUP, SLD ELECTROWEAK GROUP, SLD HEAVY FLAVOUR GROUP collaboration, *Precision electroweak measurements on the Z resonance*, *Phys. Rept.* **427** (2006) 257 [hep-ex/0509008].

[24] A. Crivellin and B. Mellado, *Anomalies in particle physics and their implications for physics beyond the standard model*, *Nature Rev. Phys.* **6** (2024) 294 [2309.03870].

[25] R. Aliberti et al., *Radiative corrections and Monte Carlo tools for low-energy hadronic cross sections in e^+e^- collisions*, *SciPost Phys. Comm. Rep.* **9** (2025) 1 [2410.22882].

[26] RBC, UKQCD collaboration, *Calculation of the hadronic vacuum polarization contribution to the muon anomalous magnetic moment*, *Phys. Rev. Lett.* **121** (2018) 022003 [1801.07224].

[27] ETM collaboration, *Electromagnetic and strong isospin-breaking corrections to the muon $g-2$ from Lattice QCD+QED*, *Phys. Rev. D* **99** (2019) 114502 [1901.10462].

[28] S. Borsányi et al., *Leading hadronic contribution to the muon magnetic moment from lattice QCD*, *Nature* **593** (2021) 51 [2002.12347].

[29] C. Lehner and A.S. Meyer, *Consistency of hadronic vacuum polarization between lattice QCD and the R-ratio*, *Phys. Rev. D* **101** (2020) 074515 [2003.04177].

[30] χQCD collaboration, *Muon g-2 with overlap valence fermions*, *Phys. Rev. D* **107** (2023) 034513 [2204.01280].

[31] C. Aubin, T. Blum, M. Golterman and S. Peris, *Muon anomalous magnetic moment with staggered fermions: Is the lattice spacing small enough?*, *Phys. Rev. D* **106** (2022) 054503 [2204.12256].

[32] M. Cè et al., *Window observable for the hadronic vacuum polarization contribution to the muon $g-2$ from lattice QCD*, *Phys. Rev. D* **106** (2022) 114502 [2206.06582].

[33] ETM collaboration, *Lattice calculation of the short and intermediate time-distance hadronic vacuum polarization contributions to the muon magnetic moment using twisted-mass fermions*, *Phys. Rev. D* **107** (2023) 074506 [2206.15084].

[34] RBC, UKQCD collaboration, *Update of Euclidean windows of the hadronic vacuum polarization*, *Phys. Rev. D* **108** (2023) 054507 [2301.08696].

[35] S. Kuberski, M. Cè, G. von Hippel, H.B. Meyer, K. Ottnad, A. Risch et al., *Hadronic vacuum polarization in the muon $g-2$: the short-distance contribution from lattice QCD*, *JHEP* **03** (2024) 172 [2401.11895].

[36] A. Boccaletti et al., *High precision calculation of the hadronic vacuum polarisation contribution to the muon anomaly*, 2407.10913.

[37] S. Spiegel and C. Lehner, *High-precision continuum limit study of the HVP short-distance window*, *Phys. Rev. D* **111** (2025) 114517 [2410.17053].

[38] RBC, UKQCD collaboration, *The long-distance window of the hadronic vacuum polarization for the muon g-2*, *Phys. Rev. Lett.* **134** (2025) 201901 [2410.20590].

[39] D. Djukanovic, G. von Hippel, S. Kuberski, H.B. Meyer, N. Miller, K. Ottnad et al., *The hadronic vacuum polarization contribution to the muon $g-2$ at long distances*, *JHEP* **04** (2025) 098 [2411.07969].

[40] ETM collaboration, *Strange and charm quark contributions to the muon anomalous magnetic moment in lattice QCD with twisted-mass fermions*, *Phys. Rev. D* **111** (2025) 054502 [2411.08852].

[41] FERMILAB LATTICE, HPQCD, MILC collaboration, *Hadronic vacuum polarization for the muon g-2 from lattice QCD: Complete short and intermediate windows*, *Phys. Rev. D* **111** (2025) 094508 [2411.09656].

[42] FERMILAB LATTICE, HPQCD, MILC collaboration, *Hadronic Vacuum Polarization for the Muon $g-2$ from Lattice QCD: Long-Distance and Full Light-Quark Connected Contribution*, *Phys. Rev. Lett.* **135** (2025) 011901 [2412.18491].

[43] A. Keshavarzi, D. Nomura and T. Teubner, *The $g-2$ of charged leptons, $\alpha(M_Z^2)$ and the hyperfine splitting of muonium*, *Phys. Rev. D* **101** (2020) 014029 [1911.00367].

[44] L. Di Luzio, A. Keshavarzi, A. Masiero and P. Paradisi, *Model-Independent Tests of the Hadronic Vacuum Polarization Contribution to the Muon g-2*, *Phys. Rev. Lett.* **134** (2025) 011902 [2408.01123].

[45] A. Kurz, T. Liu, P. Marquard and M. Steinhauser, *Hadronic contribution to the muon anomalous magnetic moment to next-to-next-to-leading order*, *Phys. Lett. B* **734** (2014) 144 [1403.6400].

[46] G. Colangelo, M. Hoferichter, M. Procura and P. Stoffer, *Dispersion relation for hadronic light-by-light scattering: theoretical foundations*, *JHEP* **09** (2015) 074 [1506.01386].

[47] P. Masjuan and P. Sánchez-Puertas, *Pseudoscalar-pole contribution to the $(g_\mu-2)$: a rational approach*, *Phys. Rev. D* **95** (2017) 054026 [1701.05829].

[48] G. Colangelo, M. Hoferichter, M. Procura and P. Stoffer, *Dispersion relation for hadronic light-by-light scattering: two-pion contributions*, *JHEP* **04** (2017) 161 [1702.07347].

[49] M. Hoferichter, B.-L. Hoid, B. Kubis, S. Leupold and S.P. Schneider, *Dispersion relation for hadronic light-by-light scattering: pion pole*, *JHEP* **10** (2018) 141 [1808.04823].

[50] G. Eichmann, C.S. Fischer, E. Weil and R. Williams, *Single pseudoscalar meson pole and pion box contributions to the anomalous magnetic moment of the muon*, *Phys. Lett. B* **797** (2019) 134855 [1903.10844].

[51] J. Bijnens, N. Hermansson-Truedsson and A. Rodríguez-Sánchez, *Short-distance constraints for the HLbL contribution to the muon anomalous magnetic moment*, *Phys. Lett. B* **798** (2019) 134994 [1908.03331].

[52] J. Leutgeb and A. Rebhan, *Axial vector transition form factors in holographic QCD and their contribution to the anomalous magnetic moment of the muon*, *Phys. Rev. D* **101** (2020) 114015 [1912.01596].

[53] L. Cappiello, O. Catà, G. D'Ambrosio, D. Greynat and A. Iyer, *Axial-vector and pseudoscalar mesons in the hadronic light-by-light contribution to the muon $(g-2)$*, *Phys. Rev. D* **102** (2020) 016009 [1912.02779].

[54] P. Masjuan, P. Roig and P. Sánchez-Puertas, *The interplay of transverse degrees of freedom and axial-vector mesons with short-distance constraints in $g-2$*, *J. Phys. G* **49** (2022) 015002 [2005.11761].

[55] J. Bijnens, N. Hermansson-Truedsson, L. Laub and A. Rodríguez-Sánchez, *Short-distance HLbL contributions to the muon anomalous magnetic moment beyond perturbation theory*, *JHEP* **10** (2020) 203 [2008.13487].

[56] J. Bijnens, N. Hermansson-Truedsson and A. Rodríguez-Sánchez, *Short-distance constraints in hadronic-light-by-light for the muon $g-2$*, *PoS* **PANIC2021** (2022) 423 [2110.13529].

[57] I. Danilkin, M. Hoferichter and P. Stoffer, *A dispersive estimate of scalar contributions to hadronic light-by-light scattering*, *Phys. Lett. B* **820** (2021) 136502 [2105.01666].

[58] D. Stamen, D. Hariharan, M. Hoferichter, B. Kubis and P. Stoffer, *Kaon electromagnetic form factors in dispersion theory*, *Eur. Phys. J. C* **82** (2022) 432 [2202.11106].

[59] J. Leutgeb, J. Mager and A. Rebhan, *Hadronic light-by-light contribution to the muon $g-2$ from holographic QCD with solved $U(1)_A$ problem*, *Phys. Rev. D* **107** (2023) 054021 [2211.16562].

[60] M. Hoferichter, B. Kubis and M. Zanke, *Axial-vector transition form factors and $e^+e^- \to f_1\pi^+\pi^-$*, *JHEP* **08** (2023) 209 [2307.14413].

[61] M. Hoferichter, P. Stoffer and M. Zillinger, *An optimized basis for hadronic light-by-light scattering*, *JHEP* **04** (2024) 092 [2402.14060].

[62] E.J. Estrada, S. Gonzàlez-Solís, A. Guevara and P. Roig, *Improved π^0, η, η' transition form factors in resonance chiral theory and their a_μ^{HLbL} contribution*, *JHEP* **12** (2024) 203 [2409.10503].

[63] J. Lüdtke, M. Procura and P. Stoffer, *Dispersion relations for the hadronic VVA correlator*, *JHEP* **04** (2025) 130 [2410.11946].

[64] O. Deineka, I. Danilkin and M. Vanderhaeghen, *Dispersive estimate of the a0(980) contribution to (g-2)μ*, *Phys. Rev. D* **111** (2025) 034009 [2410.12894].

[65] G. Eichmann, C.S. Fischer, T. Haeuser and O. Regenfelder, *Axial-vector and scalar contributions to hadronic light-by-light scattering*, *Eur. Phys. J. C* **85** (2025) 445 [2411.05652].

[66] J. Bijnens, N. Hermansson-Truedsson and A. Rodríguez-Sánchez, *Constraints on the hadronic light-by-light tensor in corner kinematics for the muon $g-2$*, *JHEP* **03** (2025) 094 [2411.09578].

[67] M. Hoferichter, P. Stoffer and M. Zillinger, *Dispersion relation for hadronic light-by-light scattering: subleading contributions*, *JHEP* **02** (2025) 121 [2412.00178].

[68] S. Holz, M. Hoferichter, B.-L. Hoid and B. Kubis, *Dispersion relation for hadronic light-by-light scattering: η and η' poles*, *JHEP* **04** (2025) 147 [2412.16281].

[69] L. Cappiello, J. Leutgeb, J. Mager and A. Rebhan, *Tensor meson transition form factors in holographic QCD and the muon $g-2$*, *JHEP* **07** (2025) 033 [2501.09699].

[70] G. Colangelo, M. Hoferichter, A. Nyffeler, M. Passera and P. Stoffer, *Remarks on higher-order hadronic corrections to the muon $g-2$*, *Phys. Lett. B* **735** (2014) 90 [1403.7512].

[71] T. Blum, N. Christ, M. Hayakawa, T. Izubuchi, L. Jin, C. Jung et al., *The hadronic light-by-light scattering contribution to the muon anomalous magnetic moment from lattice QCD*, *Phys. Rev. Lett.* **124** (2020) 132002 [1911.08123].

[72] E.-H. Chao, R.J. Hudspith, A. Gérardin, J.R. Green, H.B. Meyer and K. Ottnad, *Hadronic light-by-light contribution to $(g-2)_\mu$ from lattice QCD: a complete calculation*, *Eur. Phys. J. C* **81** (2021) 651 [2104.02632].

[73] E.-H. Chao, R.J. Hudspith, A. Gérardin, J.R. Green and H.B. Meyer, *The charm-quark contribution to light-by-light scattering in the muon $(g-2)$ from lattice QCD*, *Eur. Phys. J. C* **82** (2022) 664 [2204.08844].

[74] RBC, UKQCD collaboration, *Hadronic light-by-light contribution to the muon anomaly from lattice QCD with infinite volume QED at physical pion mass*, *Phys. Rev. D* **111** (2025) 014501 [2304.04423].

[75] Z. Fodor, A. Gérardin, L. Lellouch, K.K. Szabó, B.C. Toth and C. Zimmermann, *Hadronic light-by-light scattering contribution to the anomalous magnetic moment of the muon at the physical pion mass*, *Phys. Rev. D* **111** (2025) 114509 [2411.11719].

[76] T. Aoyama, M. Hayakawa, T. Kinoshita and M. Nio, *Complete Tenth-Order QED Contribution to the Muon $g-2$*, *Phys. Rev. Lett.* **109** (2012) 111808 [1205.5370].

[77] S. Volkov, *Calculating the five-loop QED contribution to the electron anomalous magnetic moment: Graphs without lepton loops*, *Phys. Rev. D* **100** (2019) 096004 [1909.08015].

[78] S. Volkov, *Calculation of the total 10th order QED contribution to the electron magnetic moment*, *Phys. Rev. D* **110** (2024) 036001 [2404.00649].

[79] T. Aoyama, M. Hayakawa, A. Hirayama and M. Nio, *Verification of the tenth-order QED contribution to the anomalous magnetic moment of the electron from diagrams without fermion loops*, *Phys. Rev. D* **111** (2025) L031902 [2412.06473].

[80] R.H. Parker, C. Yu, W. Zhong, B. Estey and H. Müller, *Measurement of the fine-structure constant as a test of the Standard Model*, *Science* **360** (2018) 191 [1812.04130].

[81] L. Morel, Z. Yao, P. Cladé and S. Guellati-Khélifa, *Determination of the fine-structure constant with an accuracy of 81 parts per trillion*, *Nature* **588** (2020) 61.

[82] X. Fan, T.G. Myers, B.A.D. Sukra and G. Gabrielse, *Measurement of the Electron Magnetic Moment*, *Phys. Rev. Lett.* **130** (2023) 071801 [2209.13084].

[83] A. Czarnecki, W.J. Marciano and A. Vainshtein, *Refinements in electroweak contributions to the muon anomalous magnetic moment*, *Phys. Rev. D* **67** (2003) 073006 [hep-ph/0212229].

[84] C. Gnendiger, D. Stöckinger and H. Stöckinger-Kim, *The electroweak contributions to $(g-2)_\mu$ after the Higgs boson mass measurement*, *Phys. Rev. D* **88** (2013) 053005 [1306.5546].

[85] M. Hoferichter, J. Lüdtke, L. Naterop, M. Procura and P. Stoffer, *Improved evaluation of the electroweak contribution to muon $g-2$*, *Phys. Rev. Lett.* **134** (2025) 201801 [2503.04883].

[86] R. Alemany, M. Davier and A. Hoecker, *Improved determination of the hadronic contribution to the muon (g-2) and to alpha (M(z)) using new data from hadronic tau decays*, *Eur. Phys. J. C* **2** (1998) 123 [hep-ph/9703220].

[87] V. Cirigliano, G. Ecker and H. Neufeld, *Isospin violation and the magnetic moment of the muon*, *Phys. Lett. B* **513** (2001) 361 [hep-ph/0104267].

[88] V. Cirigliano, G. Ecker and H. Neufeld, *Radiative tau decay and the magnetic moment of the muon*, *JHEP* **08** (2002) 002 [hep-ph/0207310].

[89] M. Davier, A. Hoecker, G. López Castro, B. Malaescu, X.H. Mo, G. Toledo et al., *The Discrepancy Between tau and e+e- Spectral Functions Revisited and the Consequences for the Muon Magnetic Anomaly*, *Eur. Phys. J. C* **66** (2010) 127 [0906.5443].

[90] J.A. Miranda and P. Roig, *New τ-based evaluation of the hadronic contribution to the vacuum polarization piece of the muon anomalous magnetic moment*, *Phys. Rev. D* **102** (2020) 114017 [2007.11019].

[91] M. Davier, A. Hoecker, A.-M. Lutz, B. Malaescu and Z. Zhang, *Tensions in $e^+e^- \to \pi^+\pi^-(\gamma)$ measurements: the new landscape of data-driven hadronic vacuum polarization predictions for the muon $g-2$*, *Eur. Phys. J. C* **84** (2024) 721 [2312.02053].

[92] G. López Castro, A. Miranda and P. Roig, *Isospin breaking corrections in 2π production in tau decays and e+e- annihilation: Consequences for the muon g-2 and conserved vector current tests*, *Phys. Rev. D* **111** (2025) 073004 [2411.07696].

[93] T.P. Leplumey and P. Stoffer, *Dispersive analysis of the pion vector form factor without zeros*, 2501.09643v1.

[94] G. Colangelo, M. Hoferichter and P. Stoffer, *Two-pion contribution to hadronic vacuum polarization*, *JHEP* **02** (2019) 006 [1810.00007].

[95] G. Colangelo, M. Hoferichter, B. Kubis and P. Stoffer, *Isospin-breaking effects in the two-pion contribution to hadronic vacuum polarization*, *JHEP* **10** (2022) 032 [2208.08993].

[96] P. Stoffer, G. Colangelo and M. Hoferichter, *Puzzles in the hadronic contributions to the muon anomalous magnetic moment*, *JINST* **18** (2023) C10021 [2308.04217].

[97] M. Davier, Z. Fodor, A. Gérardin, L. Lellouch, B. Malaescu, F.M. Stokes et al., *Hadronic vacuum polarization: Comparing lattice QCD and data-driven results in systematically improvable ways*, *Phys. Rev. D* **109** (2024) 076019 [2308.04221].

[98] Z. Zhang, M. Davier, A. Hoecker, G. Lopez Castro, B. Malaescu, X.H. Mo et al., *The discrepancy between tau and e+ e- spectral functions revisited and the consequences for the muon magnetic anomaly*, *PoS* **EPS-HEP2009** (2009) 373.

[99] M. Davier, A. Hoecker, B. Malaescu, C.Z. Yuan and Z. Zhang, *Reevaluation of the hadronic contribution to the muon magnetic anomaly using new e+ e- —> pi+ pi- cross section data from BABAR*, *Eur. Phys. J. C* **66** (2010) 1 [0908.4300].

[100] M. Davier, A. Hoecker, B. Malaescu and Z. Zhang, *Reevaluation of the Hadronic Contributions to the Muon $g-2$ and to alpha(MZ)*, *Eur. Phys. J. C* **71** (2011) 1515 [1010.4180].

[101] M. Davier, A. Hoecker, B. Malaescu and Z. Zhang, *Reevaluation of the hadronic vacuum polarisation contributions to the Standard Model predictions of the muon $g-2$ and $\alpha(m_Z^2)$ using newest hadronic cross-section data*, *Eur. Phys. J. C* **77** (2017) 827 [1706.09436].

[102] M. Davier, A. Hoecker, B. Malaescu and Z. Zhang, *A new evaluation of the hadronic vacuum polarisation contributions to the muon anomalous magnetic moment and to $\alpha(\mathbf{m_Z^2})$*, *Eur. Phys. J. C* **80** (2020) 241 [1908.00921].

[103] BABAR collaboration, *Precise measurement of the e+ e- —> pi+ pi- (gamma) cross section with the Initial State Radiation method at BABAR*, *Phys. Rev. Lett.* **103** (2009) 231801 [0908.3589].

[104] BABAR collaboration, *Precise measurement of the $e^+e^- \to \pi^+\pi^-(\gamma)$ cross section with the initial-state radiation method at BABAR*, *Phys. Rev. D* **86** (2012) 032013 [1205.2228].

[105] CMD-3 collaboration, *Measurement of the $e^+e^- \to \pi^+\pi^-$ cross section from threshold to 1.2 GeV with the CMD-3 detector*, *Phys. Rev. D* **109** (2024) 112002 [2302.08834].

[106] KLOE collaboration, *Measurement of $\sigma(e^+e^- \to \pi^+\pi^-\gamma(\gamma)$ and the dipion contribution to the muon anomaly with the KLOE detector*, *Phys. Lett. B* **670** (2009) 285 [0809.3950].

[107] KLOE collaboration, *Measurement of $\sigma(e^+e^- \to \pi^+\pi^-)$ from threshold to 0.85 GeV^2 using initial state radiation with the KLOE detector*, *Phys. Lett. B* **700** (2011) 102 [1006.5313].

[108] KLOE collaboration, *Precision measurement of $\sigma(e^+e^- \to \pi^+\pi^-\gamma)/\sigma(e^+e^- \to \mu^+\mu^-\gamma)$ and determination of the $\pi^+\pi^-$ contribution to the muon anomaly with the KLOE detector*, *Phys. Lett. B* **720** (2013) 336 [1212.4524].

[109] SND collaboration, *Measurement of the $e^+e^- \to \pi^+\pi^-$ process cross section with the SND detector at the VEPP-2000 collider in the energy region $0.525 < \sqrt{s} < 0.883$ GeV*, *JHEP* **01** (2021) 113 [2004.00263].

[110] CMD-2 collaboration, *Measurement of $e^+e^- \to \pi^+\pi^-$ cross-section with CMD-2 around ρ-meson*, *Phys. Lett. B* **527** (2002) 161 [hep-ex/0112031].

[111] CMD-2 collaboration, *Reanalysis of hadronic cross-section measurements at CMD-2*, *Phys. Lett. B* **578** (2004) 285 [hep-ex/0308008].

[112] CMD-2 collaboration, *Measurement of the pion form-factor in the range 1.04 GeV to 1.38 GeV with the CMD-2 detector*, *JETP Lett.* **82** (2005) 743 [hep-ex/0603021].

[113] CMD-2 collaboration, *High-statistics measurement of the pion form factor in the ρ-meson energy range with the CMD-2 detector*, *Phys. Lett. B* **648** (2007) 28 [hep-ex/0610021].

[114] CMD-2 collaboration, *Measurement of the $e^+e^- \to \pi^+\pi^-$ cross section with the CMD-2 detector in the 370 - 520 MeV c.m. energy range*, *JETP Lett.* **84** (2006) 413 [hep-ex/0610016].

[115] BESIII collaboration, *Measurement of the $e^+e^- \to \pi^+\pi^+$ cross section between 600 and 900 MeV using initial state radiation*, *Phys. Lett. B* **753** (2016) 629 [1507.08188].

[116] SND collaboration, *Study of the process $e^+e^- \to \pi^+\pi^-$ in the energy region $400 < \sqrt{s} < 1000$ MeV*, *J. Exp. Theor. Phys.* **101** (2005) 1053 [hep-ex/0506076].

[117] ALEPH collaboration, *Branching ratios and spectral functions of tau decays: Final ALEPH measurements and physics implications*, *Phys. Rept.* **421** (2005) 191 [hep-ex/0506072].

[118] CLEO collaboration, *Hadronic structure in the decay tau- —> pi- pi0 neutrino(tau)*, *Phys. Rev. D* **61** (2000) 112002 [hep-ex/9910046].

[119] OPAL collaboration, *Measurement of the strong coupling constant alpha(s) and the vector and axial vector spectral functions in hadronic tau decays*, *Eur. Phys. J. C* **7** (1999) 571 [hep-ex/9808019].

[120] BELLE collaboration, *High-Statistics Study of the tau- —> pi- pi0 nu(tau) Decay*, *Phys. Rev. D* **78** (2008) 072006 [0805.3773].

[121] E.J. Estrada, J.M. Márquez, D. Portillo-Sánchez and P. Roig, *Proton-box contribution to aμHLbL*, *Phys. Rev. D* **111** (2025) 093008 [2411.07115].

[122] E.J. Estrada and P. Roig, *Tensor Meson Pole contributions to the HLbL piece of a_μ within RχT*, *JHEP* **01** (2026) 070 [2504.00448].

[123] E.J. Estrada, A. Miranda and P. Roig, *Hadronic contributions to a_μ within Resonance Chiral Theory*, 2512.10161.

[124] M. Hoferichter and P. Stoffer, *Asymptotic behavior of meson transition form factors*, *JHEP* **05** (2020) 159 [2004.06127].

[125] G.P. Lepage, *A New Algorithm for Adaptive Multidimensional Integration*, *J. Comput. Phys.* **27** (1978) 192.

[126] G. Colangelo, M. Hoferichter, M. Procura and P. Stoffer, *Dispersive approach to hadronic light-by-light scattering*, *JHEP* **09** (2014) 091 [1402.7081].

[127] E. Estrada, E. Passemar, S. Paz, A. Rodríguez-Sánchez and P. Roig , in preparation.

[128] E. Estrada, E. Passemar, S. Paz, A. Rodríguez-Sánchez and P. Roig, *Beyond Form Factors: Precise Angular Tests in Hadronic τ Decays*, in *18th International Workshop on Tau Lepton Physics*, 1, 2026 [2601.03912].

[129] S.L. Glashow, *Partial Symmetries of Weak Interactions*, *Nucl. Phys.* **22** (1961) 579.

[130] S. Weinberg, *A Model of Leptons*, *Phys. Rev. Lett.* **19** (1967) 1264.

[131] A. Salam, *Weak and Electromagnetic Interactions*, *Conf. Proc. C* **680519** (1968) 367.

[132] P. Langacker, *The standard model and beyond* (2010).

[133] P.B. Pal, *An Introductory Course of Particle Physics*, CRC Press (7, 2014), 10.1201/b17199.

[134] M.E. Peskin and D.V. Schroeder, *An Introduction to quantum field theory*, Addison-Wesley, Reading, USA (1995), 10.1201/9780429503559.

[135] P.W. Higgs, *Broken symmetries, massless particles and gauge fields*, *Phys. Lett.* **12** (1964) 132.

[136] P.W. Higgs, *Broken Symmetries and the Masses of Gauge Bosons*, *Phys. Rev. Lett.* **13** (1964) 508.

[137] P.W. Higgs, *Spontaneous Symmetry Breakdown without Massless Bosons*, *Phys. Rev.* **145** (1966) 1156.

[138] CMS collaboration, *Measurement and QCD analysis of double-differential inclusive jet cross sections in pp collisions at $\sqrt{s} = 8$ TeV and cross section ratios to 2.76 and 7 TeV*, *JHEP* **03** (2017) 156 [1609.05331].

[139] D.J. Gross and F. Wilczek, *Ultraviolet Behavior of Nonabelian Gauge Theories*, *Phys. Rev. Lett.* **30** (1973) 1343.

[140] H.D. Politzer, *Reliable Perturbative Results for Strong Interactions?*, *Phys. Rev. Lett.* **30** (1973) 1346.

[141] M. Kobayashi and T. Maskawa, *CP Violation in the Renormalizable Theory of Weak Interaction*, *Prog. Theor. Phys.* **49** (1973) 652.

[142] A.D. Sakharov, *Violation of CP Invariance, C asymmetry, and baryon asymmetry of the universe*, *Pisma Zh. Eksp. Teor. Fiz.* **5** (1967) 32.

[143] R.P. Feynman, *Very high-energy collisions of hadrons*, *Phys. Rev. Lett.* **23** (1969) 1415.

[144] D.J. Gross, *The discovery of asymptotic freedom and the emergence of QCD*, *Proc. Nat. Acad. Sci.* **102** (2005) 9099.

[145] H. Fritzsch, M. Gell-Mann and H. Leutwyler, *Advantages of the Color Octet Gluon Picture*, *Phys. Lett. B* **47** (1973) 365.

[146] J.S. Schwinger, *On Quantum electrodynamics and the magnetic moment of the electron*, *Phys. Rev.* **73** (1948) 416.

[147] F. Mandl and G. Shaw, *QUANTUM FIELD THEORY* (1985).

[148] V. Bargmann, L. Michel and V.L. Telegdi, *Precession of the polarization of particles moving in a homogeneous electromagnetic field*, *Phys. Rev. Lett.* **2** (1959) 435.

[149] L. Michel, *Interaction between four half spin particles and the decay of the μ meson*, *Proc. Phys. Soc. A* **63** (1950) 514.

[150] R.M. Carey et al., *New measurement of the anomalous magnetic moment of the positive muon*, *Phys. Rev. Lett.* **82** (1999) 1632.

[151] MUON (G-2) collaboration, *Improved measurement of the positive muon anomalous magnetic moment*, *Phys. Rev. D* **62** (2000) 091101 [hep-ex/0009029].

[152] MUON G-2 collaboration, *Precise measurement of the positive muon anomalous magnetic moment*, *Phys. Rev. Lett.* **86** (2001) 2227 [hep-ex/0102017].

[153] MUON G-2 collaboration, *Measurement of the positive muon anomalous magnetic moment to 0.7 ppm*, *Phys. Rev. Lett.* **89** (2002) 101804 [hep-ex/0208001].

[154] MUON G-2 collaboration, *Measurement of the negative muon anomalous magnetic moment to 0.7 ppm*, *Phys. Rev. Lett.* **92** (2004) 161802 [hep-ex/0401008].

[155] G. Charpak, F.J.M. Farley and R.L. Garwin, *A New Measurement of the Anomalous Magnetic Moment of the Muon*, *Phys. Lett.* **1** (1962) 16.

[156] J. Bailey, W. Bartl, G. von Bochmann, R.C.A. Brown, F.J.M. Farley, M. Giesch et al., *Precise Measurement of the Anomalous Magnetic Moment of the Muon*, *Nuovo Cim. A* **9** (1972) 369.

[157] CERN-MAINZ-DARESBURY collaboration, *Final Report on the CERN Muon Storage Ring Including the Anomalous Magnetic Moment and the Electric Dipole Moment of the Muon, and a Direct Test of Relativistic Time Dilation*, *Nucl. Phys. B* **150** (1979) 1.

[158] J-PARC G-2 collaboration, *New g-2 experiment at J-PARC*, *Chin. Phys. C* **34** (2010) 745.

[159] M. Abe et al., *A New Approach for Measuring the Muon Anomalous Magnetic Moment and Electric Dipole Moment*, *PTEP* **2019** (2019) 053C02 [1901.03047].

[160] S. Aritome et al., *Acceleration of Positive Muons by a Radio-Frequency Cavity*, *Phys. Rev. Lett.* **134** (2025) 245001 [2410.11367].

[161] C. Zhang et al., *CANTON-μ Proposal: A Next-Generation Muon $g-2$ Measurement at Sub-0.1 ppm Precision*, 2512.11486.

[162] A. Petermann, *Magnetic moment of the mu meson*, *Phys. Rev.* **105** (1957) 1931.

[163] C.M. Sommerfield, *The magnetic moment of the electron*, *Ann. Phys. (N.Y.)* **5** (1958) 26.

[164] S. Laporta and E. Remiddi, *The Analytical value of the electron (g-2) at order alpha**3 in QED*, *Phys. Lett. B* **379** (1996) 283 [hep-ph/9602417].

[165] R. Karplus and N.M. Kroll, *Fourth-Order Corrections in Quantum Electrodynamics and the Magnetic Moment of the Electron*, *Phys. Rev.* **77** (1950) 536.

[166] T. Kinoshita and P. Cvitanovic, *Sixth-order radiative corrections to the electron magnetic moment*, *Phys. Rev. Lett.* **29** (1972) 1534.

[167] P. Cvitanović and T. Kinoshita, *Sixth Order Magnetic Moment of the electron*, *Phys. Rev. D* **10** (1974) 4007.

[168] M.J. Levine and J. Wright, *Anomalous magnetic moment of the electron*, *Phys. Rev. D* **8** (1973) 3171.

[169] R. Carroll and Y.P. Yao, *Alpha-to-the-3 contributions to the anomalous magnetic moment of an electron in the mass-operator formalism*, *Phys. Lett.* **48B** (1974) 125.

[170] R. Carroll, *Mass Operator Calculation of the electron G-Factor*, *Phys. Rev. D* **12** (1975) 2344.

[171] T. Kinoshita, *New value of the alpha**3 electron anomalous magnetic moment*, *Phys. Rev. Lett.* **75** (1995) 4728.

[172] S. Laporta, *High-precision calculation of the 4-loop contribution to the electron $g-2$ in QED*, *Phys. Lett. B* **772** (2017) 232 [1704.06996].

[173] T. Aoyama, M. Hayakawa, T. Kinoshita and M. Nio, *Tenth-Order Electron Anomalous Magnetic Moment — Contribution of Diagrams without Closed Lepton Loops*, *Phys. Rev. D* **91** (2015) 033006 [1412.8284].

[174] T. Kinoshita and W.B. Lindquist, *Eighth Order Anomalous Magnetic Moment of the electron*, *Phys. Rev. Lett.* **47** (1981) 1573.

[175] T. Kinoshita and W.B. Lindquist, *PARAMETRIC FORMULA FOR THE SIXTH ORDER VACUUM POLARIZATION CONTRIBUTION IN QUANTUM ELECTRODYNAMICS*, *Phys. Rev. D* **27** (1983) 853.

[176] T. Kinoshita and W.B. Lindquist, *EIGHTH ORDER MAGNETIC MOMENT OF THE ELECTRON. 1. SECOND ORDER VERTEX CONTAINING SECOND, FOURTH AND SIXTH ORDER VACUUM POLARIZATION SUBDIAGRAMS*, *Phys. Rev. D* **27** (1983) 867.

[177] T. Kinoshita and W.B. Lindquist, *EIGHTH ORDER MAGNETIC MOMENT OF THE ELECTRON. 2. FOURTH ORDER VERTICES CONTAINING SECOND AND FOURTH ORDER VACUUM POLARIZATION SUBDIAGRAMS*, *Phys. Rev. D* **27** (1983) 877.

[178] T. Kinoshita and W.B. Lindquist, *EIGHTH ORDER MAGNETIC MOMENT OF THE ELECTRON. 3. SIXTH ORDER VERTICES CONTAINING A SECOND ORDER VACUUM POLARIZATION SUBDIAGRAM*, *Phys. Rev. D* **27** (1983) 886.

[179] T. Kinoshita and W.B. Lindquist, *EIGHTH ORDER MAGNETIC MOMENT OF THE ELECTRON. 4. VERTEX DIAGRAMS CONTAINING PHOTON - PHOTON SCATTERING SUBDIAGRAMS*, *Phys. Rev. D* **39** (1989) 2407.

[180] T. Kinoshita and W.B. Lindquist, *EIGHTH ORDER MAGNETIC MOMENT OF THE ELECTRON. 5. DIAGRAMS CONTAINING NO VACUUM POLARIZATION LOOP*, *Phys. Rev. D* **42** (1990) 636.

[181] T. Kinoshita and M. Nio, *Revised alpha**4 term of lepton $g-2$ from the Feynman diagrams containing an internal light by light scattering subdiagram*, *Phys. Rev. Lett.* **90** (2003) 021803 [hep-ph/0210322].

[182] T. Kinoshita and M. Nio, *Improved alpha**4 term of the electron anomalous magnetic moment*, *Phys. Rev. D* **73** (2006) 013003 [hep-ph/0507249].

[183] T. Aoyama, M. Hayakawa, T. Kinoshita and M. Nio, *Revised value of the eighth-order electron $g-2$*, *Phys. Rev. Lett.* **99** (2007) 110406 [0706.3496].

[184] T. Aoyama, M. Hayakawa, T. Kinoshita and M. Nio, *Revised value of the eighth-order QED contribution to the anomalous magnetic moment of the electron*, *Phys. Rev. D* **77** (2008) 053012 [0712.2607].

[185] S. Volkov, *New method of computing the contributions of graphs without lepton loops to the electron anomalous magnetic moment in QED*, *Phys. Rev. D* **96** (2017) 096018 [1705.05800].

[186] S. Volkov, *Numerical calculation of high-order QED contributions to the electron anomalous magnetic moment*, *Phys. Rev. D* **98** (2018) 076018 [1807.05281].

[187] T. Aoyama, T. Kinoshita and M. Nio, *Theory of the Anomalous Magnetic Moment of the Electron*, *Atoms* **7** (2019) 28.

[188] T. Aoyama, T. Kinoshita and M. Nio, *Revised and Improved Value of the QED Tenth-Order Electron Anomalous Magnetic Moment*, *Phys. Rev. D* **97** (2018) 036001 [1712.06060].

[189] H. Suura and E.H. Wichmann, *Magnetic Moment of the Mu Meson*, *Phys. Rev.* **105** (1957) 1930.

[190] H.H. Elend, *On the anomalous magnetic moment of the muon*, *Phys. Lett.* **20** (1966) 682.

[191] G. Li, R. Mendel and M.A. Samuel, *Precise mass ratio dependence of fourth order lepton anomalous magnetic moments: The Effect of a new measurement of m(tau)*, *Phys. Rev. D* **47** (1993) 1723.

[192] M. Passera, *Precise mass-dependent QED contributions to leptonic g-2 at order alpha**2 and alpha**3*, *Phys. Rev. D* **75** (2007) 013002 [hep-ph/0606174].

[193] S. Laporta, *The Analytical contribution of the sixth order graphs with vacuum polarization insertions to the muon (g-2) in QED*, *Nuovo Cim.* **A106** (1993) 675.

[194] B.E. Lautrup, *On sixth-order radiative corrections to the muon g-factor*, *Nuovo Cim.* **A64** (1969) 322.

[195] B.E. Lautrup, A. Peterman and E. de Rafael, *On sixth-order radiative corrections to a(mu)-a(e)*, *Nuovo Cim.* **A1** (1971) 238.

[196] B.E. Lautrup and M.A. Samuel, *On the Light by Light Contribution to the Sixth Order Muon Anomaly*, *Phys. Lett.* **72B** (1977) 114.

[197] M.A. Samuel and C. Chlouber, *The Photon-Photon Scattering Contribution to the Anomalous Magnetic Moment of the Muon*, *Phys. Rev. Lett.* **36** (1976) 442.

[198] T. Kinoshita, *The light by light scattering contribution to the muon anomalous moment revisited*, *Phys. Rev. D* **40** (1989) 1323.

[199] T. Kinoshita, B. Nizic and Y. Okamoto, *Eighth order qed contribution to the anomalous magnetic moment of the muon*, *Phys. Rev. D* **41** (1990) 593.

[200] M.A. Samuel and G.-w. Li, *Improved analytic theory of the muon anomalous magnetic moment*, *Phys. Rev. D* **44** (1991) 3935.

[201] A. Czarnecki and M. Skrzypek, *The Muon anomalous magnetic moment in QED: Three loop electron and tau contributions*, *Phys. Lett. B* **449** (1999) 354 [hep-ph/9812394].

[202] S. Friot, D. Greynat and E. de Rafael, *Asymptotics of Feynman diagrams and the Mellin-Barnes representation*, *Phys. Lett. B* **628** (2005) 73 [hep-ph/0505038].

[203] B. Ananthanarayan, S. Friot and S. Ghosh, *Three-loop QED contributions to the $g-2$ of charged leptons with two internal fermion loops and a class of Kampé de Fériet series*, *Phys. Rev. D* **101** (2020) 116008 [2003.12030].

[204] B.E. Lautrup, *On the order of magnitude of 8th order corrections to the anomalous magnetic moment of the muon*, *Phys. Lett.* **38B** (1972) 408.

[205] S. Laporta, *The Analytical contribution of some eighth order graphs containing vacuum polarization insertions to the muon (g-2) in QED*, *Phys. Lett. B* **312** (1993) 495 [hep-ph/9306324].

[206] A. Kurz, T. Liu, P. Marquard, A. Smirnov, V. Smirnov and M. Steinhauser, *Electron contribution to the muon anomalous magnetic moment at four loops*, *Phys. Rev. D* **93** (2016) 053017 [1602.02785].

[207] A. Kurz, T. Liu, P. Marquard and M. Steinhauser, *Anomalous magnetic moment with heavy virtual leptons*, *Nucl. Phys. B* **879** (2014) 1 [1311.2471].

[208] A.L. Kataev, *Analytical eighth-order light-by-light QED contributions from leptons with heavier masses to the anomalous magnetic moment of electron*, *Phys. Rev. D* **86** (2012) 013010 [1205.6191].

[209] S. Laporta, *Analytical and numerical contributions of some tenth order graphs containing vacuum polarization insertions to the muon (g-2) in QED*, *Phys. Lett. B* **328** (1994) 522 [hep-ph/9404204].

[210] T. Kinoshita and M. Nio, *The Tenth-order QED contribution to the lepton g-2: Evaluation of dominant alpha**5 terms of muon g-2*, *Phys. Rev. D* **73** (2006) 053007 [hep-ph/0512330].

[211] A.L. Kataev, *Renormalization group and the five loop QED asymptotic contributions to the muon anomaly*, *Phys. Lett. B* **284** (1992) 401.

[212] A.L. Kataev and V.V. Starshenko, *The renormalization group inspired approaches and estimates of the tenth order corrections to the muon anomaly in QED*, *Phys. Rev. D* **52** (1995) 402 [hep-ph/9412305].

[213] A.L. Kataev, *Reconsidered estimates of the 10th order QED contributions to the muon anomaly*, *Phys. Rev. D* **74** (2006) 073011 [hep-ph/0608120].

[214] S.G. Karshenboim, *Tenth order contributions to the muon anomalous magnetic moment*, *Phys. Atom. Nucl.* **56** (1993) 857.

[215] P.A. Baikov, A. Maier and P. Marquard, *The QED vacuum polarization function at four loops and the anomalous magnetic moment at five loops*, *Nucl. Phys. B* **877** (2013) 647 [1307.6105].

[216] P.A. Baikov and D.J. Broadhurst, *Three loop QED vacuum polarization and the four loop muon anomalous magnetic moment*, hep-ph/9504398.

[217] PARTICLE DATA GROUP collaboration, *Review of particle physics*, *Phys. Rev. D* **110** (2024) 030001.

[218] ATLAS collaboration, *Observation of a new particle in the search for the Standard Model Higgs boson with the ATLAS detector at the LHC*, *Phys. Lett. B* **716** (2012) 1 [1207.7214].

[219] CMS collaboration, *Observation of a New Boson at a Mass of 125 GeV with the CMS Experiment at the LHC*, *Phys. Lett. B* **716** (2012) 30 [1207.7235].

[220] S. Peris, M. Perrottet and E. de Rafael, *Two loop electroweak corrections to the muon g-2: A New class of hadronic contributions*, *Phys. Lett. B* **355** (1995) 523 [hep-ph/9505405].

[221] M. Knecht, S. Peris, M. Perrottet and E. de Rafael, *Electroweak hadronic contributions to the muon (g-2)*, *JHEP* **11** (2002) 003 [hep-ph/0205102].

[222] C. Bouchiat and L. Michel, *La résonance dans la diffusion méson π— méson π et le moment magnétique anormal du méson μ*, *J. Phys. Radium* **22** (1961) 121.

[223] S.J. Brodsky and E. de Rafael, *SUGGESTED BOSON - LEPTON PAIR COUPLINGS AND THE ANOMALOUS MAGNETIC MOMENT OF THE MUON*, *Phys. Rev.* **168** (1968) 1620.

[224] B.E. Lautrup and E. de Rafael, *Calculation of the sixth-order contribution from the fourth-order vacuum polarization to the difference of the anomalous magnetic moments of muon and electron*, *Phys. Rev.* **174** (1968) 1835.

[225] M. Gourdin and E. de Rafael, *Hadronic contributions to the muon g-factor*, *Nucl. Phys. B* **10** (1969) 667.

[226] S.S. Schweber, H.A. Bethe and F. de Hoffmann, *Mesons and fields. Volume 1: Fields*, .

[227] A. Keshavarzi, D. Nomura and T. Teubner, *Muon $g-2$ and $\alpha(M_Z^2)$: a new data-based analysis*, *Phys. Rev. D* **97** (2018) 114025 [1802.02995].

[228] C. Arzt, M.B. Einhorn and J. Wudka, *Effective Lagrangian approach to precision measurements: The Anomalous magnetic moment of the muon*, *Phys. Rev. D* **49** (1994) 1370 [hep-ph/9304206].

[229] M.B. Einhorn and J. Wudka, *Model independent analysis of g(muon)-2*, *Phys. Rev. Lett.* **87** (2001) 071805 [hep-ph/0103034].

[230] D. Buttazzo and P. Paradisi, *Probing the muon $g-2$ anomaly with the Higgs boson at a muon collider*, *Phys. Rev. D* **104** (2021) 075021 [2012.02769].

[231] J. Aebischer, W. Dekens, E.E. Jenkins, A.V. Manohar, D. Sengupta and P. Stoffer, *Effective field theory interpretation of lepton magnetic and electric dipole moments*, *JHEP* **07** (2021) 107 [2102.08954].

[232] S. Fajfer, J.F. Kamenik and M. Tammaro, *Interplay of New Physics effects in $(g-2)_\ell$ and $h \to \ell^+\ell^-$ — lessons from SMEFT*, *JHEP* **06** (2021) 099 [2103.10859].

[233] V. Cirigliano, W. Dekens, J. de Vries, K. Fuyuto, E. Mereghetti and R. Ruiz, *Leptonic anomalous magnetic moments in ν SMEFT*, *JHEP* **08** (2021) 103 [2105.11462].

[234] L. Allwicher, L. Di Luzio, M. Fedele, F. Mescia and M. Nardecchia, *What is the scale of new physics behind the muon g-2?*, *Phys. Rev. D* **104** (2021) 055035 [2105.13981].

[235] F. Fortuna, J.M. Márquez and P. Roig, *HEFT approach to investigate the muon g-2 anomaly at a muon collider*, *Phys. Rev. D* **111** (2025) 075012 [2408.16954].

[236] J. Lüdtke, M. Procura and P. Stoffer, *Dispersion relations for hadronic light-by-light scattering in triangle kinematics*, *JHEP* **04** (2023) 125 [2302.12264].

[237] W.A. Bardeen and W.K. Tung, *Invariant amplitudes for photon processes*, *Phys. Rev.* **173** (1968) 1423.

[238] R. Tarrach, *Invariant Amplitudes for Virtual Compton Scattering Off Polarized Nucleons Free from Kinematical Singularities, Zeros and Constraints*, *Nuovo Cim. A* **28** (1975) 409.

[239] J.L. Rosner, *Higher-order contributions to the divergent part of Z(3) in a model quantum electrodynamics*, *Annals Phys.* **44** (1967) 11.

[240] H. Georgi, *Effective field theory*, *Ann. Rev. Nucl. Part. Sci.* **43** (1993) 209.

[241] A.V. Manohar, *Effective field theories*, *Lect. Notes Phys.* **479** (1997) 311 [hep-ph/9606222].

[242] A. Pich, *Effective field theory: Course*, in *Les Houches Summer School in Theoretical Physics, Session 68: Probing the Standard Model of Particle Interactions*, pp. 949–1049, 6, 1998 [hep-ph/9806303].

[243] T. Appelquist and J. Carazzone, *Infrared Singularities and Massive Fields*, *Phys. Rev. D* **11** (1975) 2856.

[244] S. Weinberg, *Effective Gauge Theories*, *Phys. Lett. B* **91** (1980) 51.

[245] S. Weinberg, *Phenomenological Lagrangians*, *Physica A* **96** (1979) 327.

[246] J. Gasser and H. Leutwyler, *Chiral Perturbation Theory to One Loop*, *Annals Phys.* **158** (1984) 142.

[247] J. Gasser and H. Leutwyler, *Chiral Perturbation Theory: Expansions in the Mass of the Strange Quark*, *Nucl. Phys. B* **250** (1985) 465.

[248] S.L. Adler, *Axial vector vertex in spinor electrodynamics*, *Phys. Rev.* **177** (1969) 2426.

[249] J.S. Bell and R. Jackiw, *A PCAC puzzle: $\pi^0 \to \gamma\gamma$ in the σ model*, *Nuovo Cim. A* **60** (1969) 47.

[250] Y. Nambu, *Quasiparticles and Gauge Invariance in the Theory of Superconductivity*, *Phys. Rev.* **117** (1960) 648.

[251] J. Goldstone, *Field Theories with Superconductor Solutions*, *Nuovo Cim.* **19** (1961) 154.

[252] J. Goldstone, A. Salam and S. Weinberg, *Broken Symmetries*, *Phys. Rev.* **127** (1962) 965.

[253] G. Ecker, *Chiral perturbation theory*, *Prog. Part. Nucl. Phys.* **35** (1995) 1 [hep-ph/9501357].

[254] A. Pich, *Chiral perturbation theory*, *Rept. Prog. Phys.* **58** (1995) 563 [hep-ph/9502366].

[255] S. Scherer, *Introduction to chiral perturbation theory*, *Adv. Nucl. Phys.* **27** (2003) 277 [hep-ph/0210398].

[256] S. Scherer and M.R. Schindler, *A Primer for Chiral Perturbation Theory*, vol. 830 (2012), 10.1007/978-3-642-19254-8.

[257] G. 't Hooft, *Symmetry Breaking Through Bell-Jackiw Anomalies*, *Phys. Rev. Lett.* **37** (1976) 8.

[258] G. 't Hooft, *Computation of the Quantum Effects Due to a Four-Dimensional Pseudoparticle*, *Phys. Rev. D* **14** (1976) 3432.

[259] R.D. Peccei and H.R. Quinn, *CP Conservation in the Presence of Instantons*, *Phys. Rev. Lett.* **38** (1977) 1440.

[260] R.D. Peccei and H.R. Quinn, *Constraints Imposed by CP Conservation in the Presence of Instantons*, *Phys. Rev. D* **16** (1977) 1791.

[261] F. Wilczek, *Problem of Strong P and T Invariance in the Presence of Instantons*, *Phys. Rev. Lett.* **40** (1978) 279.

[262] S. Weinberg, *A New Light Boson?*, *Phys. Rev. Lett.* **40** (1978) 223.

[263] S.R. Coleman, J. Wess and B. Zumino, *Structure of phenomenological Lagrangians. 1.*, *Phys. Rev.* **177** (1969) 2239.

[264] C.G. Callan, Jr., S.R. Coleman, J. Wess and B. Zumino, *Structure of phenomenological Lagrangians. 2.*, *Phys. Rev.* **177** (1969) 2247.

[265] J. Bijnens, G. Colangelo and G. Ecker, *The Mesonic chiral Lagrangian of order p**6*, *JHEP* **02** (1999) 020 [hep-ph/9902437].

[266] G. 't Hooft, *A Planar Diagram Theory for Strong Interactions*, *Nucl. Phys. B* **72** (1974) 461.

[267] G. 't Hooft, *A Two-Dimensional Model for Mesons*, *Nucl. Phys. B* **75** (1974) 461.

[268] E. Witten, *Baryons in the 1/n Expansion*, *Nucl. Phys. B* **160** (1979) 57.

[269] R. Kaiser and H. Leutwyler, *Large N(c) in chiral perturbation theory*, *Eur. Phys. J. C* **17** (2000) 623 [hep-ph/0007101].

[270] V. Bernard, N. Kaiser and U.G. Meissner, *Chiral perturbation theory in the presence of resonances: Application to pi pi and pi K scattering*, *Nucl. Phys. B* **364** (1991) 283.

[271] J.J. Sanz-Cillero, *Pion and kaon decay constants: Lattice versus resonance chiral theory*, *Phys. Rev. D* **70** (2004) 094033 [hep-ph/0408080].

[272] Z.-H. Guo and J.J. Sanz-Cillero, *Resonance effects in pion and kaon decay constants*, *Phys. Rev. D* **89** (2014) 094024 [1403.0855].

[273] T. Feldmann, P. Kroll and B. Stech, *Mixing and decay constants of pseudoscalar mesons*, *Phys. Rev. D* **58** (1998) 114006 [hep-ph/9802409].

[274] G. Ecker, J. Gasser, A. Pich and E. de Rafael, *The Role of Resonances in Chiral Perturbation Theory*, *Nucl. Phys. B* **321** (1989) 311.

[275] G. Ecker, J. Gasser, H. Leutwyler, A. Pich and E. de Rafael, *Chiral Lagrangians for Massive Spin 1 Fields*, *Phys. Lett. B* **223** (1989) 425.

[276] J. Wess and B. Zumino, *Consequences of anomalous Ward identities*, *Phys. Lett.* **37B** (1971) 95.

[277] E. Witten, *Global Aspects of Current Algebra*, *Nucl. Phys. B* **223** (1983) 422.

[278] J. Bijnens, L. Girlanda and P. Talavera, *The Anomalous chiral Lagrangian of order p**6*, *Eur. Phys. J. C* **23** (2002) 539 [hep-ph/0110400].

[279] V. Cirigliano, G. Ecker, M. Eidemüller, R. Kaiser, A. Pich and J. Portolés, *Towards a consistent estimate of the chiral low-energy constants*, *Nucl. Phys. B* **753** (2006) 139 [hep-ph/0603205].

[280] K. Kampf and J. Novotný, *Resonance saturation in the odd-intrinsic parity sector of low-energy QCD*, *Phys. Rev. D* **84** (2011) 014036 [1104.3137].

[281] G. Ecker and C. Zauner, *Tensor meson exchange at low energies*, *Eur. Phys. J. C* **52** (2007) 315 [0705.0624].

[282] C. Chen, N.-Q. Cheng, L.-W. Yan, C.-G. Duan and Z.-H. Guo, *Revisiting the tensor-meson nonet in resonance chiral theory*, *Phys. Rev. D* **108** (2023) 014002 [2302.11316].

[283] E. de Rafael, *Hadronic contributions to the muon $g-2$ and low-energy QCD*, *Phys. Lett. B* **322** (1994) 239 [hep-ph/9311316].

[284] M. Hayakawa, T. Kinoshita and A.I. Sanda, *Hadronic light by light scattering effect on muon g-2*, *Phys. Rev. Lett.* **75** (1995) 790 [hep-ph/9503463].

[285] J. Bijnens, E. Pallante and J. Prades, *Hadronic light by light contributions to the muon $g-2$ in the large N(c) limit*, *Phys. Rev. Lett.* **75** (1995) 1447 [hep-ph/9505251].

[286] J. Bijnens, E. Pallante and J. Prades, *Analysis of the hadronic light by light contributions to the muon g-2*, *Nucl. Phys. B* **474** (1996) 379.

[287] M. Hayakawa, T. Kinoshita and A.I. Sanda, *Hadronic light by light scattering contribution to muon g-2*, *Phys. Rev. D* **54** (1996) 3137 [hep-ph/9601310].

[288] M. Hayakawa and T. Kinoshita, *Pseudoscalar pole terms in the hadronic light by light scattering contribution to muon g - 2*, *Phys. Rev. D* **57** (1998) 465 [hep-ph/9708227].

[289] J. Bijnens, E. Pallante and J. Prades, *Comment on the pion pole part of the light by light contribution to the muon g-2*, *Nucl. Phys. B* **626** (2002) 410 [hep-ph/0112255].

[290] M. Knecht and A. Nyffeler, *Hadronic light by light corrections to the muon g-2: The Pion pole contribution*, *Phys. Rev. D* **65** (2002) 073034 [hep-ph/0111058].

[291] F. Jegerlehner and A. Nyffeler, *The Muon g-2*, *Phys. Rept.* **477** (2009) 1 [0902.3360].

[292] M. Hoferichter, B.-L. Hoid, B. Kubis, S. Leupold and S.P. Schneider, *Pion-pole contribution to hadronic light-by-light scattering in the anomalous magnetic moment of the muon*, *Phys. Rev. Lett.* **121** (2018) 112002 [1805.01471].

[293] K. Raya, A. Bashir and P. Roig, *Contribution of neutral pseudoscalar mesons to a_μ^{HLbL} within a Schwinger-Dyson equations approach to QCD*, *Phys. Rev. D* **101** (2020) 074021 [1910.05960].

[294] A. Gérardin, W.E.A. Verplanke, G. Wang, Z. Fodor, J.N. Guenther, L. Lellouch et al., *Lattice calculation of the $\pi 0$, η and η' transition form factors and the hadronic light-by-light contribution to the muon g-2*, *Phys. Rev. D* **111** (2025) 054511 [2305.04570].

[295] A. Gérardin, H.B. Meyer and A. Nyffeler, *Lattice calculation of the pion transition form factor with $N_f = 2 + 1$ Wilson quarks*, *Phys. Rev. D* **100** (2019) 034520 [1903.09471].

[296] ETM collaboration, *$\eta \to \gamma^*\gamma^*$ transition form factor and the hadronic light-by-light η-pole contribution to the muon g-2 from lattice QCD*, *Phys. Rev. D* **108** (2023) 054509 [2212.06704].

[297] ETM collaboration, *Pion transition form factor from twisted-mass lattice QCD and the hadronic light-by-light $\pi 0$-pole contribution to the muon g-2*, *Phys. Rev. D* **108** (2023) 094514 [2308.12458].

[298] T. Kadavy, K. Kampf and J. Novotny, *On the three-point order parameters of chiral symmetry breaking*, *JHEP* **03** (2023) 118 [2206.02579].

[299] J. Leutgeb, J. Mager and A. Rebhan, *Pseudoscalar transition form factors and the hadronic light-by-light contribution to the anomalous magnetic moment of the muon from holographic QCD*, *Phys. Rev. D* **100** (2019) 094038 [1906.11795].

[300] H. Czyz, S. Ivashyn, A. Korchin and O. Shekhovtsova, *Two-photon form factors of the π^0, η and η' mesons in the chiral theory with resonances*, *Phys. Rev. D* **85** (2012) 094010 [1202.1171].

[301] P. Roig, A. Guevara and G. López Castro, *$VV'P$ form factors in resonance chiral theory and the $\pi-\eta-\eta'$ light-by-light contribution to the muon $g-2$*, *Phys. Rev. D* **89** (2014) 073016 [1401.4099].

[302] A. Guevara, P. Roig and J.J. Sanz-Cillero, *Pseudoscalar pole light-by-light contributions to the muon $(g-2)$ in Resonance Chiral Theory*, *JHEP* **06** (2018) 160 [1803.08099].

[303] K. Melnikov and A. Vainshtein, *Hadronic light-by-light scattering contribution to the muon anomalous magnetic moment revisited*, *Phys. Rev. D* **70** (2004) 113006 [hep-ph/0312226].

[304] P.D. Ruiz-Femenía, A. Pich and J. Portolés, *Odd intrinsic parity processes within the resonance effective theory of QCD*, *JHEP* **07** (2003) 003 [hep-ph/0306157].

[305] V. Cirigliano, G. Ecker, H. Neufeld and A. Pich, *Meson resonances, large N(c) and chiral symmetry*, *JHEP* **06** (2003) 012 [hep-ph/0305311].

[306] Z.-H. Guo and J.J. Sanz-Cillero, *pi pi-scattering lengths at O(p**6) revisited*, *Phys. Rev. D* **79** (2009) 096006 [0903.0782].

[307] V. Mateu and J. Portolés, *Form-factors in radiative pion decay*, *Eur. Phys. J. C* **52** (2007) 325 [0706.1039].

[308] T. Kadavý, K. Kampf and J. Novotný, *OPE of Green functions of chiral currents*, *JHEP* **10** (2020) 142 [2006.13006].

[309] V.A. Nesterenko and A.V. Radyushkin, *Local Quark - Hadron Duality and Nucleon Form-factors in QCD*, *Phys. Lett. B* **128** (1983) 439.

[310] V.A. Novikov, M.A. Shifman, A.I. Vainshtein, M.B. Voloshin and V.I. Zakharov, *Use and Misuse of QCD Sum Rules, Factorization and Related Topics*, *Nucl. Phys. B* **237** (1984) 525.

[311] S.J. Brodsky and G.R. Farrar, *Scaling Laws at Large Transverse Momentum*, *Phys. Rev. Lett.* **31** (1973) 1153.

[312] G.P. Lepage and S.J. Brodsky, *Exclusive Processes in Perturbative Quantum Chromodynamics*, *Phys. Rev. D* **22** (1980) 2157.

[313] T. Feldmann, P. Kroll and B. Stech, *Mixing and decay constants of pseudoscalar mesons: The Sequel*, *Phys. Lett. B* **449** (1999) 339 [hep-ph/9812269].

[314] F. Jegerlehner, *The anomalous magnetic moment of the muon*, *Springer Tracts Mod. Phys.* **226** (2008) 1.

[315] F. Jegerlehner, *The Anomalous Magnetic Moment of the Muon*, *Springer Tracts Mod. Phys.* **274** (2017) 1.

[316] P. Roig and J.J. Sanz Cillero, *Consistent high-energy constraints in the anomalous QCD sector*, *Phys. Lett. B* **733** (2014) 158 [1312.6206].

[317] H. Leutwyler, *On the 1/N expansion in chiral perturbation theory*, *Nucl. Phys. Proc. Suppl.* **64** (1998) 223 [hep-ph/9709408].

[318] Z.-H. Guo and P. Roig, *One meson radiative tau decays*, *Phys. Rev. D* **82** (2010) 113016 [1009.2542].

[319] M.A. Arroyo-Ureña, G. Hernández-Tomé, G. López Castro, P. Roig and I. Rosell, *Radiative corrections to $\tau \to \pi(K)\nu\tau[\gamma]$: A reliable new physics test*, *Phys. Rev. D* **104** (2021) L091502 [2107.04603].

[320] M.A. Arroyo-Ureña, G. Hernández-Tomé, G. López Castro, P. Roig and I. Rosell, *One-loop determination of $\tau \to \pi(K)\nu_\tau\,[\gamma]$ branching ratios and new physics tests*, *JHEP* **02** (2022) 173 [2112.01859].

[321] Z.-H. Guo, *Study of tau- —> V P- nu(tau) in the framework of resonance chiral theory*, *Phys. Rev. D* **78** (2008) 033004 [0806.4322].

[322] D.G. Dumm, P. Roig, A. Pich and J. Portolés, *Hadron structure in tau —> KK pi nu (tau) decays*, *Phys. Rev. D* **81** (2010) 034031 [0911.2640].

[323] D. Gómez Dumm and P. Roig, *Resonance Chiral Lagrangian analysis of $\tau^- \to \eta^{(\prime)}\pi^-\pi^0\nu_\tau$ decays*, *Phys. Rev. D* **86** (2012) 076009 [1208.1212].

[324] D.G. Dumm, P. Roig, A. Pich and J. Portolés, *tau —> pi pi pi nu(tau) decays and the a(1)(1260) off-shell width revisited*, *Phys. Lett. B* **685** (2010) 158 [0911.4436].

[325] O. Shekhovtsova, T. Przedzinski, P. Roig and Z. Was, *Resonance chiral Lagrangian currents and τ decay Monte Carlo*, *Phys. Rev. D* **86** (2012) 113008 [1203.3955].

[326] I.M. Nugent, T. Przedziński, P. Roig, O. Shekhovtsova and Z. Wąs, *Resonance chiral Lagrangian currents and experimental data for $\tau^- \to \pi^-\pi^-\pi^+\nu_\tau$*, *Phys. Rev. D* **88** (2013) 093012 [1310.1053].

[327] K. Kampf, J. Novotný and P. Sánchez-Puertas, *Radiative corrections to double-Dalitz decays revisited*, *Phys. Rev. D* **97** (2018) 056010 [1801.06067].

[328] PARTICLE DATA GROUP collaboration, *Review of Particle Physics*, *PTEP* **2022** (2022) 083C01.

[329] BABAR collaboration, *Measurement of the gamma gamma* —> pi0 transition form factor*, *Phys. Rev. D* **80** (2009) 052002 [0905.4778].

[330] BABAR collaboration, *Measurement of the $\gamma\gamma^* \to \eta$ and $\gamma\gamma^* \to \eta'$ transition form factors*, *Phys. Rev. D* **84** (2011) 052001 [1101.1142].

[331] BELLE collaboration, *Measurement of $\gamma\gamma^* \to \pi^0$ transition form factor at Belle*, *Phys. Rev. D* **86** (2012) 092007 [1205.3249].

[332] CELLO collaboration, *A Measurement of the pi0, eta and eta-prime electromagnetic form-factors*, *Z. Phys. C* **49** (1991) 401.

[333] CLEO collaboration, *Measurements of the meson - photon transition form-factors of light pseudoscalar mesons at large momentum transfer*, *Phys. Rev. D* **57** (1998) 33 [hep-ex/9707031].

[334] L3 collaboration, *Measurement of eta-prime (958) formation in two photon collisions at LEP-1*, *Phys. Lett. B* **418** (1998) 399.

[335] BABAR collaboration, *Measurement of the $\gamma^*\gamma^* \to \eta'$ transition form factor*, *Phys. Rev. D* **98** (2018) 112002 [1808.08038].

[336] J. Schechter, A. Subbaraman and H. Weigel, *Effective hadron dynamics: From meson masses to the proton spin puzzle*, *Phys. Rev. D* **48** (1993) 339 [hep-ph/9211239].

[337] A. Bramon, R. Escribano and M.D. Scadron, *The eta - eta-prime mixing angle revisited*, *Eur. Phys. J. C* **7** (1999) 271 [hep-ph/9711229].

[338] T. Feldmann, *Quark structure of pseudoscalar mesons*, *Int. J. Mod. Phys. A* **15** (2000) 159 [hep-ph/9907491].

[339] R. Escribano and J.-M. Frere, *Study of the eta - eta-prime system in the two mixing angle scheme*, *JHEP* **06** (2005) 029 [hep-ph/0501072].

[340] S.V. Mikhailov and N.G. Stefanis, *Transition form factors of the pion in light-cone QCD sum rules with next-to-next-to-leading order contributions*, *Nucl. Phys. B* **821** (2009) 291 [0905.4004].

[341] H.L.L. Roberts, C.D. Roberts, A. Bashir, L.X. Gutierrez-Guerrero and P.C. Tandy, *Abelian anomaly and neutral pion production*, *Phys. Rev. C* **82** (2010) 065202 [1009.0067].

[342] S.S. Agaev, V.M. Braun, N. Offen and F.A. Porkert, *Light Cone Sum Rules for the pi0-gamma*-gamma Form Factor Revisited*, *Phys. Rev. D* **83** (2011) 054020 [1012.4671].

[343] S.J. Brodsky, F.-G. Cao and G.F. de Teramond, *Evolved QCD predictions for the meson-photon transition form factors*, *Phys. Rev. D* **84** (2011) 033001 [1104.3364].

[344] A.P. Bakulev, S.V. Mikhailov, A.V. Pimikov and N.G. Stefanis, *Pion-photon transition: The New QCD frontier*, *Phys. Rev. D* **84** (2011) 034014 [1105.2753].

[345] S.J. Brodsky, F.-G. Cao and G.F. de Teramond, *Meson Transition Form Factors in Light-Front Holographic QCD*, *Phys. Rev. D* **84** (2011) 075012 [1105.3999].

[346] N.G. Stefanis, A.P. Bakulev, S.V. Mikhailov and A.V. Pimikov, *Can We Understand an Auxetic Pion-Photon Transition Form Factor within QCD?*, *Phys. Rev. D* **87** (2013) 094025 [1202.1781].

[347] A.P. Bakulev, S.V. Mikhailov, A.V. Pimikov and N.G. Stefanis, *Comparing antithetic trends of data for the pion-photon transition form factor*, *Phys. Rev. D* **86** (2012) 031501 [1205.3770].

[348] S.S. Agaev, V.M. Braun, N. Offen and F.A. Porkert, *BELLE Data on the $\pi^0\gamma*\gamma$ Form Factor: A Game Changer?*, *Phys. Rev. D* **86** (2012) 077504 [1206.3968].

[349] S.S. Agaev, V.M. Braun, N. Offen, F.A. Porkert and A. Schäfer, *Transition form factors $\gamma^*\gamma \to \eta$ and $\gamma^*\gamma \to \eta'$ in QCD*, *Phys. Rev. D* **90** (2014) 074019 [1409.4311].

[350] K. Raya, L. Chang, A. Bashir, J.J. Cobos-Martínez, L.X. Gutiérrez-Guerrero, C.D. Roberts et al., *Structure of the neutral pion and its electromagnetic transition form factor*, *Phys. Rev. D* **93** (2016) 074017 [1510.02799].

[351] G. Eichmann, C.S. Fischer, E. Weil and R. Williams, *On the large-Q^2 behavior of the pion transition form factor*, *Phys. Lett. B* **774** (2017) 425 [1704.05774].

[352] N.G. Stefanis, *Pion-photon transition form factor in light cone sum rules and tests of asymptotics*, *Phys. Rev. D* **102** (2020) 034022 [2006.10576].

[353] S.J. Brodsky and G.P. Lepage, *Large Angle Two Photon Exclusive Channels in Quantum Chromodynamics*, *Phys. Rev. D* **24** (1981) 1808.

[354] Y.-H. Chen, Z.-H. Guo and H.-Q. Zheng, *Study of \eta-\eta' mixing from radiative decay processes*, *Phys. Rev. D* **85** (2012) 054018 [1201.2135].

[355] L.Y. Dai, J. Portolés and O. Shekhovtsova, *Three pseudoscalar meson production in e^+e^- annihilation*, *Phys. Rev. D* **88** (2013) 056001 [1305.5751].

[356] Y.-H. Chen, Z.-H. Guo and H.-Q. Zheng, *Radiative transition processes of light vector resonances in a chiral framework*, *Phys. Rev. D* **90** (2014) 034013 [1311.3366].

[357] Y.-H. Chen, Z.-H. Guo and B.-S. Zou, *Unified study of $J/\psi \to PV$, $P\gamma^{(*)}$ and light hadron radiative processes*, *Phys. Rev. D* **91** (2015) 014010 [1411.1159].

[358] PRIMEX collaboration, *A New Measurement of the π^0 Radiative Decay Width*, *Phys. Rev. Lett.* **106** (2011) 162303 [1009.1681].

[359] PRIMEX-II collaboration, *Precision measurement of the neutral pion lifetime*, *Science* **368** (2020) 506.

[360] KLOE-2 collaboration, *Measurement of η meson production in $\gamma\gamma$ interactions and $\Gamma(\eta \to \gamma\gamma)$ with the KLOE detector*, *JHEP* **01** (2013) 119 [1211.1845].

[361] F. Stollenwerk, C. Hanhart, A. Kupść, U.-G. Meißner and A. Wirzba, *Model-independent approach to $\eta \to \pi^+\pi^-\gamma$ and $\eta' \to \pi^+\pi^-\gamma$*, *Phys. Lett. B* **707** (2012) 184 [1108.2419].

[362] J. Leutgeb and A. Rebhan, *Hadronic light-by-light contribution to the muon $g-2$ from holographic QCD with massive pions*, *Phys. Rev. D* **104** (2021) 094017 [2108.12345].

[363] S. Holz, M. Hoferichter, B.-L. Hoid and B. Kubis, *Precision Evaluation of the η- and η'-Pole Contributions to Hadronic Light-by-Light Scattering in the Anomalous Magnetic Moment of the Muon*, *Phys. Rev. Lett.* **134** (2025) 171902 [2411.08098].

[364] J.S.R. Chisholm, *Rational approximants defined from double power series*, *Math. Comp.* **27** (1973) 841.

[365] J.S.R. Chisholm and J. McEwan, *Rational approximants defined from double power series*, *Proc. R. Soc. Lond. A* **336** (1974) 421.

[366] R. Hughes Jones, *General rational approximants in N-variables*, *Journal of Approximation Theory* **16** (1976) 201.

[367] P. Masjuan and P. Sánchez-Puertas, *Phenomenology of bivariate approximants: the pi0 to e+e- case and its impact on the electron and muon g-2*, 1504.07001.

[368] P. Masjuan and P. Sánchez-Puertas, *η and η' decays into lepton pairs*, *JHEP* **08** (2016) 108 [1512.09292].

[369] R. Escribano, S. Gonzàlez-Solís, P. Masjuan and P. Sánchez-Puertas, *η' transition form factor from space- and timelike experimental data*, *Phys. Rev. D* **94** (2016) 054033 [1512.07520].

[370] A. Nyffeler, *Precision of a data-driven estimate of hadronic light-by-light scattering in the muon $g-2$: Pseudoscalar-pole contribution*, *Phys. Rev. D* **94** (2016) 053006 [1602.03398].

[371] X.-K. Guo, Z.-H. Guo, J.A. Oller and J.J. Sanz-Cillero, *Scrutinizing the η-η' mixing, masses and pseudoscalar decay constants in the framework of U(3) chiral effective field theory*, *JHEP* **06** (2015) 175 [1503.02248].

[372] F. Guerrero and A. Pich, *Effective field theory description of the pion form-factor*, *Phys. Lett. B* **412** (1997) 382 [hep-ph/9707347].

[373] G.P. Lepage and S.J. Brodsky, *Exclusive Processes in Quantum Chromodynamics: Evolution Equations for Hadronic Wave Functions and the Form-Factors of Mesons*, *Phys. Lett. B* **87** (1979) 359.

[374] V. Braun, G. Korchemsky and D. Müller, *The Uses of conformal symmetry in QCD*, *Prog. Part. Nucl. Phys.* **51** (2003) 311 [hep-ph/0306057].

[375] G.P. Lepage, *Adaptive multidimensional integration: VEGAS enhanced*, *J. Comput. Phys.* **439** (2021) 110386 [2009.05112].

[376] T. Lin, M. Bruno, X. Feng, L.-C. Jin, C. Lehner, C. Liu et al., *Lattice QCD calculation of the π^0-pole contribution to the hadronic light-by-light scattering in the anomalous magnetic moment of the muon*, *Rep. Prog. Phys.* **88** (2025) 080501 [2411.06349].

[377] J. Leutgeb, J. Mager and A. Rebhan, *Superconnections in AdS/QCD and the hadronic light-by-light contribution to the muon $g-2$*, *Phys. Rev. D* **111** (2025) 114001 [2411.10432].

[378] J.H. Kuhn, A.I. Onishchenko, A.A. Pivovarov and O.L. Veretin, *Heavy mass expansion, light by light scattering and the anomalous magnetic moment of the muon*, *Phys. Rev. D* **68** (2003) 033018 [hep-ph/0301151].

[379] Z. Ye, J. Arrington, R.J. Hill and G. Lee, *Proton and Neutron Electromagnetic Form Factors and Uncertainties*, *Phys. Lett. B* **777** (2018) 8 [1707.09063].

[380] C. Alexandrou, S. Bacchio, M. Constantinou, J. Finkenrath, K. Hadjiyiannakou, K. Jansen et al., *Proton and neutron electromagnetic form factors from lattice QCD*, *Phys. Rev. D* **100** (2019) 014509 [1812.10311].

[381] R.J. Hill and G. Paz, *Model independent extraction of the proton charge radius from electron scattering*, *Phys. Rev. D* **82** (2010) 113005 [1008.4619].

[382] W.M. Alberico, S.M. Bilenky, C. Giunti and K.M. Graczyk, *Electromagnetic form factors of the nucleon: New Fit and analysis of uncertainties*, *Phys. Rev. C* **79** (2009) 065204 [0812.3539].

[383] J. Arrington, W. Melnitchouk and J.A. Tjon, *Global analysis of proton elastic form factor data with two-photon exchange corrections*, *Phys. Rev. C* **76** (2007) 035205 [0707.1861].

[384] JPAC collaboration, *Exclusive tensor meson photoproduction*, *Phys. Rev. D* **102** (2020) 014003 [2005.01617].

[385] SND collaboration, *Search for direct production of the $f_1(1285)$ resonance in e^+e^- collisions*, *Phys. Lett. B* **800** (2020) 135074 [1906.03838].

[386] I. Danilkin and M. Vanderhaeghen, *Light-by-light scattering sum rules in light of new data*, *Phys. Rev. D* **95** (2017) 014019 [1611.04646].

[387] G.A. Schuler, F.A. Berends and R. van Gulik, *Meson photon transition form-factors and resonance cross-sections in e+ e- collisions*, *Nucl. Phys. B* **523** (1998) 423 [hep-ph/9710462].

[388] P. Colangelo, F. Giannuzzi and S. Nicotri, *Hadronic light-by-light scattering contributions to $(g-2)_\mu$ from axial-vector and tensor mesons in the holographic soft-wall model*, *Phys. Rev. D* **109** (2024) 094036 [2402.07579].

[389] H.-Y. Cheng, Y. Koike and K.-C. Yang, *Two-parton Light-cone Distribution Amplitudes of Tensor Mesons*, *Phys. Rev. D* **82** (2010) 054019 [1007.3541].

[390] V.M. Braun, N. Kivel, M. Strohmaier and A.A. Vladimirov, *Electroproduction of tensor mesons in QCD*, *JHEP* **06** (2016) 039 [1603.09154].

[391] T.M. Aliev and M.A. Shifman, *Old Tensor Mesons in QCD Sum Rules*, *Phys. Lett. B* **112** (1982) 401.

[392] BELLE collaboration, *Study of π^0 pair production in single-tag two-photon collisions*, *Phys. Rev. D* **93** (2016) 032003 [1508.06757].

[393] G. Källén, *Elementary particle physics*, Addison-Wesley, Reading, MA (1964).

[394] M. Knecht, S. Narison, A. Rabemananjara and D. Rabetiarivony, *Scalar meson contributions to a_μ from hadronic light-by-light scattering*, *Phys. Lett. B* **787** (2018) 111 [1808.03848].

[395] W. Qin, L.-Y. Dai and J. Portolés, *Two and three pseudoscalar production in e^+e^- annihilation and their contributions to $(g-2)_\mu$*, *JHEP* **03** (2021) 092 [2011.09618].

[396] R. Escribano, J.A. Miranda and P. Roig, *Radiative corrections to the τ-$\to$(P1P2)$-\nu\tau$ (P1,2=π,K) decays*, *Phys. Rev. D* **109** (2024) 053003 [2303.01362].

[397] P. Masjuan, A. Miranda and P. Roig, *τ data-driven evaluation of Euclidean windows for the hadronic vacuum polarization*, *Phys. Lett. B* **850** (2024) 138492 [2305.20005].

[398] S.-J. Wang, Z. Fang and L.-Y. Dai, *Two body final states production in electron-positron annihilation and their contributions to $(g-2)_\mu$*, *JHEP* **07** (2023) 037 [2302.08859].

[399] P. Roig and P. Sánchez-Puertas, *Axial-vector exchange contribution to the hadronic light-by-light piece of the muon anomalous magnetic moment*, *Phys. Rev. D* **101** (2020) 074019 [1910.02881].

[400] A. Pich and J. Portolés, *The Vector form-factor of the pion from unitarity and analyticity: A Model independent approach*, *Phys. Rev. D* **63** (2001) 093005 [hep-ph/0101194].

[401] D. Gómez Dumm and P. Roig, *Dispersive representation of the pion vector form factor in $\tau \to \pi\pi\nu_\tau$ decays*, *Eur. Phys. J. C* **73** (2013) 2528 [1301.6973].

[402] S. Gonzàlez-Solís and P. Roig, *A dispersive analysis of the pion vector form factor and $\tau^- \to K^- K_S \nu_\tau$ decay*, *Eur. Phys. J. C* **79** (2019) 436 [1902.02273].

[403] G. Eichmann, C.S. Fischer and R. Williams, *Kaon-box contribution to the anomalous magnetic moment of the muon*, *Phys. Rev. D* **101** (2020) 054015 [1910.06795].

[404] A. Miramontes, A. Bashir, K. Raya and P. Roig, *Pion and Kaon box contribution to a_μ^{HLbL}*, *Phys. Rev. D* **105** (2022) 074013 [2112.13916].

[405] A.S. Miramontes, K. Raya, A. Bashir, P. Roig and G. Paredes-Torres, *Radially excited pion: electromagnetic form factor and the box contribution to the muon's g-2**, *Chin. Phys.* **49** (2025) 083108 [2411.02218].

[406] A. Miranda, P. Roig and P. Sánchez-Puertas, *Axial-vector exchange contribution to the hyperfine splitting*, *Phys. Rev. D* **105** (2022) 016017 [2110.11366].

[407] V. Pascalutsa, V. Pauk and M. Vanderhaeghen, *Light-by-light scattering sum rules constraining meson transition form factors*, *Phys. Rev. D* **85** (2012) 116001 [1204.0740].

[408] F. Jegerlehner, *Leading-order hadronic contribution to the electron and muon $g-2$*, *EPJ Web Conf.* **118** (2016) 01016 [1511.04473].

[409] M. Knecht, S. Peris, M. Perrottet and E. de Rafael, *New nonrenormalization theorems for anomalous three point functions*, *JHEP* **03** (2004) 035 [hep-ph/0311100].

[410] L.D. Landau, *On the angular momentum of a system of two photons*, *Dokl. Akad. Nauk Ser. Fiz.* **60** (1948) 207.

[411] C.-N. Yang, *Selection Rules for the Dematerialization of a Particle Into Two Photons*, *Phys. Rev.* **77** (1950) 242.

[412] V. Pauk and M. Vanderhaeghen, *Single meson contributions to the muon's anomalous magnetic moment*, *Eur. Phys. J. C* **74** (2014) 3008 [1401.0832].

[413] L.-Y. Dai, J. Fuentes-Martín and J. Portolés, *Scalar-involved three-point Green functions and their phenomenology*, *Phys. Rev. D* **99** (2019) 114015 [1902.10411].

[414] G. Colangelo, M. Hoferichter, M. Procura and P. Stoffer, *Rescattering effects in the hadronic-light-by-light contribution to the anomalous magnetic moment of the muon*, *Phys. Rev. Lett.* **118** (2017) 232001 [1701.06554].

[415] J. Bijnens, N. Hermansson-Truedsson, L. Laub and A. Rodríguez-Sánchez, *The two-loop perturbative correction to the $(g-2)_\mu$ HLbL at short distances*, *JHEP* **04** (2021) 240 [2101.09169].

[416] J. Bijnens, N. Hermansson-Truedsson and A. Rodríguez-Sánchez, *Constraints on the hadronic light-by-light in the Melnikov-Vainshtein regime*, *JHEP* **02** (2023) 167 [2211.17183].

[417] J. Mager, L. Cappiello, J. Leutgeb and A. Rebhan, *Longitudinal short-distance constraints on hadronic light-by-light scattering and tensor meson contributions to the muon $g-2$*, *Phys. Rev. Lett.* **135** (2025) 091901 [2501.19293].

[418] J.M. Márquez, G.L. Castro and P. Roig, *Michel parameters in the presence of massive Dirac and Majorana neutrinos*, *JHEP* **11** (2022) 117 [2208.01715].

[419] L. Gan, B. Kubis, E. Passemar and S. Tulin, *Precision tests of fundamental physics with η and η' mesons*, *Phys. Rept.* **945** (2022) 1 [2007.00664].

[420] S. Tulin, *New weakly-coupled forces hidden in low-energy QCD*, *Phys. Rev. D* **89** (2014) 114008 [1404.4370].

[421] R. Escribano, S. Gonzàlez-Solís and E. Royo, *Sensitivity of the $\eta(')\to\pi 0\gamma\gamma$ and $\eta'\to\eta\gamma\gamma$ decays to a sub-GeV leptophobic U(1)B boson*, *Phys. Rev. D* **106** (2022) 114007 [2207.14263].

[422] R. Escribano, S. Gonzàlez-Solís and E. Royo, *Assessment of the $a_2(1320)$ tensor-meson contribution to $\eta/\eta' \to \pi^0\gamma\gamma$ decays*, 2510.00787.

[423] R. Escribano, E. Royo and P. Sanchez-Puertas, *New-physics signatures via CP violation in $\eta^{(\prime)} \to \pi^0\mu^+\mu^-$ and $\eta \to \eta\mu^+\mu^-$ decays*, *JHEP* **05** (2022) 147 [2202.04886].

[424] KLOE-2 collaboration, *Measurement of $\eta \to \pi^0\gamma\gamma$ branching fraction with the KLOE detector*, 2505.09285.

[425] H. Dembinski and P. Ongmongkolkul Version 2.32.0, Released Nov 9, 2025, https://pypi.org/project/iminuit/.

[426] H. Dembinski Version 0.2.2, Released: Aug 16, 2023, https://pypi.org/project/jacobi/.

[427] A. Pich, *Precision Tau Physics*, *Prog. Part. Nucl. Phys.* **75** (2014) 41 [1310.7922].

[428] P. Roig, *Hadronic and radiative decays of the tau lepton*, Ph.D. thesis, Valencia U., 2010. 1301.7626.

[429] A. Rodríguez-Sánchez, *Hadronic tau decays*, 2504.21732.

[430] V. Cirigliano, J. Jenkins and M. Gonzalez-Alonso, *Semileptonic decays of light quarks beyond the Standard Model*, *Nucl. Phys. B* **830** (2010) 95 [0908.1754].

[431] A. Guevara, G. López Castro and P. Roig, *Weak radiative pion vertex in $\tau^- \to \pi^-\nu_\tau\ell^+\ell^-$ decays*, *Phys. Rev. D* **88** (2013) 033007 [1306.1732].

[432] A. Guevara, G.L. Castro and P. Roig, *Improved description of dilepton production in τ-$\to\nu\tau$P- decays*, *Phys. Rev. D* **105** (2022) 076007 [2111.09994].

[433] M. Antonelli, V. Cirigliano, A. Lusiani and E. Passemar, *Predicting the τ strange branching ratios and implications for V_{us}*, *JHEP* **10** (2013) 070 [1304.8134].

[434] F.V. Flores-Baéz and J.R. Morones-Ibarra, *Model Independent Electromagnetic corrections in hadronic τ decays*, *Phys. Rev. D* **88** (2013) 073009 [1307.1912].

[435] J.H. Kuhn and E. Mirkes, *Structure functions in tau decays*, *Z. Phys. C* **56** (1992) 661.

[436] D.A.L. Aguilar, J. Rendón and P. Roig, *CP violation in two-meson Tau decays induced by heavy new physics*, *JHEP* **01** (2025) 105 [2409.05588].

[437] W.J. Marciano and A. Sirlin, *Electroweak Radiative Corrections to tau Decay*, *Phys. Rev. Lett.* **61** (1988) 1815.

[438] E. Braaten and C.-S. Li, *Electroweak radiative corrections to the semihadronic decay rate of the tau lepton*, *Phys. Rev. D* **42** (1990) 3888.

[439] J. Erler, *Electroweak radiative corrections to semileptonic tau decays*, *Rev. Mex. Fis.* **50** (2004) 200 [hep-ph/0211345].

[440] R. Omnès, *On the Solution of certain singular integral equations of quantum field theory*, *Nuovo Cim.* **8** (1958) 316.

[441] I. Rosell, J.J. Sanz-Cillero and A. Pich, *Quantum loops in the resonance chiral theory: The Vector form-factor*, *JHEP* **08** (2004) 042 [hep-ph/0407240].

[442] A. Pich, I. Rosell and J.J. Sanz-Cillero, *Form-factors and current correlators: Chiral couplings L(10)mu) **r(mu) and C(87)**r(mu) at NLO in 1/N(C)*, *JHEP* **07** (2008) 014 [0803.1567].

[443] J.A. Miranda and P. Roig, *Effective-field theory analysis of the $\tau^- \to \pi^- \pi^0 \nu_\tau$ decays*, *JHEP* **11** (2018) 038 [1806.09547].

[444] S. Gonzàlez-Solís, A. Miranda, J. Rendón and P. Roig, *Exclusive hadronic tau decays as probes of non-SM interactions*, *Phys. Lett. B* **804** (2020) 135371 [1912.08725].

[445] BELLE-II collaboration, *The Belle II Physics Book*, *PTEP* **2019** (2019) 123C01 [1808.10567].

[446] BABAR collaboration, *Measurement of the spectral function for the $\tau^- \to K^- K_S \nu_\tau$ decay*, *Phys. Rev. D* **98** (2018) 032010 [1806.10280].

[447] S. Gonzàlez-Solís, A. Miranda, J. Rendón and P. Roig, *Effective-field theory analysis of the $\tau^- \to K^-(\eta^{(\prime)}, K^0)\nu_\tau$ decays*, *Phys. Rev. D* **101** (2020) 034010 [1911.08341].

[448] S. Weinberg, *Charge symmetry of weak interactions*, *Phys. Rev.* **112** (1958) 1375.

[449] C. Leroy and J. Pestieau, *Tau Decay and Second Class Currents*, *Phys. Lett. B* **72** (1978) 398.

[450] A. Pich, *'Anomalous' η Production in Tau Decay*, *Phys. Lett. B* **196** (1987) 561.

[451] S. Descotes-Genon and B. Moussallam, *Analyticity of $\eta\pi$ isospin-violating form factors and the $\tau \to \eta\pi\nu$ second-class decay*, *Eur. Phys. J. C* **74** (2014) 2946 [1404.0251].

[452] R. Escribano, S. Gonzàlez-Solís and P. Roig, *Predictions on the second-class current decays $\tau^- \to \pi^- \eta^{(\prime)} \nu_\tau$*, *Phys. Rev. D* **94** (2016) 034008 [1601.03989].

[453] BABAR collaboration, *Studies of tau- —> eta K-nu and tau- —> eta pi- nu(tau) at BaBar and a search for a second-class current*, *Phys. Rev. D* **83** (2011) 032002 [1011.3917].

[454] BABAR collaboration, *Study of high-multiplicity 3-prong and 5-prong tau decays at BABAR*, *Phys. Rev. D* **86** (2012) 092010 [1209.2734].

[455] A. Guevara, G. López-Castro and P. Roig, *$\tau^- \to \eta^{(\prime)} \pi^- \nu_\tau \gamma$ decays as backgrounds in the search for second class currents*, *Phys. Rev. D* **95** (2017) 054015 [1612.03291].

[456] G. Hernández-Tomé, G. López Castro and P. Roig, *G-parity breaking in $\tau^- \to \eta^{(\prime)}\pi^-\nu_\tau$ decays induced by the $\eta^{(\prime)}\gamma\gamma$ form factor*, *Phys. Rev. D* **96** (2017) 053003 [1707.03037].

[457] G. Hernández-Tomé, G. López Castro and D. Portillo-Sánchez, *τ-$\to\pi$-$\eta\nu\tau$ decay induced by QED one-loop effects*, *Phys. Rev. D* **108** (2023) 113001 [2308.08067].

[458] BELLE collaboration, *Precise measurement of hadronic tau-decays with an eta meson*, *Phys. Lett. B* **672** (2009) 209 [0811.0088].

[459] S. Arteaga, L.-Y. Dai, A. Guevara and P. Roig, *Tension between e+e-$\to\eta\pi$-π+ and τ-$\to\eta\pi$-π0$\nu\tau$ data and nonstandard interactions*, *Phys. Rev. D* **106** (2022) 096016 [2209.15537].

[460] E.A. Garcés, M. Hernández Villanueva, G. López Castro and P. Roig, *Effective-field theory analysis of the $\tau^- \to \eta^{(\prime)}\pi^-\nu_\tau$ decays*, *JHEP* **12** (2017) 027 [1708.07802].

[461] M. Jamin, A. Pich and J. Portolés, *What can be learned from the Belle spectrum for the decay - tau- —> nu(tau) K(S) pi-*, *Phys. Lett. B* **664** (2008) 78 [0803.1786].

[462] D.R. Boito, R. Escribano and M. Jamin, *K pi vector form-factor, dispersive constraints and tau —> nu(tau) K pi decays*, *Eur. Phys. J. C* **59** (2009) 821 [0807.4883].

[463] V. Bernard, D.R. Boito and E. Passemar, *Dispersive representation of the scalar and vector Kπ form factors for $\tau \to K\pi\nu_\tau$ and $K_{\ell 3}$ decays*, *Nucl. Phys. B Proc. Suppl.* **218** (2011) 140 [1103.4855].

[464] V. Bernard, *First determination of $f_+(0)|V_{us}|$ from a combined analysis of $\tau \to K\pi\nu_\tau$ decay and πK scattering with constraints from $K_{\ell 3}$ decays*, *JHEP* **06** (2014) 082 [1311.2569].

[465] R. Escribano, S. González-Solís, M. Jamin and P. Roig, *Combined analysis of the decays $\tau^- \to K_S\pi^-\nu_\tau$ and $\tau^- \to K^-\eta\nu_\tau$*, *JHEP* **09** (2014) 042 [1407.6590].

[466] M. Jamin, J.A. Oller and A. Pich, *Scalar K pi form factor and light quark masses*, *Phys. Rev. D* **74** (2006) 074009 [hep-ph/0605095].

[467] D.R. Boito, R. Escribano and M. Jamin, *K π vector form factor constrained by $\tau->$ K piν_τ and K_{l3} decays*, *JHEP* **09** (2010) 031 [1007.1858].

[468] B. Moussallam, *Analyticity constraints on the strangeness changing vector current and applications to tau —> K pi nu(tau), tau —> K pi pi nu(tau)*, *Eur. Phys. J. C* **53** (2008) 401 [0710.0548].

[469] M. Jamin, J.A. Oller and A. Pich, *S wave K pi scattering in chiral perturbation theory with resonances*, *Nucl. Phys. B* **587** (2000) 331 [hep-ph/0006045].

[470] M. Jamin, J.A. Oller and A. Pich, *Strangeness changing scalar form-factors*, *Nucl. Phys. B* **622** (2002) 279 [hep-ph/0110193].

[471] M. Jamin, A. Pich and J. Portolés, *Spectral distribution for the decay tau —> nu(tau) K pi*, *Phys. Lett. B* **640** (2006) 176 [hep-ph/0605096].

[472] M. Finkemeier and E. Mirkes, *The Scalar contribution to tau –> k pi tau-neutrino*, *Z. Phys. C* **72** (1996) 619 [hep-ph/9601275].

[473] BELLE collaboration, *Study of tau- —> K(S) pi- nu(tau) decay at Belle*, *Phys. Lett. B* **654** (2007) 65 [0706.2231].

[474] J. Gasser and H. Leutwyler, *Low-Energy Expansion of Meson Form-Factors*, *Nucl. Phys. B* **250** (1985) 517.

[475] FLAG collaboration, *FLAG Review 2024*, 2411.04268.

[476] BABAR collaboration, *Search for CP Violation in the Decay* $\tau^- - > \pi^- K_S^0 (>= 0\pi^0)\nu_t au$, *Phys. Rev. D* **85** (2012) 031102 [1109.1527].

[477] V. Cirigliano, A. Crivellin and M. Hoferichter, *No-go theorem for nonstandard explanations of the* $\tau \to K_S \pi \nu_\tau$ *CP asymmetry*, *Phys. Rev. Lett.* **120** (2018) 141803 [1712.06595].

[478] J. Rendón, P. Roig and G. Toledo Sánchez, *Effective-field theory analysis of the* $\tau^- \to (K\pi)^- \nu_\tau$ *decays*, *Phys. Rev. D* **99** (2019) 093005 [1902.08143].

[479] F.-Z. Chen, X.-Q. Li, S.-C. Peng, Y.-D. Yang and H.-H. Zhang, *CP asymmetry in the angular distributions of* $\tau \to K_S \pi \nu_\tau$ *decays. Part II. General effective field theory analysis*, *JHEP* **01** (2022) 108 [2107.12310].

[480] R. Escribano, P. Masjuan and P. Sánchez-Puertas, η *and* η' *transition form factors from rational approximants*, *Phys. Rev. D* **89** (2014) 034014 [1307.2061].